UNIVERSITY OF SOUTHAMPTON

Faculty of Medicine

Collectin Interactions with Rhinovirus

by

Jacqueline Sarah Pugh

Thesis for the degree of Doctor of Philosophy

September 2012

UNIVERSITY OF SOUTHAMPTON

ABSTRACT

FACULTY OF MEDICINE

Doctor of Philosophy

COLLECTIN INTERACTIONS WITH RHINOVIRUS

by Jacqueline Sarah Pugh

The collectins surfactant protein A (SP-A) and SP-D are found in the lining fluid of the lung and form an important component of innate pulmonary defenses; they consist of a N-terminal region, a collagenous region, a neck region and a carbohydrate recognition domain (CRD). SP-A and SP-D bind to and have antiviral properties *in vivo* against the enveloped viruses respiratory syncytial virus (RSV) and influenza A virus (IAV). A recombinant fragment of SP-D (rfhSP-D) has also been developed and is composed of the neck, CRD and a short collagenous region of SP-D. The rfhSP-D retains the ability to bind to RSV and IAV. Human rhinovirus (HRV) is a non-enveloped virus and is the predominant cause of the common cold. HRV can also cause exacerbations in patients with chronic airway disease. Based on the known antiviral effects of SP-A and SP-D, and their localisation in the upper and lower airways, the present thesis sought to investigate the research question '**Can SP-A, SP-D and rfhSP-D bind to and inhibit infectivity of HRV**?'

Methods to purify and detect HRV were established and used in experiments with SP-A and SP-D purified from bronchoalveolar lavage and rfhSP-D expressed in *Escherichia coli*. A novel interaction between SP-D and rfhSP-D with HRV was identified using co-immunoprecipitation and surface plasmon resonance; no such interaction was detected with SP-A. Binding was calcium dependent and inhibited by the presence of sugars, indicating that binding is via the CRD. Monolayers of HeLa cells, 16HBE cells or undifferentiated primary nasal epithelial cells were infected with HRV co-incubated with collectins and the infection level was assessed using flow cytometry. The presence of collectins did not significantly alter the infection level. This is the first report of a component of the innate immune system binding to the surface of HRV.

List of Contents

List of Figures ix

List of Tables xv

Declaration of Authorship xvii

Acknowledgements xix

List of Abbreviations xxi

1. Chapter 1: Introduction 1

1.1 Pulmonary Surfactant 1

1.1.1 Surfactant Lipids 1

1.1.2 Surfactant Proteins 1

1.1.2.1 SP-B and SP-C 5

1.2 SP-A and SP-D 2

1.2.1 Isolation of SP-A and SP-D 3

1.2.2 Structure of SP-A and SP-D 4

1.2.2.1 Carbohydrate Recognition Domain 5

1.2.2.2 Neck Region 8

1.2.2.3 Collagenous Region 8

1.2.2.4 N-terminal Region 9

1.2.3 SP-A and SP-D Function 10

1.2.3.1 Chemotaxis 10

1.2.3.2 Alteration of Cytokine Production 11

1.2.3.3 Lymphocyte Proliferation 11

1.2.3.4 Antigen Presentation 12

1.2.3.5 Clearance of Apoptotic Cells 12

1.2.3.6 Interaction of SP-A and SP-D with Influenza A virus 13

1.2.3.7 Interaction of SP-A and SP-D with Respiratory Syncytial Virus 15

1.2.3.8 Interaction of SP-A and SP-D with Other Viruses 17

1.2.3.9 Interaction of SP-A and SP-D with Bacteria **17**
1.2.3.10 Interaction of SP-A and SP-D with Yeast and Fungi **18**
1.3 Human Rhinovirus **18**
1.3.1 Structure of HRVs **19**
1.3.2 HRV Replication Cycle **20**
1.3.2.1 Receptor Binding **23**
1.3.2.2 HRV Uncoating and Entry of Viral RNA into the Host Cell Cytoplasm..... **24**
1.3.2.3 HRV Replication **25**
1.3.2.4 HRV Virion Assembly **26**
1.3.3 Host Immune Response to HRV Infection **26**
1.3.3.1 Cellular Immune Response to HRV **26**
1.3.3.2 Humoral Immune Response **28**
1.3.4 HRV and Chronic Airway Disease **28**
1.4 Thesis Aims **30**
2. Chapter 2: General Materials and Methods **31**
2.1.1 Sodium Dodecyl Sulfate Polyacrylamide Gel Electrophoresis (SDS-PAGE) **31**
2.1.2 Western Blotting **31**
2.1.3 Cell Culture **32**
2.1.4 Viable Cell Counting **33**
2.1.5 Frozen Storage and Regeneration of Cell Stock **33**
2.1.6 Mycoplasma Testing **34**
2.1.7 Endotoxin Levels in Purified Proteins and HRV Preparations **34**
2.1.8 Flow cytometry **34**
2.1.9 Ultraviolet Inactivation of HRV **35**
2.1.10 Statistics **35**
3. Chapter 3: Validation of Viral Techniques **37**
3.1 Introduction **37**

3.2 Materials and Methods **38**
3.2.1 Optimisation of R16-7 for Western Blotting **38**
3.2.2 50 % tissue culture infectious dose ($TCID_{50}$) **38**
3.2.3 Immunocytochemistry **39**
3.2.4 Fluorescent Focus Assay **40**
3.2.5 Amplification of HRV1B and HRV16 Stocks **41**
3.2.6 Purification of HRV **41**
3.2.7 Transmission Electron Microscopy **43**
3.3 Results **43**
3.3.1 Optimisation of R16-7 for Western Blotting **43**
3.3.2 Refinement of $TCID_{50}$ **47**
3.3.3 Optimisation of R16-7 for Immunocytochemistry **48**
3.3.4 Fluorescent Focus Assay **50**
3.3.5 Amplification of HRV **51**
3.3.6 Purification of HRV Stocks **54**
3.3.7 Transmission Electron Microscopy of HRV **64**
3.4 Discussion **66**
4. Chapter 4: Source and Purification of Collectins **73**
4.1 Introduction **73**
4.2 Materials and Methods **74**
4.2.1 Expression and Purification of rfhSP-D **74**
4.2.2 Purification of nhSP-D from Amniotic Fluid **76**
4.2.3 Purification of nhSP-D from Bronchoalveolar Lavage Fluid ... **77**
4.2.4 Purification of nhSP-A from Bronchoalveolar Lavage Fluid ... **78**
4.2.5 Protein Concentration Determinisation **79**
4.2.6 Validation of Collectin Biological Activity **79**
4.3 Results **80**
4.3.1 Expression and Purification of rfhSP-D **80**
4.3.2 Removal of Endotoxin from rfhSP-D **83**

4.3.3 Purification of nhSP-D from Amniotic Fluid **86**
4.3.4 Purification of nhSP-D from BAL **88**
4.3.5 Purification of nhSP-A from BAL **90**
4.3.6 Validation of Collectin Biological Activity **93**
4.4 Discussion **95**
5. Chapter 5: Binding Studies between Collectins and Rhinovirus **99**
5.1 Introduction **99**
5.2 Materials and Methods **99**
5.2.1 Ligand Blot **99**
5.2.2 Solid Phase Binding Assay **100**
5.2.3 Co-immunoprecipitation **101**
5.2.4 Surface Plasmon Resonance **101**
5.3 Results **104**
5.3.1 HRV and rfhSP-D Ligand Blot **104**
5.3.2 Solid Phase HRV and SP-D Binding Assay **105**
5.3.3 Co-immunoprecipitation **113**
5.3.4 SPR **118**
5.4 Discussion **135**
5.4.1 Ligand Blot **135**
5.4.2 Solid Phase Binding Assay **136**
5.4.3 Co-immunoprecipitation **139**
5.4.4 SPR **141**
5.4.5 Conclusions and Future Directions **145**
6. Chapter 6: Effect of Collectins on *In Vitro* Rhinovirus Infection **147**
6.1 Introduction **147**
6.2 Materials and Methods **147**
6.2.1 Fluorescent Focus Reduction Assay **147**
6.2.2 Flow Cytometry **148**
6.2.3 Cytokine Analysis **149**

6.2.4 Primary Nasal Epithelial Cell Culture **150**
6.3 Results **150**
6.3.1 Validation of Flow Cytometry **150**
6.3.2 *In Vitro* HRV Infection of HeLa Cells **153**
6.3.3 Effect of Pre-incubation of Collectins on HeLa Cells prior to *In Vitro* HRV Infection **154**
6.3.4 Effect of Co-incubation of Collectins and HRV prior to *In Vitro* Infection of HeLa Cells **155**
6.3.5 Cytokine Analysis **158**
6.3.6 *In Vitro* HRV Infection of 16HBE Cells **160**
6.3.7 Effect of Co-incubation of Collectins and HRV prior to *In Vitro* Infection of PNEC Cultures **162**
6.4 Discussion **166**
6.4.1 Flow Cytometry to Detect HRV Infection **166**
6.4.2 Collectins and *In Vitro* Infection of HeLa cells **166**
6.4.3 Effect of Collectins on Cytokine Release by HeLa Cells in Response to HRV Infection **172**
6.4.4 Collectins and *In Vitro* Infection of 16HBE cells **179**
6.4.5 Collectins and *In Vitro* Infection of PNECs **180**
6.4.6 Future Directions **182**
7. Chapter 7: Summary and Future Directions **185**
8. Appendices **193**
8.1 Appendix 1: Amplification of HRV16 ..... **193**
8.1.1 Infection Media **193**
8.2 Appendix 2: Preliminary Murine Studies **193**
8.3 Introduction **193**
8.4 Materials and Methods **194**
8.4.1 Source of Wild-Type and Knockout Mice **194**
8.4.2 BAL of Animals **194**

8.4.3 Cytospin Preparations of Alveolar Macrophages **195**

8.4.4 Infection of Mice with HRV **195**

8.4.5 Analysis of Infection of Mice..... **196**

8.5 Results..... **197**

8.5.1 Characterisation of iDKO Mice..... **197**

8.5.2 HRV Infection of iDKO Mice **199**

8.6 Discussion..... **201**

9. References **205**

List of Figures

Figure 1-1 SP-A, SP-D and rfhSP-D structure. **5**

Figure 1-2 Electrostatic surface of (A) SP-A and (B) SP-D..... **7**

Figure 1-3 Schematic of HRV structure..... **20**

Figure 1-4 HRV replication cycle..... **22**

Figure 3-1 Initial optimisation of western blot using R16-7 antibody to detect HRV..... **44**

Figure 3-2 Optimisation of western blot using R16-7 antibody to detect HRV. **45**

Figure 3-3 Optimisation of blocking solution and concentration of secondary antibodies to detect HRV..... **46**

Figure 3-4 $TCID_{50}$ assay to determine viral infectivity of HRV1B on HeLa cells at passage >100 (A) and passage >60 (B) and HRV16 on HeLa cells at passage >100 (C) and passage >60 (D)..... **48**

Figure 3-5 Immunohistochemistry to detect HRV..... **49**

Figure 3-6 Immunocytochemistry negative controls..... **50**

Figure 3-7 Fluorescent focus assay to determine viral titre..... **51**

Figure 3-8 $TCID_{50}$ assay to determine viral titre of HRV16 amplified on (A) high (>100) and (B) low (>60) passage HeLa cells. **52**

Figure 3-9 Western Blot and SDS-PAGE of PEG precipitated HRV16..... **55**

Figure 3-10 Western blot of steps of PEG precipitation of HRV16..... **57**

Figure 3-11 Western blot analysis of sucrose density gradient purified HRV16..... **58**

Figure 3-12 Western blot analysis of sucrose density gradient purified HRV16..... **59**

Figure 3-13 Secondary removal of HRV1B by PEG precipitation after ultracentrifugation of HRV1B infected HeLa cell lysate. **63**

Figure 3-14 Transmission electron microscope images of purified (A) HRV1B and (B) HRV16. ..... **65**

Figure 4-1 Affinity purification of rfhSP-D using ManNAc-Sepharose column. **81**

Figure 4-2 Gel filtration of rfhSP-D using a Superdex 200 column. **81**

Figure 4-3 SDS-PAGE and western blot analysis of rfhSP-D stock and fractions from gel filtration using a Superdex 200 column shown in Figure 4-2. ..... **83**

Figure 4-4 Chromatogram of endotoxin removal from rfhSP-D stock using Detoxi-Gel. **84**

Figure 4-5 SDS-PAGE of stages of endotoxin removal from rfhSP-D using Detoxi gel shown in Figure 4-4. ..... **85**

Figure 4-6 Chromatogram of affinity purification of nhSP-D from amniotic fluid using ManNAc-agarose. **86**

Figure 4-7 SDS-PAGE (A. and C.) and western blot (B. and D.) analysis of nhSP-D purification from amniotic fluid. **88**

Figure 4-8 Gel filtration of nhSP-D using a Superose 6 column. **89**

Figure 4-9 Western blot analysis of nhSP-D preparations purified from BAL. **90**

Figure 4-10 Purified stock of nhSP-A. **91**

Figure 4-11 Verification of no contamination of nhSP-A preparation with nhSP-D. **92**

Figure 4-12 Effect of multimeric nhSP-D (A), dodecameric nhSP-D (B), rfhSP-D (C) and nhSP-A (D) on infectivity of IAV. **94**

Figure 5-1 Ligand blot of HRV16 and rfhSP-D. **105**

Figure 5-2 Solid phase binding assay of rfhSP-D and (A) Hep-2C cell lysate and (B) RSV A2 infected Hep-2C cell lysate. **107**

Figure 5-3 Solid phase binding assay of rfhSP-D and (A) HeLa cell lysate and (B) HRV16 infected HeLa cell lysate. **108**

Figure 5-4 Solid phase binding assay of rfhSP-D binding to sucrose density gradient purified HRV16. ..... **109**

Figure 5-5 Optimisation of blocking solution for solid phase binding assay. **110**

Figure 5-6 Further optimisation of the blocking solution for solid phase binding assay. **111**

Figure 5-7 Further Optimisation of Blocking Solution for Solid Phase Binding Assay. **112**

Figure 5-8 Diagram of co-immunoprecipitation experimental principle. **113**

Figure 5-9 Co-immunoprecipitation negative control for nonspecific binding. **115**

Figure 5-10 Co-immunoprecipitation of rfhSP-D with HRV16 or HRV1B in virus buffer and a negative control with no HRV. **116**

Figure 5-11 Negative control of nhSP-A and virus buffer alone subjected to co-immunoprecipitation conditions. **117**

Figure 5-12 Co-immunoprecipitation of rfhSP-D and HRV16 or HRV1B in virus buffer. **118**

Figure 5-13 SPR response analyses of collectin and HRV1B interactions. **119**

Figure 5-14 SPR response analyses of collectin and HRV16 interactions. **120**

Figure 5-15 Kinetics analysis of HRV16 SPR response when flowed over immobilised rfhSP-D. **121**

Figure 5-16 SPR response analyses of HRV1B and BSA interactions with SP-D. **125**

Figure 5-17 SPR response analyses of protein and HRV1B interactions in the presence and absence of calcium ions. **126**

Figure 5-18 SPR response analyses of protein and HRV16 interactions in the presence and absence of calcium ions. **127**

Figure 5-19 SPR response analyses of nhSP-A and HRV1B or HRV16 interactions in the presence and absence of calcium ions. **128**

Figure 5-20 SPR response analyses of collectin and HRV1B interactions in the presence and absence of the anti-HRV mAb, R16-7..... **129**
Figure 5-21 SPR response analyses of HRV1B in the presence maltose. **131**
Figure 5-22 SPR analysis of the effect of sugars on the interaction between HRV and SP-D. **133**
Figure 6-1 Comparison of (A) uninfected vs (B) HRV16 infected HeLa cells using flow cytometry. **151**
Figure 6-2 Comparison of HRV16 infection of (A) HeLa cells and (B) 16HBE cells assessed by FFA and flow cytometry (FACS). **152**
Figure 6-3 Determining viral dose for *in vitro* HeLa cell studies. **153**
Figure 6-4 Effect of pre-treatment of HeLa cells with rfhSP-D prior to infection with HRV16. ..... **155**
Figure 6-5 HRV1B infection of HeLa cells in the presence of rfhSP-D *in vitro*. **156**
Figure 6-6 HRV16 infection of HeLa cells in the presence of rfhSP-D *in vitro*. **157**
Figure 6-7 Analysis of cytokines in cell supernatant from HeLa cells infected with HRV16 co-incubated with multimeric nhSP-D prior to infection. **159**
Figure 6-8 Determining viral dose for *in vitro* 16HBE cell studies..... **161**
Figure 6-9 HRV16 infection in the presence of rfhSP-D *in vitro* in 16HBE cells. **162**
Figure 6-10 HRV1B infection of PNECs in the presence and absence of multimeric nhSP-D..... **164**
Figure 6-11 Effect of co-incubation of HRV1B with multimeric nhSP-D on the level of HRV1B infection of PNECs. **165**
Figure 6-12 A model showing the potential binding site of SP-D on HRV.. **169**
Figure 8-1 Cytospin of alveolar macrophages from (A) iDKO mice withdrawn from tetracycline for 48 hours (B) iDKO receiving tetracycline (C) wild type mice and (D) wild type rat. **198**

Figure 8-2 Western blot analysis of SP-D content of BAL from wild type and iDKO mice with and without treatment with tetracycline..... **199**

Figure 8-3 HRV1B RNA detected in the lungs of HRV1B infected mice. **200**

List of Tables

Table 3-1 Optimisation of HRV amplification. **53**

Table 3-2 Viral titre of each population from the sucrose density gradient as identified by western blotting (Figure 3-12). **61**

Table 3-3 Comparison of PEG precipitation and ultracentrifugation to concentrate HRV prior to purification on sucrose gradients. **62**

Table 3-4 Comparison of dialysis and Amicon filter to remove sucrose from purified HRV preparations. **64**

Table 5-1 Binding of HRV1B and HRV16 to immobilised SP-D..... **122**

Table 5-2 Molar ratios of SP-D binding to HRV1B and HRV16. ..... **124**

Table 5-3 IC_{50} values for sugar inhibition of HRV1B and HRV16 binding to SP-D..... **134**

Declaration of Authorship

I, Jacqueline Sarah Pugh, declare that the thesis entitled Interactions of Collectins with Rhinovirus and the work presented in the thesis are both my own, and have been generated by me as the result of my own original research.

I confirm that:

1. This work was done wholly or mainly while in candidature for a research degree at this University;
2. Where any part of this thesis has previously been submitted for a degree or any other qualification at this University or any other institution, this has been clearly stated;
3. Where I have consulted the published work of others, this is always clearly attributed;
4. Where I have quoted from the work of others, the source is always given. With the exception of such quotations, this thesis is entirely my own work;
5. I have acknowledged all main sources of help;
6. Where the thesis is based on work done by myself jointly with others, I have made clear exactly what was done by others and what I have contributed myself;
7. None of this work has been published before submission

Signed: ……..

Date:……

Acknowledgements

I would like to thank many people for their help and support whilst undertaking my PhD project, without them it would not have been possible.

Firstly I would like to thank my supervisors Professor Howard Clark and Dr. Jens Madsen for their continual support and guidance throughout the project. They have encouraged me throughout and been excellent supervisors. In addition, Jens has been a fantastic teacher, helping me to develop my laboratory skills as well as a being a good friend.

I also very much want to thank the rest of the Child Health group, in particular Rosie and Zofi. Both listened to my experimental woes and gave me encouragement, so for that I am very grateful. Thank you Paul for passing on your protein purification wisdom.

From GlaxoSmithKline I am indebted to Dr. Ian Kirby and Emilie Charles who willingly divulged their vast surface plasmon resonance knowledge, and dedicated time to helping me whilst using their facilities in Stevenage. Dr. Roberto Solari, my industrial supervisor, gave great support and suggested alternate perspectives on addressing challenges I was faced with.

My project was funded by the BBSRC and GlaxoSmithKline, I would like to express my thanks for this funding as, without it, the project would have not been possible.

Finally I would like to thank my friends and family; this is not an exhaustive list as support from everyone around me has been vital over the past four years. Thank you to Kerry and Sarah for lending a military wife's ear when things were all getting too much. Thank you to Kerry and Louise for lending a bed in the final months of lab work when I couldn't face a long drive home. To my husband James, you are my rock and motivator; I do not know how I would have completed the last four years without your support and belief in me – even if sometimes from afar. I would also like to thank my parents, as well as Carole and Tom for their love, encouragement and support as always; Chloe also deserves a mention as she never failed to make me smile.

List of Abbreviations

ALI	Air-liquid interface
APC	Allophycocyanin
BAL	Bronchoalveolar lavage
BSA	Bovine serum albumin
CCL-5	Chemokine (C-C motif) ligand 5
COPD	Chronic obstructive pulmonary disease
CPE	Cytopathic effect
CRD	Carbohydrate recognition domain
DAPI	4',6-diamidino-2-phenylindole
DC	Dendritic cell
DMEM	Dulbecco's Modified Eagle Medium
DMSO	Dimethyl sulphoxide
ECL	Enhanced chemiluminescence
EDC	1-ethyl-3-(3-dimethylaminopropyl) carbodiimide hydrochloride
EDTA	Ethylenediaminetetraacetic Acid
ELISA	Enzyme-linked immunosorbant assay
FBS	Heat inactivated fetal bovine serum
FFA	Fluorescent focus assay
FFRA	Fluorescent focus reduction assay
ffu	Fluorescence forming units
FITC	Fluorescein isothiocyanate
GαM-AF594	Goat-anti-mouse alexafluor594 conjugated secondary antibody
GαM-HRP	Goat-anti-mouse HRP conjugated secondary antibody
HA	Hemagglutinin

HBEC	Human bronchial epithelial cells
HIV	Human immunodeficiency virus
HRP	Horse radish peroxidase
HRV	Human rhinovirus
HSV	Herpes simplex virus
IAV	Influenza A virus
IFN	Interferon
ICAM-1	Intercellular adhesion molecule-1
iDKO	Inducible SP-D knockout mice
IGEPAL® CA-630	Octylphenoxy polyethoxyethanol
kDa	Kilodaltons
LAL	Limulus amebocyte lysate
LB	Luria broth
LDLR	Low density lipoprotein receptor
mAB	Monoclonal antibody
ManNAc	N-Acetyl-D-mannosamine
MDCK	Madin-Darby canine kidney
MEM	Minimum essential medium
MWCO	Molecular weight cut off
NA	Neuraminidase
NF-κB	Nuclear factor κB
NHS	N-hydroxysuccinimide
nhSP-A	Full length native human surfactant protein A
nhSP-D	Full length native human surfactant protein D
OGP	Octyl β-D-glucopyranoside
PCR	Polymerase chain reaction
PDB	Protein data bank
PBS	Phosphate buffered saline (105 mM KH_2PO_4, 154 mM NaCl, 5.6 mM Na_2HPO_4, pH 7.4)

PEG	Polyethylene glycol
PBEC	Primary bronchial epithelial cell
PNEC	Primary nasal epithelial cell
PVDF	Polyvinylidene fluoride
pPCR	Quantitative real time polymerase chain reaction
rfhSP-D	Recombinant fragment of human surfactant protein D
RPMI	Roswell Park Memorial Institute (RPMI) 1640 medium
RSV	Respiratory syncytial virus
SARS-CoV	Severe acute respiratory syndrome coronavirus
SDS-PAGE	Sodium dodecyl sulfate polyacrylamide gel electrophoresis
SIRPα	Signal regulatory protein α
SP-D$^{-/-}$	SP-D deficient genotype
SPR	Surface plasmon resonance
TBS	Tris-buffered saline (20 mM Tris, 150 mM NaCl, pH 7.4)
TBS-$CaCl_2$	Tris-buffered saline containing calcium (20 mM Tris, 150 mM NaCl, 5 mM $CaCl_2$, pH 7.4)
TBW	Tris-buffered water (5 mM Tris, pH 7.4)
$TCID_{50}$	50 % Tissue culture infectious dose
TEM	Transmission electron microscopy
TMB	3,3',5,5'-tetramethyl-benzidine
TNF	Tumor necrosis factor

1. Chapter 1: Introduction

1.1 Pulmonary Surfactant

Pulmonary surfactant is an essential component of the lung, made up of a complex mixture of lipid (~90 %) and protein (~10 %). The most critical function of pulmonary surfactant is the reduction in surface tension at the air-liquid interface in the lung, thereby preventing alveolar collapse [1]. Neonatal respiratory distress syndrome (RDS) occurs in premature babies who have immature lungs and therefore a deficiency in pulmonary surfactant. The introduction of exogenous surfactant treatment to these premature babies greatly reduced the mortality associated with premature birth [2-4]. In addition pulmonary surfactant has a well-documented role in the innate immunity of the lung (see section 1.2.3).

1.1.1 Surfactant Lipids

The surface tension reducing properties of pulmonary surfactant are attributed mainly to the lipid component of surfactant, although the surfactant associated proteins do play a role. The main constituent (~80 %) of the lipid portion of pulmonary surfactant is phosphatidlycholine, of which approximately half is dipalmitoylphosphatidylcholine (DPPC). The saturated DPPC is able to pack densely forming a layer capable of maintaining low surface tension [5].

1.1.2 Surfactant Proteins

There are four surfactant proteins, native human surfactant protein-A (SP-A), SP-B, SP-C and SP-D. The proteins are separated into two groups. The proteins SP-B and SP-C are hydrophobic proteins that are involved in the

reduction of surface tension, whereas SP-A and SP-D are hydrophilic glycoproteins primarily involved in innate immunity in the lung.

1.1.2.1 SP-B and SP-C

The proteins SP-B and SP-C are expressed by type II alveolar epithelial cells, SP-B is also expressed by Clara cells. Both proteins are associated with the lipid component of surfactant and promote surface film formation at the air-liquid interface of the lung; it has been demonstrated that SP-B enhances lipid insertion into the lipid layer at the air-liquid interface [6]. The importance of SP-B is revealed by a mutation in the SP-B gene that causes SP-B deficiency and leads to fatal neonatal respiratory disease [7]. SP-B deficiency is also linked with aberrant processing of SP-C protein; the mechanism for this remains elusive [8]. Mutations that lead to SP-C deficiencies result in respiratory dysfunction and interstitial lung diseases [9, 10].

An anti-inflammatory role for SP-B, in addition to its essential role in reducing surface tension, has been shown by studying SP-B overexpressing mice ($SP\text{-}B^{(+/+/+)}$). When these mice are challenged with endotoxin they have fewer inflammatory cells and proinflammatory cytokines in their BAL compared to $SP\text{-}B^{(+/-)}$ mice [11].

1.2 SP-A and SP-D

The proteins SP-A and SP-D are part of the collectin family, which also consists of mannan-binding lectin, bovine collectin conglutinin, collectin-46 collectin-43 and collectin 11 [12-15]. Collectins are so called due to their collagenous and lectin domains. SP-A and SP-D form an important part of

the innate pulmonary defences and control of inflammation. The lung is the primary site of SP-A and SP-D synthesis, where they are predominantly produced by alveolar type II cells; however non-ciliated Clara cells and submucosal cells also produce SP-A and SP-D [16, 17]. There is approximately ten-fold more SP-A than SP-D within the surfactant lining fluid in the lung. Expression of SP-A and SP-D is not restricted to the lungs; they are expressed in many extrapulmonary sites where they may have a role in host defence. Both SP-A and SP-D are present in human nasal mucosa, tears, saliva and amniotic fluid [18-22]. SP-A is also expressed in the thymus, prostrate, mesentery, and the female genital tract [23-25]. SP-D is found in many extrapulmonary sites. It is secreted onto mucosal surfaces throughout the body [17].

1.2.1 Isolation of SP-A and SP-D

SP-A and SP-D can be isolated from amniotic fluid and bronchoalveolar lavage (BAL) taken from patients with alveolar proteinosis; however, yields are low and the SP-D exists in various oligomeric forms [26]. Mammalian and baculovirus expression systems also produce SP-D; however, the yield is still low [27, 28]. Difficulty of isolation, varying structure and low yields results in SP-D being an unattractive pharmacological agent. In contrast to this, a recombinant fragment of SP-D (rfhSP-D) with biological activity *in vivo* has been developed [29-31]. The rfhSP-D consists of the neck and CRD of the SP-D molecule, with only a short collagenous region. The rfhSP-D can potentially be produced uniformly on a large scale from bacterial and yeast expression systems that give a higher yield, and thus rfhSP-D is a viable pharmacological agent [32].

1.2.2 Structure of SP-A and SP-D

There are four structural domains of SP-A and SP-D; the N-terminal non-collagenous domain, the collagenous region, the neck region and the C-type carbohydrate recognition domain (CRD) (Figure 1-1) [33-35]. Monomers of SP-A and SP-D associate with one another at the neck region to form trimers [36]. In the case of SP-A there are two transcribed genes, SFTPA1 and SFTPA2, forming SP-A1 and SP-A2 chains respectively [37, 38].

Higher order oligomers are formed via disulfide and non-disulfide bonds between the amino terminuses of the chains. The most common SP-A oligomer is an octadecamer consisting of six trimers in a bunch of tulips formation; whereas the most common SP-D oligomer is a dodecamer consisting of four trimers in a crucifix formation (Figure 1-1) [13, 39, 40]. In SP-A isolated from patients with alveolar proteinosis multimers of SP-A have been observed using electron microscopy [41, 42]. Multimers of SP-D consisting of upwards of 32 homotrimers can also naturally form and are seen in some healthy individuals and patients with pulmonary alveolar proteinosis [39, 43].

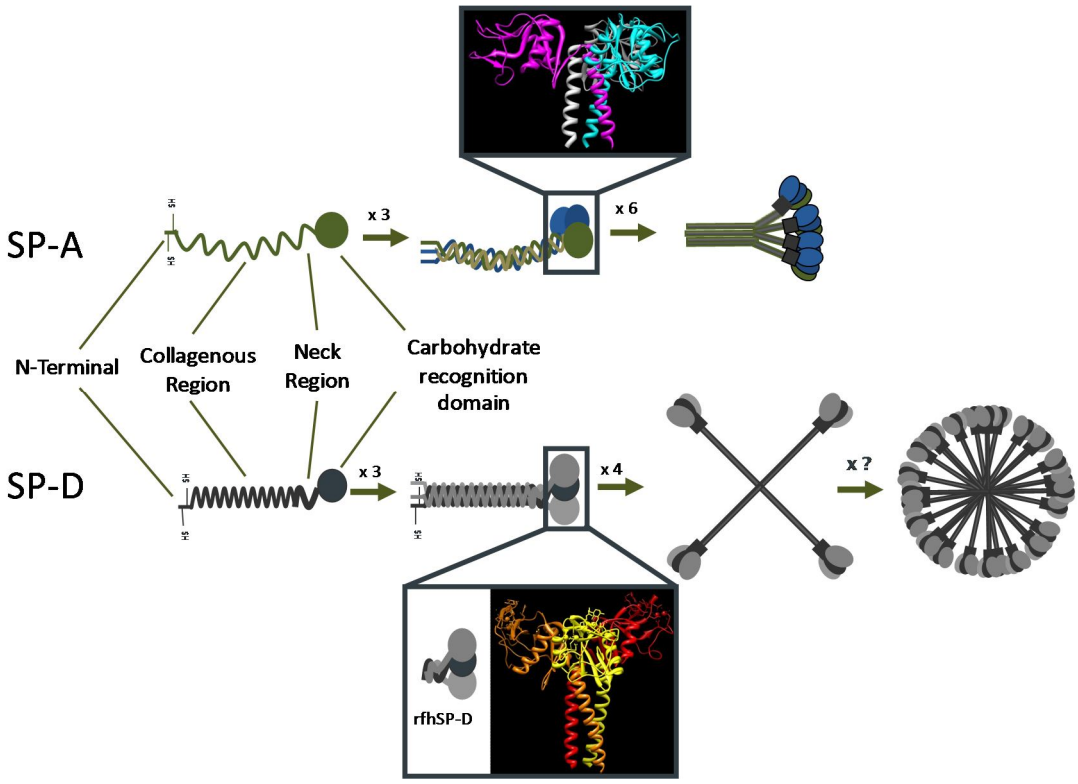

Figure 1-1 SP-A, SP-D and rfhSP-D structure. The four structural domains of the SP-A and SP-D monomers are shown. Three monomers associate with one another at the neck region to form trimers. Trimers oligomerise to form higher order multimers, the most common of which for SP-A is an octadecamer consisting of six trimers in a bunch of tulips formation and for SP-D the most common is a dodecamer, consisting of four trimers in a crucifix formation. SP-D also forms higher order multimers with an unknown number of trimers. A schematic diagram and a ribbon representation of the crystal structure of the rfhSP-D, which consists of the neck region, CRD and a short collagen section is shown. Each colour represents a different monomer. Crystal structure images produced using the UCSF Chimera package version 1.6, protein data bank (PDB) codes 1PW9 and 3PAR for rfhSP-D and rat SP-A respectively.

1.2.2.1 Carbohydrate Recognition Domain

The CRD of SP-A and SP-D confers lectin activity and is primarily responsible for the recognition of pathogens. The overall structure of the collectins varies; however, there are 18 highly conserved residues within the CRD [44, 45].

The structures of the CRDs of SP-A and SP-D have been resolved at high resolution using x-ray crystallography. The structure of the CRD of a recombinant fragment of SP-D in the native form has been described by Hakansson *at al.* and Shrive *et al.* [34, 46]. Head *et al*. resolved the CRD structure of rat SP-A [47]. These have shown subtle differences in the structures of SP-A and SP-D that may help explain their different ligand specificities.

The structure of the CRD is primarily composed of two anti-parallel β-sheets. One of these is four-stranded and interacts with the neck region; the other is five-stranded and in conjunction with some of the loop structure and a Ca^{2+} ion forms the carbohydrate binding site [34, 35]. This primary Ca^{2+} ion, termed Ca1, is present in the CRD of all collectins. The presence of Ca1 causes a symmetric conformation in all three chains of SP-D; it also changes the charge of the cleft. The coordination of Ca1 in the absence of a carbohydrate ligand is completed by two water molecules, but when bound to carbohydrate this is conducted by oxygen atoms from the terminal monosaccharide [46]. The distance between two carbohydrate binding Ca^{2+} ions was found to be approximately 5 nm [34]. A recent study by Shang *et al.* demonstrated that there is a ligand associated conformational change in the carbohydrate binding site of SP-A. This has not been reported for SP-D [48]. No contacts between the individual CRDs of SP-A or SP-D have been found in the x-ray crystallography studies.

There are two further Ca^{2+} ions in the CRD of SP-D, termed Ca2 and Ca3, seen in crystallography studies [46]. These Ca^{2+} ions are in close proximity to Ca1 and are coordinated by water molecules and acidic side chains. No equivalent Ca^{2+} ions are seen in the structure of rat SP-A [47].

The surface of SP-D is largely positive, mainly due non-conserved lysine residues. The crystal structure of a recombinant fragment of SP-D shows that there is a Ca^{2+} ion that interacts with Glu232 which is in contact with the lysine residues on each chain. The Ca^{2+} ion changes the conformational structure of the chains thereby removing the neutralising effect that the glutamate residues have on the lysine residues; this results in a positively charged "funnel" in the cavity between the three lectin domains which is absent in SP-A, as can be seen in Figure 1-2 [46].

There is N-glycosylation in the CRD of SP-A from all species studied, and based on size-shift studies of deglycosylated SP-A this is a carbohydrate group of 5-10 kDa [49]. The only other collectin with known N-glycosylation in the CRD is porcine SP-D [50]. The functional effect of the glycosylation on carbohydrate binding has not been well studied.

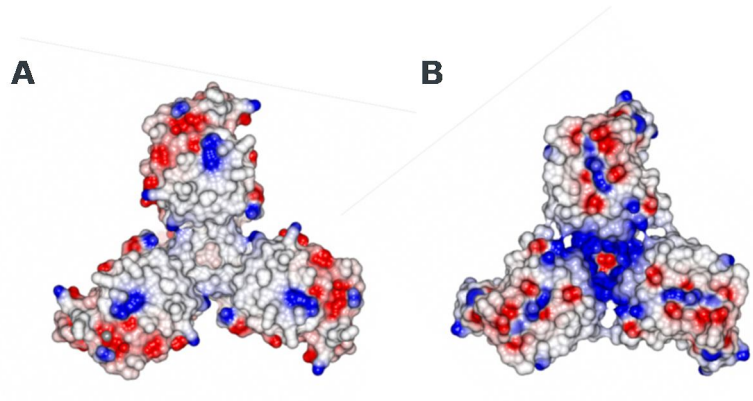

Figure 1-2 Electrostatic surface of (A) SP-A and (B) SP-D. The electrostatic surfaces of the CRD of rat SP-A (PBD code 3PAR) and human SP-D (PBD code 1B08) are shown. A Ca^{2+} ion is present in the SP-A structure and three Ca^{2+} ions are present in the SP-D structure. The positive and negative charges are represented by blue and red respectively. Surface charges calculated and images created using CCP4 software version 2.6.2 [51, 52].

1.2.2.2 Neck Region

A 34-41 amino acid section of the SP-A and SP-D molecule forms the neck region. The amino acid sequence results in the formation of an α-helix, three of these come together in the trimer to form the α-helical coiled-coil structure which makes about eight helical turns [34, 36]. Hydrophobic interactions stabilise the trimeric coiled-coil [36, 47]. The characteristic amino acid sequence of an α-helical coiled-coil is that of the repeating heptad pattern, 'a-b-c-d-e-f-g' where 'a' and 'd' are typically hydrophobic residues. The neck region of SP-D does tend to follow this rule; however, the neck region of SP-A deviates from this and consequently the interactions in the neck region are weaker. Experiments using mutated rat SP-D have helped elucidate that the neck region is important for the formation of a stable collagenous region and is required for the formation of trimers [53].

The orientation of the neck and CRD domains of the SP-A molecule results in a 'T' shape, in contrast, the SP-D molecule has a 'Y' shape [47]. This could have implications for the interaction of the molecules with ligands.

1.2.2.3 Collagenous Region

The collagenous region of the collectins consists of the classic collagen structure, repeating units of glycine-X-Y, where X and Y can be any amino acid but are often proline or hydroxyproline. Three chains coil around one another in a right handed manner, forming a helix with the glycine residues inside the helix. The hydoxylation of some prolines and lysines is required for the stabilisation of the helical collagen structure at 37 °C. It is believed that intrachain hydrogen bonds form and thus stabilise the structure [54]. Early structural studies of SP-D suggested that in the molecule approximately 24 % of the lysine residues and 33 % of the proline residues

were hydroxylated [55]. Of all the collectins SP-D has one of the largest collagenous regions (59 Gly-X-Y repeats, 46 nm long), and SP-A has one of the shortest (23 Gly-X-Y repeats, 20 nm long) [37, 55]. There is an interruption in the Gly-X-Y repeats of the collagen domain of SP-A, and this gives a 60° kink in the helix, as revealed by electron microscopy [56]. Another difference between SP-A and SP-D is that SP-D is glycosylated within the collagenous region, at residue Asn70, whereas SP-A is not [39]. The functional importance of the glycosylation of SP-D is not clear; it was initially hypothesised that it may be necessary for the formation of trimers and therefore dodecamer formation. This was however disproved as Chinese hamster ovary (CHO)-K1 expressed rat SP-D engineered to lack the glycosylation shows normal assembly and secretion [57].

1.2.2.4 N-terminal Region

The N-terminal region of SP-D is 25 amino acids whereas the N-terminal region of SP-A is much shorter with 7 amino acids [37, 55, 58]. Within the N-terminal region stabilising disulphide bonds form between the monomeric units that form trimers; the formation of further disulphide bonds result in oligomerisation of SP-A and SP-D. There are two cysteine residues at positions 15 and 20 that have been shown by mutational studies of rat SP-D to be required for the stabilisation of the dodecameric form of SP-D [59]. Mutational analysis of SP-A has shown that although the N-terminal region is required for the formation of SP-A oligomers, the formation of disulphide bonds is not essential [60, 61].

1.2.3 SP-A and SP-D Function

The role of SP-A and SP-D in the lung is well documented; they provide innate defence and modulate the inflammatory response to inhaled micro-organisms, including viruses, fungi and bacteria [62-68]. The CRD is responsible for recognition of carbohydrate molecules commonly present on the surface of pathogens, to which it binds in a calcium dependent manner. It is also thought that binding of SP-D may involve electrostatic interactions due to the large electrostatic potential in the cavity between the three lectin domains; this may interact with targets on micro-organisms which have a negative charge, such as lipopolysaccharide which is found in cell walls of Gram-negative bacteria [34]. In addition to interactions with microorganisms, it has also been documented that SP-A and SP-D can recognise and aid in the clearance of materials in the lung such as pollen, house dust mite allergens and apoptotic cells [69-71].

1.2.3.1 Chemotaxis

SP-A and SP-D are chemotactic for alveolar macrophages and neutrophils and are consequently thought to have an important role in recruitment and retention of these cells in immune responses [72, 73]. Experimental evidence suggests that the chemotaxis associated with SP-D is mediated by the CRD binding to the phagocyte as the presence of sugars and CRD directed antibodies inhibit this function [72]. The CRD is further implicated as a neck-CRD recombinant fragment of SP-D retains the ability to elicit neutrophil chemotaxis *in vitro* [74]. Unlike that of SP-D, SP-A chemotaxis of alveolar macrophages may be mediated via the collagen region [75].

1.2.3.2 Alteration of Cytokine Production

It has been proposed that SP-A and SP-D are dual mediators of inflammation, depending on the presence of pathogens and how the collectins are interacting with receptors. Gardai *et al.* suggest that in the absence of pathogens SP-A and SP-D bind to signal inhibitory protein (SIRP)-α, expressed on mononuclear phagocytes and pulmonary epithelial cells, via the CRD which consequently inhibits production of pro-inflammatory cytokines. When SP-A and SP-D are associated with pathogens it is believed they engage with the calreticulin/CD91 complex via the collagen domain, and thus cause a pro-inflammatory response [76].

SP-A and SP-D are pattern recognition molecules and can therefore modulate the immune response to pathogens through direct interactions with pathogen-associated molecular patterns (PAMPs), as well as by other mechanisms. For example, SP-A down-regulates zymosan induction of tumor necrosis factor (TNF)-α secretion from alveolar macrophages; this is via a mechanism involving SP-A alteration of the interaction of zymosan with toll-like receptor (TLR)-2, despite not binding to zymosan [77]. Binding of SP-A to CD14 on alveolar macrophages inhibits binding of smooth LPS (which is not a ligand for SP-A) to CD14, which reduces TNF-α production [78]. In contrast, TNF-α production from alveolar macrophages in response to rough LPS remains unchanged in the presence of SP-A, even though rough LPS is a SP-A ligand [78]. This highlights that the effect of SP-A is dependent on various factors.

1.2.3.3 Lymphocyte Proliferation

Inhibition of T-cell proliferation has been reported for both SP-A and SP-D, this is thought to be mediated by two different mechanisms. The first is an

IL-2 dependent mechanism in which SP-A and SP-D were shown to inhibit anti-CD3 antibody and phytohaemagglutinin stimulated T cell proliferation mediated by inhibition of IL-2 production [79, 80]. The second mechanism is an IL-2 independent mechanism that involves attenuation of calcium signalling [81, 82].

1.2.3.4 Antigen Presentation

Both SP-A and SP-D bind to dendritic cells (DCs). DCs are the most potent antigen presenting cells and are found in the airway epithelium, the lung parenchyma and within the alveolar space [83]. The interaction of SP-A and SP-D with DCs is only partially inhibited by ethylenediaminetetraacetic acid (EDTA) suggesting both CRD and non-CRD mediated binding [84]. Pre-treatment of immature DCs with SP-A inhibits DC maturation *in vitro* and *in vivo*. SP-A also inhibits the chemotaxis of DCs [85, 86]. In contrast, SP-D has been shown to enhance *E .coli* uptake and presentation by murine bone-marrow derived DCs [87]. A later study found that SP-D inhibited antigen presentation by murine lung DCs [88]. These experiments suggest that the SP-A and SP-D may have important regulatory roles in the lung resulting in the maintenance of a hyporesponsive immunologic environment. The overall role of SP-A and SP-D in enhancing phagocytic uptake and preventing DC maturation and T cell proliferation reduces the occurrence of potentially damaging inflammatory responses.

1.2.3.5 Clearance of Apoptotic Cells

Apoptosis is the process of programmed cell death, essential for the maintenance of tissue homeostasis and resolution of the inflammatory response [89]. The importance of SP-D, but not SP-A, in clearance of

apoptotic cells from the lung is evident from *in vivo* murine studies in mice overexpressing SP-D or SP-A [90]. In addition to this, SP-$D^{-/-}$ mice show accumulation of apoptotic and necrotic alveolar macrophages and intranasal administration of rfhSP-D reduces the number of apoptotic macrophages [91] .

1.2.3.6 Interaction of SP-A and SP-D with Influenza A virus

Influenza A virus (IAV) is an important pathogen that has been responsible for causing three worldwide pandemics in the last century, the "Spanish influenza" in 1918, the "Asian influenza" in 1957, and the "Hong Kong influenza" in 1968; it is estimated that the Spanish influenza killed approximately 50 million people globally [92]. IAV are negative sense, single stranded RNA viruses, which have a lipid envelope derived from the plasma membrane of the cell in which it replicated [93].

The initial step in IAV infection is attachment of the hemagglutinin (HA) to sialic acids on the surface of the host cell. For human strains this is predominantly respiratory epithelial cells. Human IAV strains preferentially bind sialic acid residues attached to galactose by an α2, 6 linkage, the most common linkage found on human respiratory epithelial cells [94]. After attachment the virus is endocytosed into the host cell, where it replicates before budding. The budding process involves both the viral HA and the neuraminidase (NA); the HA anchors IAV to the host cell while the NA activity removes the sialic acid thus releasing the virus. NA also removes sialic acid from the viral envelope to prevent aggregation of viral particles [95].

Both SP-A and SP-D neutralise IAV but by different mechanisms. SP-D binds to high-mannose oligosaccharides close to the sites on the HA that bind sialic acid. SP-D is therefore thought to sterically prevent cellular attachment [62, 96, 97]. SP-D binding is dependent on the glycosylation of the HA and requires calcium, as shown by calcium chelation resulting in decreased anti-IAV effects of SP-D [62]. SP-D also binds to the NA of IAV, inhibiting the enzyme activity [98]. This could be another mechanism by which SP-D limits IAV infection as antibody blockade of IAV NA inhibits the release of progeny virus [99]. *In vivo* murine studies also highlight the importance of SP-D in the immune response to IAV infection. When infected intranasally with glycosylated strains of IAV, SP-D$^{-/-}$ mice show reduced clearance of the virus and increased production of inflammatory cytokines, compared with wild type mice [100, 101]. These differences can be rectified by intra-tracheal co-administration of SP-D, demonstrating the importance of SP-D in IAV immunity [100].

A highly sialylated glycan present on the CRD of SP-A is a target for the IAV HA. This was elucidated as deglycosylation of SP-A prevents its neutralising effect on IAV and the interaction is not inhibited by EDTA or sugars, confirming lectin independent activity [65]. In agreement with this SP-A anti-IAV activity is not dependent on glycosylation of the IAV HA as is seen with SP-D; in a study by Hartshorn *et al.* SP-A was in fact shown to be more effective against IAV strains with less HA glycosylation [102]. This therefore renders SP-A effective against strains of IAV that are resistant to SP-D. The contribution of SP-A to IAV defence is less than that of SP-D, as exemplified by studies using knockout mice. SP-A$^{-/-}$ mice do tend to show increased viral titres and inflammatory response after infection with IAV, but this is much less than the responses observed in SP-D$^{-/-}$ mice. In addition, in double knockout mice lacking both SP-A and SP-D, the response

observed upon infection with a glycosylated strain of IAV is almost the same as that seen for SP-D$^{-/-}$ mice [101].

In addition to preventing attachment of IAV to host cells and therefore preventing viral replication, binding of SP-A and SP-D to IAV also causes viral aggregation. SP-A only forms small aggregates of IAV, but SP-D forms very large aggregates. SP-D mediated aggregation of IAV is highly dependent on the level of multimerisation of SP-D; multimers are more effective than dodecamers whilst trimers only induce minimal or no agglutination [27, 59]. SP-A and SP-D can also enhance uptake by neutrophils, which is linked to the capacity of the molecule to agglutinate IAV with SP-D being more potent than SP-A and SP-D multimers being the most effective [103, 104]. Another anti-IAV function of SP-A and SP-D is that they have been shown to enhance the IAV-induced neutrophil respiratory burst; it is however worth noting that in these experiments the collectin preparations do not appear to have been analysed for endotoxin contamination [62, 102]. SP-D has also been shown to protect neutrophils from the depressing effects of IAV on the neutrophil respiratory burst in response to other stimuli [103].

1.2.3.7 Interaction of SP-A and SP-D with Respiratory Syncytial Virus

Within the first two years of life it is estimated that 98 % of children will have been infected with respiratory syncytial virus (RSV); approximately 1 % of children who are infected require hospitalisation as the virus can cause acute bronchiolitis or pneumonia [105]. RSV can also cause significant respiratory illness in the elderly as well as in adults who are immunocompromised or have chronic airways disease [106].

RSV is an enveloped, negative stranded RNA virus. There are two major glycoproteins on the viral envelope, G and F. The G protein is responsible for attachment to the host cell whereas the F protein is involved in fusion of the host cell and viral membranes [107, 108].

Experiments using SP-A$^{-/-}$ and SP-D$^{-/-}$ mice demonstrate that SP-A and SP-D are important in the immune response to RSV. RSV clearance is reduced in both SP-A$^{-/-}$ and SP-D$^{-/-}$ mice, and this is linked to increased inflammation and inflammatory cell recruitment to the lung post infection [63, 64]. Increased susceptibility to severe RSV infection has been observed with some SP-A and SP-D genetic polymorphisms, further implicating them as important molecules in the defence against RSV [109, 110].

SP-D binds the G glycoprotein of RSV via the CRD in a calcium dependent manner, as shown by inhibition of binding in the presence of EDTA; binding is also inhibited in the presence of mannan further implicating the CRD [111]. In addition to SP-D, rfhSP-D is also able to bind to and inhibit RSV replication both *in vitro* and *in vivo* [111]. SP-A binds to the F glycoprotein, also in a calcium dependent manner [112]. The mechanism by which SP-A and SP-D inhibit RSV infection *in vivo* has not been fully elucidated. Two *in vitro* studies found that SP-A enhances RSV uptake by HEp-2 cells; this suggests that binding to the F protein does not inhibit its activity [113, 114]. This therefore indicates SP-A must have other immunomodulatory effects during RSV infection as opposed to preventing the initial fusion and therefore infection of host cells. SP-A and SP-D may also increase phagocytosis of RSV, as in SP-D$^{-/-}$ mice phagocytosis by alveolar macrophages is reduced compared with wild type mice [64, 115].

1.2.3.8 Interaction of SP-A and SP-D with Other Viruses

Interactions of SP-A and SP-D with other viruses, in addition to IAV and RSV, have also been described. SP-A opsonises herpes simplex virus (HSV) for phagocytosis by rat alveolar macrophages [116]. The binding between SP-A and HSV is similar to that seen with IAV, in that there is an interaction between the HSV and the sialylated carbohydrate in the CRD of SP-A [117]. Interactions of both SP-A and SP-D with human immunodeficiency virus (HIV) have also been described; they bind to the envelope glycoprotein gp120 in a calcium dependent manner [118, 119]. The localisation of SP-A and SP-D in the genito-urinary tract suggest they may affect transmission of the virus. SP-D recognition of the severe acute respiratory syndrome coronavirus (SARS-CoV) envelope glycoprotein (S-protein) has also been demonstrated but the functional consequence is not yet known [120].

1.2.3.9 Interaction of SP-A and SP-D with Bacteria

Both SP-A and SP-D have been shown to interact with a broad spectrum of Gram-negative and Gram-positive bacteria via the collectin CRD. The specific bacteria targeted by SP-A and SP-D include *Staphylococcus aureus*, *Klebsiella pneumonia*, *Mycobacterium tuberculosis* and *Escherichia coli* [66, 67, 121-125]. The consequence of SP-A and SP-D binding varies depending on the bacteria, but can include agglutination, direct killing by permeabilisation of the bacterial cell walls and enhancement of phagocytosis and increased respiratory burst by macrophages and neutrophils [76, 121, 126-129]. An indirect consequence of the presence of SP-A, observed with *Streptococcus pneumonia*, is enhanced phagocytosis as a result of up-regulation of cell surface expression of scavenger receptor A on alveolar macrophages [130].

1.2.3.10 Interaction of SP-A and SP-D with Yeast and Fungi

Interactions of SP-A and SP-D with yeasts and fungi have been described and have been shown to have protective roles in preventing infection in the lungs. SP-A and SP-D bind to a glycoprotein associated with the trophozoites and cysts of *Pneumocystis carinii* via the CRD; the interaction can enhance the attachment to macrophages [131, 132]. SP-A and SP-D also bind to *Aspergillus fumigatus* conidia in a calcium dependent manner, suggesting a CRD interaction with glycoconjugates [133]. A protective effect of SP-A, SP-D and rfhSP-D against *A. fumigatus* has been demonstrated *in vivo* in an immunosuppressed mouse model that was intranasally challenged with *A. fumigatus* [68]. The pathogenic unencapsulated (but not the encapsulated) form of *Cryptococcus neoformans* is bound by SP-A and SP-D. SP-D binding results in agglutination of the organism but this is not observed with SP-A [134]. The pathogenic encapsulated form evades immune recognition by SP-A and SP-D

1.3 Human Rhinovirus

Human rhinovirus (HRV) infections are the main cause of the common cold [135]; they were first isolated in the 1950's by Pelon *et al.* and Price [136, 137]. HRV is part of the *Picornaviridae* family, which contain non-enveloped single stranded RNA viruses. HRV has recently been classified within the genus of enteroviruses by the International Committee on Taxonomy of Viruses due to their high sequence homology (www.ictvonline.org/virusTaxonomy.asp) [138].

There have been over 100 serotypes of HRV identified. HRV classification was originally based upon their susceptibility to capsid binding antivirals,

and was later confirmed through phylogenetic studies [139, 140]. This subdivides the HRVs into HRV-A, HRV-B and the newly identified HRV-C [138, 141]. A fourth species, HRV-D was also proposed in 2009 by Palmenberg *et al.* after sequencing of all known HRV genomes, however this has not been adopted [141]. An alternative method of HRV classification is based upon the cellular receptor to which the HRV binds. Minor group HRVs, comprising 12 serotypes of HRV-A, infect cells by binding to the low density lipoprotein receptor (LDLR), very LDLR and LDLR-related protein [142, 143]. Major group HRVs, comprising the remaining serotypes of HRV-A and all members of HRV-B bind to the intercellular adhesion molecule-1 (ICAM-1) to gain entry to cells [144-146]. In addition, some major group HRVs may also bind to heparin sulphate [147, 148]. The receptor to which the newly identified HRV-C species binds is currently unknown; however, experiments using blocking antibodies suggest that it is neither ICAM-1 nor LDLR [149].

HRVs are an important pathogen as although in healthy individuals the infection is self-limiting, the economic burden is considerable due to missed days from work and school [150]. In patients with chronic airway diseases such as asthma and chronic obstructive pulmonary disease (COPD) a HRV infection can cause exacerbations that may lead to irreversible lung damage and hospitalisation [151-153]. HRV is detected in approximately two thirds of asthma exacerbations in children and is a major cause of exacerbations in adults [153, 154]. Currently, there are no effective treatments specifically for HRV infections.

1.3.1 Structure of HRVs

HRVs are composed of four structural viral proteins, VP1, VP2, VP3 and VP4

Figure 1-3 [155]. HRVs are icosahedral viruses and have 60 copies of each of the viral proteins and are approximately 25-30 nm in diameter. The viral capsid is composed of VP1-3 (approximately 30 kDa each). Variations in these proteins are responsible for the antigenic diversity between HRVs. VP4 (approximately 7 kDa) is not on the surface of the virus, it is found internally in contact with the positive sense viral RNA [156]. On each of the fivefold axes of the icosahedron there is a star-shaped dome, around which there is a depression, or canyon Figure 1-3 [155]. The canyon is approximately 2.5 nm deep and between 1.2 and 3 nm wide [155].

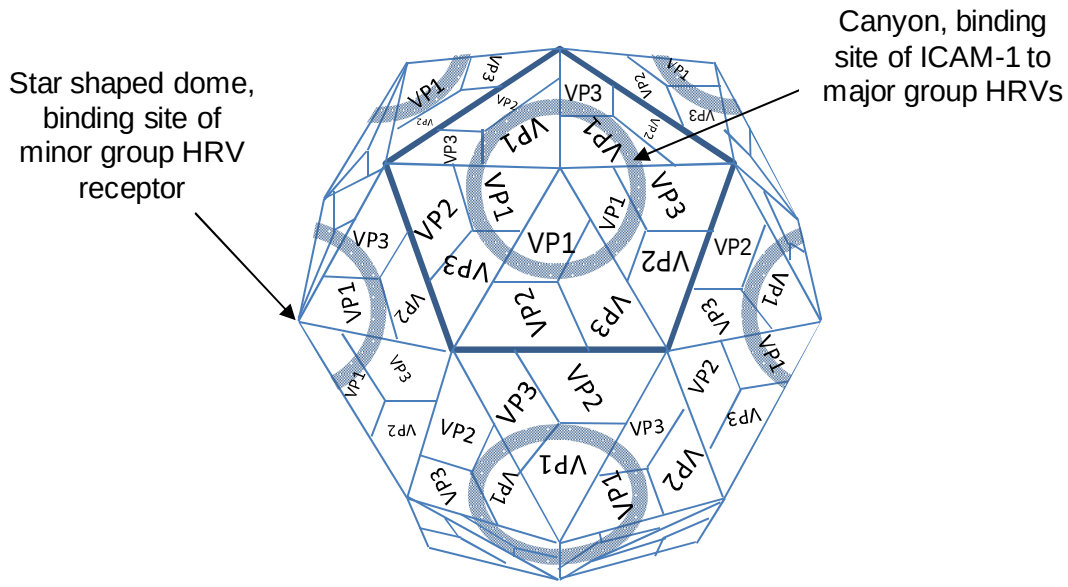

Figure 1-3 Schematic of HRV structure. The icosahedral structure of HRV and the location of the external proteins VP1, VP2 and VP3 can be seen. There are 60 copies of each of the proteins. Shading indicates the location of a canyon. The major and minor HRV receptor binding sites are indicated.

1.3.2 HRV Replication Cycle

The replication of all HRV serotypes follow the same viral life cycle (Figure 1-4). The initial step of HRV infection is binding to cellular receptors

(ICAM-1 or LDLR) on the host cell surface. Uncoating of the virus is then initiated, releasing the positive-stranded viral RNA into the host cell cytoplasm where it can be replicated.

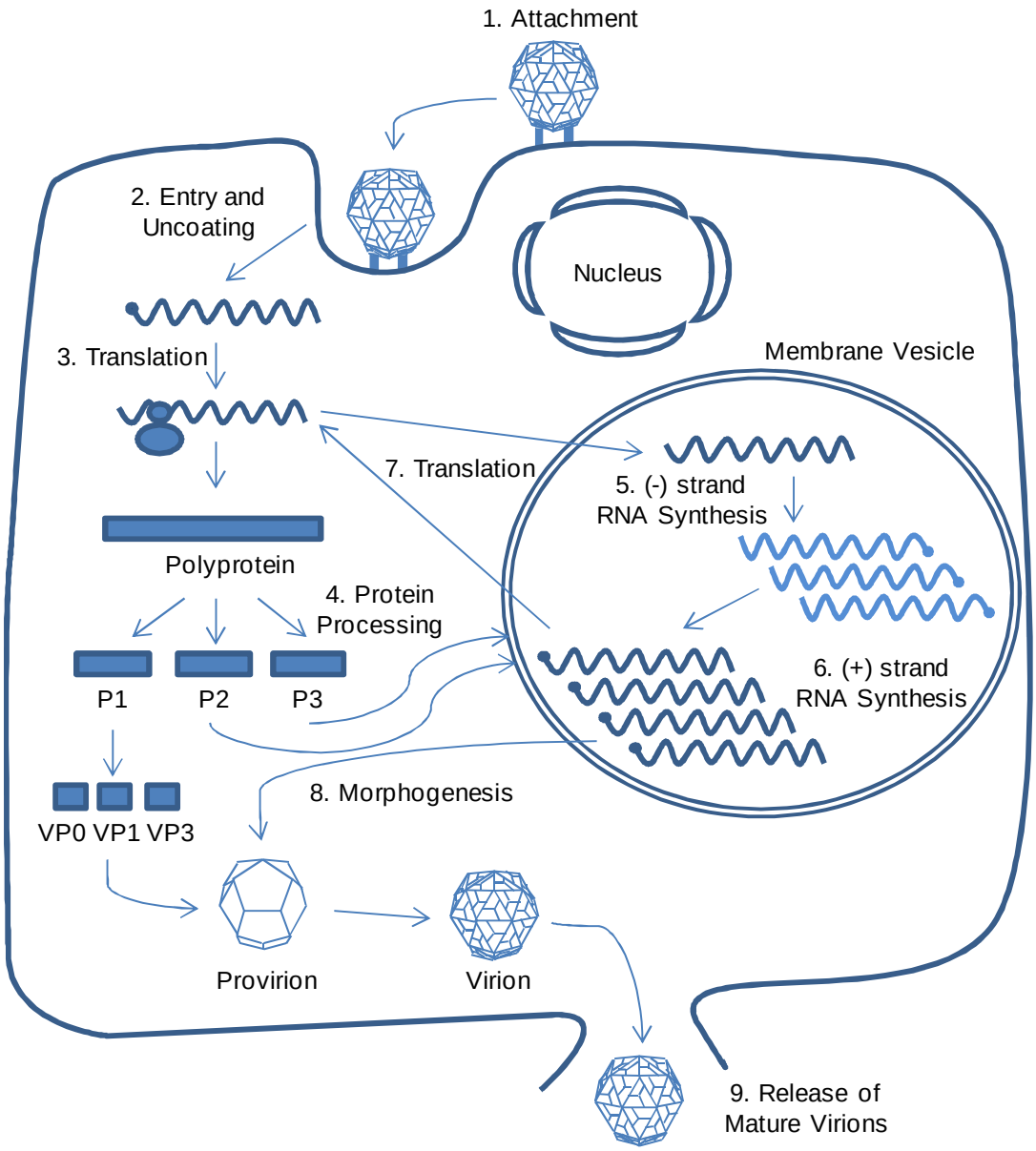

Figure 1-4 HRV replication cycle. **1.** HRV attaches to the cellular receptor. **2.** HRV is endocytosed and the RNA genome is released into the host cell cytoplasm. **3.** The RNA is translated into a polyprotein. **4.** The polyprotein is cleaved forming structural proteins and non-structural proteins, including enzymes involved in the replicative cycle. **5.** The (+) strand viral RNA is copied by the viral RNA polymerase 3D to form (-) strand RNA. **6.** The (-) strand RNA is copied to produce more (+) stand RNA. **7.** The newly synthesised (+) strand RNA is translated to produce additional viral proteins. **8.** The (+) strand RNA is packaged into provirions; VP0 within the provirions is cleaved forming VP2 and VP4 which thereby produces infectious virions. **9.** The mature virions are released by cell lysis.

1.3.2.1 Receptor Binding

The major group receptor, ICAM-1, is expressed in the nasal epithelium; the site of entry for HRVs [146, 157]. HRV infection causes increased expression of ICAM-1, via a mechanism involving up-regulation of nuclear factor κB (NF-κB) [158]. The physiological role of ICAM-1 is to facilitate leukocyte migration to sites of inflammation via binding to leukocyte function associated antigen (LFA)-1 and macrophage-1 antigen (Mac-1) on the surface of leukocytes [159, 160]. The ICAM-1 molecule consists of five extracellular domains, D1 to D5. Mutagenesis studies demonstrated that the binding site for major group HRVs is within the tip of D1, the immunoglobulin domain at the end distal to the cellular membrane [161, 162]. Further confirmation of the site of HRV binding was given by the high degree of complementarity in the physical shape and charge between D1 and major HRVs [163]. The canyon on the HRV virion is the site of ICAM-1 binding. The "canyon hypothesis" was first proposed by Rossmann *et al.* after resolving the structure of HRV14. The authors suggested that the canyon may be the receptor binding site as it would be inaccessible to neutralising antibodies and thereby the residues would not be subjected to "immune selection" [155]. Indeed the amino acid residues within the canyon of different HRVs were found to be more conserved than other surface residues [164]. It was however later discovered using X-ray crystallography and cryo-electron microscopy that antibodies are able to penetrate into the canyon [165]. This suggests the canyon does not conceal these residues of the virus from the immune system.

The receptor binding site for the minor group HRV was revealed using cry-electron microscopy and found to be on the star-shaped dome close to the fivefold axis on the surface of HRV [166, 167]. The star-shaped dome of the

capsid has a uniform positive charge, and LDLRs are negatively charged due to acidic amino acid residues. This suggests electrostatic interactions are likely to occur between minor HRVs and their receptors. There is one important difference between minor and major group HRVs that may explain their different receptor specificities. All minor group HRVs have a lysine residue at position 224 of VP1 that is a critical residue involved in interactions with acidic residues in the LDLR. This lysine is absent in all but one of the major HRVs [167]. The physiological function of the LDLR family is in the maintenance of cholesterol homeostasis [168]. As with major HRV infection that stimulates ICAM-1 up-regulation, infection with the minor group HRV, HRV2, causes up-regulation of LDLR [169].

1.3.2.2 HRV Uncoating and Entry of Viral RNA into the Host Cell Cytoplasm

In receptor sensitive serotypes of major HRVs (e.g. HRV14), binding to ICAM-1 causes the loss of VP4 and release of the viral RNA, thereby initiating uncoating [170]. HRV14 is then believed to be internalised via clatherin-mediated endocytosis [171]. At neutral pH some HRVs are stable upon binding to ICAM-1; HRV16 is an example of such a serotype. HRV16 is thought to enter host cells by receptor mediated endocytosis and uncoating is likely to be induced by low pH (pH 5.5-6.0) within the endosome [172]. Zhao *et al.* believe that low pH may trigger protonation of the nitrogen atoms of histidine residues surrounding the fivefold axis, leading to a conformational change and expulsion of a Zn^{+} ion that they believe stabilises the virus, thus triggering uncoating [173].

Binding of minor HRVs, exemplified by HRV2, to the cellular receptor does not initiate uncoating [174]. The function of LDLR is to mediate internalisation of the virion into acidic endosomes ($pH \leq 5.6$).

How the viral RNA enters the cytoplasm from the endosome is not well understood but is clearly different for the major and minor sub-groups of HRV. The viral RNA of the major group HRV, HRV14, is thought to pass into the cytoplasm by rupturing the endosomal membrane [175]. In contrast, the viral RNA of the minor group HRV, HRV2, is transferred into the host cytoplasm via a pore in the endosomal membrane [176, 177].

1.3.2.3 HRV Replication

Once the viral RNA, consisting of approximately 7200 nucleotides, is in the cytoplasm the HRV can be replicated [178]. The 5' end of the viral RNA contains the internal ribosome entry site (IRES) which can bind ribosomes [179, 180]. The viral RNA is translated into a single polyprotein that contains P1, P2 and P3. P1 is further processed into the structural proteins VP3, VP1 and the proprotein VP0, while P2 and P3 code for non-structural proteins [181, 182]. There are a total of seven non-structural proteins that are involved in protein maturation and RNA replication; they include two proteases (2A and 3C), an RNA dependent polymerase (3D) and an ATPase (2C) [183]. The first step in replication of the viral RNA is the production of a negative-strand RNA. The negative stand RNA is used as a template to produce new positive-strand RNA, which is then translated or incorporated as genomic RNA into progeny viral particles. The RNA synthesis steps are catalysed by the 3D polymerase [184, 185].

1.3.2.4 HRV Virion Assembly

The viral proteins assemble to form virions. The first step is the formation of protomers made up of VP1, VP3 and VP0. Five protomers assemble to form pentamers [186, 187]. The formation of the provirion then pursues in which the viral RNA is packaged and VP0 remains uncleaved. The cleavage of VP0 into VP2 and VP4 results in formation of infectious viral particles [188]. The mature HRV virions are released from the cell by lysis.

1.3.3 Host Immune Response to HRV Infection

The host response to HRV infections is complex and still a matter of investigation. Not all persons who are infected with HRV will develop the symptoms associated with a common cold, such as sneezing, sore throat, cough, nasal obstruction and nasal discharge [189]. This suggests that although the host response is fundamental for resolving the infection, it may also be responsible for the symptoms experienced.

1.3.3.1 Cellular Immune Response to HRV

The airway epithelial cells are the site of HRV infection but they are also very important in the immune response to the virus. Infection causes the release of numerous cytokines by epithelial cells, including IL-1β, IL-2, IL-4, IL-6, IL-8, IL-13, IL-16, TNF-α and RANTES. Infection of airway epithelial cells increases HRV receptor expression, which can increase viral uptake into the cells but also aids the recruitment of inflammatory cells to assist in the antiviral response.

Airway macrophages express both ICAM-1 and LDLR, however, there has been little or no replication of HRV detected within these cells [190, 191].

Activation of macrophages by HRV leads to release of TNF-α, interferon (IFN)-γ, IL-8 and IL-10 [190, 192-194]. IL-8 is chemotactic for neutrophils and promotes neutrophil degranulation and respiratory burst [195]. ICAM-1 expression is up-regulated by TNF-α; this can both increase the viral attachment and therefore replication of HRV as well as enhancing inflammatory cell recruitment [196]. Macrophages may therefore play an important role in HRV induced airway inflammation.

Increases in neutrophil and eosinophil numbers are observed in nasal lavage upon infection with HRV. The cell numbers peak two days after infection. The increase in neutrophils correlates with an increase in IL-8 detected in nasal secretions [193, 197]. An antiviral role for neutrophils during HRV infection still remains unclear. However, an *in vitro* study found that HRV enters but does not replicate within neutrophils and can elicit the release of cytokines such as IL-8, MIP-1α and MIP-1β from neutrophils [198]. Release of RANTES, a chemokine for eosinophils, has been detected *in vivo* in mice infected with HRV and from the nasal lavage of infected children who have wheeze [199, 200]. This suggests RANTES may have an important role in recruitment and activation of eosinophils. An increased number of eosinophils in nasal lavage prior to experimental HRV infection was found to result in less severe cold symptoms [201]. This inverse correlation may be a consequence of eosinophil granular products which are RNAses and appear to increase viral clearance [202].

T-cell and natural killer (NK) cell infiltration to the airway epithelium is observed in volunteers experimentally infected with HRV [203]. These cells may aid the clearance of HRV by release of cytokines such as IFN-γ [204]. NK cells can also directly destroy virus infected cells.

1.3.3.2 Humoral Immune Response

HRV specific IgG and IgA antibodies are produced following infection with HRV [205]. After experimental infection with HRV, antibodies are detected within one to two weeks, peaking five weeks post infection. IgG levels are sustained for at least one year after HRV infection but IgA levels slowly decline [206]. HRV specific antibody not being detected in the serum or secretions of infected individuals until after HRV infection has been resolved suggests that it is not responsible for the resolution of infection. The presence of existing antibodies are however protective against re-infection with the same HRV serotype, or lessened clinical symptoms [206, 207].

1.3.4 HRV and Chronic Airway Disease

It is well established that HRV is a major cause of exacerbations of chronic lung diseases such as asthma and COPD. Virus is detected in approximately 50 % of COPD exacerbations, and of these approximately 50 % are caused by HRV [151]. In school aged children Johnston *et al.* found that 80-85 % of asthma exacerbations were caused by viruses, and 66 % of these were due to HRV [153]. HRV also causes the majority of virally induced asthma exacerbations in adults [154].

It is not entirely clear how HRV infections result in exacerbation of airway diseases. Several mechanisms have been proposed including, airway injury by the virus, increased production of proinflammatory mediators and a deficient response in the asthmatic lung resulting in a prolonged and more severe infection [208, 209]. In addition to infecting the upper airways HRV can also infect and replicate in the respiratory epithelium of the lower airways, which is important in the pathogenesis of HRV induced asthma exacerbations [209, 210]. HRV infection induces mRNA expression and

protein production of IL-6, IL-8, IL-16 and RANTES in the lower airways [209]. IL-6 and IL-8 are both proinflammatory cytokines which may contribute to exacerbations caused by HRV. IL-8 causes an influx of neutrophils into the lung; neutrophil activation results in neutrophil elastase production which would contribute to airway obstruction and up-regulation of goblet cell mucus production [211]. Experimental evidence suggests that IL-16 is a key cytokine in the recruitment of lymphocytes that contribute to the pathogenesis of asthma [212, 213]. It is therefore possible that IL-16 is responsible for the large bronchial influx of lymphocytes observed during experimental HRV infection and thus a cause of HRV induced airway inflammation [203].

Several studies have found that there is a defective cellular type 1 response to HRV infection in asthmatics compared with that of healthy controls [208, 214, 215]. Human bronchial epithelial cells (HBECs) from asthmatics have been shown *in vitro* to support HRV replication much more efficiently than those from healthy controls [208]. HBECs from asthmatics had impaired production of the antiviral cytokine IFN-β, which was linked to defective apoptosis of HRV infected cells, thus resulting in late cell lysis and release of vast numbers of infectious HRV particles. This may explain why HRV infections in asthmatics are of longer duration and lead to much more severe lower respiratory tract symptoms and airway obstruction than observed in non-asthmatics [152]. A recent phase II clinical trial of inhaled IFN-β given to moderate and severe asthmatics, at the onset of a natural cold, has had positive results; indicating the IFN-β treatment prevented worsening of asthma symptoms (Synairgen Research Ltd., Southampton, UK, press release, 10th August 2012).

1.4 Thesis Aims

Previous studies demonstrating SP-A and SP-D binding to RSV and IAV and antiviral effects against these respiratory viruses, as well as the localisation of the proteins in the nasal epithelium, allude to these collectins being optimal candidates for an involvement in HRV infection. Therefore, the question sought to be investigated in this thesis was: **Can SP-A, SP-D and rfhSP-D bind to and inhibit infectivity of HRV?** The aim of this project was to investigate whether SP-A, SP-D and rfhSP-D bind to HRV and to investigate if this inhibits infection. No previous studies had looked at HRV infection with relation to the presence of SP-A, SP-D or rfhSP-D.

If SP-A, SP-D and rfhSP-D bind to and inhibit the infectivity of HRV this could lead to the development of these proteins as therapeutics to neutralise HRV, a major cause of exacerbations of chronic lung diseases such as asthma and COPD [153]. Currently, there are no specific treatments to HRV infections and therefore a therapy would be of immense value both socially, by increasing quality of life for patients, and economically, due to reduced absences from work and school, and hospitalisation of patients.

2. Chapter 2: General Materials and Methods

2.1.1 Sodium Dodecyl Sulfate Polyacrylamide Gel Electrophoresis (SDS-PAGE)

Reduced samples (19 µl sample, 8 µl NuPAGE LDS sample buffer, 3 µl reducing agent (both Invitrogen, Paisley, UK)) were heated for five minutes at 95 °C and run alongside 10 µl of Seablue® Plus 2 standard (Invitrogen) to allow molecular weight comparison of the sample protein bands. Gels were run at 200 V, 120 mA on either 4-12 % or 12 % NuPage® Bis-Tris gels in 1 x MES SDS running buffer (both Invitrogen) until the dye front ran to the end of the gel. Gels were stained using SimplyBlue™ SafeStain (Invitrogen) or Silver Stain Kit (Bio-Rad, Hemel Hempstead, UK) as per manufacturer's instructions.

2.1.2 Western Blotting

Samples were run as described for SDS-PAGE and proteins were transferred to polyvinylidene fluoride (PVDF) mini membranes using an iBlotter (Invitrogen). Membranes were washed in phosphate buffered saline (PBS) with 0.05 % (v/v) Tween® 20 (Sigma-Aldrich, Gillingham, UK) (PBS-Tween). Membranes were blocked in PBS-Tween containing 2 % (w/v) skimmed milk (Marvel), or as indicated, for one hour at 37 °C to eradicate non-specific binding.

For western blots to detect nhSP-D and rfhSP-D, the primary antibody, a polyclonal rabbit-anti-rfhSP-D was diluted to 1.61 µg/ml in blocking solution and incubated at 37 °C for one hour. After washing, the western blot was developed using an anti-rabbit secondary solution and detection kit, as per

the manufacturer's instructions (Invitrogen), or a goat-anti-rabbit-HRP conjugated antibody diluted to 1 μg/ml in blocking solution (Invitrogen). The goat-anti-rabbit-HRP conjugated antibody was incubated on the membrane for one hour at 37 °C, the membrane was washed and reactivity detected with Enhanced Chemiluminescence (ECL)™ Advance (GE Healthcare Life Sciences, Little Chalfont). The secondary antibody used in each experiment is indicated in figure.

Western blots were imaged by enclosing the membrane in clingfilm being careful to ensure no air bubbles are present and overlaying photographic film (Fuji Film, Bedford, UK) and exposing to the membrane from less than one minute to a maximum of ten minutes. Film was developed in Fotospeed FX20 Print Developer (First Call Photographic, Taunton, Somerset) for one minute, rinsed in water, and fixed in Fotospeed PD5 Rapid Fixer (First Call Photographic) for one minute and finally rinsed before air drying. When necessary an initial exposure was used to determine the subsequent exposure time.

2.1.3 Cell Culture

HeLa cells were routinely cultured in Dulbecco's Modified Eagle Medium GlutaMAX™ (Invitrogen) (DMEM), supplemented with 10 % (v/v) foetal bovine serum (FBS) (Sigma-Aldrich), 50 U/ml penicillin and 50 U/ml streptomycin (both Invitrogen).

16HBE cells (human bronchial epithelial cell line) were cultured in Minimum Essential Medium GlutaMAX™ (Invitrogen) (MEM), supplemented with 10 % (v/v) FBS (Sigma-Aldrich), 50 U/ml penicillin and 50 U/ml streptomycin (both Invitrogen).

Both HeLa cells and 16HBE cells were incubated in a humidified atmosphere at 37 °C, 5 % CO_2. Routine passage of cells was conducted by removing cells from the flask surface using 0.25 % trypsin-EDTA (Invitrogen).

2.1.4 Viable Cell Counting

Cells were diluted with 0.4 % (w/v) Trypan Blue in 0.81% NaCl and 0.06% K_2HPO_4 (Sigma-Aldrich). An Improved Neubauer haemocytometer (depth 0.1 mm; 1/400 mm^2) was used to count the number of viable cells in both the top and bottom chambers. The viable cell count was calculated using the following equation:

$$\text{Viable cells/ml} = (\text{viable cell number}) \times (\text{dilution factor}) \times 10^3$$

Cells were diluted in the appropriate maintenance media for the cell type, as detailed in section 2.1.3, to the required concentration and plated as required.

2.1.5 Frozen Storage and Regeneration of Cell Stock

Post-trypsinisation, cells were pelleted at 160 x g for 7 minutes at 4 °C. Cells were resuspended to 3 x 10^6 cells/ml with maintenance media containing 10 % (v/v) dimethylsulphoxide (DMSO) and frozen in 1 ml aliquots in cryovials (Nunc, Denmark) at a rate of -1 °C per minute in a -80 °C freezer using a cryogenic freezing container.

To regenerate cell stocks, frozen cells were quickly defrosted and 19 ml of pre-warmed maintenance medium was added, cells were transferred into a 75 cm^2 flask. After four hours, once cells had adhered, the medium was

exchanged for fresh maintenance medium to eliminate DMSO and routinely cultured.

2.1.6 Mycoplasma Testing

Cells were periodically tested for mycoplasma contamination using Venor GeM-qEP Mycoplasma detection kit for real time PCR (Minerva Biolabs) as per manufacturers' instructions.

2.1.7 Endotoxin Levels in Purified Proteins and HRV Preparations

Endotoxin levels were tested using the LAL QCL-1000® (Lonza, Basel Switzerland) assay as per the manufacturer's instructions. In brief, preparations were serially diluted and analysed to obtain readings that were within the linear portion of the standard curve (0.1 – 1.0 EU/ml). The standard curve was diluted in the sample diluent to ensure inhibition of the endotoxin detection reaction was not occurring. A spiked sample containing endotoxin of a known concentration was also included. Levels of endotoxin were 27 EU/mg rfhSP-D protein (22 EU/ml) and 1.6 EU/mg nhSP-A (2.4 EU/ml). The sucrose density gradient purified HRV16 stock had 0.6 EU/ml and HRV1B stock had 2.0 EU/ml.

2.1.8 Flow cytometry

Cells were trypsinised and trypsin was neutralised with colourless RPMI containing 10 % FCS. Cells were pelleted by centrifuging at 160 x g for 5 minutes at 4 °C, supernatants were removed and pellets resuspended in 150 µl BD Cytofix/Cytoperm™ (BD biosciences, Franklin Lakes, NJ, USA) and left for 20 minutes on ice. Cells were washed in 1.5 ml BD Perm/Wash™ (BD

biosciences) and re-centrifuged. To detect HRV, the primary antibody R16-7 (kindly provided by Dr Wai-Ming Lee, University of Wisconsin, USA) was applied at 70 ng/ml in 100 µl permwash, and was left 30 minutes on ice before washing as before. Secondary antibody goat-anti-mouse-allophycocyanin (APC) (Invitrogen) was applied in 100 µl at 1 µg/ml and left on ice in the dark for 30 minutes. The antibody was washed off as previously and pellets were resuspended in FACS buffer (1 mM EDTA, 0.5 % bovine serum albumin (BSA)). Cells were analysed using a FACS Aria (BD biosciences) and FlowJo version 7.6.5 (Tree Star, Ashland, USA).

2.1.9 Ultraviolet Inactivation of HRV

HRV1B and HRV16 were ultraviolet (UV) inactivated using a UV crosslinker (UVP #CL-1000, Ultra-violet products Ltd., Cambridge, UK). HRV in virus buffer (10 mM Tris, 50 mM $MgCl_2$) was placed in a 24 well plate, 500 µl/well, on ice into the crosslinker with the lid removed. HRV was inactivated using 120,000 $\mu J/cm^2$ UV light for 50 minutes. UV inactivated HRV was aliquoted and stored at -80 °C.

2.1.10 Statistics

Experiments were analysed for statistical significance. The experiments analysed are indicted in figure legends. The data was found to be normally distributed and therefore were compared using one-way analysis of variance (ANOVA), the test was performed using GraphPad Prism version 5 (GraphPad Software, La Jolla, CA, USA); differences were considered significant if $p<0.05$.

3. Chapter 3: Validation of Viral Techniques

3.1 Introduction

As HRV had not previously been used in the laboratory several techniques such as amplification, purification, detection and quantification of HRV had to be established.

Amplification was optimised in this laboratory to ensure a maximal yield was obtained. Following amplification in HeLa cells the HRV infected cell lysate was purified. The purification of HRV was undertaken to ensure the utmost scientific rigor was maintained. Some laboratories undertaking HRV research do not purify, or only partially purify, the HRV preparations that they use [158, 200, 216-220]. Purification removes components of an infected cell lysate which could influence the observed response to infection of cells *in vitro* and animals *in vivo*. Apoptotic cells and cytokines, for example, would be present in an infected cell lysate and could alter the cytokine response observed upon infection with HRV. Apoptotic cells can be partially accounted for by using an uninfected cell lysate control, however, in an infected cell lysate the number of apoptotic cells is likely to be much higher. Cytokines in an infected as opposed to uninfected cell lysate will differ due to the antiviral response of the cells. Of the laboratories that do purify HRV there is no single accepted method to purify HRV. Purification methods can involve concentration of HRV by precipitation using Polyethylene Glycol (PEG) or pelleting HRV by ultracentrifugation, followed by purification by ultracentrifugation on linear or stepwise sucrose or caesium chloride gradients [194, 221-225]. As purification of HRV had not previously been conducted in this laboratory development of a method was required.

Immuno-detection of HRV was by the means of a mouse monoclonal antibody (mAb), R16-7, directed against VP2 of the HRV viral capsid. This antibody was kindly provided by Dr Wai-Ming Lee, University of Wisconsin, USA. The antibody had not previously been used in this laboratory and therefore the conditions of immuno-detection had to be optimised.

3.2 Materials and Methods

3.2.1 Optimisation of R16-7 for Western Blotting

Western blots to detect HRV were made as described in section 2.1.2. After blocking in the indicated blocking solution for one hour at 37 °C the primary antibody R16-7 was diluted as indicated in blocking solution and incubated on the membrane overnight at 4 °C. The membrane was washed for 25 minutes with five changes of PBS-Tween. The secondary antibody, a goat-anti-mouse IgG horseradish peroxidise (HRP) conjugated antibody (GαM-HRP) (Invitrogen) was diluted as indicated in blocking solution and incubated on the membrane for one hour at 37 °C. The membrane was washed as before and Enhanced Chemiluminescence (ECL)™ Advance (GE Healthcare) was applied and immediately imaged as detailed in section 2.1.2.

3.2.2 50 % tissue culture infectious dose ($TCID_{50}$)

HeLa cells were seeded onto 96 well plates (Nunc, Nunclon™ Surface) at a density of 2.6 x 10^4 cells/well in maintenance medium and left three hours at 37 °C, 5 % CO_2 to adhere. Medium was removed and replaced with serum starved medium (DMEM (Invitrogen) supplemented with 2 % (v/v) FBS, 50 IU/ml penicillin, 50 mg/ml streptomycin); a 10 fold serial dilution of virus was performed in a 180 µl final volume in sextuples for each serial dilution.

Control wells with serum starved medium without virus were included on each plate. The plate was left for one hour on a mini see-saw rocker at 30 osc/minute and room temperature. Plates were incubated for five days at 33 °C, 5 % CO_2, after which 50 ul/well crystal violet solution (0.13 % (w/v) crystal violet, 5 % (v/v) formaldehyde, 5 % (v/v) ethanol in 1 x PBS) was added to the wells. Plates were incubated for 30 minutes at room temperature in the dark. Wells were washed with tap water and air dried. Wells were counted as a cytopathic effect (CPE) if less than 50 % of the surface of the well was covered in crystal violet stained cells; these numbers were used in the Spearman-Karber formula to calculate the tissue culture infectious dose, at which virus particles will infect 50 % of cells ($TCID_{50}$):

$$TCID_{50} = [10 \text{ ^ } {}^{-(I-(d(s-0.5)))}]/0.18 \text{ ml}$$

where I= Log_{10} of lowest dilution (eg x1 = 0)

d = Log_{10} of difference of stepwise dilutions (eg x 10=1)

s = number of rows of wells with CPE

0.18 ml is the final volume of media in each well

3.2.3 Immunocytochemistry

HeLa cells were seeded in a 96 well plate at a density of 2.6 x 10^4 cells/well in maintenance medium and left three hours at 37 °C, 5 % CO_2 to adhere. Cells were washed twice in serum free medium and inoculated with HRV diluted in serum starved medium. Plates were rocked at 30 osc/minute for one hour at room temperature before transferring to 33 °C, 5 % CO_2 for 17 hours. Cells were washed twice with PBS and fixed in 1 % (w/v) paraformaldehyde in PBS for one hour at room temperature; the cells were then washed twice in PBS and kept in PBS at 4 °C until staining. The primary antibody, R16-7, was

applied at the indicated concentration diluted in PBS containing 0.03 % (v/v) Triton®X-100 (Sigma-Aldrich) to allow intracellular staining, left at room temperature for one hour, rocking at 30 osc/minute, then washed three times in PBS with 0.03 % (v/v) Triton®X-100. Controls omitting primary antibody, or secondary antibody, or both were also included. Secondary antibody, goat-anti-mouse IgG-AlexaFluor594 (GαM-AF594), was diluted to the indicated concentration in PBS with 0.03 % (v/v) Triton®X-100, left at room temperature for one hour in the dark, rocking at 30 osc/minute. After washing as before nuclei were stained using 4',6-diamidino-2-phenylindole (DAPI), diluted in PBS to 1 µg/ml for five minutes at room temperature and washed in PBS with 0.03 % (v/v) Triton®X-100. Plates were stored at 4 °C in PBS until visualisation.

Immunofluorescence was visualised using an Olympus IX microscope (Olympus, Southend-on-Sea, UK) and images produced using CellP software (Olympus).

3.2.4 Fluorescent Focus Assay

HRV infection and fluorescent staining was carried out as described for immunocytochemistry. The primary R16-7 antibody was diluted to 0.05 µg/ml, and the secondary GαM-AF594 antibody was diluted to 0.5 µg/ml.

Infected cells, or fluorescent foci, were counted directly using an Olympus IX microscope. To calculate viral titre from the number of fluorescent foci the following formula was used:

$$\frac{\text{Area of well}}{\text{Area of image}} \times \text{Number of infected cells} = \text{Number of infected cells/well}$$

$$\frac{\text{Number of infected cells / well}}{\text{Volume of HRV added to well}} = \text{fluorescence forming units (ffu)/ml}$$

3.2.5 Amplification of HRV1B and HRV16 Stocks

The amplification protocol was adapted from that used by Synairgen Research Ltd. (Southampton, UK) In brief, HeLa cells were cultured to ~85 % confluence and infected with HRV1B or HRV16 stock (both obtained from ATCC) in infection media (details in Appendix 1) at a ratio of 2:1 (v/v). Cells were left for one hour at room temperature on a mini see-saw rocker at 35 osc/minute. Infection media was added to a final ratio of 1:4 (HRV to infection media), the cells were incubated at 33 °C, 5 % CO_2, until 80 % cell death was observed using an inverted light microscope (usually approximately 18 hours). HeLa cells were freeze-thawed twice at -80 °C and the media was centrifuged at 160 x g for seven minutes to remove large cellular debris. The supernatant was filtered using a 0.2 μm PVDF syringe filter and used to infect subsequent rounds of HeLa cells. Stocks were stored at -80 °C.

3.2.6 Purification of HRV

The HRV from HeLa cell lysate infected with HRV1B or HRV16 was concentrated by either Polyethylene Glycol (PEG) precipitation or ultracentrifugation.

To PEG precipitate the HRV, the cell lysate was concentrated using 100 K MWCO Amicon Ultra Centrifugal Filtration Units (Merck Millipore, Billerica, USA) at 4000 x g for 20 minutes. The retained HRV was precipitated by adding 7 % (w/v) PEG 6000 (BDH Chemicals Ltd., Poole) and 0.5 M NaCl (where indicated); this was left on ice with occasional mixing for

two hours and then spun at 4000 x g at 4 °C for one hour. The pellet containing precipitated HRV and HeLa cell debris was resuspended in virus buffer (10 mM Tris, 50 mM $MgCl_2$), 1/20th the original volume. Large insoluble matter was removed by centrifugation at 3000 x g at 4 °C for 15 minutes and then the supernatant was filtered using a 0.2 μm PVDF syringe filter. The supernatant was further concentrated using 100 K MWCO Amicon Ultra Centrifugal Filtration Units, to wash residual PEG from the preparation the filters were topped up with virus buffer and re-spun, this wash step was repeated a total of four times. The HRV was stored at -80 °C until proceeding to sucrose density gradient ultracentrifugation.

To pellet HRV by ultracentrifugation the infected HeLa cell lysate was spun at 141,000 x g for 1 hour at 4 °C in a SW28 swing rotor (Beckman Coulter, High Wycombe, UK). The supernatant was discarded and the HRV containing pellet was resuspended in 1/50th the original volume in virus buffer and left to soak overnight at 4 °C. The resuspended pellets were clarified by centrifugation at 4000 x g for five minutes before proceeding immediately to sucrose density gradient ultracentrifugation.

Sucrose was dissolved in virus buffer. Two methods were employed, either a stepwise gradient or a linear gradient. A stepwise gradient was produced by layering 5 ml of 30 % sucrose onto 5 ml of 35 % sucrose, and 5 ml of 25 % on top of this and so on until 10 % was reached. Each layer was frozen before addition of the next sucrose layer. A continuous linear sucrose density gradient, 15 – 45 % was produced by layering 15 % sucrose on top of 45 % sucrose, laying the tube flat for two hours at 4 °C and carefully righting the tube immediately prior to use. Octylphenoxy polyethoxyethanol (IGEPAL® CA-630) (Sigma-Aldrich) detergent was added to 1 % (v/v) to the concentrated HRV and left at 4 °C for 30 minutes to disrupt binding between

virus and HeLa cell proteins; this was layered on top of the sucrose gradient. The sucrose gradients were centrifuged at 80,000 x g in a SW28 swing rotor for four hours at 4 °C. The gradient was fractioned into 500 µl or 1 ml aliquots and stored at -80 °C.

Sucrose density gradient purified HRV was either dialysed using Slide-A-Lyser dialysis cassette (3.5 K MWCO) (Thermo Scientific, Pierce, Rockford, USA) into buffer, or spun in 100 K MWCO Amicon Ultra Centrifugal Filtration Units and washed three times with virus buffer before final resuspension in virus buffer. Purified HRV in virus buffer was stored in aliquots at -80 °C.

3.2.7 Transmission Electron Microscopy

Sucrose density gradient purified HRV was buffer exchanged into ultrapure water and concentrated using 100 K MWCO Amicon Ultra Centrifugal Filtration Units (Merck Millipore). The HRVs were fixed in glutaraldehyde at a final concentration of 2.5 %. A 5 µl volume of HRV was allowed to dry onto a 50 µm formvar and carbon coated copper grid for ten minutes. Uranyl acetate (2 % w/v) was applied to the grid for ten seconds before blotting off. The grids were viewed using a Hitachi H-7000 microscope (Hitachi, Maidenhead, UK).

3.3 Results

3.3.1 Optimisation of R16-7 for Western Blotting

The R16-7 primary antibody, directed against the HRV viral capsid protein VP2, had not previously been used in this laboratory. Western blotting using the antibody therefore had to be optimised.

The R16-7 antibody recognised both reduced and non-reduced HRV samples of the minor group HRV, HRV1B, and the major group HRV, HRV16, at a concentration of 0.23 μg/ml, Figure 3-1. The reduced samples gave distinct bands at 37 kDa corresponding to the size of VP0 (a precursor to the proteins VP2 and VP4) and 30 kDa corresponding to the size of VP2 .

In the non-reduced samples a band at 90 kDa is visible, this corresponds to the size of P1 (precursor to VP0, VP1 and VP3), Figure 3-1.

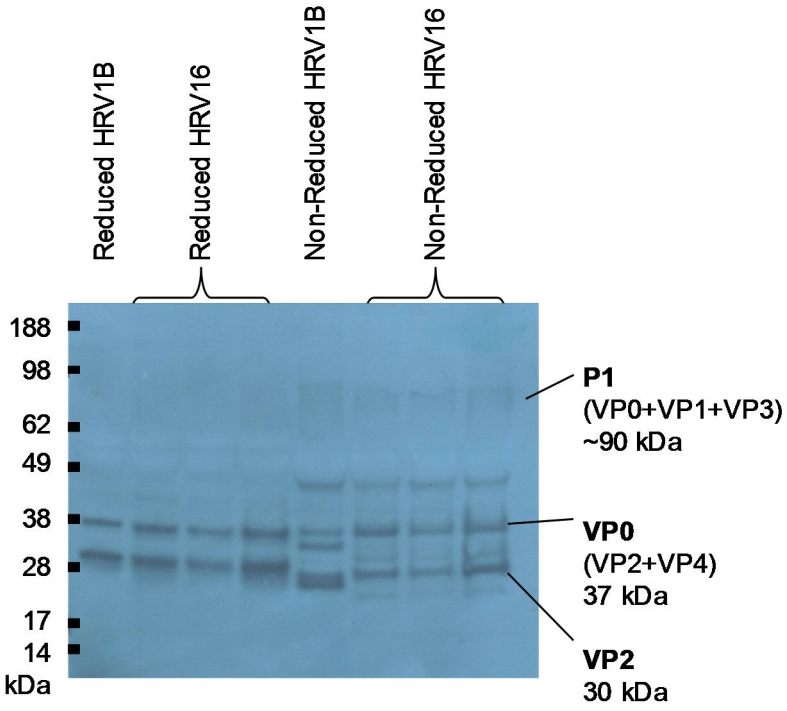

Figure 3-1 Initial optimisation of western blot using R16-7 antibody to detect HRV. Reduced and non-reduced HRV1B and HRV16 samples were run on a 4-12% NuPAGE gel (Invitrogen). Membrane was blocked in 1 % (w/v) BSA in PBS-Tween and probed using R16-7 primary antibody (0.23 μg/ml) and GαM-HRP conjugated secondary antibody (1 μg/ml). HRP was detected using ECL.

Due to limited stock of the R16-7 antibody a lower concentration, 0.14 μg/ml, was evaluated showing that both HRV1B and HRV16 were still detected, Figure 3-2. A negative control, HeLa cell lysate from cells that had not been infected with HRV1B or HRV16 but had otherwise been subjected to the same conditions was also included; no bands are visible in this sample, however negative staining can be seen at 49 kDa.

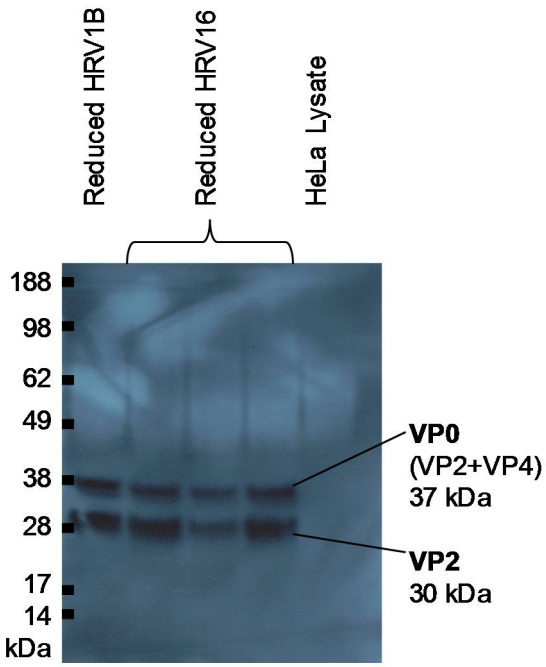

Figure 3-2 Optimisation of western blot using R16-7 antibody to detect HRV. Reduced HRV1B, HRV16 and HeLa cell lysate samples were run on a 4-12% NuPAGE gel. The membrane was blocked in 1 % BSA (w/v) in PBS-Tween and probed using the R16-7 primary antibody (0.14 μg/ml) and GαM-HRP conjugated secondary antibody (1 μg/ml). HRP was detected using ECL.

A new ECL kit was purchased and resulted in very high background, the appropriate blocking solution and antibody concentrations therefore had to be re-established, Figure 3-3.

Blocking the membrane with 1 % (w/v) BSA in PBS-Tween resulted in very high background that blocked any signal given by the antibodies bound to proteins on the membrane; a five second exposure resulted in the signal being concealed (Figure 3-3 A and C). Blocking with 2 % (w/v) skimmed milk in PBS-Tween stopped the background staining observed with 1 % BSA blocking solution; the HRV proteins were detected with the secondary antibody at both 1 μg/ml and 0.5 μg/ml (Figure 3-3 B and D respectively), the signal was however stronger with 1 μg/ml and this was therefore decided to be the concentration to be used in future western blots.

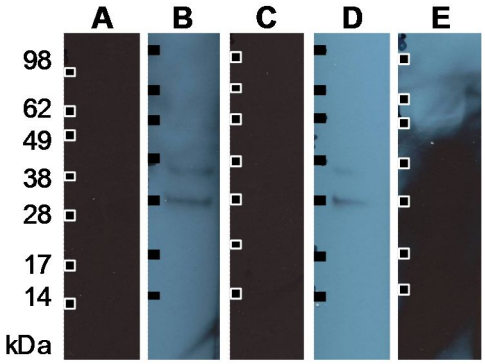

	Blocking Solution	R16-7 Concentration / μg/ml	GαM-HRP Concentration / μg/ml
A	1 % BSA	0.14	1.0
B	2 % Skimmed Milk	0.14	1.0
C	1 % BSA	0.14	0.5
D	2 % Skimmed Milk	0.14	0.5
E	1 % BSA	None	1.0

Figure 3-3 Optimisation of blocking solution and concentration of secondary antibodies to detect HRV. HRV16 infected HeLa cell lysate was run on SDS-PAGE and transferred to PVDF membrane. The membrane was incubated with blocking solution and R16-7 primary antibody and GαM-HRP conjugated secondary antibody as indicated in the table.

3.3.2 Refinement of $TCID_{50}$

The $TCID_{50}$ assay is a measure of viral titre; this was a new method in the laboratory and thus required optimisation. $TCID_{50}$ results from the same virus stocks conducted on HeLa cells at passage >60 and passage >100 were compared. HRV1B and HRV16 were tested. The higher passage HeLa cells were more submissive to the virus, and showed higher $TCID_{50}$ value (HRV1B: 2.6×10^5 $TCID_{50}$/ml, HRV16: 3.8×10^4 $TCID_{50}$/ml) than the same stock applied to the lower passage HeLa cells, (HRV1B: 1.8×10^4 $TCID_{50}$/ml, HRV16: 18 $TCID_{50}$/ml) Figure 3-4. The low passage HeLa cells did not show any CPE with the HRV16, Figure 3-4 D. Due to the higher passage HeLa cells being more susceptible to the HRV16 infection and due to HRV16 being used in experiments in this project, the higher passage HeLa cells were used in subsequent $TCID_{50}$ assays.

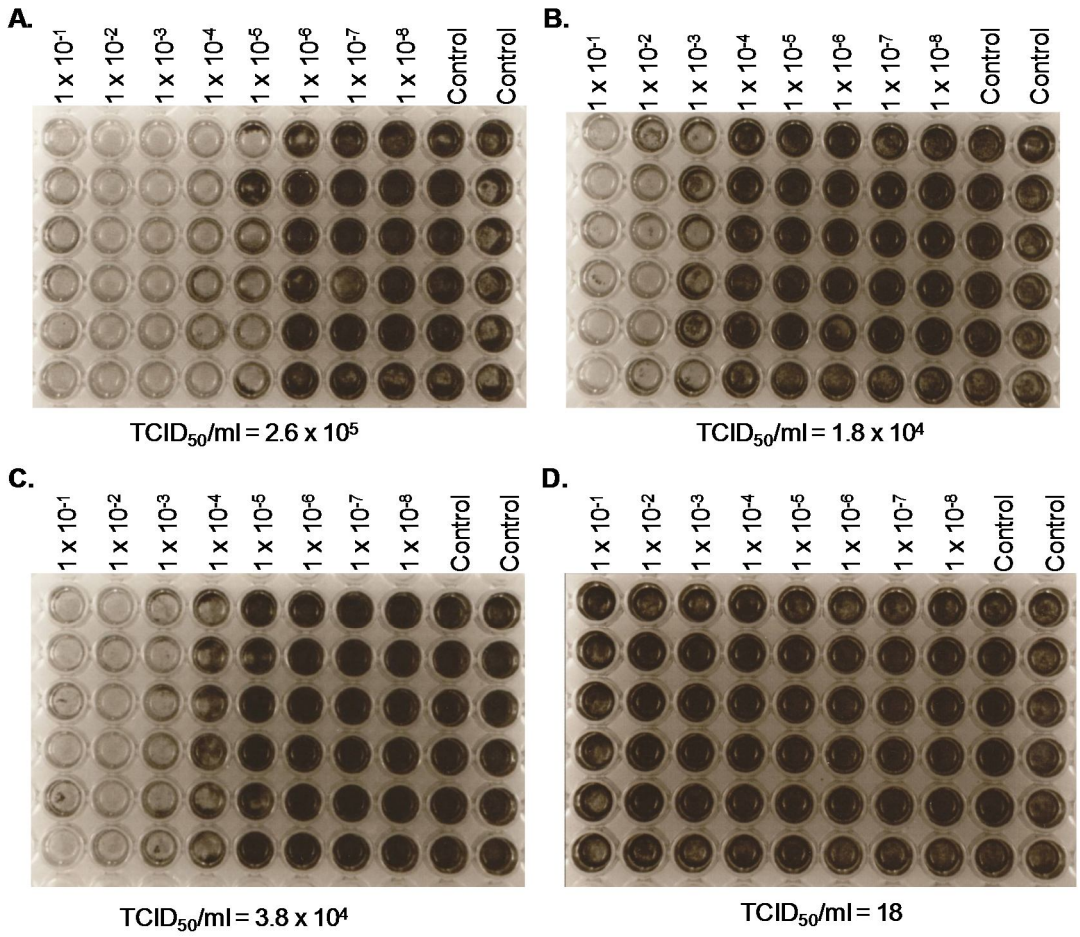

Figure 3-4 $TCID_{50}$ assay to determine viral infectivity of HRV1B on HeLa cells at passage >100 (A) and passage >60 (B) and HRV16 on HeLa cells at passage >100 (C) and passage >60 (D). HeLa cells were infected with HRV1B or HRV16 serially diluted from 1 x 10^{-1} to 1 x 10^{-8}. Control wells had media only and were not infected. Plates were left 5 days at 33 °C before staining with crystal violet.

3.3.3 Optimisation of R16-7 for Immunocytochemistry

Infection of HeLa cells by HRV *in vitro* was detected using immunocytochemistry; this was also a new method in the laboratory and therefore required optimisation. This was conducted on higher passage HeLa cells due to the information gained from $TCID_{50}$ experiments. Various concentrations of the primary antibody (R16-7) and secondary antibody (GαM-AF549) were conducted; appropriate negative controls in which

primary only or secondary only were applied to HRV infected cells, or both antibodies applied to HRV uninfected cells, were also performed.

HRV was detectable with the primary antibody at a concentration of 43.75 ng/ml and the secondary at 0.5 μg/ml, Figure 3-5. Successful detection of HRV16 infected cells is confirmed as the cells stained using the R16-7 anti-HRV antibody are displaying CPE; they are rounded and morphologically different to the uninfected cells surrounding them, Figure 3-5 B. The negative controls did not have any fluorescence (Figure 3-6).

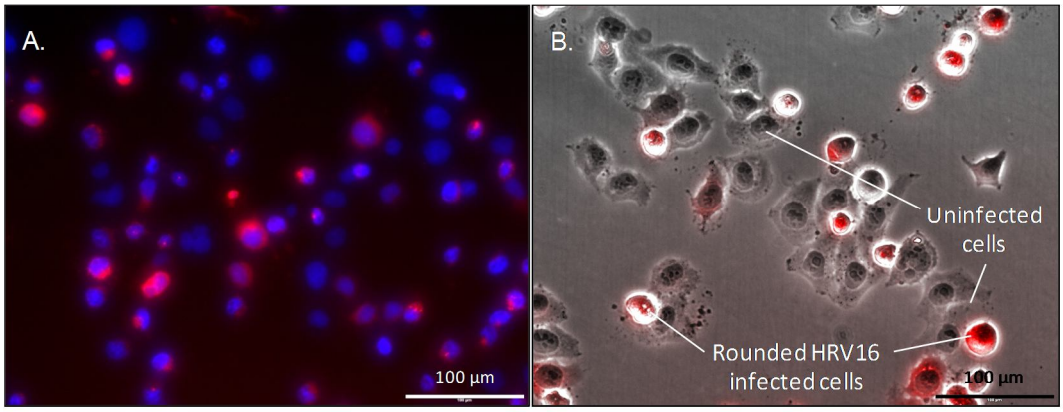

Figure 3-5 Immunohistochemistry to detect HRV. Monolayers of HeLa cells were infected with HRV16 and left at 33 °C for 17 hours. Cells were then fixed with 1 % paraformaldehyde and permeabilised with washes using PBS containing 0.03 % (v/v) Triton®X-100 (Sigma-Aldrich). Primary antibody, R16-7 at 43.75 ng/ml was applied and left for 1 hour at room temperature, after thorough washing the secondary antibody at GαM-A549 at 0.5 μg/ml was applied and also left 1 hour at room temperature. Nuclei were counterstained with DAPI. Images were viewed using an Olympus IX microscope and images produced using Cell^{P} software (**A**) Overlay of DAPI and TRITC filter images. (**B**) Overlay of phase contrast and TRITC filter. Red indicates a HRV16 infected cell.

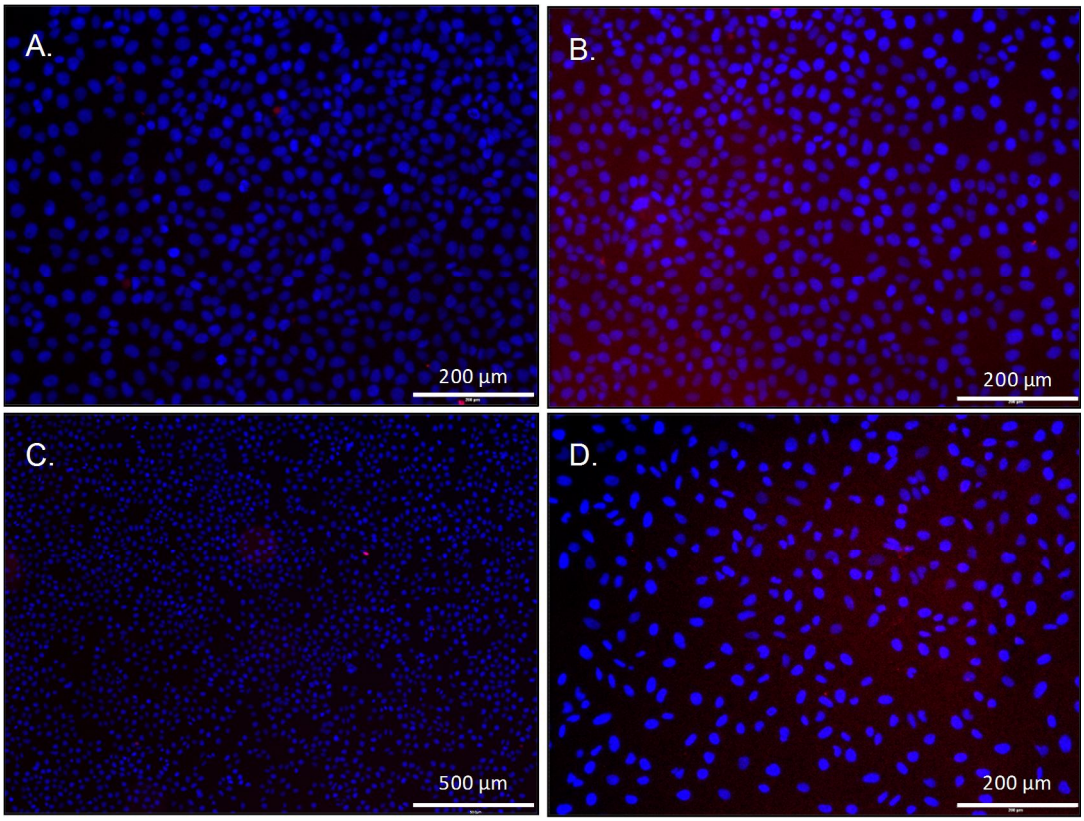

Figure 3-6 Immunocytochemistry negative controls. Monolayers of HeLa cells were or were not (as indicated) infected with HRV16 and left 17 hours at 33°C. Cells were fixed with 1 % paraformaldehyde and stained with antibodies as indicated (primary antibody – R16-7 at 43.75 ng/ml, secondary antibody – GαM-A549 at 0.5 µg/ml) Nuclei were counterstained using DAPI. (**A**) Uninfected cells stained with primary and secondary antibodies. (**B**) HRV16 infected cells stained with primary antibody only. (**C**) HRV16 infected cells stained with secondary antibody only. (**D**) HRV16 infected cells with neither primary nor secondary antibodies.

3.3.4 Fluorescent Focus Assay

The $TCID_{50}$ method is an effective and reliable way of measuring viral titre, however the assay takes five days before viral titre can be assessed and thus a quicker method was preferable. The fluorescent focus assay (FFA) can provide a measure of viral titre within two days. The antibodies for the FFA were optimised as discussed in section 3.3.3. A comparison between titres measured using the $TCID_{50}$ and FFA were made; this was conducted by setting up two identical 96 well plates with serially diluted HRV16, as

described for the $TCID_{50}$ assay. The FFA plate was washed, fixed and stained as described in 3.2.3, 17 hours post infection. The fluorescent foci were counted directly under fluorescent microscopy. The $TCID_{50}$ plate was stained after five days. The viral titre was determined by both techniques as described in the methods sections 3.2.2 and 3.2.4.

The average viral titre from triplicate wells of HRV16 diluted 1 in 10 as determined by FFA was 1.8×10^5 ffu/ml; this is comparable to the viral titre as determined by $TCID_{50}$ conducted at the same time of 2.6×10^5 $TCID_{50}$/ml. As can be seen in Figure 3-7 approximately 13 % of cells were infected with HRV16.

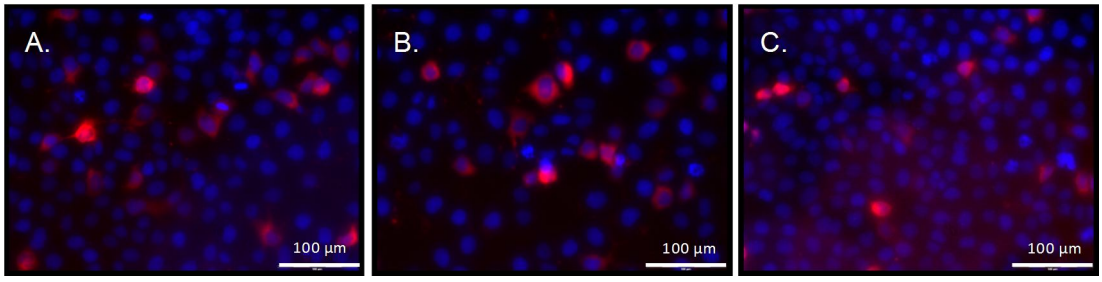

Figure 3-7 Fluorescent focus assay to determine viral titre. High passage HeLa cells were infected with HRV16, at a 1 in 10 dilution, repeated three times, **A**, **B** and **C**, 17 hours post infection HRV16 was detected using R16-7 primary antibody (43.75 ng/ml) and a GαM-AF549 conjugated secondary antibody (0.5 µg/ml) (Red). Nuclear staining with DAPI (Blue). Images are a DAPI and TRITC overlay.

3.3.5 Amplification of HRV

HRV1B and HRV16 amplification was undertaken to produce stocks of HRV1B and HRV16, which after purification could be used to investigate interactions with nhSP-A, nhSP-D and rfhSP-D.

Amplification of HRV had not previously been undertaken in the laboratory and thus the most successful method of amplifying HRV infection had to be established. CPE were identified as cell rounding and de-adherence of the monolayer from the surface of the tissue culture flask. Due to differences observed between HeLa cells at different passages in the $TCID_{50}$ assay, HRV16 was amplified on HeLa cells at passage >60 and passage >100 and compared by $TCID_{50}$, Figure 3-8. There was a high level of visible cell death in the higher passage HeLa cells after 17 hours of infection, and therefore the flask was frozen at this point. In the lower passage HeLa cells there was not a high level of cell death after 48 hours, however, this is the longest period of time the cells are left before HRV harvesting and thus the cells were frozen at this point. (The 48 hour time point was recommended by personal communication with staff at Synairgen plc). The HRV16 amplification in higher passage HeLa cells produced a $TCID_{50}$/ml of 3.7×10^7; the HRV16 amplification in lower passage HeLa cells produced a $TCID_{50}$/ml of 1.8×10^5.

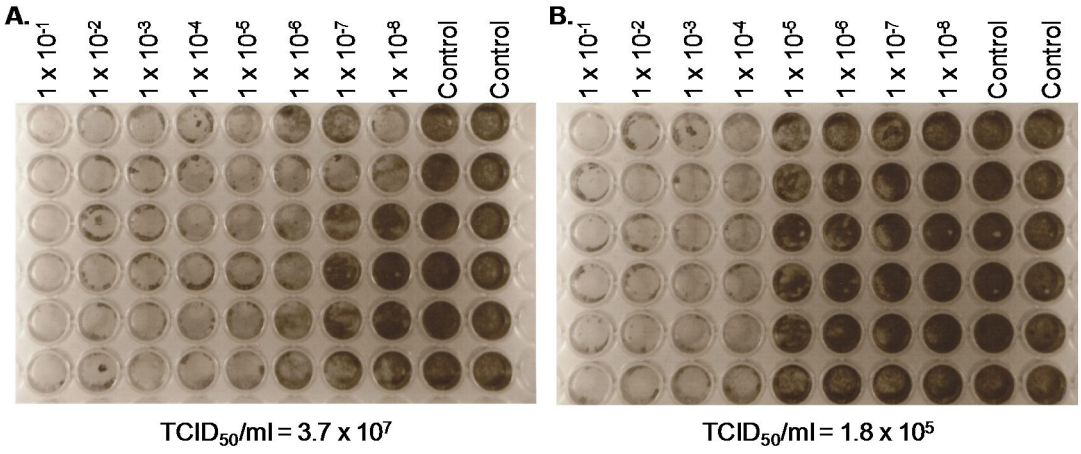

Figure 3-8 $TCID_{50}$ assay to determine viral titre of HRV16 amplified on (A) high (>100) and (B) low (>60) passage HeLa cells. Two 80 % confluent T75 flasks of HeLa cells at either high or low passage were infected with 4 ml of HRV16 HeLa cell lysate and left for A. 17 hours (high passage) or B. 48 hours (low passage) until 80 % cell death was seen or the maximum time point of 48 hours was reached. Cell lysate from these flasks were assessed for viral titre by the $TCID_{50}$ assay.

To ensure the yield from amplification was maximal, regimes of different ratios of HRV to infection media was undertaken. The method obtained from Synairgen plc recommended using a 2:1 ratio of HRV to infection media during rocking and a final ratio of 1:1. Ratios were altered as detailed in Table 3-1. An initially low volume during rocking maximises contact between HRV particles and cell surface receptors, the volume of media is increased after attachment to optimise availability of factors required for replication.

Ratio HRV16: infection media during rocking	**Ratio HRV16: infection media during 33 °C incubation**	**Repeat 1 Titre ($TCID_{50}$/ml)**	**Repeat 2 Titre ($TCID_{50}$/ml)**
2:1	1:1	5.6×10^5	3.8×10^6
2:1	1:2	3.1×10^5	8.2×10^5
2:1	1:3	1.8×10^5	3.8×10^6
2:1	1:4	5.6×10^5	1.8×10^5
2:1	1:5	3.1×10^5	3.8×10^5
1.3:1	1:2	5.6×10^5	8.2×10^5
1:1	1:3	5.6×10^5	1.8×10^6
0.8:1	1:4	8.2×10^5	8.2×10^5
0.66:1	1:5	3.8×10^5	2.6×10^5

Table 3-1 Optimisation of HRV amplification. HRV16 and infection media were applied to HeLa cells at the indicated ratios during a one hour rocking period at room temperature. Infection media was added to the indicated final ratio before incubation at 33 °C for 17 hours. The yield from each infection regime was determined using a $TCID_{50}$ assay conducted on HeLa cells.

In the first repeat the maximal HRV16 yield was obtained by infecting HeLa cells with 0.8:1 HRV16 to infection media initially and then increasing this to 1:4 after incubation. In the second repeat the maximal HRV16 yield was obtained by infecting HeLa cells with 2:1 HRV16 to infection media initially and then increasing this to 1:1 or 1:3 after incubation.

HRV1B and HRV16 stocks were analysed to ensure that stocks were not contaminated with mycoplasma using a PCR based detection kit; results were negative for both stocks (data not shown).

3.3.6 Purification of HRV Stocks

Purification of HRV1B and HRV16 was required for binding studies and preferable for all *in vitro* and *in vivo* experiments to ensure that conclusions drawn from these experiments are due to HRV virions and not contaminants from the cell lysate.

The first approach used to concentrate HRV before applying to a sucrose gradient for isolation of viral particles was PEG precipitation. This was conducted by mixing HRV16 infected HeLa cell lysate with 7 % PEG6000, centrifuging and then reconstituting the HRV16 containing pellet in virus buffer, 1/20th of the original volume. The pellet and supernatant fractions were analysed by SDS-PAGE and western blot to determine if the HRV16 had been successfully removed from the supernatant into a concentrated form in the pellet,
Figure 3-9.

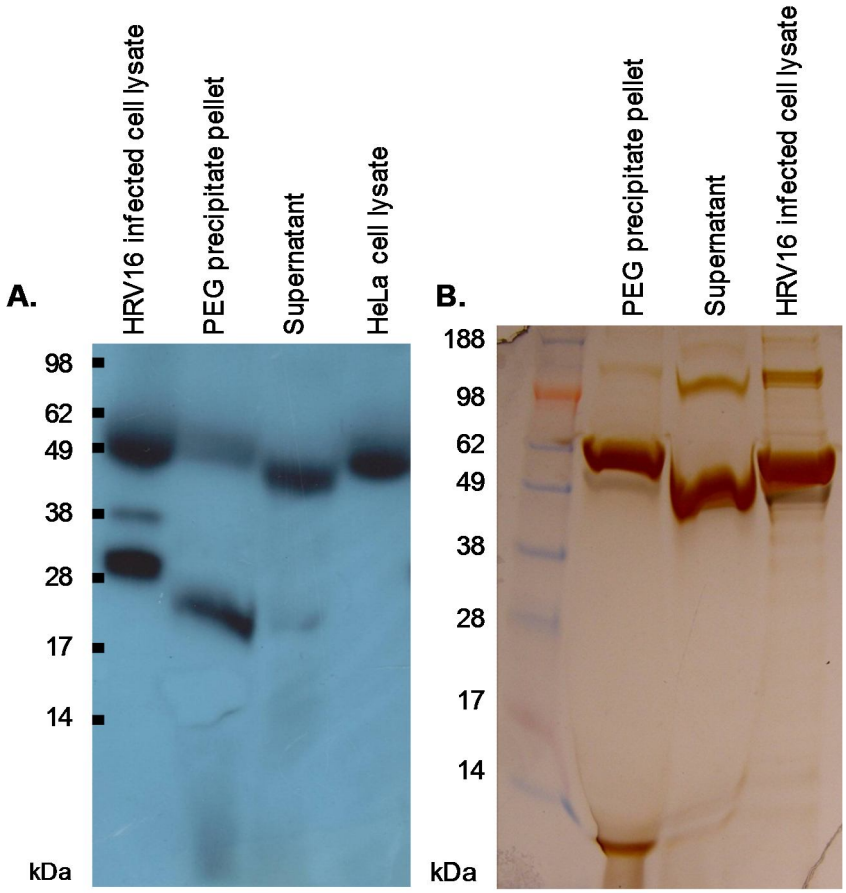

Figure 3-9 Western Blot and SDS-PAGE of PEG precipitated HRV16. HRV16 was PEG precipitated with 7 % PEG6000 by mixing for two hours at room temperature, this was centrifuged and the HRV16 containing pellet was resuspended in virus buffer at 1/20th the original volume. The resuspended pellet and supernatant from the PEG precipitation were analysed by SDS-PAGE followed by (A) western blot using R16-7 primary antibody or (B) silver staining.

Remaining PEG6000 in the pelleted sample interfered with the running of the gel; however, virus was detectable in the western blot. There is a band visible on the western blot, Figure 3-9 A, in the PEG precipitate pellet sample, this is slightly lower than at ~30kDa which is the appropriate size of VP2, however, this is likely due to the abnormal running of the gel. A band at the same position is faintly visible in the supernatant suggesting the HRV16 was not fully removed by PEG precipitation.

The silver stained SDS-PAGE gel, Figure 3-9 B, did not detect any protein at ~30 kDa that corresponded to the staining observed in the western blot, suggesting the HRV proteins were not of a high enough concentration to be detected by this method. The PEG precipitation pellet did however show a strong band at approximately 10 kDa.

The PEG precipitation method was further refined to reduce the loss of HRV16 during the procedure, shown by the presence of HRV16 in the supernatant after the virus should have been precipitated out of solution. During precipitation with 7 % PEG6000, 0.5 M NaCl was also added to encourage HRV16 precipitation. After centrifugation and resuspension of the HRV16 PEG pellet the HRV16 was syringe filtered and concentrated in a 100 K MWCO Amicon Ultra Centrifugal Filtration Unit. Each stage of the PEG precipitation process was analysed by western blot to determine if the HRV16 had been successfully concentrated and to determine if there was any loss of HRV16, Figure 3-10.

There is a clear band in the supernatant of the centrifugation step to remove the PEG precipitated HRV16 (lane 2, Figure 3-10) suggesting that not all of the HRV16 was removed by the PEG and NaCl precipitation. The band is slightly lower than expected for HRV16, as observed in Figure 3-9 A, this is again likely due to PEG affecting the running of the SDS-PAGE. A band at 37 kDa corresponding to the size of VP0 and a 30 kDa band corresponding to VP2 is visible in the pellet from the spin to remove insoluble matter when the HRV16 containing PEG pellet was resuspended, lane 3 Figure 3-10. This is due to PEG being difficult to re-suspend. No loss of HRV16 into the flow through was observed during the concentration or buffer exchange using 100 K MWCO Amicon Ultra Centrifugal Filtration Unit as no bands are visible on the blot, lane 4 Figure 3-10.

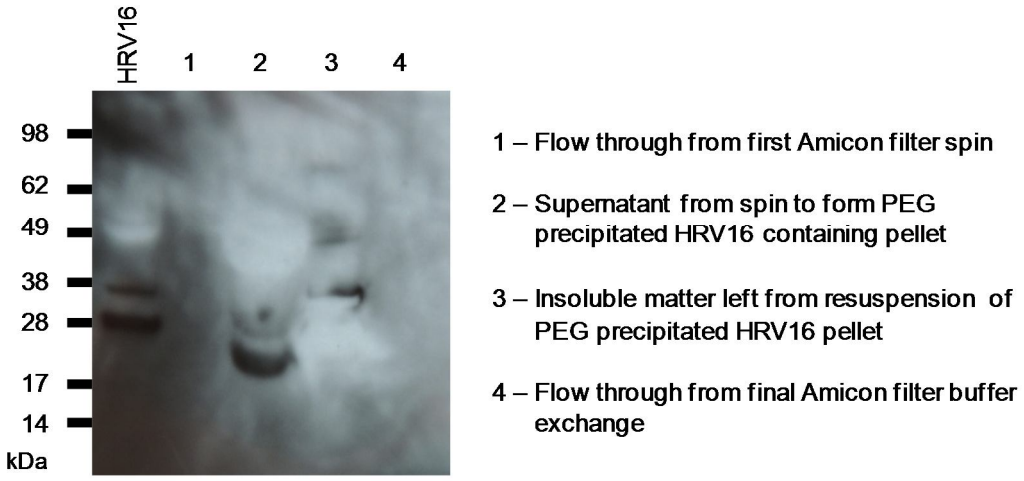

Figure 3-10 Western blot of steps of PEG precipitation of HRV16. A sample was taken after each step of the PEG precipitation procedure. Samples and a HRV16 positive control were reduced and run on a 12 % NuPAGE gel, transferred to PVDF membrane and probed using a R16-7 primary antibody (0.14 μg/ml) and GαM-HRP secondary antibody (1 μg/ml).

The HRV16 concentrated by PEG precipitation was further purified by ultracentrifugation on a stepwise 10 to 35 % (w/v) sucrose density gradient. As there was no visible band of protein on the sucrose gradient all fractions were analysed by SDS-PAGE followed by western blotting using the R16-7 antibody. All western blots were performed with positive and negative controls, which were successful, but no HRV16 was detected in any of the fractions (data not shown). This further purification step therefore required refinement.

Ultracentrifugation on a stepwise 10 to 35 % (w/v) sucrose density gradient was repeated with a more concentrated PEG precipitated HRV16 sample. When analysed by western blot, Figure 3-11 B and C, all fractions tested contained both the mature HRV protein VP2 and its precursor VP0; no fractions contained only VP2 (mature HRV alone), therefore the purification

method required further refinement. The fractions analysed were from the interface of each of the layers of sucrose, as shown on Figure 3-11 A.

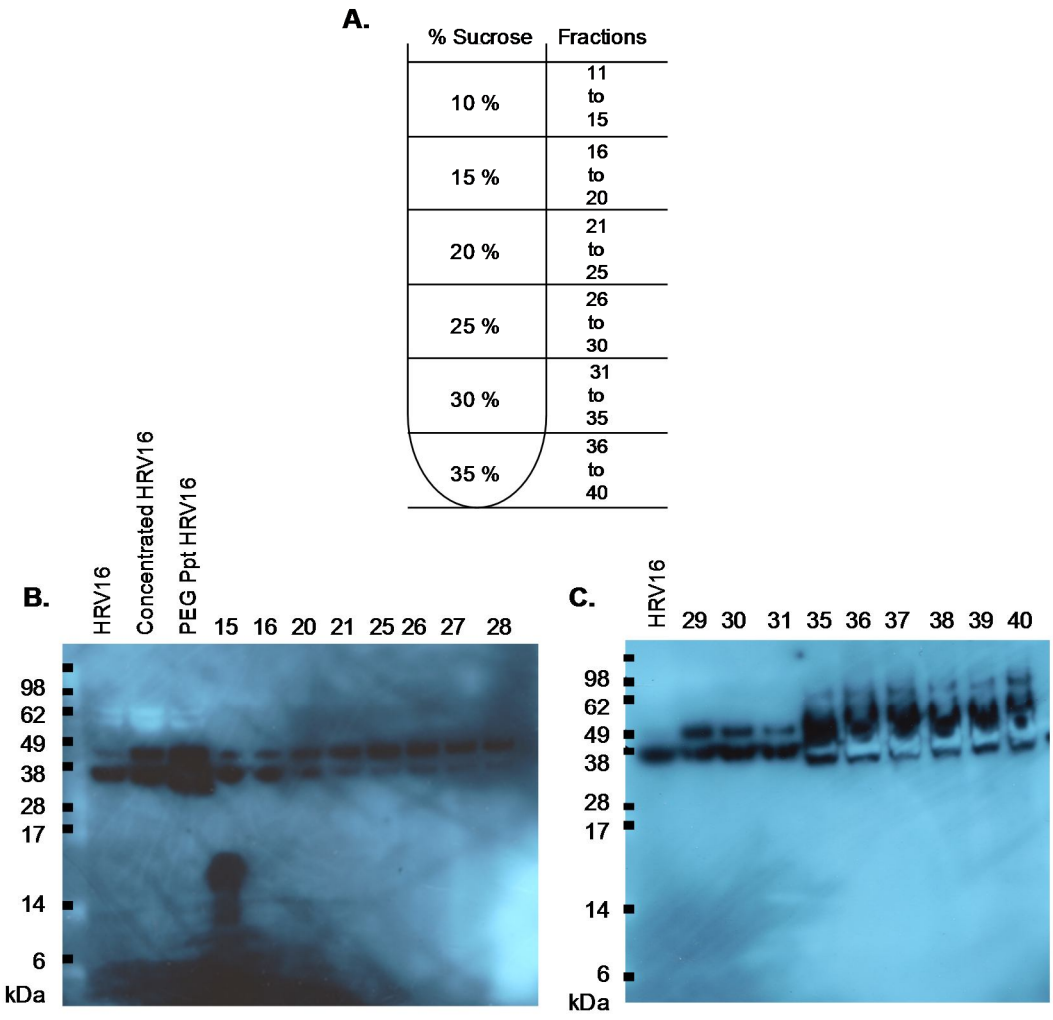

Figure 3-11 Western blot analysis of sucrose density gradient purified HRV16. PEG precipitated HRV16 was layered onto a 10-35 % (w/v) stepwise sucrose density gradient, as represented diagrammatically in **A** and centrifuged at 80,000 x g for four hours. The gradient was fractioned into 1 ml fractions and reduced samples and a HRV16 positive control were run on SDS-PAGE using a 12 % Nu-PAGE gel and analysed by western blot on PVDF using the R16-7 antibody (**B** and **C**).

A third batch of PEG precipitated HRV16 was purified by ultracentrifugation on a linear 15-45 % (w/v) sucrose density gradient. Before addition of the

HRV16 to the sucrose gradient, the detergent IGEPAL® CA-630 was added to the HRV16 to dissociate HRV16 from contaminating proteins. After ultracentrifugation the sucrose density gradient was fractioned into sequential 0.5 ml fractions and analysed by western blotting to identify those containing mature HRV16, Figure 3-12.

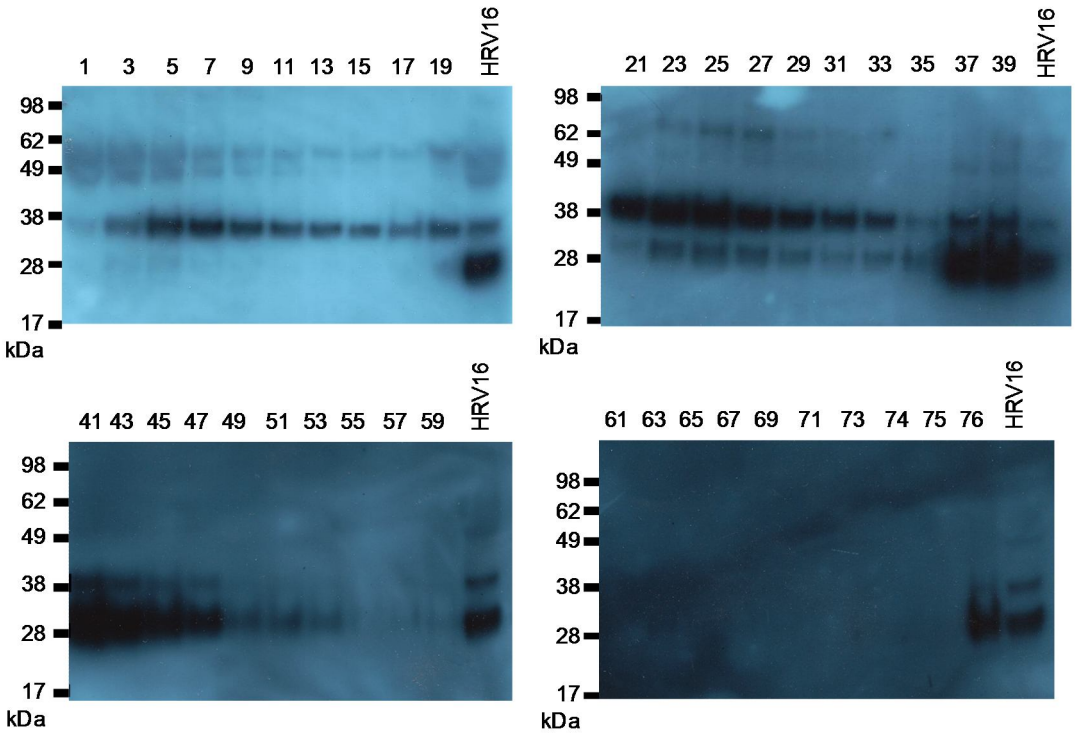

Figure 3-12 Western blot analysis of sucrose density gradient purified HRV16. PEG precipitated HRV16 was layered onto a 15-45 % (w/v) linear sucrose density gradient and centrifuged at 80,000 x g for four hours. The gradient was fractioned into 0.5 ml fractions and reduced samples and a HRV16 positive control were run on a 12 % Nu-PAGE gel and analysed by western blot using R16-7 primary antibody.

Purification of HRV16 on a linear sucrose density gradient resulted in production of five distinct populations within the gradient, identifiable on the western blots (figure 5.11). Fractions (0.5 ml) were taken from the top of the gradient, fraction 1, to the bottom of the gradient, fraction 76. All fractions were stored at -80 °C until analysis. Fractions 1 to 20 contained a high concentration of VP0, shown by a dark band at 37 kDa. Factions 1 to 20

also contained several high molecular weight proteins, possibly HRV16 proteins bound to HeLa cell proteins and a HeLa protein at 49 kDa has been observed in previous western blots (Figure 3-2) is also seen in these fractions. Fractions 21 to 35 have a darker band at 37 kDa, than seen in fractions 1 to 20 and also a band at 30 kDa, corresponding to the size of VP2. High molecular weight proteins are also observed in these fractions. Fractions 36 to 40 have a very dark band at 30 kDa and a less dark band at 37 kDa but these fractions also contain the high molecular weight bands observed in the afore mentioned fractions. Fractions 41 to 54 have a dark band visible at 30 kDa, corresponding to the size of VP2 and a faint band at 37 kDa. No viral proteins at all were detected in fractions 55 to 75 by western blot, in fraction 76 there were some viral proteins detected, this is the bottom of the tube and may be aggregated HRV16 or HRV16 bound to high density proteins that have pelleted due to being able to pass through the gradient.

The 0.5 ml fractions in each population identified by the western blot analysis (Figure 3-12) of the HRV16 purified by sucrose density gradient ultracentrifugation were pooled and analysed for infectivity using the $TCID_{50}$ assay. The $TCID_{50}$ values for each population and the HRV16 infected HeLa cell lysate from which the HRV16 was purified are given in Table 3-2, the percentage of total yield for each population is also shown.

Fraction	Volume / ml	$TCID_{50}$ / ml	Total HRV / $TCID_{50}$	Percentage of yield (total yield = 2.2×10^6 $TCID_{50}$)
Cell lysate that was purified	282	1.8×10^{11}	5.1×10^{13}	
1 to 20	10	No infectivity	0	0
21 to 35	7.5	5.6×10^2	4.2×10^3	0.2
36 to 40	2.5	8.2×10^5	2.1×10^6	93.2
41 to 54	7	1.8×10^4	1.3×10^5	5.6
55 to 75	10.5	1.8×10^3	1.9×10^4	0.8

Table 3-2 Viral titre of each population from the sucrose density gradient as identified by western blotting (Figure 3-12). Each population from the sucrose density gradient ultracentrifugation to purify HRV16 was assessed for viral titre using the $TCID_{50}$ assay. The original untreated HRV16 infected HeLa lysate was also assessed. The percentage of the overall HRV16 yield is shown for each population.

No infectivity was detected for fractions 1 to 20, and only a low titre for fractions 21 to 35. Fractions 36 to 40 and 41 to 54 had viral titres of 8.2×10^5 /ml and 1.8×10^4 /ml respectively. As can be seen from the yield calculations the 93.2 % of infectious HRV16 was within fractions 36 to 40. Fraction 55 to 75 had a titre of 1.8×10^3 /ml. All of the populations had titres much lower than that of the infected HeLa cell lysate from which the HRV16 was purified which had a titre of 1.8×10^{11} /ml.

Due to PEG precipitation of HRV16 being ineffective at removing all HRV16 from solution ultracentrifugation was employed as an alternative method of concentrating the HRV, as used by other laboratories [221, 224, 226]. This

also did not remove all of the HRV from the cell lysate supernatant as tested by western blot (data not shown) but due to being a quick method was trialled to examine how much HRV was lost during the process. The amount of virus retained during purification is shown in Table 3-3. The purification process results in great losses of HRV, however the method of PEG precipitation resulted in a greater loss than ultracentrifugation. Due to this observation subsequent purifications of HRV were conducted by initially concentrating the HRV using ultracentrifugation.

	Method of HRV infected cell lysate concentration				
	PEG precipitation			Ultracentrifugation	
Total HRV in cell lysate	6.9×10^9 ffu/ml	5×10^{10} $TCID_{50}$/ml	5.04×10^9 ffu/ml	3.36×10^9 ffu/ml	1×10^{10} ffu/ml
Total HRV in purified virus	6.5×10^7 ffu/ml	1.26×10^5 $TCID_{50}$/ml	3.24×10^6 ffu/ml	3.3×10^8 ffu/ml	1.8×10^8 ffu/ml
HRV Retained / %	0.94	0.00004	0.06	9.8	2

Table 3-3 Comparison of PEG precipitation and ultracentrifugation to concentrate HRV prior to purification on sucrose gradients. Titre of purified HRV is that at the end of the purification process once purified HRV is in virus buffer and ready to use.

As it was observed that not all HRV was removed from the cell lysate by ultracentrifugation a second step involving PEG precipitation of the already ultracentrifuged cell lysate was undertaken. The PEG precipitated supernatant was loaded onto a linear sucrose gradient and analysed by western blot after ultracentrifugation and fractioning, Figure 3-13. No HRV was detected in any of the fractions.

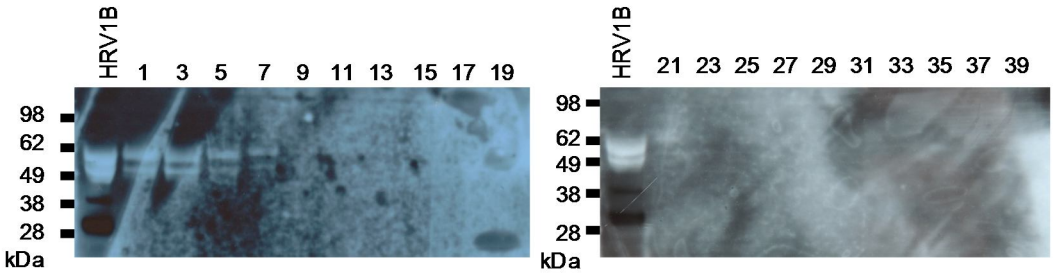

Figure 3-13 Secondary removal of HRV1B by PEG precipitation after ultracentrifugation of HRV1B infected HeLa cell lysate. Western blot analysis of fractions of sucrose gradient loaded with PEG precipitated HRV1B infected cell lysate that had previously been ultracentrifuged to remove HRV1B.

The purification process results in a preparation of HRV in sucrose; this was not desirable for use in experiments in this project as sucrose may interfere with collectin interactions with HRV. The sucrose was removed by dialysis or buffer exchange using 100 K MWCO Amicon Ultra Centrifugal Filtration Units. The two methods were assessed to evaluate loss of HRV during each technique. This was conducted by measuring viral titres of HRV before and after removal of sucrose, Table 3-4. Both techniques resulted in large losses of HRV, the Amicon filter exchange method did however result in lower loss of HRV and was also quicker to carry out and thus became the preferred method.

	Method of sucrose removal		
	Dialysis	Amicon filter	
HRV prior to sucrose removal / ffu	1.9×10^8	5.6×10^7	6.3×10^8
HRV post sucrose removal / ffu	6.9×10^7	2.7×10^7	3.3×10^8
Total loss / %	63.7	51.8	47.6

Table 3-4 Comparison of dialysis and Amicon filter to remove sucrose from purified HRV preparations. HRV was either dialysed using a Slide-A-Lyser dialysis cassette (3.5 K MWCO) (Thermo Scientific, Pierce) in 1 L of buffer with four buffer changes, or buffer exchanged using 100 K MWCO Amicon Ultra Centrifugal Filtration Units (Merck Millipore) and three washes with virus buffer. Virus titre was assessed using the FFA before and after sucrose removal.

3.3.7 Transmission Electron Microscopy of HRV

To ensure that ultracentrifugation had not resulted in deformation of the viral particles and to observe if there were any contaminants the HRV stocks were subjected to transmission electron microscopy. The HRVs were fixed and negatively stained using uranyl acetate. Figure 3-14 shows both HRV1B and HRV16 viral particles that are spherical and have a diameter of approximately 25-30 nm. All of the viral particles appear to be "full", i.e. no empty capsids that are incapable of replication. The HRV1B stock appears to contain a higher number of viral particles than the HRV16 stock; this is expected based on a higher viral titre of HRV1B observed *in vitro*.

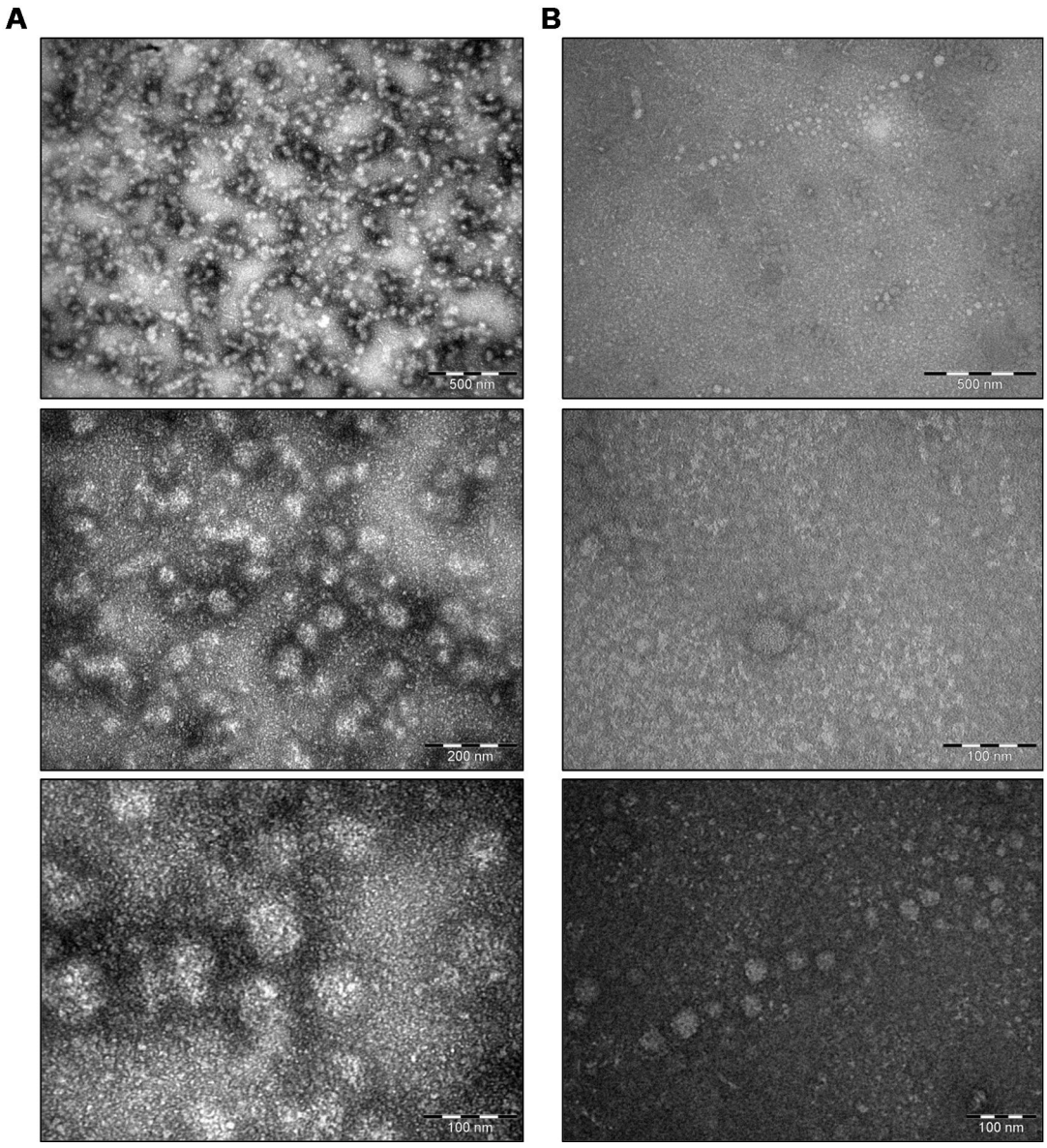

Figure 3-14 Transmission electron microscope images of purified (A) HRV1B and (B) HRV16. Sucrose density gradient purified HRV1B and HRV16 were concentrated using 100 K MWCO Amicon Ultra Centrifugal Filtration Units and exchanged into sterile ultrapure water. After glutaraldehyde fixing the HRVs were applied to formvar coated grids and subsequently stained using 2 % (w/v) uranyl acetate. Images taken with a Hitachi H-7000 electron microscope.

3.4 Discussion

To address the hypothesis of whether nhSP-A, nhSP-D and rfhSP-D bind to HRV and whether they inhibit HRV infection several experimental techniques had to be established.

Western blotting to detect HRV had to be optimised. The best parameters to detect the viral protein VP2 of HRV1B and HRV16 were found to be 0.14 μg/ml of the primary antibody R16-7 and 1 μg/ml of the secondary antibody GαM-HRP with blocking maintained throughout using 2 % (w/v) skimmed milk in PBS-Tween. No previous literature had indicated that R16-7 could recognise HRV1B in addition to HRV16, and so to our knowledge this is the first report of this finding. In addition to VP2, the VP2 precursors VP0 and P1 were detected using R16-7, these are 37 and 90 kDa proteins respectively; this is in accordance with the literature where other groups have also found that the antibody reacts with these proteins [227].

Optimisation was required for the $TCID_{50}$ assay used to measure viral titre. $TCID_{50}$ represents the dose that will give rise to CPE in 50 % of inoculated cultures and therefore gives a measure of viral titre. HeLa cells of lower passage (>60) were found to be less susceptible to infection by HRV1B as the $TCID_{50}$ value on these cells was much lower than on cells of higher passage number (>100). No CPEs were observed when HRV16 was applied to cells of lower passage, whilst CPE was observed on cells of higher passage. It is unclear why this is so; it is possible that as the cells go through increasing numbers of passages their properties change; for instance they may start expressing an increased level cell surface receptors. Increased ICAM-1 or LDLR expression would lead to increased adsorption of virus (HRV16 and HRV1B respectively) to the cell surface which would in turn elevate

internalisation and replication of HRV. Levels of ICAM-1 and LDLR mRNA and protein expression in the high and low passage HeLa cells could be measured and compared using quantitative polymerase chain reaction (PCR) or fluorescent activated cell sorting (FACS) respectively, as conducted by Papi et al [158]. It is also possible that a point mutation in ICAM-1 or LDLR may have occurred with increasing passages, thereby adapting better to the virus. This could be investigated by sequencing the ICAM-1 and LDLR genes in the high and low passage HeLa cells. The increased susceptibility of the higher passage HeLa cells may also be as a result of the older cells being unable to mount the same antiviral response as the lower passage HeLa cells. The antiviral response could be investigated using an enzyme-linked immunosorbent assay (ELISA) to measure cytokines at the protein level or PCR to measure cytokines at the mRNA level. Due to differences in the susceptibility of the HeLa cells at different passages all subsequent experiments in this investigation were conducted on HeLa cells that were of similar passage number (within ten passages); this allows comparisons to be drawn between experiments undertaken with the same conditions.

Immunocytochemistry to detect HRV *in vitro* required optimisation prior to development of the FFA as this had not been conducted in our laboratory with the mAb R16-7. HRV16 was detected using R16-7 at a low concentration of 43.75 ng/ml and the secondary antibody, GαM-AF549, at a concentration of 0.5 μg/ml. Immunocytochemistry was applied as a FFA to determine viral titre, as previously described for other viruses [111, 228, 229]. The infected cells were stained 17 hours post infection. This time point was chosen as at this point the HRV has infected and replicated within the cell to allow a great enough signal to be seen but secondary infection cannot yet be detected. Any secondary infection of neighbouring cells wouldn't be detected as preliminary experiments in which plates were left just six hours

before staining did not show any infection. The FFA was validated by comparing viral titre results with those obtained using the $TCID_{50}$ assay. The optimal infection rate to use is around 20 %, rather than the 13 % obtained in the initial experiment, this increases the number of cells counted and thus the accuracy of the viral titre measurement. This was accomplished in subsequent FFAs by titrating the volume of HRV that cells were infected with until the desired infection rate of 20 % was achieved. The level of HRV infection is expressed by counting the number of viral foci in relation to the number of cells.

Amplification of HRV1B and HRV16 stocks was required as these are the HRVs chosen for use in this project. HRV1B is a minor group HRV whereas HRV16 is a major group HRV. It was explored whether high or low passage HeLa cells were most successful at supporting HRV amplification, and hence which yielded the most virus. It was found that the higher passage HeLa cells yielded greater viral titres than lower passage HeLa cells, hence all amplification was conducted on high passage HeLa cells. To optimise yields the ratio of HRV to infection media during amplification was addressed; the ratios were based on recommendations from Synairgen plc. The results were variable and did not give a clear answer, however, the second repeat suggested that an initial ratio of HRV to infection media of 2:1 was favourable as this resulted in viral titres of 3.6×10^6 $TCID_{50}$/ml in two flasks. Both the repeats suggested a final ratio of HRV to infection media of 1:3 or 1:4 was favourable and so a final ratio of 1:4 was chosen as this maximised yield as the titre was high and also resulted in a large volume of HRV infected cell lysate.

To investigate nhSP-A, nhSP-D and rfhSP-D interactions with HRV it was necessary to purify HRV. This ensures experimental observations are due to

the HRV virions and, or, the interaction of nhSP-A, nhSP-D and rfhSP-D in the experimental system into which they are used and not due to other factors present in the HRV infected HeLa cell lysate. Binding studies also require pure HRV virions. There are many varying methods of HRV purification documented in the literature [194, 221-224, 230-232]. Some previously reported purification methods involve two steps, PEG precipitation and sucrose density gradient ultracentrifugation [194, 223]. This was undertaken on a small sample of HRV16 stock to refine the method. The initial PEG precipitation was successful as the PEG precipitated pellet contained a greater concentration of HRV16 protein than the supernatant from which the HRV16 was expected to be removed. However, not all of the HRV16 was removed suggesting further optimisation was required. It appeared that remaining PEG in the sample interfered with the running of the SDS-PAGE as the viral protein band detected using the R16-7 HRV specific antibody is slightly lower than expected. On a silver stained gel of PEG precipitated HRV16 a band corresponding to the size of reduced VP2 was not observed, suggesting that the proteins detected in the western blot were not of a high enough concentration to be detected by this method. A band at approximately 10 kDa was however detected; this may be VP4, a 7 kDa viral protein that may have been affected by the abnormal running of the gel. This band was not detected by the western blot, however it has not been reported that the R16-7 antibody is able to detect this viral protein and this band has not been detected in any other western blots conducted in this study.

A second PEG precipitation in which 0.5 M NaCl was included with the PEG6000 was performed to optimise the precipitation of HRV. Again, not all HRV16 was removed by precipitation. HRV16 was also lost in the insoluble

matter after resuspension of the HRV16 containing PEG pellet, the PEG is very difficult to re-suspend and consequently this is difficult to avoid.

The second step of HRV16 purification, sucrose density gradient ultracentrifugation, required refinement. An initial attempt using a stepwise gradient resulted in the virus not being detected by western blot in any of the fractions. This may be due to such a small sample of the HRV16 being loaded onto the top of the gradient it could have resulted in the HRV16 being diluted beyond the detection limits of the western blot. It is also possible that the gradient may have been disturbed and thus the HRV16 would not have concentrated at one point on the gradient thus being diluted within the sucrose. The sucrose gradient was repeated with a more concentrated PEG precipitated HRV16 sample; all fractions analysed by western blot contained HRV16 protein and there were no fractions containing only mature HRV16. This may have been due to the HRV16 proteins being bound to contaminating HeLa cell proteins which interfered with separation by density. To rectify this, a detergent, IGEPAL® CA-630, was added to the PEG precipitated HRV16 before addition to a continuous linear sucrose gradient, this step had previously been used by Abraham *et al.* [223]. Western blotting of fractions from this purification showed five distinct populations of virus proteins. One population taken from the top of the gradient contained a high concentration of the VP0 precursor protein and high molecular weight proteins. These are possibly fragments of HRV16 that are still bound to HeLa cell proteins, despite addition of detergent, which have a high molecular weight but low density. A second population, slightly lower within the gradient, contained a band that corresponds to VP2, but in addition a high concentration of VP0 and the contaminating high molecular weight proteins observed in the aforementioned population. In a third population a higher concentration of VP2 was observed and less of the VP0

precursor but again contained faint bands of contaminating high molecular weight proteins. The fourth population, just below the middle of the 15-45 % linear sucrose gradient contained a very strong band corresponding to the molecular weight of VP2, and a faint band corresponding to VP0; this is the pure virus that can be used in binding and infectivity studies. The fifth population had either a very faint band or no viral proteins at all detectable by western blot.

Each of the five populations from the sucrose density gradient were analysed for viral titre by the $TCID_{50}$ assay. The most infectious was the third population (fractions 36 to 40) with a $TCID_{50}$ of 8.2×10^5 / ml; this coincides with the western blot as this population contained the darkest band at 30 kDa, corresponding to VP2. The next most infectious was the population containing the pure virus (fractions 41 to 54) with a $TCID_{50}$ of 1.8×10^4 / ml. The viral titre of these populations is much lower than the titre of the HRV16 infected HeLa cell lysate from which the HRV16 was purified ($TCID_{50}$ of 1.8×10^{11} / ml); this highlights the losses that were observed previously during PEG precipitation.

To optimise yield of pure HRV from the sucrose density gradient ultracentrifugation of infected HeLa cell lysate was employed rather than PEG precipitation to concentrate the HRV. Pelleting of virus prior to purification has been conducted by other laboratories [221, 224, 226]. This was to negate problems with resuspension of the HRV containing PEG pellet where a large volume of HRV appeared to be lost. Pelleting the HRV by this method also resulted in great losses of HRV but the losses were less than observed with PEG precipitation. The residual HRV that was in the supernatant after ultracentrifugation could not be recovered from the HeLa cell lysate by subsequent PEG precipitation.

Sucrose removal from the purified HRV preparations was another stage at which large amount of HRV was lost, Table 3-4. Of the two techniques tried (dialysis and Amicon filter buffer exchange) the Amicon filter resulted in a slightly lower loss of HRV than dialysis and therefore was the chosen method. This is an unavoidable step in the purification process as the presence of sucrose in the preparations could interfere with collectin interactions with HRV. The undesirable loss of up to 50 % of HRV at this sucrose removal stage therefore had to be tolerated.

TEM of the purified HRV preparations confirmed the presence of viral particles, identified as 25-30 nm spherical particles as reported in the literature [233-235]. The morphology of the viral particles is not very distinctive, but this is in keeping with published reports of HRV TEM[236]. All of the viral particles appear to be "full" i.e. no empty capsids that are incapable of replication that are observed in some preparations [235, 236]. This may be due to the sucrose density gradient used to purify the HRV resulting in separation of "full" and "empty" capsids as they are likely to have different densities. However, it is interesting to note that some reports suggest that the appearance of "empty" capsids may be due to the staining solution being able to penetrate the particles and not because they lack RNA [234]. This was concluded as high and low density fractions that were, and were not infectious, contained similar proportions of both "empty" and "full" particles [235].

4. Chapter 4: Source and Purification of Collectins

4.1 Introduction

In order to conduct studies into interactions between collectins and HRV it was necessary to purify nhSP-A and nhSP-D as well as to express and purify rfhSP-D. Pure surfactant protein preparations were required to be able to attribute differences observed during experiments involving HRV and surfactant proteins to these constituents, and not to contaminants. The nhSP-D was purified from both amniotic fluid and BAL from patients with alveolar proteinosis; this was conducted using affinity chromatography. Affinity chromatography is commonly used to purify nhSP-D from amniotic fluid and BAL, the technique exploits the sugar binding capacity of the molecule in a calcium environment [26, 237]. The nhSP-D binds to the sugar containing matrix whilst in a calcium containing buffer, and can be eluted from the matrix by addition of EDTA. nhSP-A was purified using butanol extraction to delipidate a BAL pellet containing the nhSP-A, this method was developed by Jo Rae Wright and had not previously been used in this laboratory [238]. All preparations of the native proteins were analysed using western blot and SDS-PAGE to ensure pure protein preparations were obtained.

As discussed in section 1.2.1 rfhSP-D has pharmacological advantages over nhSP-D as it is able to be expressed in high yielding systems in a uniform manner. The rfhSP-D contains eight Gly-Xaa-Yaa repeats from the collagen region, the neck region and the CRD of nhSP-D. The bacterial clone for rfhSP-D was developed by Strong *et al.* [29]. The rfhSP-D was expressed in *E. coli*, the inclusion bodies were then solubilised and refolded to produce functional rfhSP-D, and this was purified using affinity chromatography and

gel filtration. The rfhSP-D purity was assessed using western blotting and SDS-PAGE.

4.2 Materials and Methods

4.2.1 Expression and Purification of rfhSP-D

Plates were streaked using a glycerol stock of the *E. coli* BLD21 DE3 containing pALMI-53 kanamycin resistant clone on an agar plate containing 25 μg/ml kanamycin monosulphate (Sigma-Aldrich). The plate was incubated overnight at 37 °C. A single colony was selected to inoculate 50 ml of Luria broth (LB), with the antibiotic maintained. This was grown overnight at 37 °C with shaking at 300 r.p.m. One litre of Magic Media (Invitrogen) was inoculated with 50 ml of the previously inoculated LB; this was cultured for 22 hours before harvesting the bacteria by centrifugation at 2,700 x g for 20 minutes.

Pellets were resuspended in Bugbuster® Mastermix (Novagen®, Merck-Millipore) (6 ml Bugbuster® to 1 g of pellet). The lysate was centrifuged at 16,000 x g for 20 minutes, the supernatant was removed and resuspension in Bugbuster® Mastermix was repeated with six times the volume of Bugbuster® Mastermix diluted one in ten with ultrapure water, before centrifuging as before to obtain the inclusion body pellet. The pellet was resuspended to 10 mg/ml, based on OD280 measurements, in solubilisation buffer (20 mM Tris, 150 mM NaCl, 5 mM $CaCl_2$, 5 % (v/v) glycerol, 8 M urea) at pH 7.4. Particulate matter was removed by centrifuging at 9,000 x g for 20 minutes. The supernatant was dialysed by placing in SnakeSkin™ dialysis tubing (10 KDa molecular weight cut off) (Thermo Scientific, Pierce) and exchanging solubilisation buffers from 4 M urea, 2 M urea, 1 M urea to 0 M

urea; each buffer was left for three hours at room temperature or overnight at 4 °C with gentle stirring. Finally 0 M urea without glycerol was exchanged every one to two hours for a total of ten litres. The dialysate was centrifuged at 9,000 x g for 15 minutes. The rfhSP-D was purified using affinity chromatography to separate the correctly refolded, biologically active rfhSP-D from denatured rfhSP-D, using the ÄktaAmicro™ (GE Healthcare). The dialysed supernatant was loaded onto a ManNAc-Sepharose column, equilibrated in 20 mM Tris and 150 mM NaCl (TBS) containing 5 mM $CaCl_2$ (TBS-$CaCl_2$) at pH 7.4. The ManNAc-Sepharose column was produced in-house as per the protocol published by Sorensen et al. [237]. In brief, ManNAc (Sigma-Aldrich) was immobilised onto Sepharose CL-4B (GE Healthcare) using divinylsulfone-mediated covalent crosslinking. The Sepharose CL-4B gel (20 ml) was activated with 0.5 M Na_2CO_3 and divinylsulfone for 90 minutes at room temperature. The gel was washed in water and further washed in 0.5 M Na_2CO_2. ManNAc (10 % w/v) was coupled to the activated Sepharose CL-4B by overnight incubation in 0.5 M Na_2CO_3, the final column volume was 20 ml. After washing with water the reactive groups were blocked by incubation with 100 mM ethanolamine for two hours at room temperature. After a final wash with water the gel was stored in TBS until use. After loading the dialysed supernatant onto the ManNAc-Sepharose column the non-specific proteins were eluted with a high salt buffer wash of TBS containing 1 M NaCl at pH 7.4. The column was then equilibrated back to TBS-$CaCl_2$, pH 7.4 and rfhSP-D protein fractions were eluted with TBS containing 10 mM EDTA at pH 7.4. The peak fractions were gel filtered on a Superdex 200 column (GE Healthcare) using TBS containing 5 mM EDTA at pH 7.4 as the running buffer. Protein was frozen at -20 °C until required.

Endotoxin levels in the rfhSP-D preparations were reduced by the use of a Detoxi-gel endotoxin removing column (Thermo Scientific, Pierce) on the ÄktaAmicro™. The Detoxi-gel column was regenerated by washing with three column volumes of milliQ water, three column volumes of 1 % (w/v) sodium deoxycholate (Sigma-Aldrich) in Limulus Amebocyte Lysate (LAL) reagent water (Lonza), then another three column volumes of LAL reagent water and finally three column volumes of sterile PBS. The rfhSP-D was concentrated using Amicon Ultra 30,000 MWCO centrifugal filters and loaded onto the column. Unbound rfhSP-D, not containing endotoxin, that was eluted from the column with PBS was collected in sterile tubes and frozen at -20°C until endotoxin level testing as detailed in section 2.1.7. The column was regenerated as before but the final PBS wash was replaced by 20 % (v/v) ethanol.

4.2.2 Purification of nhSP-D from Amniotic Fluid

Amniotic fluid was collected with informed consent as per ethics number 09/H0502/9 approved by the Southampton and South West Hampshire Research Ethics Committee. Amniotic fluid was pooled, brought to 10 mM EDTA, filtered using a 100 μm mesh to remove large particulate matter and centrifuged for 20 minutes at 10,000 x g. The supernatant containing the nhSP-D was brought to 25 mM $CaCl_2$ and 0.05 % emulphogene (polyoxythylene 10-tridecyl ether) (Sigma-Aldrich) and adjusted to pH 7.4 by addition of bicarbonate buffer. 0.2 % (w/v) azide was also added to prevent bacterial growth, this was then stirred for 30 minutes at room temperature. ManNAc-Agarose beads were equilibrated in TBS-$CaCl_2$ buffer by centrifuging the beads at 160 x g and replacing the buffer three times. The equilibrated beads were added to the amniotic fluid and stirred overnight at room temperature to allow binding of nhSP-D to the beads. The amniotic

fluid was then filtered through a scintered funnel to recover the beads which were then washed with excess of TBS-$CaCl_2$ buffer. The beads were transferred into a 20 cm XK16 column (GE Healthcare) and allowed to pack down under gravity. Using an ÄktaAmicro™ TBS-$CaCl_2$ was run through the column for one column volume before swapping to TBS containing 1 M NaCl run for one and a half column volumes to dissociate non-specifically bound proteins from the ManNAc-Agarose beads. Elution of nhSP-D from the beads was conducted by running two column volumes of TBS containing 10 mM EDTA through the column.

4.2.3 Purification of nhSP-D from Bronchoalveolar Lavage Fluid

BAL from therapeutic lung washings of alveolar proteinosis patients was collected with informed consent as per ethics number 10/H0504/9 approved by the Southampton and South West Hampshire Research Ethics Committee. The method published by Strong *et al.* was followed [26]. BAL was pooled and made to 10 mM EDTA and pH 7.4 using 20 mM Tris; this was stirred for one hour at room temperature before centrifugation at 10,000 x g for 45 minutes. The nhSP-D containing supernatant was kept at -20 °C until being processed further by Mr Paul Townsend. $CaCl_2$ was slowly added to defrosted BAL supernatant to a concentration of 50 mM. ManNAc-Sepharose beads were equilibrated in TBS-$CaCl_2$ buffer and added to the nhSP-D containing supernatant; this was stirred overnight at 4 °C. The ManNAc-Sepharose beads were packed into a column and washed with a high salt buffer (TBS containing 1 M NaCl) to elute non-specifically bound proteins. Bound nhSP-D was eluted with TBS containing 100 mM $MnCl_2$, and immediately buffer exchanged in to TBS containing 5 mM EDTA, pH 7.4, using 30 K MWCO Amicon Ultra Centrifugal Filtration Units (Merck Millipore). The nhSP-D was further purified using gel filtration

chromatography using a Superose 6 column (GE Healthcare), equilibrated with TBS containing 5 mM EDTA, pH 7.4.

4.2.4 Purification of nhSP-A from Bronchoalveolar Lavage Fluid

nhSP-A was extracted from pellets resulting from centrifugation of BAL from alveolar proteinosis patients as detailed in section 4.2.3. The method used was established by Jo Rae Wright, the protocol was obtained via direct communication; the method is similar to that published [238]. The pellet was drop-wise added to a 50 times volume excess of 1-butanol and stirred at room temperature for 30 minutes. This was spun at 10,000 x g for 30 minutes at 4 °C; pellets were resuspended in 1-butanol and re-spun. The pellets were dried under a steady flow of nitrogen and the dry pellets were resuspended in 20 mM Octyl β-D-glucopyranoside (OGP) (Sigma-Aldrich), 150 mM NaCl, 5 mM Tris, (OGP/NaCl/Tris) pH 7.4 and dounced. This was centrifuged at 114,500 x g for 30 minutes at 4 °C and the resulting pellet resuspended in OGP/NaCl/Tris and dounced before repeating the centrifugation. The pellet was resuspended in Tris-buffered water (TBW) (5 mM Tris, pH 7.4) and made to 100 mM OGP before mixing for 30 minutes at room temperature. To remove endotoxin polymyxin B beads (Sigma-Aldrich) were added to the nhSP-A preparation and dialysed for 48 hours at room temperature in four changes of TBW using SnakeSkin™ dialysis tubing (10,000 Da MWCO) (Thermo Scientific, Pierce). The nhSP-A was centrifuged at 3000 x g for 10 minutes to remove polymyxin beads, the supernatant was aliquoted and stored at -20 °C until use.

4.2.5 Protein Concentration Determination

The protein concentration of surfactant protein preparations was calculated according to Beer-Lambert Law: $OD280 = \varepsilon_{OD280} \times C \times L$. Where OD280 is the optical density of the sample at 280 nm, ε is the extinction coefficient, C is concentration and L is the length of the light path. The extinction coefficients used were 18825 $M^{-1} cm^{-1}$ for nhSP-D, 15720 $M^{-1} cm^{-1}$ for rfhSP-D and 28920 $M^{-1} cm^{-1}$ for nhSP-A as calculated using the ExPASy Server ProtParam programme (http://www.expasy.org/tools/protparam.html).

4.2.6 Validation of Collectin Biological Activity

The biological activity of the purified nhSP-A, nhSP-D and rfhSP-D proteins were validated using an *in vitro* cell culture infectivity assay with IAV based on the assay conducted by Hawgood and colleagues [101]. The assays were conducted by Jacqueline Pugh and Zofi McKenzie. The assays were carried out on Madin-Darby canine kidney (MDCK) cells that had been seeded three hours prior to infection at 1.5×10^5 cells per well in a 48 well plate (Greiner Bio-One Ltd, Stonehouse, UK) in Roswell Park Memorial Institute 1640 (RPMI) medium (Invitrogen) containing 10 % FCS (Sigma-Aldrich) and 50 U/ml penicillin and 50 U/ml streptomycin (both Invitrogen). The strain of IAV used was X-79. X-79 is a H3N2 strain of IAV, it is a laboratory derived strain that is a reassortment of A/PR/8/34 (H1N1) in the core and A/Philippines/82 (H3N2) on the surface. The X-79 strain has been adapted for mouse studies [239]. The X-79 IAV purified on a sucrose gradient (kind gift of Zofi McKenzie) was incubated with the indicated concentration of collectin in serum free RPMI medium for one hour at room temperature with agitation. The volume of IAV was established by preliminary experiments to result in 20 % of cells being infected. The inoculum was applied to the MDCK cells that had been washed twice with serum free RPMI medium.

The inoculum was incubated on the cells for one hour at 37 °C and 5 % CO_2 before being washed twice with serum free RPMI media and incubated with 250 µl serum free RPMI medium per well for 17 hours at 37 °C and 5 % CO_2.

The cells were removed from the plate and stained for flow cytometry as described in section 2.1.8, except the primary antibody was a monoclonal mouse-anti-IAV nucleoprotein (Abcam, Cambridge, UK) used at a concentration of 6.87 µg/ml and the wash buffer and antibody diluent was PBS containing 0.3 % Triton X-100.

4.3 Results

4.3.1 Expression and Purification of rfhSP-D

For studies investigating interactions between rfhSP-D and HRVs large stocks of rfhSP-D were required. *E. coli* transformed to express rfhSP-D were grown, inclusion bodies were isolated and solubilised in urea. After dialysis of the rfhSP-D to refold the protein the rfhSP-D was purified by affinity chromatography to isolate correctly folded and functional rfhSP-D. In buffer containing 5 mM $CaCl_2$ to facilitate rfhSP-D binding, rfhSP-D was applied to a ManNAc-Sepharose column. A 1 M NaCl wash was conducted to elute non-specifically bound protein before washing using an EDTA buffer to dissociate rfhSP-D from the column and thus recover pure, functional rfhSP-D, Figure 4-1.

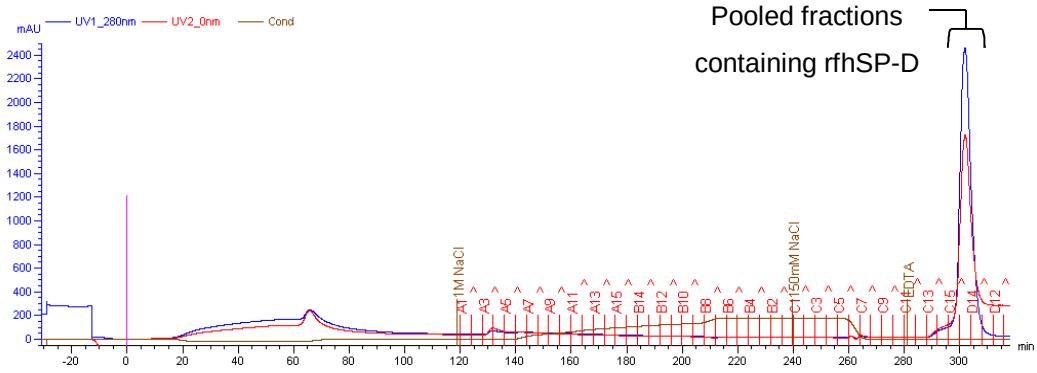

Figure 4-1 Affinity purification of rfhSP-D using ManNAc-Sepharose column. Chromatogram of affinity chromatography to purify rfhSP-D. Sample containing rfhSP-D was loaded onto a ManNAc-Sepharose column at time 0 minutes in TBS-$CaCl_2$, a TBS containing 1 M NaCl wash was conducted to elute non-specifically bound protein before returning to TBS-$CaCl_2$ buffer. Flowing EDTA buffer over the column eluted rfhSP-D, as indicated.

Affinity purified rfhSP-D was gel filtered using a Superdex 200 column to further increase rfhSP-D purity. The rfhSP-D protein eluted at 70 ml, as expected for a 60 kDa protein. A representative chromatogram can be seen in Figure 4-2.

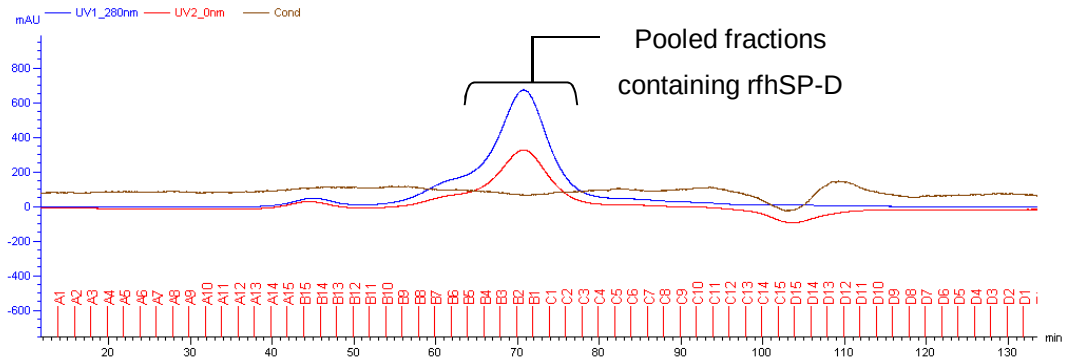

Figure 4-2 Gel filtration of rfhSP-D using a Superdex 200 column. The rfhSP-D was applied to the column in TBS containing 5 mM EDTA at pH 7.4, the rfhSP-D eluted as expected for a protein with an approximate molecular weight of 60 kDa. Fractions, as indicated, containing purified rfhSP-D were pooled.

A pure preparation of rfhSP-D was produced as can be seen by the 18 kDa band on the SDS-PAGE gel and western blot (Figure 4-3), corresponding to the size of reduced rfhSP-D. Two further bands at approximately 40 kDa and 60 KDa can be seen in the rfhSP-D positive control and the rfhSP-D stock; as this was also detected on the western blot. The fractions corresponding to the chromatogram in Figure 4-2 are also shown in Figure 4-3 A. The peak fractions B5 to C2 were pooled to form the rfhSP-D stock. B9, B8 and B7 fractions are from the slight shoulder observed on the gel filtration chromatogram (Figure 4-2); on the SDS-PAGE (Figure 4-3 A) some lower molecular weight proteins of approximately 10 kDa can be seen, these may be degraded protein.

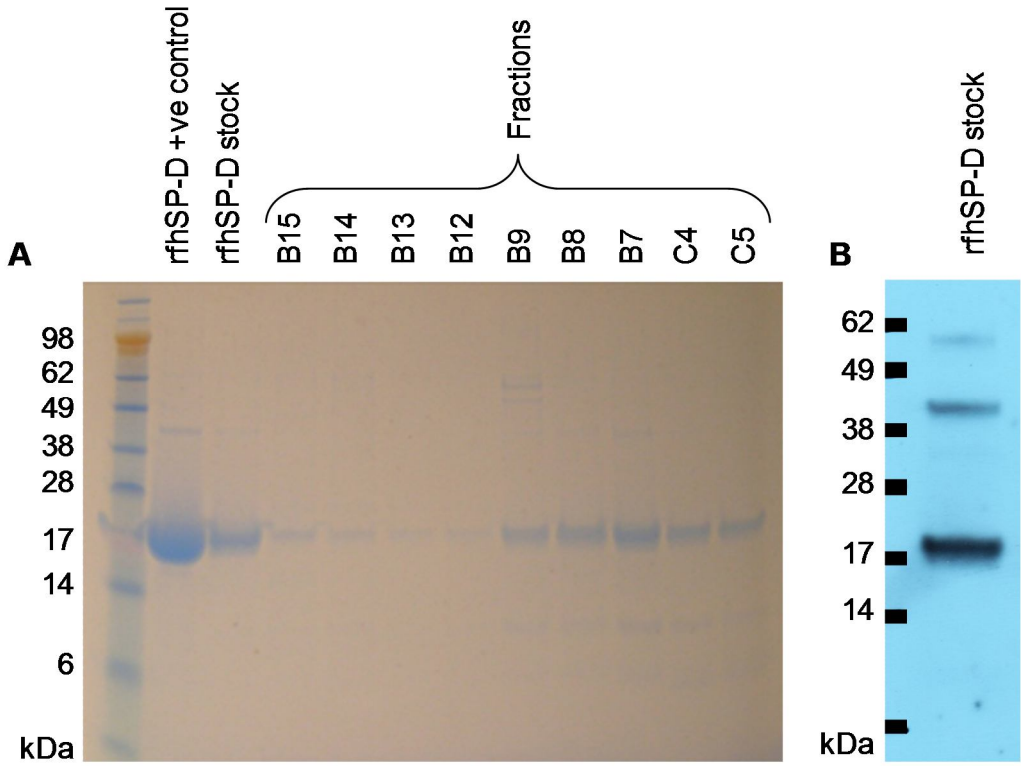

Figure 4-3 SDS-PAGE and western blot analysis of rfhSP-D stock and fractions from gel filtration using a Superdex 200 column shown in Figure 4-2. rfhSP-D was expressed in an *E.coli* system and purified using affinity chromatography and gel filtration. Reduced samples were run on a 12 % NuPAGE gel and either stained using SimplyBlue™ Safestain (**A**); or transferred to PVDF membrane and probed using a rabbit-anti-rfhSP-D antibody and detected using Western Breeze secondary detection kit (Invitrogen) (**B**).

4.3.2 Removal of Endotoxin from rfhSP-D

Endotoxin must be removed from rfhSP-D preparations due to the nature of the rfhSP-D expression system resulting in high endotoxin levels in rfhSP-D preparations. Endotoxin contamination may result in cellular responses that are not attributable to the rfhSP-D, or reduce the binding capacity of rfhSP-D due to endotoxin occupying binding sites. A Detoxi-gel column was used to remove rfhSP-D that was bound to endotoxin, allowing non endotoxin

bound rfhSP-D to be recovered; a typical chromatogram showing this process is shown in Figure 4-4.

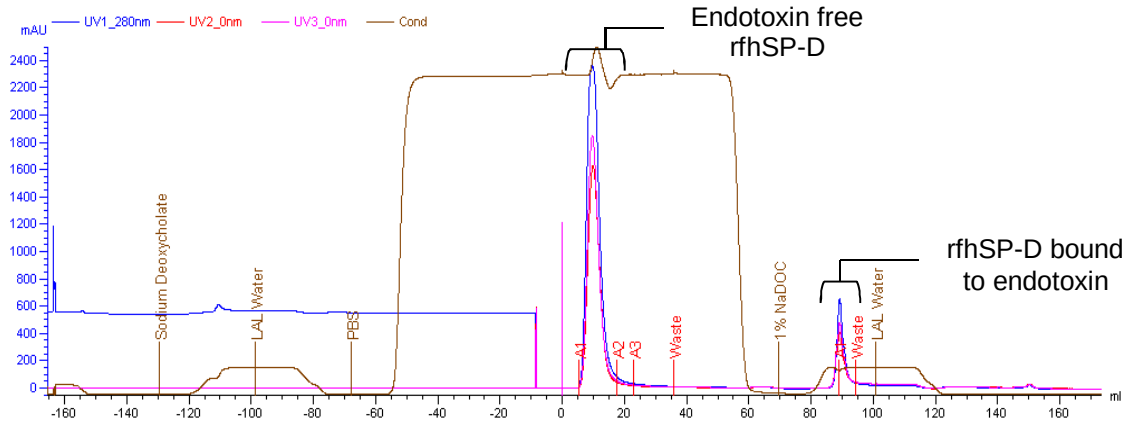

Figure 4-4 Chromatogram of endotoxin removal from rfhSP-D stock using Detoxi-Gel. After preparing the column by running a sodium deoxycholate buffer, endotoxin free water and then PBS (the sample buffer), rfhSP-D purified by affinity chromatography and gel filtration was passed over the Detoxi gel to remove endotoxin contamination from stock of rfhSP-D.

A peak containing endotoxin free rfhSP-D can be seen in the chromatogram, Figure 4-4, approximately 5 ml after the rfhSP-D was loaded onto the column, at 0 ml. A second peak of rfhSP-D can be seen after the final 1 % sodium deoxycholate wash, this wash removes protein that has bound to the column, and is therefore the rfhSP-D that was bound to endotoxin.

The chromatogram, Figure 4-4, correlates with analysis of each stage of endotoxin removal by SDS-PAGE, Figure 4-5. The flow through just before the first peak (Figure 4-5, lane 2) contained no protein. The pre-treatment sample was concentrated prior to loading onto the Detoxi-gel, a large band at 18 kDa shows the presence of rfhSP-D (Figure 4-5, lane 3). Faint bands can also be seen at approximately 6 and 12 kDa, suggesting breakdown products of the rfhSP-D; another band at approximately 40 kDa which may correspond to a dimer of rfhSP-D. The first peak (Figure 4-5, lane 4) clearly

contains rfhSP-D as a clear band is visible at 18 kDa. The A3 sample (Figure 4-5, lane 5) taken after the first peak shows that no rfhSP-D was still coming off the column. The post endotoxin sodium deoxycholate wash that created a second peak did contain rfhSP-D, and this is the endotoxin contaminated rfhSP-D that was therefore bound to the column (Figure 4-5, lane 6).

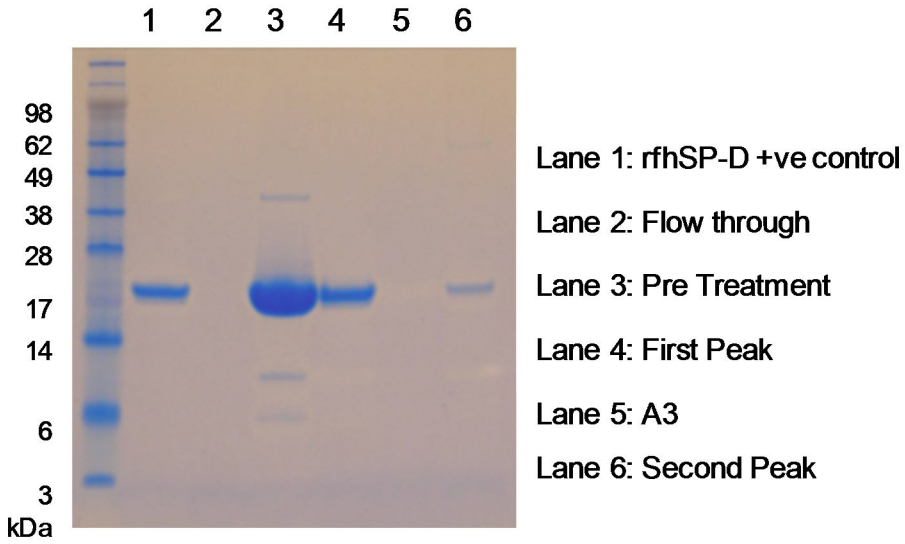

Figure 4-5 SDS-PAGE of stages of endotoxin removal from rfhSP-D using Detoxi gel shown in Figure 4-4. rfhSP-D was passed over Detoxi-gel column in PBS buffer, stages were analysed by reducing samples and running on a 12 % NuPAGE gel and stained using SimplyBlue™ SafeStain.

The Detoxi-gel treated rfhSP-D was tested for endotoxin levels using the quantitative LAL assay as per manufacturer's instructions. From an average of duplicate wells the rfhSP-D stock was found to contain 58 Endotoxin Units (EU)/mg rfhSP-D prior to Detoxi-gel treatment and 27 EU/mg rfhSP-D after Detoxi-gel treatment.

4.3.3 Purification of nhSP-D from Amniotic Fluid

Binding studies between nhSP-D and HRVs require pure stocks of nhSP-D. Isolation and purification of nhSP-D from amniotic fluid was conducted using ManNAc-agarose affinity chromatography, the chromatogram is shown in Figure 4-6.

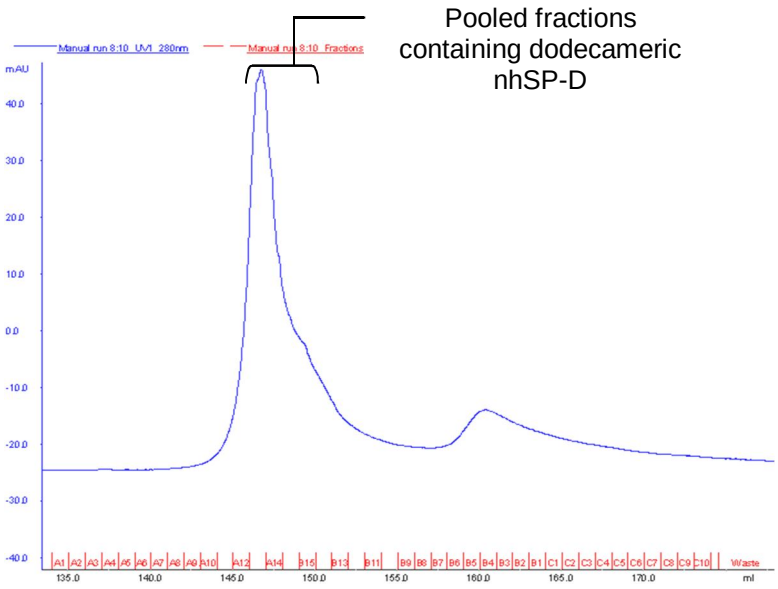

Figure 4-6 Chromatogram of affinity purification of nhSP-D from amniotic fluid using ManNAc-agarose. nhSP-D was isolated and purified from amniotic fluid by affinity chromatography using ManNAc-agarose beads in the presence of calcium and eluted in the presence of EDTA. Shown here is the EDTA elution and nhSP-D can be seen in fractions A12, A13, A14, A15, B15, B14, B13 and B12, as indicated.

Amniotic fluid samples taken before processing, after centrifugation to remove cellular debris, post addition of ManNAc-agarose beads and post affinity chromatography were analysed by SDS-PAGE and western blot for the presence of nhSP-D, Figure 4-7.

The SDS-PAGE (Figure 4-7 A.) demonstrates that samples 1, 2 and 3 contained a large number of proteins; the western blot of the same samples

(Figure 4-7 B.) identifies the protein band at 49 kDa as nhSP-D. The amniotic fluid preparation to which ManNAc-agarose beads had been added shows that not all the nhSP-D was removed by the beads as after removal some nhSP-D remained (Figure 4-7 B. Sample 3).

The fractions taken before the peak containing nhSP-D, A10 and A11 contained nhSP-D at a lower concentration than the pooled peaks (A12, A13, A14, A15, B15, B14, B13 and B12) as shown by a less dark band on the western blot (Figure 4-7 B.). A second band at approximately 98 kDa was detected on the western blot, corresponding to a dimer of nhSP-D that has not been fully reduced. Fractions B5, B4 and B3 are from the second peak seen on the gel filtration chromatogram, Figure 4-6, these fractions also contained nhSP-D with a molecular weight of 49 kDa as shown by western blotting.

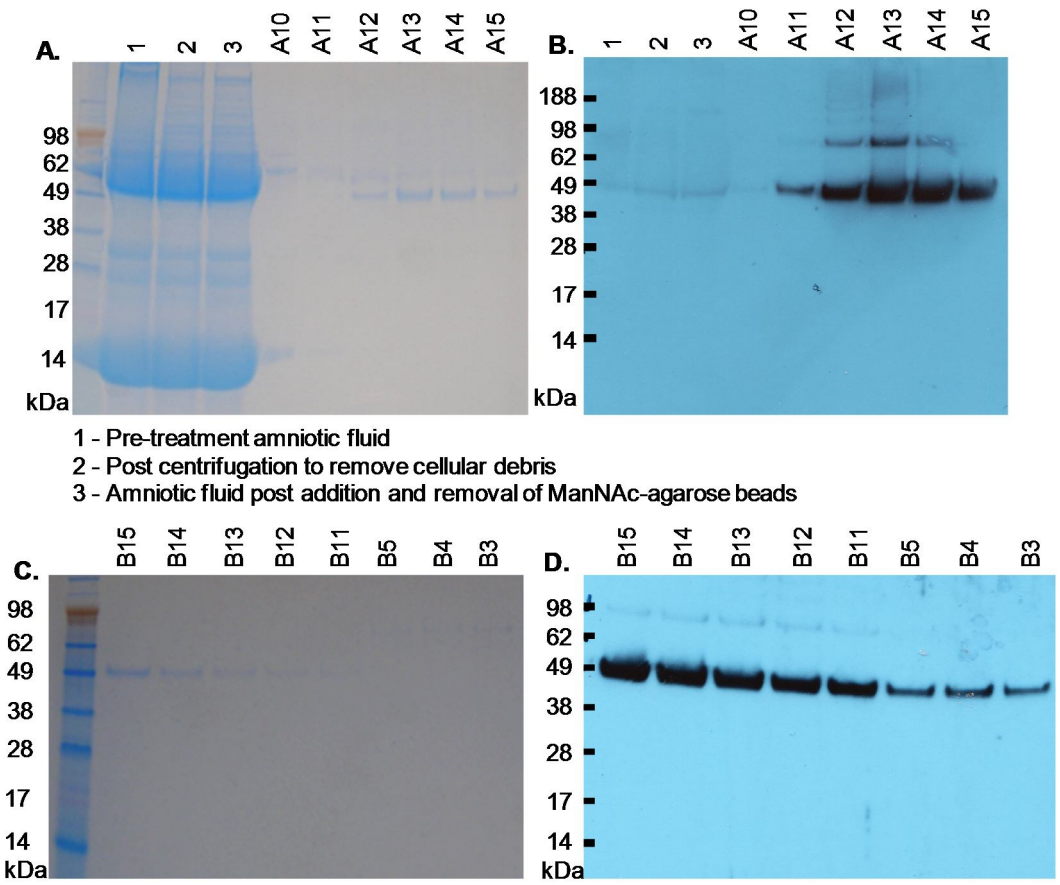

Figure 4-7 SDS-PAGE (A. and C.) and western blot (B. and D.) analysis of nhSP-D purification from amniotic fluid. Amniotic fluid samples and fractions from affinity chromatography, as indicated, were analysed. Reduced samples were run on 12 % NuPAGE gels; for western blotting proteins were transferred to PVDF membrane and probed using a biotinylated rabbit-anti-SP-D primary antibody. SDS-PAGE gels were stained using SimplyBlue™ SafeStain.

4.3.4 Purification of nhSP-D from BAL

nhSP-D was purified from BAL of alveolar proteinosis patients using affinity chromatography and gel filtration, Figure 4-8. Affinity chromatography and gel filtration were conducted by Paul Townsend.

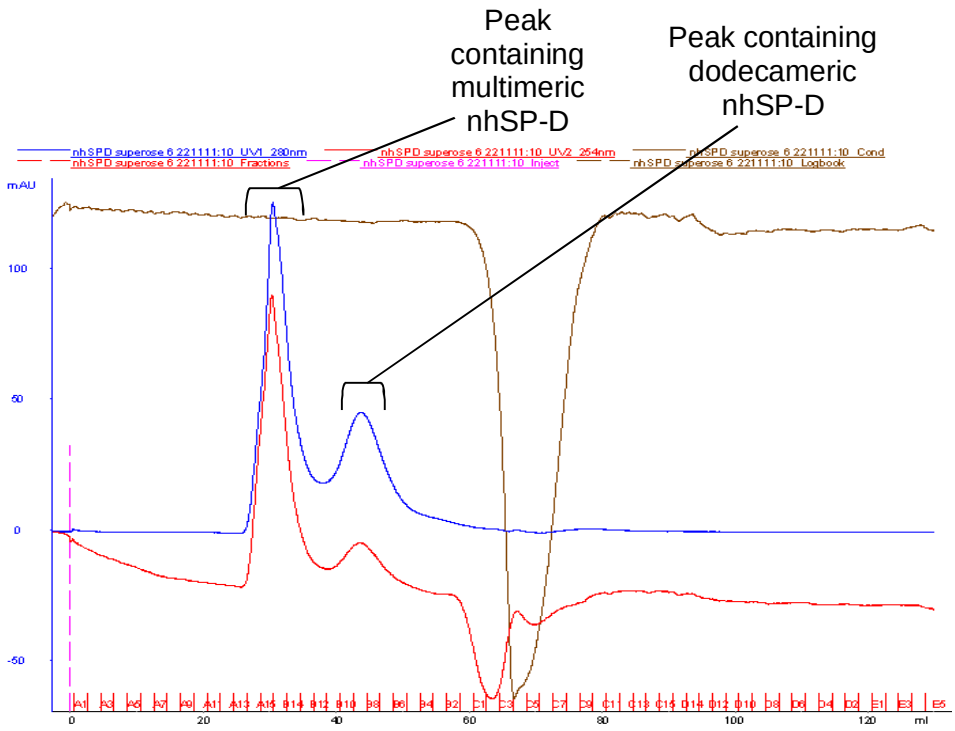

Figure 4-8 Gel filtration of nhSP-D using a Superose 6 column. The nhSP-D purified from BAL by affinity chromatography using ManNAc-Sepharose beads was further purified by applying to a Superose 6 column in TBS containing 20 mM EDTA at pH 7.4. Fractions corresponding to dodecameric nhSP-D and multimeric nhSP-D, as indicated, were pooled. Purification conducted by Paul Townsend.

The purified nhSP-D preparations were analysed by SDS-PAGE and western blot. As can be seen in Figure 4-9 the multimeric and dodecameric nhSP-D preparations purified from BAL both contain a band at 49 kDa, corresponding to the size of reduced nhSP-D. There is an additional band present at 90 kDa in both preparations corresponding to the size of dimerised nhSP-D. There is a higher molecular weight band in the multimeric nhSP-D preparation that could correspond to the size of trimeric nhSP-D, however above 98 kDa the accuracy of size determination is limited due to the nature of the protein standard used. SDS-PAGE analysis showed no further bands, and was consistent with the nhSP-D purified from amniotic fluid see in Figure 4-7 A and C.

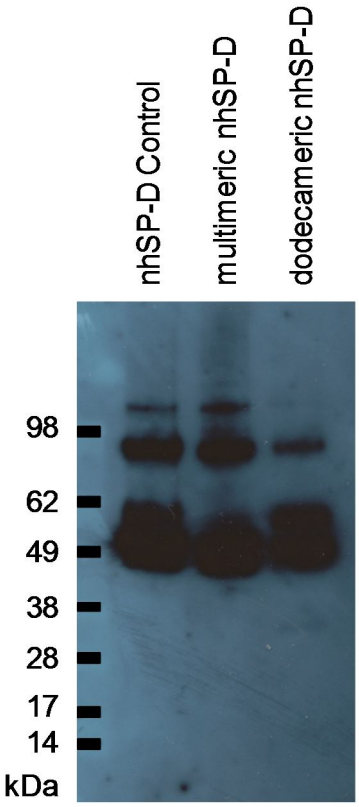

Figure 4-9 Western blot analysis of nhSP-D preparations purified from BAL. Reduced samples were run on a 12 % NuPAGE gel and transferred to PVDF. The membrane was probed using a rabbit-anti-rfhSP-D antibody and this was detected using a goat-anti-mouse-HRP conjugated secondary antibody (Invitrogen) and ECL™ Advance (GE Healthcare Life Sciences).

4.3.5 Purification of nhSP-A from BAL

Stocks of nhSP-A were produced using butanol extraction from BAL from patients with alveolar proteinosis. This is a well-established method developed by Jo Rae Wright.

Figure 4-10 shows western blot and SDS-PAGE analysis of purified nhSP-A; on both the western blot and SDS-PAGE gel a clear band can be seen at 36 kDa, this corresponds to the size of nhSP-A. Two further bands are present at 60 KDa and approximately 90 KDa; these are likely to be dimerised and

trimerised nhSP-A respectively as they were detected by the anti-nhSP-A primary antibody. On SDS-PAGE there are no bands present other than those corresponding to nhSP-A, indicating that this is a clean protein preparation.

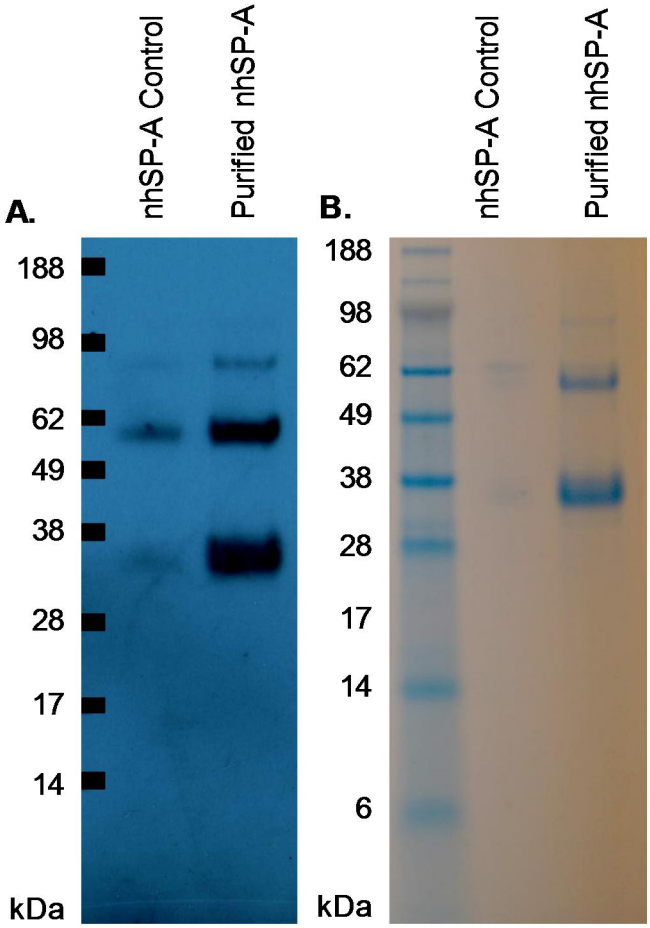

Figure 4-10 Purified stock of nhSP-A. nhSP-A was purified from BAL of patients with alveolar proteinosis using butanol extraction. Pure nhSP-A was assessed using western blot (**A**), using a rabbit-anti-nhSP-A primary antibody and Invitrogen western breeze secondary antibody and chemiluminescent substrate; SDS-PAGE (**B**), samples were run on a 12 % NuPAGE gel and stained with SimplyBlue™ SafeStain.

As part of rigorous quality control to ensure the purity of nhSP-A, a western blot of nhSP-A probed with an anti-rfhSP-D antibody was conducted to

ensure no contamination with nhSP-D. The western blot, Figure 4-11, showed no 49 kDa band corresponding to the size of nhSP-D in the purified nhSP-A stock, Figure 4-10. There are bands at 36 kDa, 60 kDa, and 90 kDa as would be expected if the blot had been probed for nhSP-A, as these correspond to the size of nhSP-A oligomers.

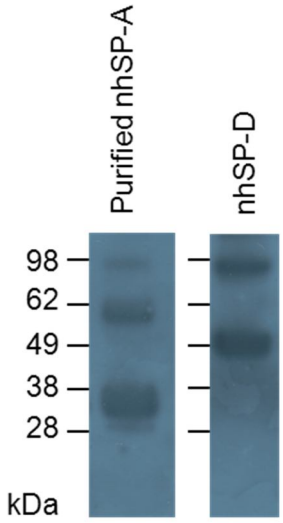

Figure 4-11 Verification of no contamination of nhSP-A preparation with nhSP-D. nhSP-A was purified from BAL from patients with alveolar proteinosis using butanol extraction. Purified nhSP-A was assessed using SDS-PAGE and western blot to ensure no contamination of the protein with nhSP-D. Proteins were run on a 12 % NuPAGE gel, transferred to PVDF and probed using an anti-rfhSP-D primary antibody (which also detects nhSP-D) and Invitrogen western breeze secondary antibody and chemiluminescent substrate.

At the end of the purification process for nhSP-A polymyxin beads were added to the preparation to remove endotoxin bound nhSP-A. This resulted in removal of the majority of endotoxin as using the LAL assay the endotoxin level in the nhSP-A was found to be 1.6 EU/mg nhSP-A.

4.3.6 Validation of Collectin Biological Activity

The biological activity of the purified collectins were validated using an *in vitro* cell culture infectivity assay with IAV, based on a method developed by Hawgood and colleagues [101]. Assessment of infectivity was using the technique of flow cytometry to ensure the collectins functioned as expected when incubated with X-79 IAV. The X-79 (H3N2) strain of IAV is a laboratory derived strain that is a reassortment of A/PR/8/34 (H1N1) and A/Philippines/82 (H3N2) adapted for mouse studies, it is highly glycosylated and has been shown in *in vitro* studies to be inhibited by SP-D and SP-A [101]. IAV has been shown to be neutralised by nhSP-A and nhSP-D, whereas rfhSP-D has no effect [65, 104, 229, 240, 241].

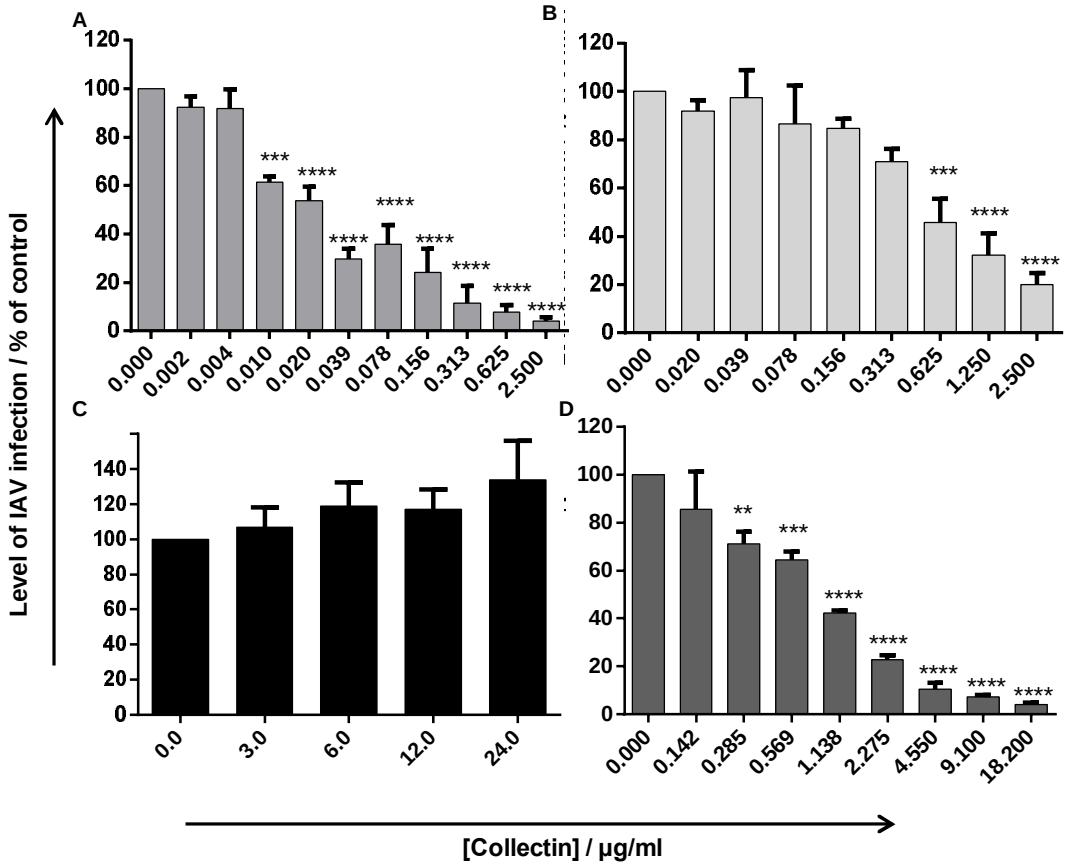

Figure 4-12 Effect of multimeric nhSP-D (A), dodecameric nhSP-D (B), rfhSP-D (C) and nhSP-A (D) on infectivity of IAV. Infectivity was assessed by flow cytometry. IAV was pre-incubated for one hour with collectins before addition to monolayers of MDCK cells, after one hour at 37 °C cells were washed with serum free RPMI and incubated for 17 hours at 37 °C, 5 % CO_2. Cells were removed from the plate with trypsin, fixed in 1 % paraformaldehyde in PBS, washed with PBS containing 0.3 % Triton X-100 and incubated with a mouse anti-IAV NP primary antibody which was detected using a goat-anti-mouse-APC conjugated secondary antibody. The number of IAV infected cells was quantified using a FACS ARIA and analysed using FlowJo software version 7.6.5. Data is normalised to the infected control with no collectin. Values are means + S.E.M of at least three experiments, conducted by Jacqueline Pugh or Zofi McKenzie. * $p<0.05$, ** $p<0.01$, *** $p<0.001$, **** $p<0.0001$ indicates mean is significantly different to mean of control where no collectin is present determined using one-way ANOVA.

Figure 4-12 shows that multimeric nhSP-D, dodecameric nhSP-D and nhSP-A all inhibited IAV infection in a dose dependent manner, whereas rfhSP-D did not inhibit infection.

4.4 Discussion

The aim of this project was to investigate if there was an interaction between collectins, SP-A and SP-D, and HRV. The collectin preparations used were nhSP-A, dodecameric nhSP-D, multimeric nhSP-D and rfhSP-D. As discussed previously, rfhSP-D has advantages over nhSP-D as a therapeutic and in this project rfhSP-D was tested against two preparations of nhSP-D, dodecameric nhSP-D and multimeric nhSP-D. Dodecameric nhSP-D is the oligomeric form of nhSP-D consisting of four trimers bound at the N-terminus in a crucifix formation, whereas multimeric nhSP-D has a higher order of multimerisation with as many as eight dodecameric nhSP-D molecules associated with one another [39]. Stocks of rfhSP-D were expressed and purified. When the rfhSP-D stock was analysed by SDS-PAGE and western blot under reducing conditions an 18 kDa band, corresponding to the size of monomeric rfhSP-D, was clearly seen. Two further faint bands of approximately 40 kDa and 60 kDa are also visible; this is likely dimerised and trimerised rfhSP-D that has not been fully reduced as it was detected with the anti-rfhSP-D antibody. In fractions taken either side of the peak containing rfhSP-D small bands of approximately 10 kDa were observed, these are possibly degraded fragments of rfhSP-D.

nhSP-D was purified from amniotic fluid using affinity chromatography. On the chromatogram it is possible to see two peaks, both of which contained a 49 kDa band, corresponding to the size of reduced monomeric nhSP-D. The first peak is the dodecameric nhSP-D stock. The second peak contains

multimeric nhSP-D, these bound with greater avidity to the column due to the synergistic action of the CRDs and thus took longer to dissociate. It is worth noting that in some previous reports of nhSP-D analysis by SDS-PAGE the protein appears as a 43 kDa band, whilst in the system used in this project nhSP-D is a 49 kDa band [26, 237]. This discrepancy is likely due to the different buffer systems used as a laboratory using the same buffer system as in this laboratory also observe monomeric nhSP-D as a 49 kDa band [242].

Purification of nhSP-D from BAL of alveolar proteinosis patients was conducted by Paul Townsend. Analysis post affinity chromatography was conducted by Jacqueline Pugh. SDS-PAGE and western blot of the dodecameric and multimeric nhSP-D showed a band at 49 kDa, corresponding to the size of reduced monomeric nhSP-D.

Butanol extracted nhSP-A was assessed using western blot and SDS-PAGE; the SDS-PAGE shows three bands, 36 kDa, 60 kDa and 90 kDa. These correspond to the size of reduced monomeric nhSP-A, dimerised nhSP-A or trimerised nhSP-A respectively. The proteins were confirmed as being nhSP-A as they were detected using an anti-nhSP-A antibody on western blot. The western blot to detect contaminating nhSP-D showed that no nhSP-D was present in the nhSP-A stock. The western blot did however demonstrate that there is cross reactivity between either the anti-rfhSP-D antibody or the secondary anti-rabbit antibody solution and nhSP-A as bands corresponding to the size of nhSP-A were detected.

The preparations of nhSP-A, nhSP-D and rfhSP-D require further attention to reduce endotoxin levels if used in animal studies; the rfhSP-D endotoxin level was 27 EU/mg of protein despite treatment with the Detoxi gel column.

The nhSP-D has not been treated to remove endotoxin is therefore not recommended to be used for animal studies before the level of endotoxin has been determined. Surfactant proteins obtained from BAL of alveolar proteinosis patients are likely to contain high levels of endotoxin due to both nhSP-A and nhSP-D being reported as binding endotoxin and due to these patients commonly suffering a large number of respiratory infections [67, 78, 128, 243]. Whilst the nhSP-A endotoxin level was reduced to 1.6 EU/mg protein this is possibly still higher than is suitable for animal studies. For *in vivo* animal models endotoxin must be reduced before use to prevent eliciting an inflammatory response; the proteins could therefore be tested in an animal before use in experiments to ensure they do not elicit such a response. Previous experiments have shown that SP-D preparations with endotoxin levels up to 0.5 EU/ml do not elicit an inflammatory response in mouse models [244]. This suggests that this level of endotoxin is below that capable of causing inflammation or that the endotoxin bound to SP-D rendered it unable to elicit inflammation. In a study conducted by Wright and colleagues it was found that nhSP-A and nhSP-D treated to remove endotoxin did not elicit nitrate production by alveolar macrophages *in vitro*, this highlights the need to monitor endotoxin levels in these preparations [245]. In binding studies it should be borne in mind that endotoxin in these preparations may reduce HRV binding as the endotoxin may occupy binding sites required by the collectins to bind HRV [246]. The presence of endotoxin in the preparations may alter cellular responses observed when added to cell culture. The functional capacity of endotoxin treated and untreated preparations of SP-D was found to be the same by Restrepo *et al*., as both treated and untreated preparations were able to bind to and stimulate macrophage phagocytosis of *P. aeruginosa* [247]. This suggests that the functional activity of nhSP-A and nhSP-D can be maintained despite endotoxin contamination.

To confirm biological activity of the collectin preparations an IAV neutralisation assay was utilised as it is well documented in the literature that nhSP-D and nhSP-A neutralise the infectivity of IAV [65, 104, 229, 240, 241]. It was demonstrated that all of the preparations of purified native proteins reduced IAV infection in a dose dependent manner. The proteins are therefore biologically active and thus suitable for use in assays to assess their ability to neutralise HRV. The current preparation of rfhSP-D did not reduce the level of IAV infection; this is consistent with previous findings in various laboratories [240].

5. Chapter 5: Binding Studies between Collectins and Rhinovirus

5.1 Introduction

Binding between collectins and other respiratory viruses such as IAV and RSV has been demonstrated [64, 65, 111, 113, 114, 248]. There had been no studies reporting investigations of collectins binding to HRVs. Four different methods were employed in this thesis to deduce if nhSP-A, nhSP-D or rfhSP-D can bind to HRV1B or HRV16; these were a ligand blot, a solid phase binding assay, co-immunoprecipitation and surface plasmon resonance (SPR).

5.2 Materials and Methods

5.2.1 Ligand Blot

SDS-PAGE gels of reduced HRV16 infected and uninfected HeLa cell lysate (19 μl cell lysate per lane was loaded, HRV16 infected cell lysate had a $TCID_{50}$/ml of 3.8×10^4) were run and transferred to PVDF membrane as detailed for western blotting (section 2.1.2). The membranes were blocked in 1 % (w/v) BSA in PBS-Tween for one hour at 37 °C. rfhSP-D was applied to the membrane at the indicated concentration diluted in 5 mM $CaCl_2$ in PBS. The membrane was incubated in rfhSP-D for two hours at 37 °C before washing for 25 minutes with five changes of PBS-Tween. A biotinylated anti-rfhSP-D primary antibody was applied to the membrane at a 1 in 4000 dilution in 1 % (w/v) BSA in PBS-Tween left overnight at 4 °C. The membrane was washed as previously detailed before addition of ExtrAvidin® Peroxidase conjugate (Sigma-Aldrich) diluted 1 in 200 in 1 % (w/v) BSA in PBS-Tween and left 30 minutes at 37 °C. Finally, the membrane

was washed as before and developed as detailed for the western blot (section 2.1.2).

5.2.2 Solid Phase Binding Assay

A volume of 100 µl/well of bicarbonate buffer, pH 9.6, either alone or containing the protein to be immobilised to the 96 well maxisorp plate (Nunc) was added as indicated; this was left overnight at 4 °C. The plate was washed four times with 150 µl/well of TBS-$CaCl_2$ containing 0.05 % (v/v) Tween® 20 (TBS-$CaCl_2$-Tween). Unbound sites were then blocked for one hour at 37 °C using blocking buffer diluted in TBS-$CaCl_2$-Tween as indicated. The plate was washed as before. Either 100 µl/well rfhSP-D or nhSP-D diluted to the appropriate concentration in TBS-$CaCl_2$-Tween was added to the plate and left for one hour at 37 °C. Unbound proteins were washed from the plate as before. The detection antibody, a biotinylated monoclonal mouse anti-human SP-D (Catalogue number: HYB 246-04B, Antibody shop, Gentofte, Denmark) was diluted to 0.5 µg/ml in TBS-$CaCl_2$-Tween and 100 µl/well was left for one hour at 37 °C. The plate was washed as previously, then 100 µl/well Streptavidin-HRP (Sigma-Aldrich) diluted 1: 30,000 in TBS-$CaCl_2$-Tween was added and left 1 hour at room temperature. After washing, as before, the plate was developed by addition of 100 µl/well 3,3',5,5'-tetramethyl-benzidine (TMB) liquid substrate for ELISA reagent (Sigma-Aldrich) until an appropriate colour change was observed; the colour development was stopped using 50 µl/well of 0.5 M H_2SO_4. Absorbance was read at 450 nm using a SpectraMax® 340PC^{384} absorbance microplate reader (Molecular devices, Wokingham, UK).

5.2.3 Co-immunoprecipitation

Sucrose density gradient purified HRV1B (1 ml at 1.10 x 10^7) or HRV16 (1 ml at 1.73 x 10^6) were incubated with 12 μg/ml rfhSP-D for one hour at room temperature with agitation. To bind HRV16 to protein G beads, 2.8 μg/ml of anti-HRV antibody, R16-7, was added and left for a further hour before addition of 20 μl of protein G Agarose beads (Thermo Scientific, Pierce). To bind rfhSP-D to Dynabeads® protein A polystyrene beads (Dynal Biotech, Oslo, Norway) 2 μg/ml of rabbit anti-rfhSP-D antibody was added and left for an hour before addition of 20 μl of the Dynabeads® protein A polystyrene beads. All beads were washed five times in wash buffer (16 mM Tris-HCl, 3 mM Tris-Base, 100 mM NaCl, 5 mM $CaCl_2$, 1 % NP-40, pH 7.4) before use by suspending in 500 μl wash buffer and centrifuging at 13,400 x g for one minute. After beads were added they were left to incubate overnight at 4 °C with agitation.

Tubes were spun to pellet beads and supernatant removed. To wash unbound protein from the beads, 500 μl of wash buffer was added and centrifuged at 13,400 x g. Beads were resuspended in 500 μl of wash buffer and transferred to a clean tube, and centrifuged as before; this was repeated a total of five times. To remove proteins from the beads 6.25 μl NuPAGE® SDS sample buffer and 2.5 μl reducing agent (both Invitrogen) were added and heated for 10 minutes at 70 °C. The samples were then run on 12 % NuPAGE® Bis-Tris gels and transferred to PVDF membrane and probed for either rfhSP-D or HRV as described for western blotting, in section 2.1.2.

5.2.4 Surface Plasmon Resonance

All SPR experiments were conducted using a BIACORE®3000 (Biacore) which allows real-time biomolecular interaction analysis (BIA) using SPR

technology. Proteins were immobilised onto a CM5 chip (GE Healthcare) by amine coupling using an amine coupling kit (GE Healthcare). This involves activation of the chip surface using a mix of 1-ethyl-3-(3-dimethylaminopropyl) carbodiimide hydrochloride (EDC) and N-hydroxysuccinimide (NHS). The proteins were diluted to 59 µg/ml for dodecameric nhSP-D, 40 µg/ml for multimeric nhSP-D, 24 µg/ml for rfhSP-D and 181 µg/ml for nhSP-A in 10 mM NaOAc buffer (pH 5.0) (Bio-Rad) and flowed over the flow cell at 10 µl/min for seven minutes. The running buffer during immobilisation was HBS-N buffer (0.01 M HEPES, 0.15 M NaCl, and pH 7.4) (GE Healthcare). To inactivate the chip surface 1 M ethanolamine-HCl pH 8.5 was used. An empty flow cell was used as a background control for binding.

To detect binding to the immobilised proteins UV inactivated HRV16 or HRV1B was dialysed overnight at 4 °C into HBS-N running buffer containing 5 mM $CaCl_2$ (HBS-N-5 mM $CaCl_2$) (GE Healthcare); varying concentrations of each dialysed virus was titrated and flowed over the flow cells at 10 µl/min for five minutes in HBS-N-5 mM $CaCl_2$ at 25 °C. Inhibition studies were also conducted in which HRV16 or HRV1B were diluted with different concentrations of sugars. Complexes were allowed to disassociate for five minutes and the chip surface was regenerated with a 20 µl pulse of 20 mM EDTA. Flow cells were re-equilibrated with five washes of HBS-N-5 mM $CaCl_2$ at 10 µl/min for five minutes.

To establish if binding is calcium dependent, UV inactivated HRV16 and HRV1B were diluted 1 in 9 in either a HBS-N-5 mM $CaCl_2$ or HBS-EP buffer (Teknova, Hollister, California, USA) (containing 3 mM EDTA). The HRVs were flowed over the immobilised proteins as described above. Running buffer for the experiment was the buffer in which the HRV had been diluted.

To map the site of binding to HRV, a 1 in 9 dilution of HRV1B was pre-incubated with R16-7 mAb at several concentrations, as indicated, for one hour at room temperature with agitation. The HRV1B/R16-7 mixture or R16-7 alone was flowed over immobilised dodecameric nhSP-D, multimeric nhSP-D and rfhSP-D.

In all experiments the response for binding to an empty flow cell were subtracted from responses for binding to flow cells containing immobilised proteins. To account for any non-specific binding data was double referenced by subtracting responses of buffer alone passed over the immobilised proteins. Data was analysed using BIAevaluation software version 4.1 and BIAsimulation software version 3.1. Concentration of HRV preparations was determined using a NanoDrop 1000 spectrophotometer (Thermo Scientific) and the formula 1 OD_{260} = 9.4 x 10^{12} virus particles (v.p.)/ml [249]. The association rate constant (k_a), dissociation rate constant (k_d) and the equilibrium dissociation constant ($K_D = k_d / k_a$) were calculated using the BIAevaluation software version 4.1 using the Langmuir binding model for kinetic analysis. Molar ratios for binding were calculated as described by Doss and colleagues using the formula *ab/cd*, where *a* is the level of binding at five minutes, *b* is the oligomeric mass of immobilised SP-D, *c* is the mass of HRV (8000 kDa), and *d* is the amount of SP-D immobilised to the biosensor surface (in RUs) [250]. The molar ratio represents the moles of analyte (HRV) bound per moles of immobilised ligand (SP-D) at the end of the five minute binding phase. The molar ratios were calculated assuming oligomeric molecular masses of 1.7 MDa, 512 kDa and 54 kDa for multimeric nhSP-D, dodecameric nhSP-D and rfhSP-D respectively.

5.3 Results

5.3.1 HRV and rfhSP-D Ligand Blot

As an initial investigation into whether rfhSP-D can bind HRV16 a ligand blot was conducted as this had previously been used to identify binding of the collectin MBP to IAV [251]. Reduced HRV16 infected HeLa cell lysate was run on SDS-PAGE and transferred to PVDF membrane; this was incubated with rfhSP-D at the indicated concentrations, Figure 5-1. Bound rfhSP-D was detected using an anti-rfhSP-D antibody. A HRV16 western blot, stained with the monoclonal RV16-7 antibody directed against VP2 of the HRV capsid, was also conducted on a HRV16 infected HeLa cell lysate sample. The HRV probed for western blot was run and transferred to PVDF simultaneously with PVDF membranes that were incubated with rfhSP-D.

The anti-HRV16 western blot shows presence of VP0 (37 kDa) and VP2 (30 kDa) showing HRV16 proteins are present on the membrane Figure 5-1 F. The membranes incubated in rfhSP-D and then probed for the presence of rfhSP-D (Figure 5-1 A-D) all showed a band at approximately 100 kDa, this was visible in HRV16 infected HeLa cell lysate samples as well as in the uninfected HeLa cell lysate samples, with all concentrations of rfhSP-D (except $0.01\ \mu g/ml$, Figure 5-1 E). With the highest concentration of rfhSP-D ($100\ \mu g/ml$), two more bands were visible, at approximately 65 kDa and 48 kDa, both in the uninfected and HRV16 infected HeLa cell lysate samples. An RSV infected cell lysate, a virus to which rfhSP-D binds, was analysed as a positive experimental control to verify if rfhSP-D would bind to the virus under reduced conditions in a ligand blot; as can be seen in Figure 5-1 A rfhSP-D did not bind the RSV sample, except to bands which appear to be components of the cell lysate.

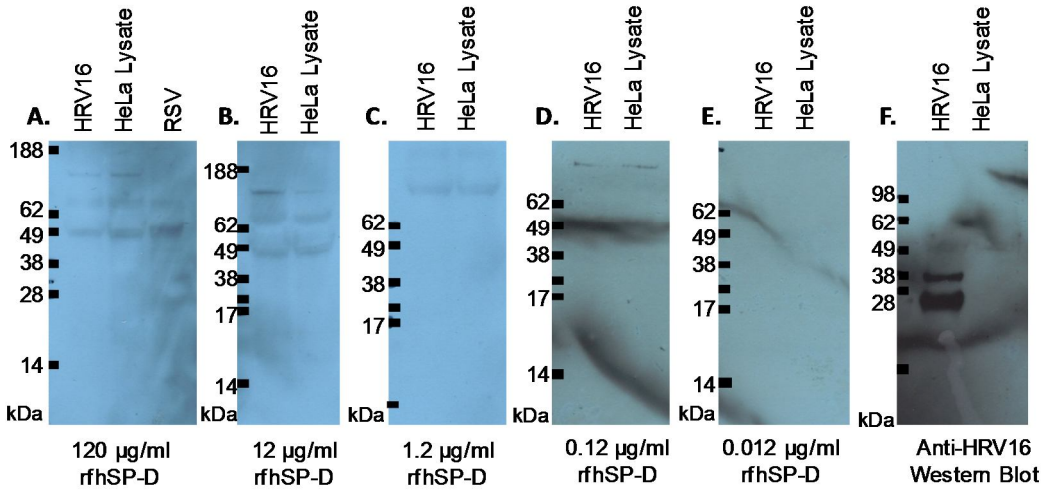

Figure 5-1 Ligand blot of HRV16 and rfhSP-D. Reduced HRV16 infected HeLa cell lysate samples (HRV16) and uninfected HeLa cell lysate (HeLa lysate) were run on SDS-PAGE and transferred to a PVDF membrane; rfhSP-D was incubated on the membrane at various concentrations in 5 mM $CaCl_2$ and after thorough washing with 5 mM $CaCl_2$ maintained, rfhSP-D detected using an anti-rfhSP-D antibody (**A-E**). An anti- HRV16 western blot was also performed on an identical HRV16 infected HeLa cell lysate sample performed simultaneously alongside the rfhSP-D probed membranes (**F**).

5.3.2 Solid Phase HRV and SP-D Binding Assay

To examine if SP-D is able to bind HRV a solid phase binding assay was conducted, this involved immobilisation of HRV16 onto 96 well maxisorp plates and the addition of SP-D in a 5 mM $CaCl_2$ buffer, followed by SP-D detection by an antibody to observe if SP-D had bound to the HRV16.

Hep-2 cell lysate infected with RSV A2 was also immobilised as a positive control as SP-D has been shown to bind RSV A2 [111]; to ensure binding was not to Hep-2C cell proteins a negative control of uninfected Hep-2C cell lysate was also conducted. A titration of rfhSP-D was carried out on varying dilutions of virus infected or uninfected cell lysate, Figure 5-2. Initially

HRV16 infected HeLa cell lysate was used and therefore a negative control of uninfected HeLa cell lysate was included, Figure 5-3.

The positive control for the solid phase binding assay, RSV A2 infected Hep-2C cell lysate did not show successful rfhSP-D binding. There is binding of rfhSP-D to the uninfected Hep-2C cell lysate that is above the level of binding to the equivalent dilution of RSV A2 infected Hep-2C cell lysate (Figure 5-2).

Binding of rfhSP-D to HRV16 infected HeLa cell lysate was no greater than the binding observed to uninfected HeLa cell lysate, Figure 5-3.

A positive control for detection using the biotinylated monoclonal mouse anti-human SP-D antibody and streptavidin-HRP detection method was also included; this involved binding 0.12 μg of rfhSP-D to the maxisorp plate and detecting the immobilised rfhSP-D as was conducted for the other wells. This was successful as an absorbance of 4.0 at 450 nm was recorded.

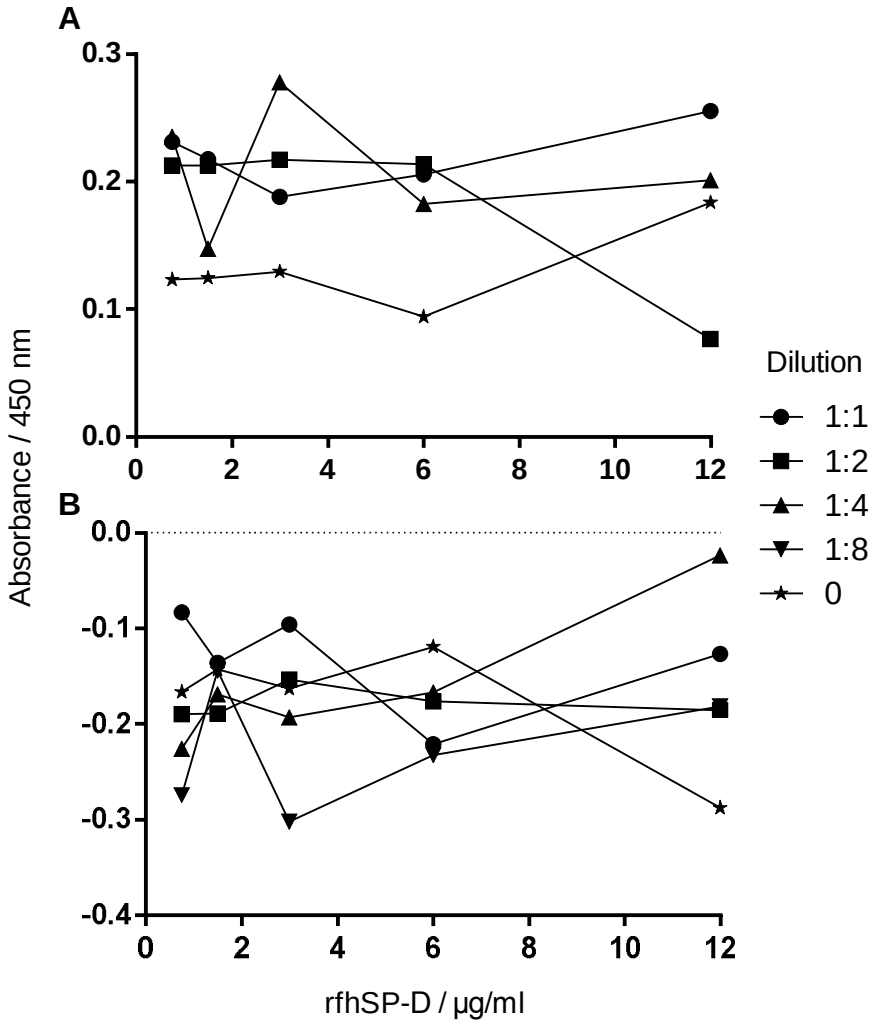

Figure 5-2 Solid phase binding assay of rfhSP-D and (A) Hep-2C cell lysate and (B) RSV A2 infected Hep-2C cell lysate. Uninfected and RSV A2 infected Hep-2C cell lysate at different dilutions was immobilised onto maxisorp plates. Varying concentrations of rfhSP-D were added to the immobilised proteins and detected using a biotinylated monoclonal mouse anti-nhSP-D antibody and streptavidin-HRP. RSV A2 data is corrected for background binding to uninfected Hep-2C cell lysate.

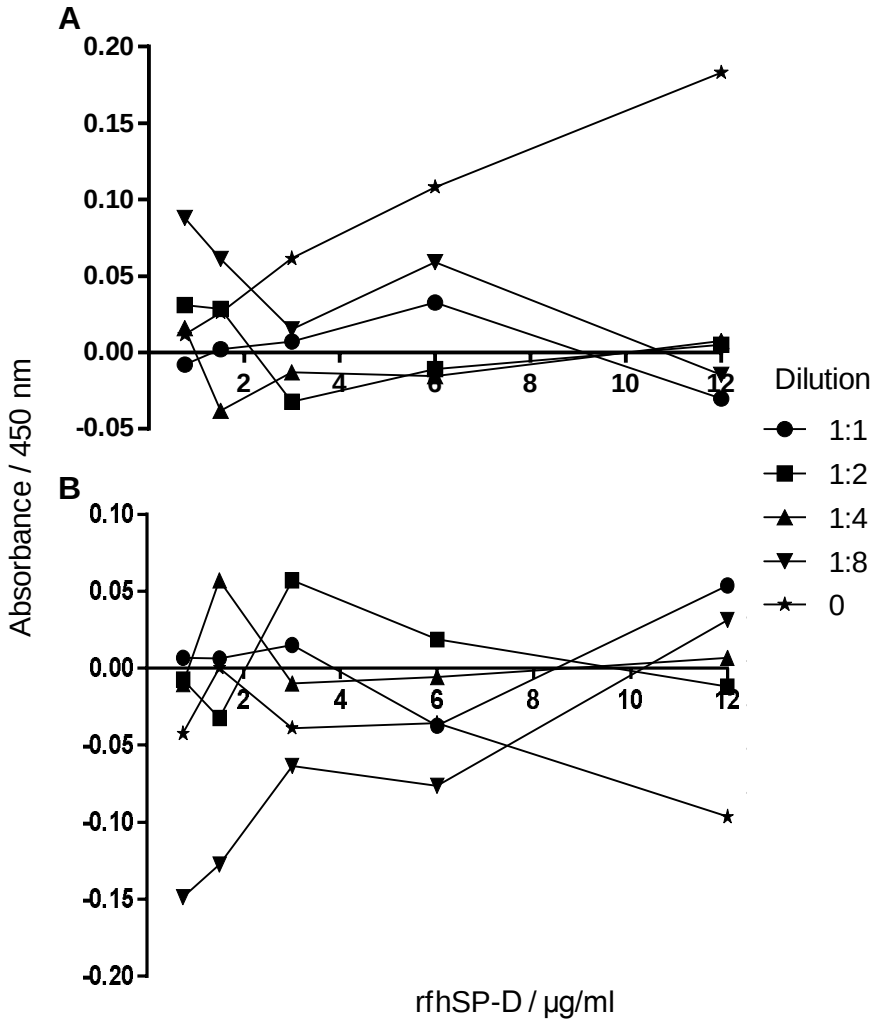

Figure 5-3 Solid phase binding assay of rfhSP-D and (A) HeLa cell lysate and (B) HRV16 infected HeLa cell lysate. Uninfected and HRV16 infected HeLa cell lysate at different dilutions was immobilised onto maxisorp plates. Varying concentrations of rfhSP-D were added to the immobilised proteins and detected using a biotinylated monoclonal mouse anti-nhSP-D antibody and streptavidin-HRP. All data is corrected to background, where no rfhSP-D was added, and HRV16 infected cell lysate data is also corrected for binding to uninfected HeLa cell lysate.

As it appeared there was binding to cellular proteins in both the Hep-2C lysate and HeLa lysate the solid phase binding study was repeated with sucrose density gradient purified HRV16, still in sucrose (Figure 5-4). As previously, maxisorp plates were coated with HRV16 and then rfhSP-D was added, but at a constant concentration of 12 µg/ml. When corrected for non-

specific rfhSP-D binding when no HRV16 was applied and for background when no rfhSP-D was added to the plate there doesn't appear to be any clear rfhSP-D binding to the sucrose purified HRV16.

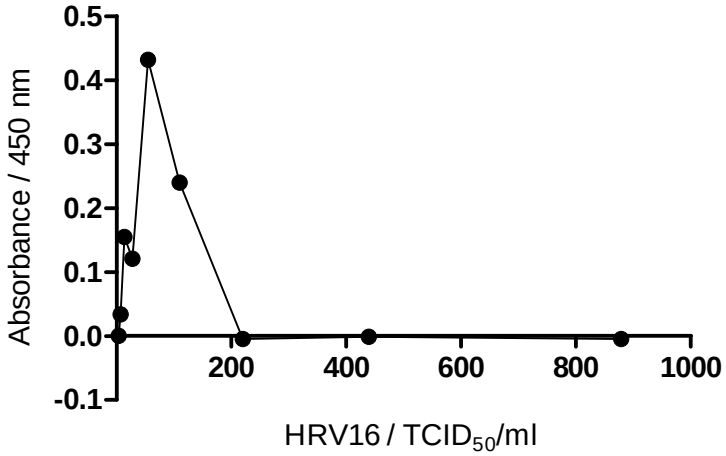

Figure 5-4 Solid phase binding assay of rfhSP-D binding to sucrose density gradient purified HRV16. Sucrose density gradient purified HRV16 at varying dilutions was immobilised onto a maxisorp plate (Nunc), rfhSP-D at 12 μg/ml was added to the immobilised HRV16 and detected using a biotinylated monoclonal mouse anti-nhSP-D antibody and streptavidin-HRP. All data is corrected to background, where no rfhSP-D was added, and where rfhSP-D was added but no HRV16.

High non-specific rfhSP-D background binding was observed, which may be masking true binding of rfhSP-D to HRV16, therefore the blocking solution was addressed. To determine the best blocking solution, the plates were treated as before, except without the addition of any protein in the initial coating of the plates. In previous solid phase binding assays a block of 2 % (w/v) BSA had been used; this was titrated and non-specific binding of both rfhSP-D and nhSP-D was analysed, Figure 5-5 A. A skimmed milk solution was also investigated as a possible blocking solution, Figure 5-5 B.

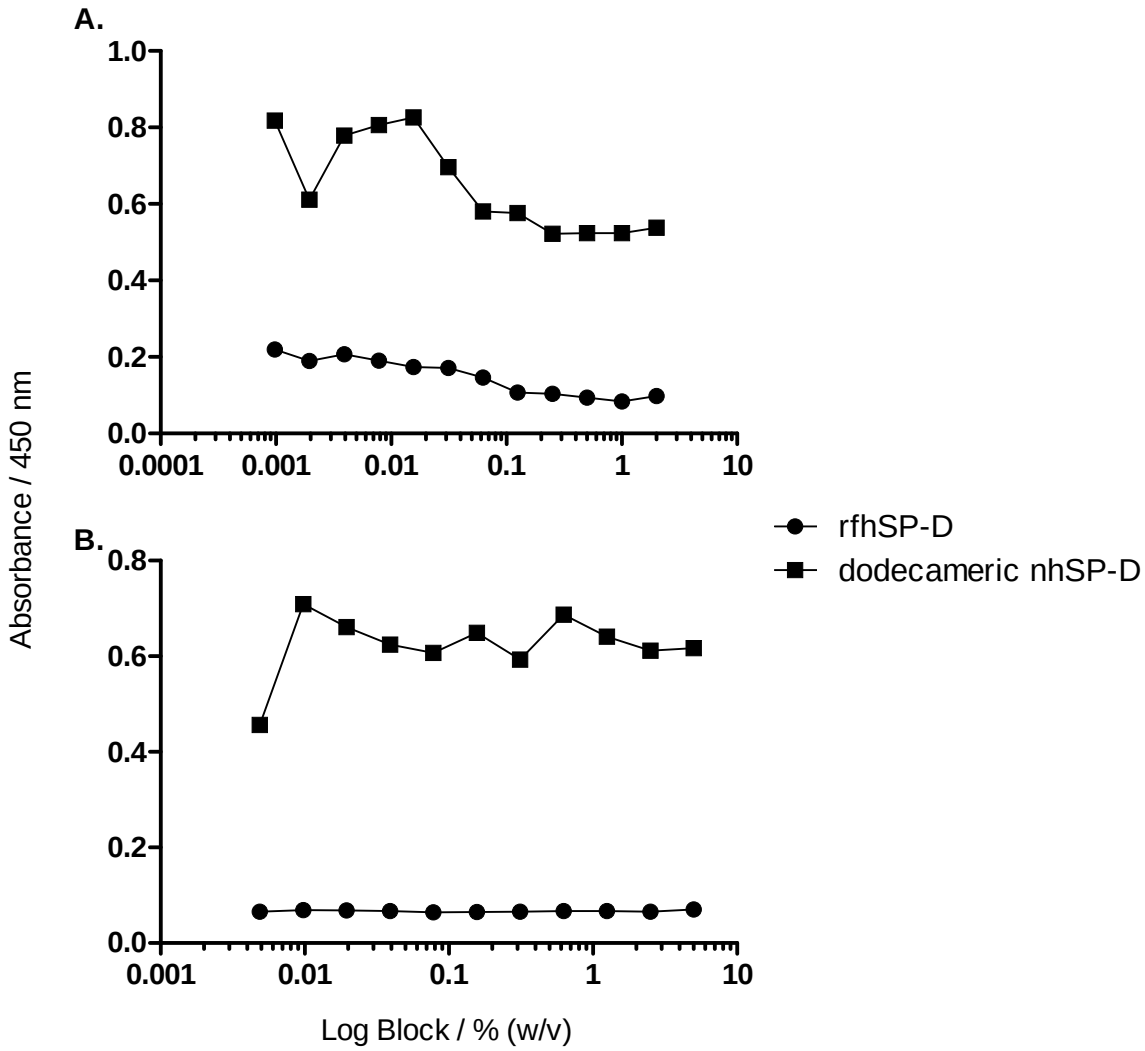

Figure 5-5 Optimisation of blocking solution for solid phase binding assay. (A) BSA or **(B)** skimmed milk were applied to maxisorp plates to coat wells before applying rfhSP-D or nhSP-D at 12 μg/ml and 20 μg/ml respectively and detecting using a biotinylated monoclonal mouse anti-nhSP-D antibody and streptavidin-HRP. All data is an average of duplicate wells**.**

Non-specific binding of dodecameric nhSP-D was high with all concentrations of both BSA and skimmed milk, Figure 5-5. Non-specific dodecameric nhSP-D binding was reduced to the lowest absorbance of 0.52 with 0.25 % (w/v) BSA, this plateaued so higher concentrations of BSA did not reduce non-specific binding further. Non-specific rfhSP-D binding was reduced to the lowest absorbance of 0.08 with 1 % (w/v) BSA. Skimmed milk

did not effectively reduce non-specific binding of either dodecameric nhSP-D or rfhSP-D.

To address the high level of non-specific dodecameric nhSP-D binding, an increased concentration of BSA was tested, a 5 % (w/v) BSA solution, as well as a combination of 5 % (w/v) BSA and 5 % (w/v) skimmed milk, Figure 5-6.

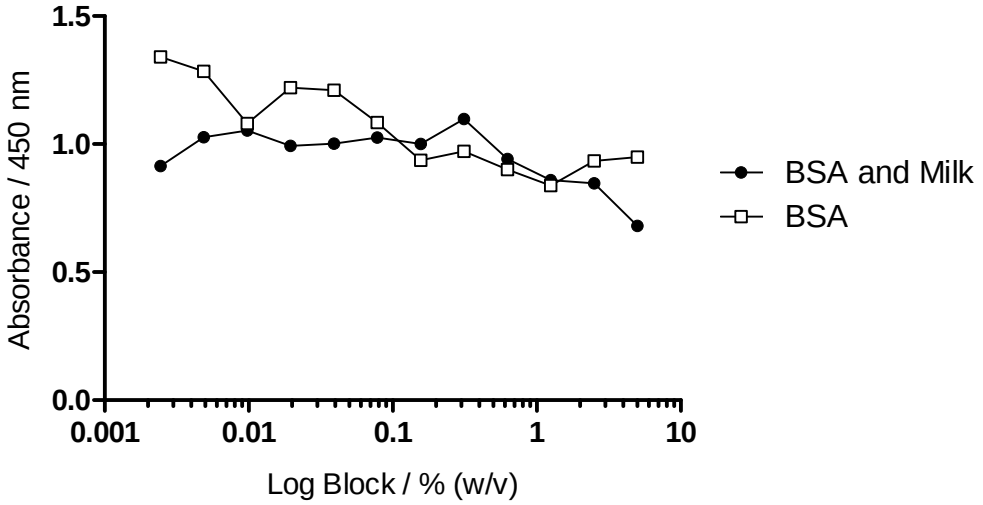

Figure 5-6 Further optimisation of the blocking solution for solid phase binding assay. BSA only or BSA and skimmed milk were applied to maxisorp plates to coat wells before applying dodecameric nhSP-D at 20 μg/ml and detecting using a biotinylated monoclonal mouse anti-nhSP-D antibody and streptavidin-HRP. All data is an average of duplicate wells.

Non-specific nhSP-D binding levels, despite being much reduced from using wash buffer only as a blocking solution (Abs at 450 nm = 1.25), still remained very high with both a blocking solution containing 5 % (w/v) BSA and a combination of 5 % (w/v) BSA and 5 % (w/v) skimmed milk.

In the previous experiments exploring the most effective blocking solution the coating buffer was applied to empty wells, in the absence of any protein. It was hypothesised that this resulted in the surface charge of the plate

surface being altered and thus becoming more "sticky" to the SP-D. A coating of protein (either HRV infected HeLa lysate or uninfected HeLa lysate diluted 1: 410 or 10 μg BSA per well) was applied to the maxisorp plates before blocking with BSA solution to see if this reduced non-specific binding. HRV16 infected and uninfected HeLa lysate had similarly high levels of dodecameric nhSP-D binding whereas the BSA coated wells had much lower nhSP-D binding, this didn't vary with the concentration of blocking solution used, Figure 5-7.

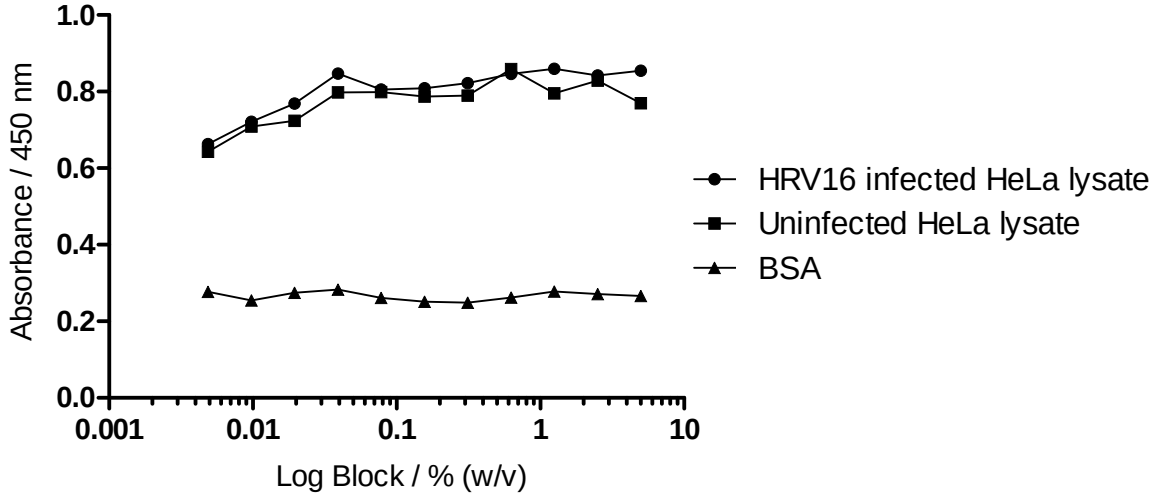

Figure 5-7 Further Optimisation of Blocking Solution for Solid Phase Binding Assay. Maxisorp plates were coated with either HRV16 infected or uninfected HeLa cell lysate or BSA. A titration of BSA blocking solution was then conducted from 5 to 0.0049 % (w/v). Dodecameric nhSP-D was applied at 20 μg/ml and detected using a biotinylated monoclonal mouse anti-nhSP-D antibody and streptavidin-HRP. All data is an average of duplicate wells.

Due to high background encountered using this solid phase binding assay, alternative methods were explored to determine whether there was an interaction between HRV and collectins.

5.3.3 Co-immunoprecipitation

To determine if rfhSP-D is able to bind HRV16, HRV16 infected HeLa cell lysate or sucrose purified HRV16 were incubated with rfhSP-D and a co-immunoprecipitation experiment performed. Negative control experiments were also conducted. The experimental set up is as is shown in Figure 5-8, the protein A or G bead captures the anti-HRV or anti-rfhSP-D antibody which in turn captures either HRV or rfhSP-D respectively. If rfhSP-D interacts with the antibody immobilised HRV it will precipitate with the beads and be visible on western blot, or likewise if the HRV interacts with the antibody immobilised rfhSP-D it will also be precipitated with the bead and thus be visible by western blot.

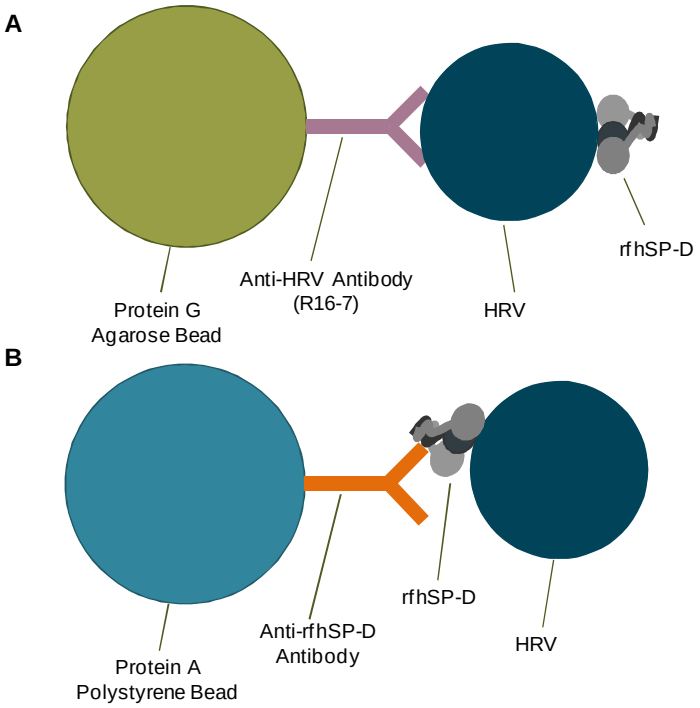

Figure 5-8 Diagram of co-immunoprecipitation experimental principle. HRV and rfhSP-D are co-incubated for one hour, antibody to either rfhSP-D or HRV are then added. The antibody and protein complex is then bound to either protein A or protein G beads as shown; this allows the complex to be drawn out of solution by centrifugation. Diagram not to scale.

Negative control experiments were conducted to rule out any possible non-specific interactions between components of the co-immunoprecipitation experiment that could lead to a false positive result. In addition to those shown in Figure 5-9, negative controls in which R16-7 or HRV16 infected cell lysate were run on SDS-PAGE and transferred to PVDF to probe using rfhSP-D antibodies yielded no bands after an overnight incubation with substrate; this was also the case for protein G beads incubated with the anti-HRV R16-7 antibody (data not shown). When HRV16 infected cell lysate was incubated with R16-7 without the presence of rfhSP-D and run on SDS-PAGE and probed on western blot for rfhSP-D no bands were seen after a 90 minute exposure (data not shown). As HRV infected HeLa cell lysate was a potential component (as opposed to purified HRV) uninfected HeLa cell lysate was also included in the negative control experiments. In Figure 5-9 the first supernatants (SN1) and supernatants from the final wash (SN6) of the experiments conducted using beads are shown. No bands corresponding to rfhSP-D can be seen in any of the final washes (SN6), indicating there was no residual unbound rfhSP-D. The negative controls were successful as there was no non-specific binding, except when rfhSP-D was incubated with HeLa cell lysate alone as well as in the presence of protein G beads, bands corresponding to those of rfhSP-D can be seen, Figure 5-9, blot ii, lanes C and D. Due to the negative control experiments clearly showing that rfhSP-D binds to a component in the uninfected HeLa cell lysate a HRV infected HeLa cell lysate was unsuitable for use in the co-immunoprecipitation. It would not be possible to deduce if binding observed in a HRV infected HeLa cell lysate was due to the presence of HRV. The next step was therefore to use HRV that had been purified by ultracentrifugation on a sucrose density gradient; this would establish if rfhSP-D bound to HRV16, without the complication of rfhSP-D binding to HeLa cell proteins.

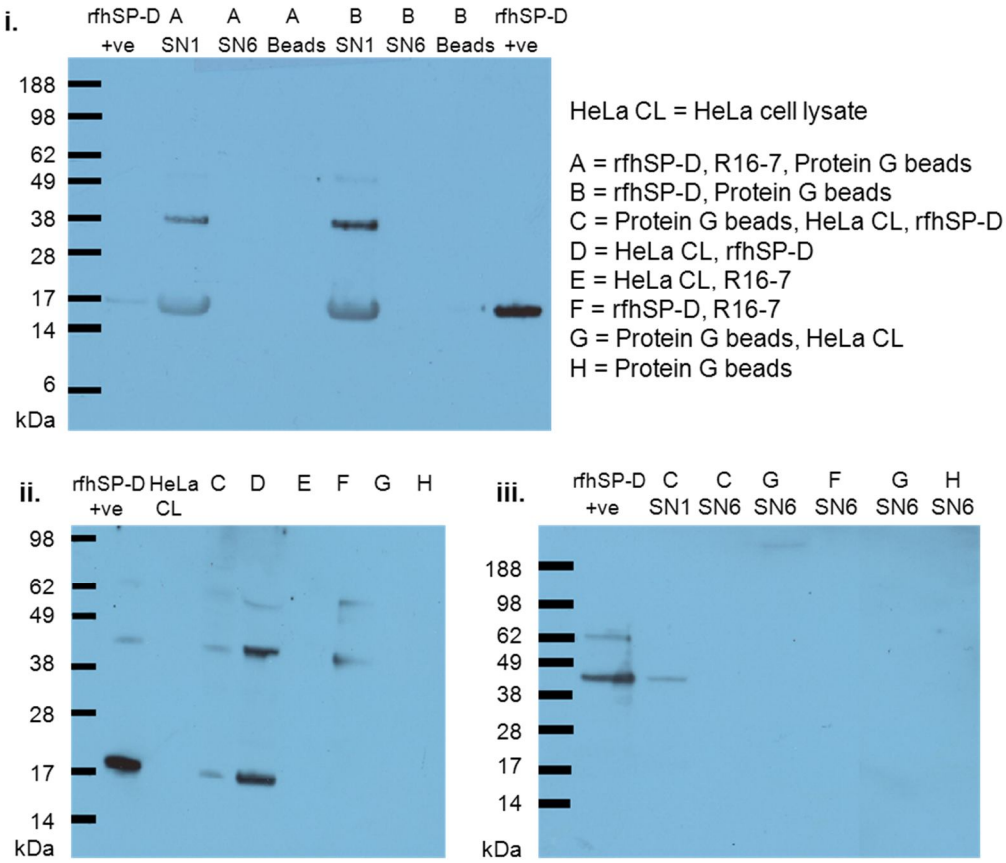

Figure 5-9 Co-immunoprecipitation negative control for nonspecific binding. The indicated components were incubated together before washing five times. The supernatant from the first wash (SN1) and last wash (SN6) are shown. The samples were reduced and run on SDS-PAGE. Proteins were transferred to PVDF membrane and probed using a rabbit-anti-rfhSP-D antibody ($1.61\ \mu g/ml$) and detected using an anti-rabbit AP conjugated secondary antibody solution (Invitrogen) and Novex AP chemiluminescence (Invitrogen).

The sucrose density gradient purified HRV was in a suspension of virus buffer, the negative control experiments of beads with rfhSP-D were therefore repeated in the presence of an equal volume of virus buffer in place of HRV; no rfhSP-D was detected by western blot (data not shown). There was no rfhSP-D detected in the absence of HRV, when only virus buffer along with beads, R16-7 and rfhSP-D was present (Figure 5-10 "Virus Buffer" Beads lane). In the presence of HRV16 no rfhSP-D was detected when the beads were reduced (Figure 5-10 "HRV16" Beads lane), however with

HRV1B rfhSP-D was precipitated with the beads (Figure 5-10 "HRV1B" Beads lane).

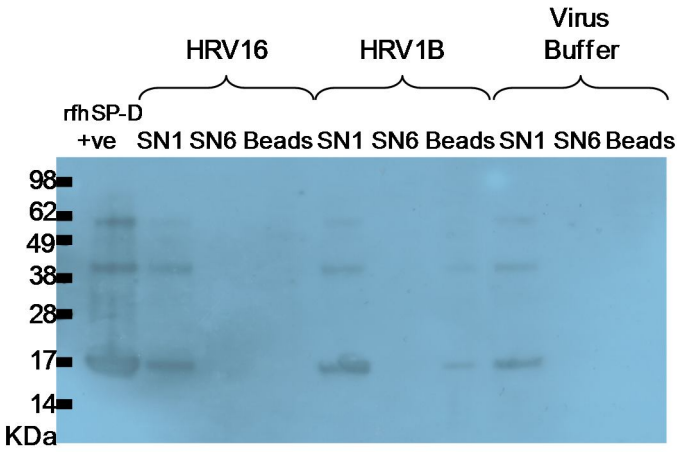

Figure 5-10 Co-immunoprecipitation of rfhSP-D with HRV16 or HRV1B in virus buffer and a negative control with no HRV. Experiment was conducted as for Figure 5-9, but sucrose purified HRVs in virus buffer were used, or virus buffer alone incubated with rfhSP-D, R16-7 and protein G beads. SN1 is the first supernatant removed after co-incubation overnight; SN6 is the supernatant of the final wash. Western blot was probed for rfhSP-D.

To establish if binding between HRVs and nhSP-A could be observed using this method an initial control was done. A 9 μg/ml nhSP-A solution and 50 μl of virus buffer were added together and treated as though the other components of the co-immunoprecipitation experiment had been added, including five washes. This resulted, as seen in Figure 5-11, in nhSP-A being detected by western blot. This suggests the protein had become insoluble in the assay conditions used, making this co-immunoprecipitation method unsuitable for binding analysis.

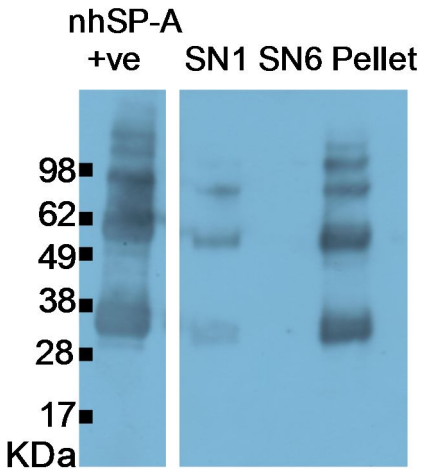

Figure 5-11 Negative control of nhSP-A and virus buffer alone subjected to co-immunoprecipitation conditions. nhSP-A and virus buffer were added together and treated as though it were a co-immunoprecipitation experiment, only not adding in other components of the experiment. After five washes the pellet was reduced and run on a 12 % NuPAGE gel, transferred to PVDF and probed using a rabbit-anti-nhSP-A antibody and anti-rabbit AP conjugated secondary antibody solution (Invitrogen). AP was detected using Novex AP chemiluminescence (Invitrogen).

The experimental set up was swapped to see if binding between rfhSP-D and HRV16 could be detected, as per Figure 5-8 B. The rfhSP-D is captured via an anti-rfhSP-D antibody onto protein A beads and any HRV bound to the rfhSP-D will therefore be precipitated and detectable on western blot probed with an anti-HRV antibody.

The negative controls for the western blot, running beads alone, R16-7 alone and rfhSP-D alone are shown in Figure 5-12, the blots were probed using the anti-HRV antibody R16-7. A band in the bead only control is clearly visible at 60 kDa. When the anti-rfhSP-D antibody was run alone there are two bands visible, one at 25 kDa, and one at 60 kDa. In the experiments containing HRV1B or HRV16 the bands corresponding to the anti-rfhSP-D antibody and beads are the only ones present, there is no band at 28 kDa as would be expected for HRV1B and HRV16.

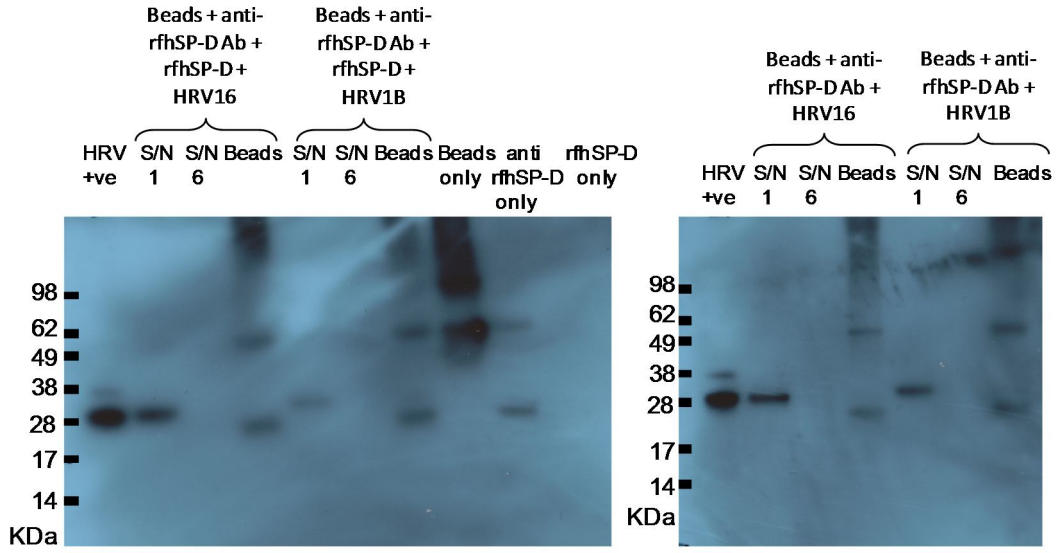

Figure 5-12 Co-immunoprecipitation of rfhSP-D and HRV16 or HRV1B in virus buffer. rfhSP-D and HRV16 or HRV1B in virus buffer were incubated together for one hour before addition of anti-rfhSP-D antibody. Protein A beads were then added and left overnight. The supernatant was removed, SN1, and the beads were washed five times, the supernatant from the last wash is shown, SN6. Beads were then reduced and loaded onto a 12 % NuPAGE gel, transferred to PVDF and probed using a mouse mAb, R16-7 detected using a goat-anti-mouse-HRP conjugated antibody and HRP chemiluminescent substrate.

5.3.4 SPR

The highly sensitive method of SPR was used to identify binding between multimeric nhSP-D, dodecameric nhSP-D, rfhSP-D and nhSP-A with HRV1B or HRV16. The collectins were immobilised to individual flow cells of a CM5 Biacore chip and binding to UV inactivated HRV1B and HRV16 were measured by flowing the virus over the surface and measuring changes in SPR.

Titrated HRV1B and HRV16 were flowed over the immobilised collectins, Figure 5-13 and Figure 5-14 respectively, in the presence of calcium. HRV1B and HRV16 both bound to all forms of SP-D and this binding was titratable.

Maximal binding was observed with neat HRV on all immobilised forms of SP-D. No binding of either HRV1B or HRV16 to nhSP-A was detected.

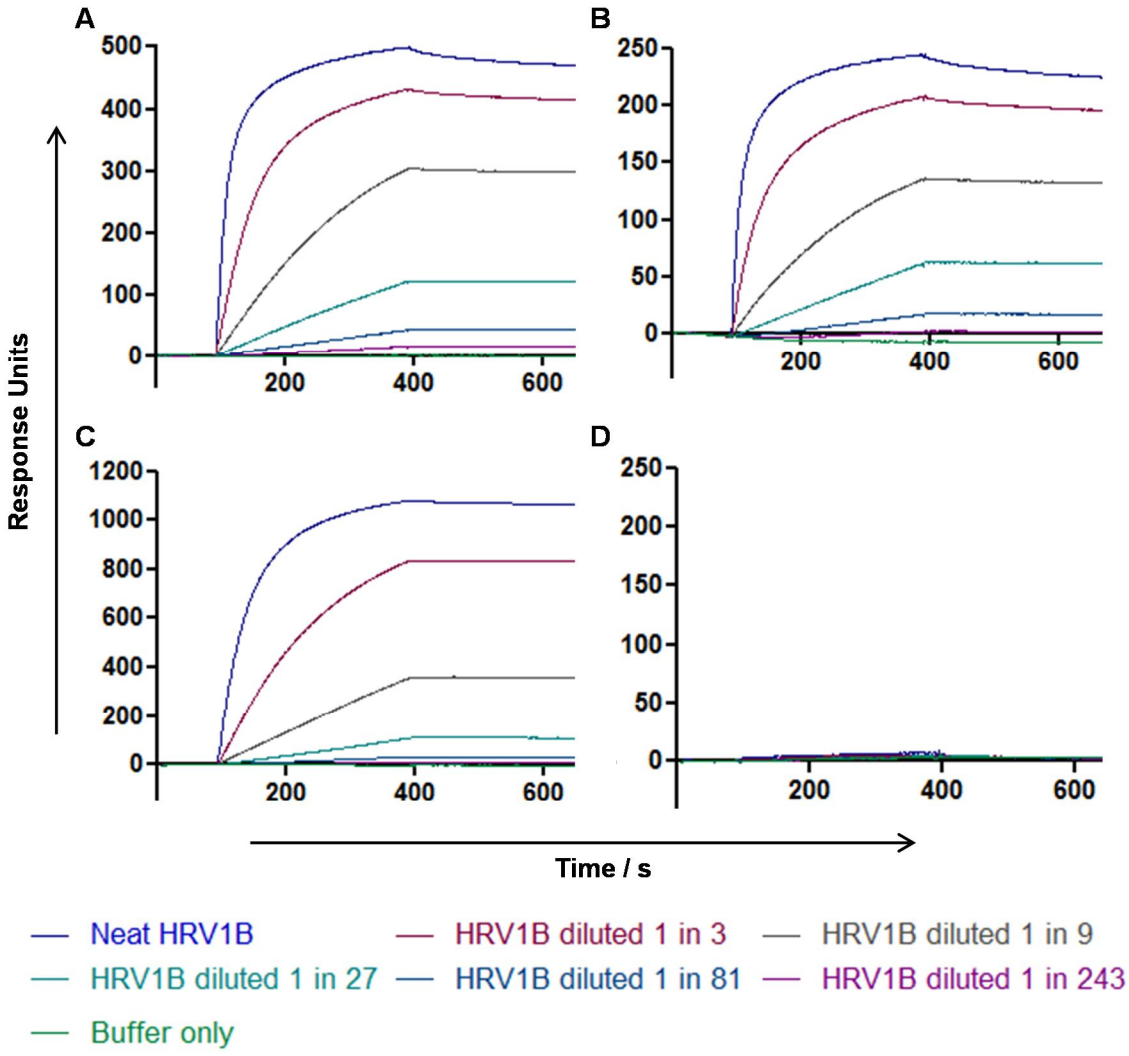

Figure 5-13 SPR response analyses of collectin and HRV1B interactions. HRV1B (neat followed by five 3-fold dilutions in buffer containing 5 mM $CaCl_2$) or buffer alone, were allowed to bind to **(A)** multimeric nhSP-D, **(B)** dodecameric nhSP-D, **(C)** rfhSP-D or **(D)** nhSP-A immobilised on a CM5 chip via amine coupling. Data is corrected for non-specific binding of HRV1B to an empty flow cell and also for buffer alone binding to the immobilised proteins.

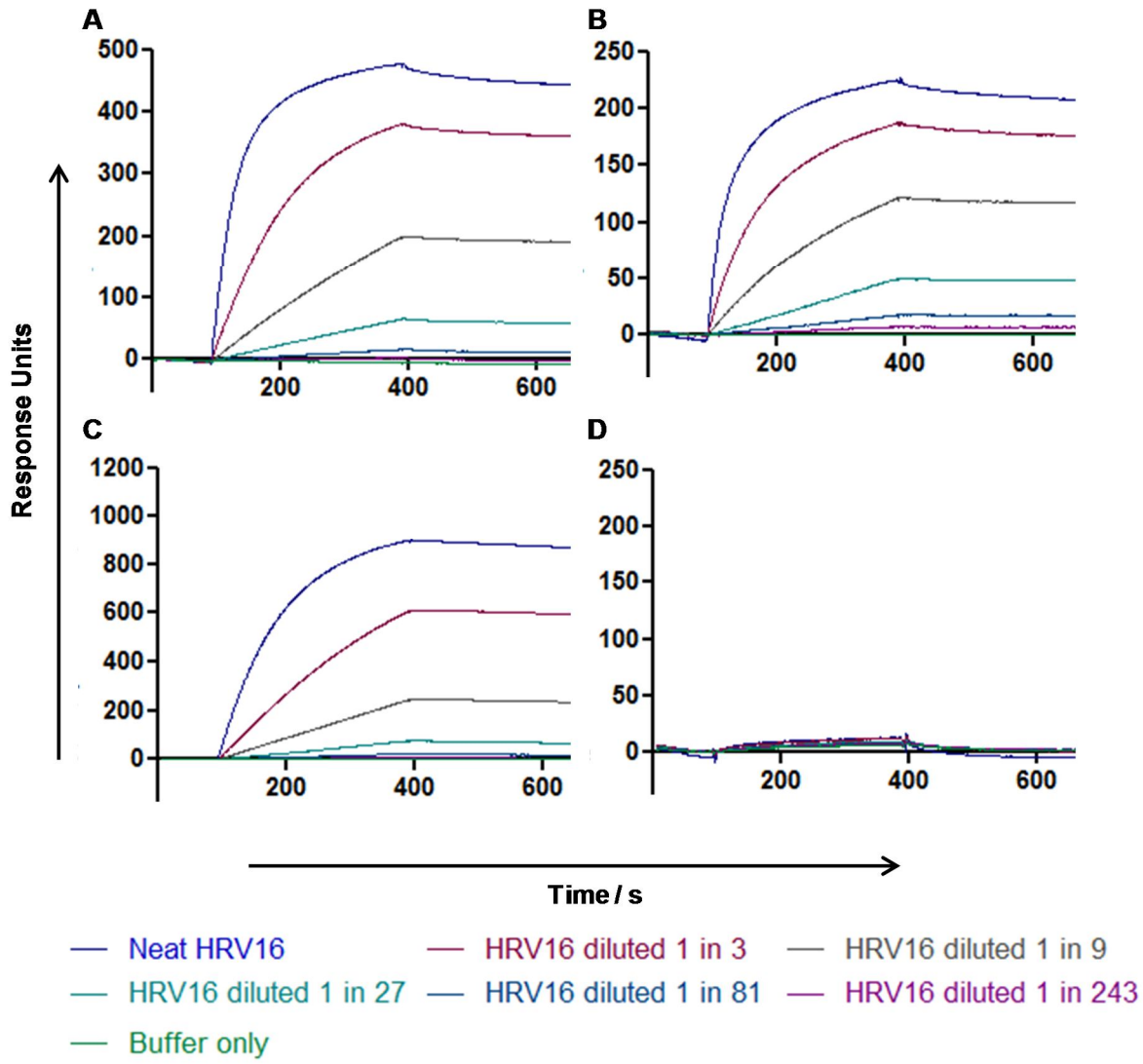

Figure 5-14 SPR response analyses of collectin and HRV16 interactions. HRV16 (neat followed by five 3-fold dilutions, diluted in buffer containing 5 mM $CaCl_2$) or buffer alone, were allowed to bind to **(A)** multimeric nhSP-D, **(B)** dodecameric nhSP-D, **(C)** rfhSP-D or **(D)** nhSP-A immobilised on a CM5 chip via amine coupling. Data is corrected for non-specific binding of the HRV16 to an empty flow cell and also for buffer alone binding to the immobilised proteins.

All binding curves of titrated HRV1B and HRV16 binding to SP-D were analysed to calculate kinetic values, the association rate constant (k_a) and dissociation rate constant (k_d), assuming 1:1 monomeric ligand to analyte binding using BIAevaluation software (version 4.1.1, Biacore). An example kinetic fit is shown in Figure 5-15. The k_a and k_d values for HRV1B and

HRV16 on the immobilised SP-D are shown in Table 5-1. Kinetics analysis was assessed using BIAsimulation software (version 3.1, Biacore) and all kinetics curves were found to represent the binding curves.

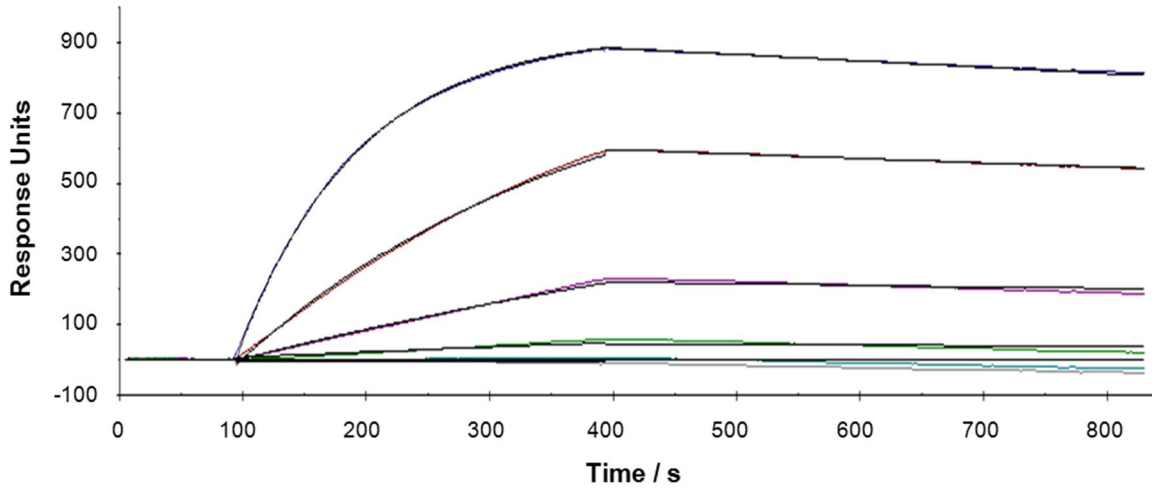

Figure 5-15 Kinetics analysis of HRV16 SPR response when flowed over immobilised rfhSP-D. HRV16 (neat followed by five 3-fold dilutions, top to bottom) or buffer containing 5 mM $CaCl_2$, were allowed to bind to rfhSP-D immobilised on a CM5 chip. Kinetics curves were generated using simultaneous fit using BIAevaluation software version 4.1.1, the kinetics curves are shown as black lines overlaid on the coloured binding curves of the titrated HRV16.

		HRV1B			HRV16		
		k_a ($M^{-1}s^{-1}$)	k_d (s^{-1})	K_D (pM)	k_a ($M^{-1}s^{-1}$)	k_d (s^{-1})	K_D (pM)
Protein Immobilised	multimeric nhSP-D	5.04×10^7	4.8×10^{-8}	0.000953	2.06×10^6	1.45×10^{-4}	70.6
	dodecameric nhSP-D	7.75×10^7	1.13×10^{-4}	1.46	2.31×10^6	1.48×10^{-4}	60.4
	rfhSPD	3.16×10^7	1.49×10^{-5}	0.47	9.4×10^5	2.15×10^{-4}	229

Table 5-1 Binding of HRV1B and HRV16 to immobilised SP-D. Kinetics curves of titrated HRV1B and HRV16 binding to SP-D were analysed using BIAevaluation software version 4.1.1.

The dissociation of the binding for HRV16 was similar for all forms of SP-D with k_ds of 1.45×10^{-4} s^{-1} for multimeric nhSP-D, 1.48×10^{-4} s^{-1} for dodecameric nhSP-D and 2.15×10^{-4} s^{-1} for rfhSP-D. HRV1B had the greatest binding affinity with multimeric nhSP-D, then rfhSP-D and the lowest affinity with dodecameric nhSP-D, the k_d values were 4.8×10^{-8} s^{-1}, 1.49×10^{-5} s^{-1}, and 1.13×10^{-4} s^{-1} respectively (Table 5-1).

The k_a or "on rate" was greatest for HRV1B compared to HRV16 on all immobilised forms of SP-D. For both HRVs the largest k_a was with dodecameric nhSP-D with values of 7.75×10^7 M^{-1} s^{-1} and 2.31×10^6 M^{-1} s^{-1} for HRV1B and HRV16 respectively. The multimeric nhSP-D had the next highest "on rate" for both HRV1B and HRV16, with k_a values of 5.04×10^7 M^{-1} s^{-1} and 2.06×10^6 M^{-1} s^{-1} respectively. With rfhSP-D and HRV1B the k_a was 3.16×10^7 M^{-1} s^{-1} compared to 9.4×10^5 M^{-1} s^{-1} for HRV16; this was the form of SP-D with the slowest "on rate". In summary the k_a values were in the order of dodecameric nhSP-D >multimeric nhSP-D >rfhSP-D for both HRVs tested.

The equilibrium dissociation constant (K_D) was calculated using BIAevaluation software. The low K_D values (in the pico- or femto- mole range) show that there is a strong affinity between SP-D with HRV1B and HRV16. For HRV1B the highest affinity was with multimeric nhSP-D, then rfhSP-D and then dodecameric nhSP-D with K_D values of 0.000953 pM, 0.47 pM and 1.46 pM respectively. For HRV16 the highest affinity was with dodecameric nhSP-D, then multimeric nhSP-D and then rfhSP-D with K_D values of 60.4 pM, 70.6 pM and 229 pM respectively.

The molar ratios (Table 5-2) were calculated for HRV1B at a concentration of 8.46×10^{10} v.p./ml and HRV16 at a concentration of 1.97×10^{11} v.p./ml as calculated using the formula 1 $OD_{260} = 9.4 \times 10^{12}$ v.p./ml [249]. The molar ratios, representing the moles of HRV bound per moles of immobilised SP-D, show that the multimeric nhSP-D has the most binding sites for HRV1B and HRV16 as the molar ratios are 0.0245 and 0.00414 respectively. This is almost twice the molar ratio for dodecameric nhSP-D which had molar ratios of 0.0142 and 0.0066 for HRV1B and HRV16 respectively. The rfhSP-D had the lowest molar ratio of all the forms of SP-D with a molar ratio of 0.0003 for HRV1B and 0.001 for HRV16, this is ~80 to ~100 times less than observed with the multimeric nhSP-D and each HRV.

		HRV1B		HRV16	
		Molar Ratio	**SEM**	**Molar Ratio**	**SEM**
Protein Immobilised	**multimeric nhSP-D**	0.0245	0.00182	0.0111	0.00414
	dodecameric nhSP-D	0.0142	0.00079	0.0066	0.00220
	rfhSPD	0.0003	0.00002	0.0001	0.00003

Table 5-2 Molar ratios of SP-D binding to HRV1B and HRV16. Binding was expressed as a molar ratio, representing the moles of analyte (HRV1B or HRV16) bound per moles of immobilised ligand (SP-D). Molar ratios were calculated using the formula *ab/cd*, where *a* = level of binding at five minutes, *b* = oligomeric mass of immobilised SP-D, *c* = mass of HRV (8000 kDa), and *d* = amount of SP-D immobilised to the biosensor surface (in RUs). The molar ratios were calculated assuming oligomeric molecular masses of 1.7 MDa, 512 kDa and 54 kDa for multimeric nhSP-D, dodecameric nhSP-D and rfhSP-D respectively. The concentration of HRV1B flowed over the immobilised SP-D was 8.46×10^{10} v.p./ml and the concentration of HRV16 used was 1.97×10^{11} v.p./ml. Molar ratios are mean of ≥ 4 separate experiments.

To ensure SP-D binding to HRV was specific a negative control using BSA at 1 μg/ml was conducted. Binding to HRV1B can be seen but there is no binding to BSA, Figure 5-16.

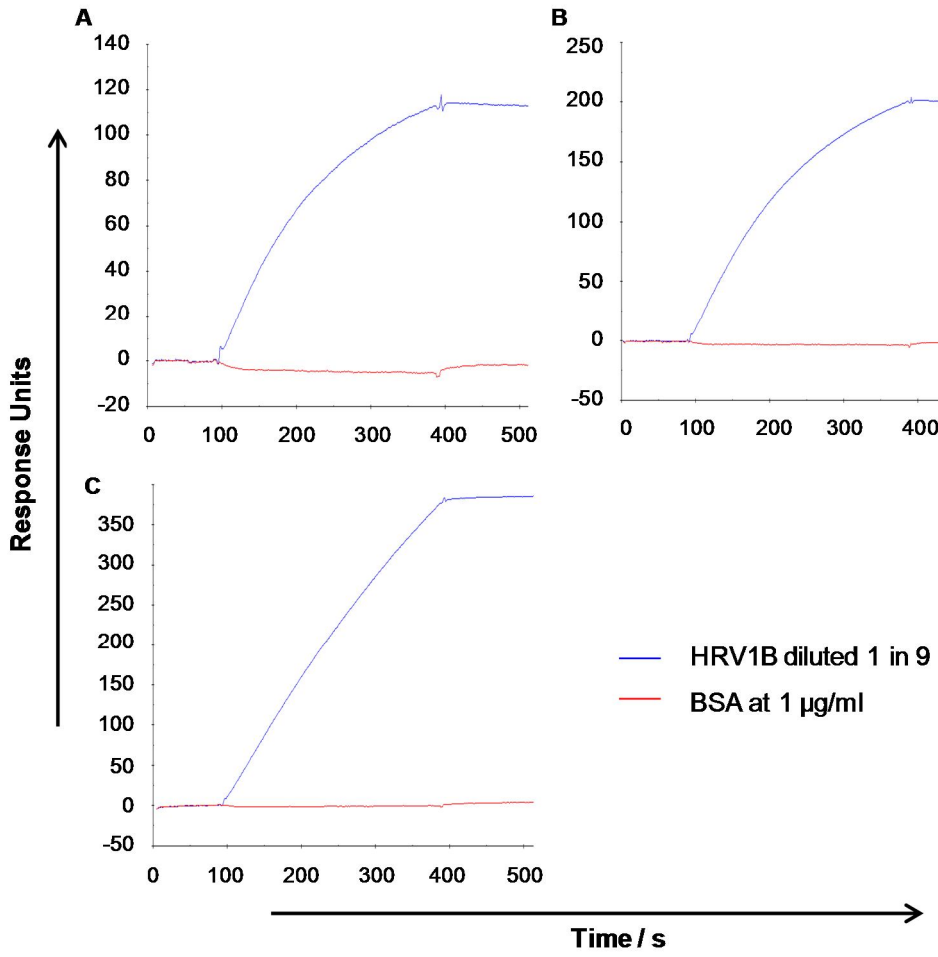

Figure 5-16 SPR response analyses of HRV1B and BSA interactions with SP-D. HRV1B diluted 1 in 9 (blue) and BSA at 1 µg/ml (red) both in buffer containing 5 mM $CaCl_2$ were allowed to bind to **(A)** multimeric nhSP-D, **(B)** dodecameric nhSP-D or **(C)** rfhSP-D immobilised on a CM5 chip via amine coupling. Data is corrected for non-specific binding of the HRV to an empty flow cell and for buffer alone binding to the immobilised proteins.

To establish if binding between HRV1B and HRV16 is calcium dependent the HRVs were diluted in either buffer containing 5 mM $CaCl_2$ or 3 mM EDTA to sequester calcium ions. The HRVs were flowed over the flow cells in the appropriate buffer and binding was measured by detecting changes in SPR. The presence of 3 mM EDTA in the running buffer resulted in abolition of binding of HRV1B and HRV16 to multimeric nhSP-D, rfhSP-D and nhSP-D where binding was observed when the running buffer contained 5 mM $CaCl_2$

(Figure 5-17 and Figure 5-18). No binding was seen between nhSP-A and HRV1B or HRV16 in either running buffer Figure 5-19.

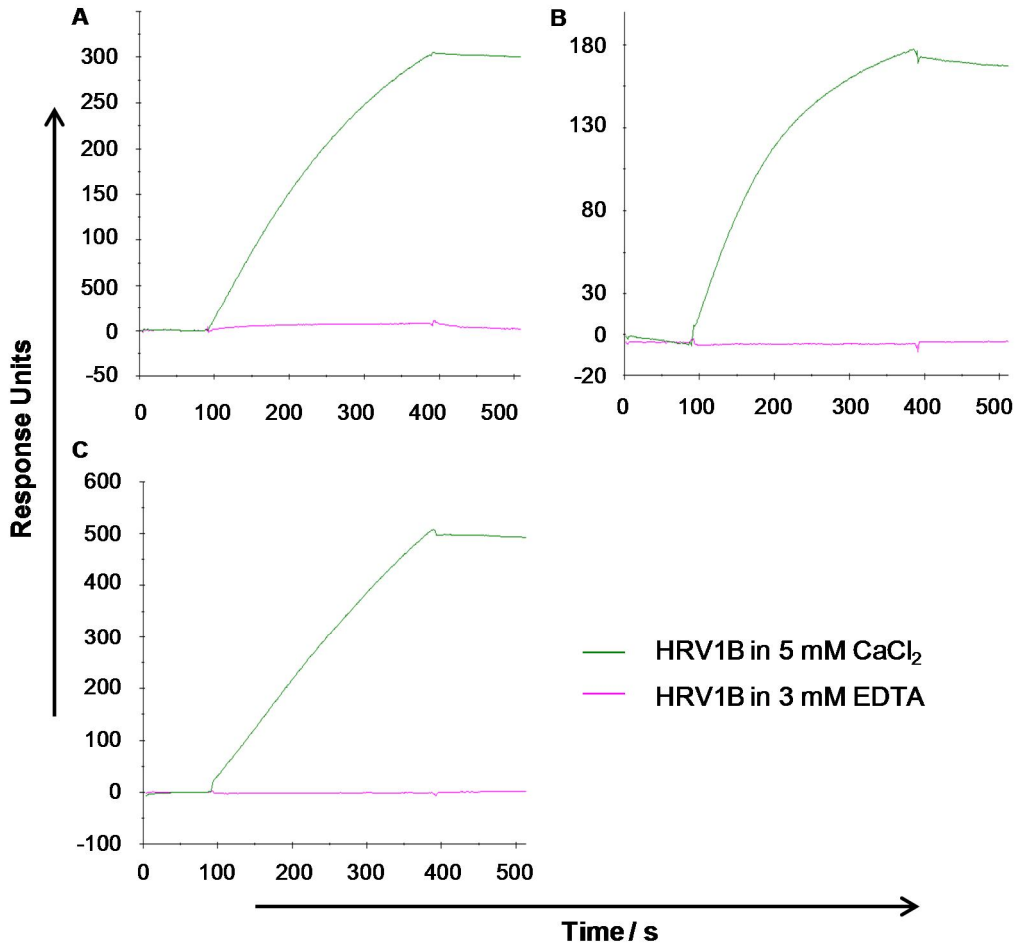

Figure 5-17 SPR response analyses of protein and HRV1B interactions in the presence and absence of calcium ions. HRV1B was diluted 1 in 9 in buffer containing either 5 mM $CaCl_2$ (green) or 3 mM EDTA (pink), the HRV1B was allowed to bind in the respective buffer to **(A)** multimeric nhSP-D, **(B)** nhSP-D or **(C)** rfhSP-D immobilised on a CM5 chip via amine coupling. Data is corrected for non-specific binding of the HRV1B to an empty flow cell and also for buffer alone binding to the immobilised proteins.

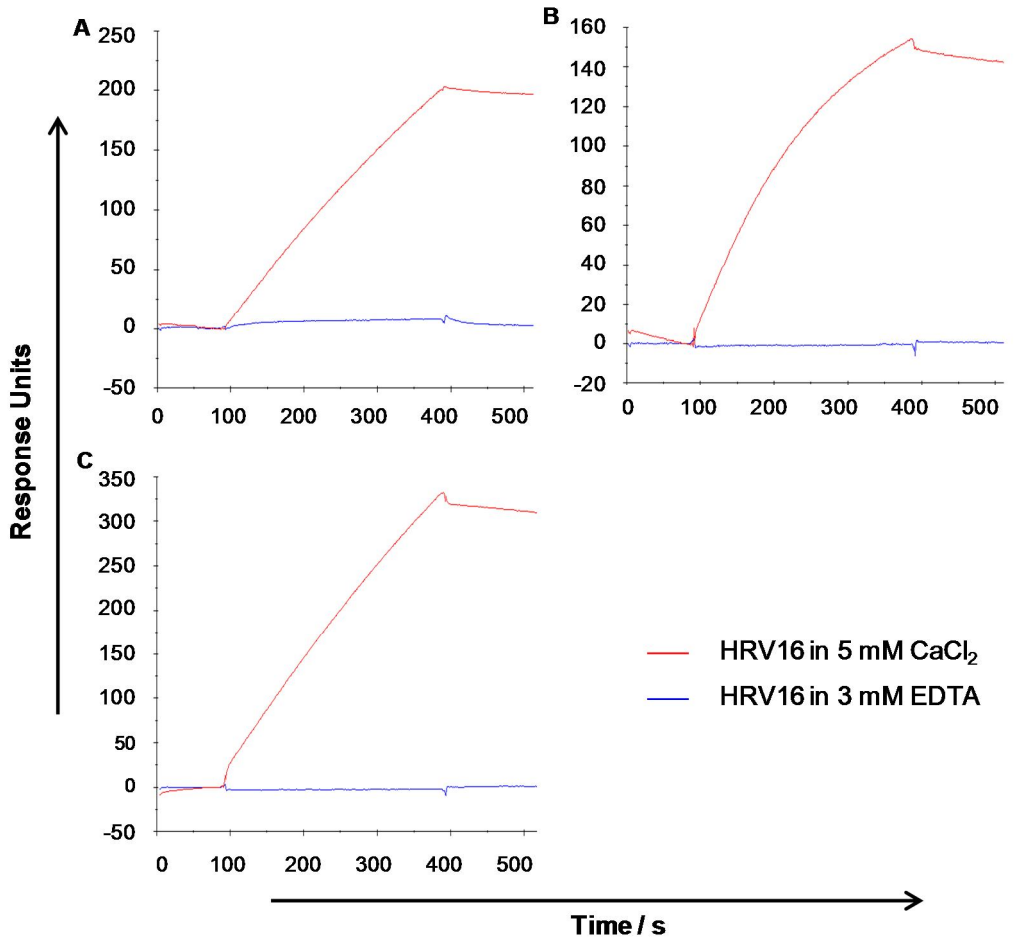

Figure 5-18 SPR response analyses of protein and HRV16 interactions in the presence and absence of calcium ions. HRV16 was diluted 1 in 9 in buffer containing either 5 mM $CaCl_2$ (red) or 3 mM EDTA (blue), the HRV16 was flowed over the surface of a CM5 chip in the respective buffer on which **(A)** multimeric nhSP-D, **(B)** nhSP-D or **(C)** rfhSP-D had been immobilised via amine coupling. Data is corrected for non-specific binding of the HRV16 to an empty flow cell and also for buffer alone binding to the immobilised proteins.

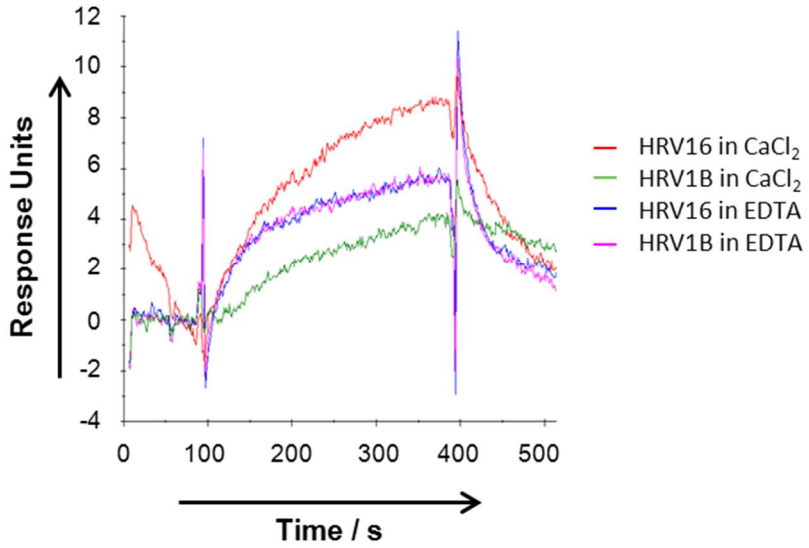

Figure 5-19 SPR response analyses of nhSP-A and HRV1B or HRV16 interactions in the presence and absence of calcium ions. HRV was diluted 1 in 9 in buffer containing either 5 mM $CaCl_2$ (red/green) or 3 mM EDTA (blue/pink), the HRV was allowed to bind in the respective buffer to nhSP-A immobilised on a CM5 chip via amine coupling. Data is corrected for non-specific binding of HRV to an empty flow cell and for buffer alone binding to the immobilised proteins. N.B. very small scale.

To attempt to map the binding site of SP-D on HRV the mAb R16-7 directed against VP2 on the HRV capsid surface was pre-incubated at various concentrations, as shown in Figure 5-20, with HRV1B. None of the concentrations of R16-7 blocked HRV1B binding to any of the forms of SP-D. With the highest concentration of R16-7 (20 μg/ml) there is a large excess of antibody to HRV virions, approximately 9.4×10^{10} antibodies and 1.43×10^{5} virions.

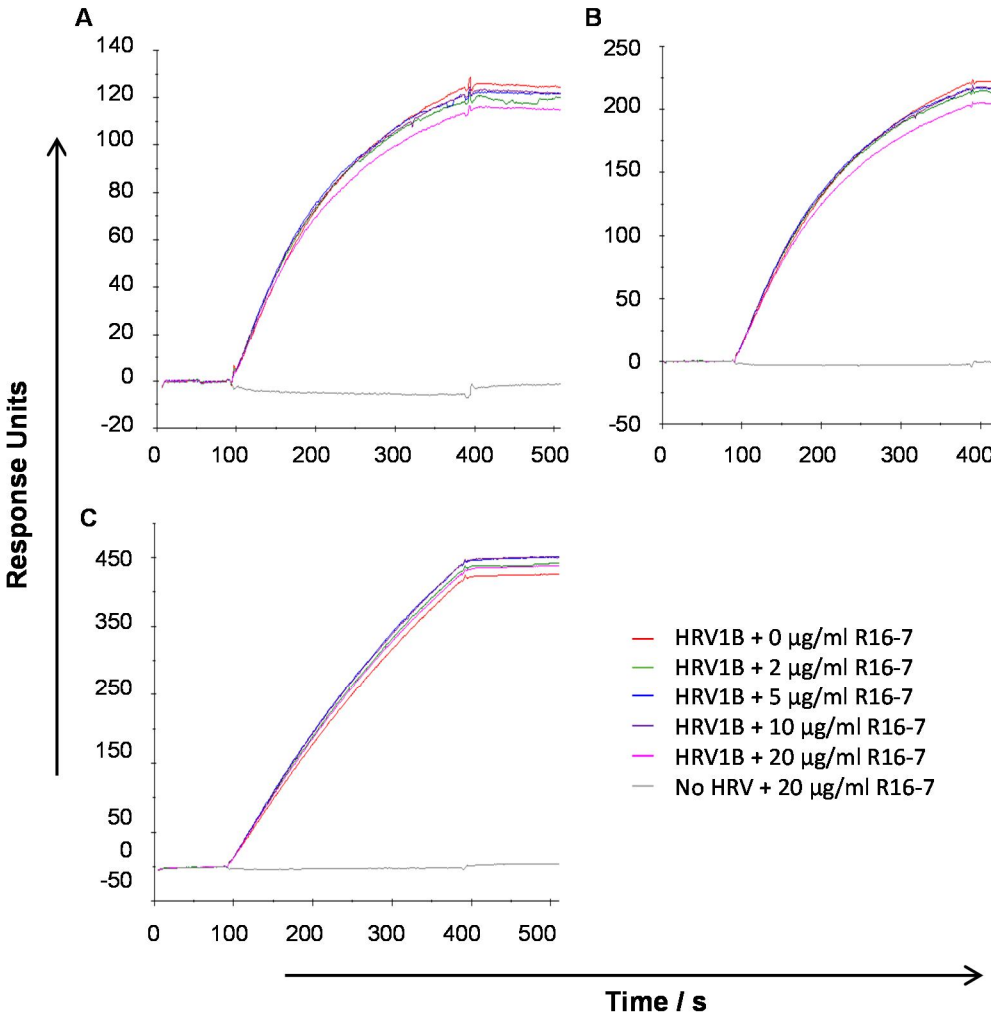

Figure 5-20 SPR response analyses of collectin and HRV1B interactions in the presence and absence of the anti-HRV mAb, R16-7. HRV1B was diluted 1 in 9 in buffer containing 5 mM $CaCl_2$ with or without a one hour pre-incubation with varying concentrations of the mAb R16-7 directed against the HRV capsid protein VP2. HRV1B was allowed to bind to **(A)** multimeric nhSP-D, **(B)** dodecameric nhSP-D or **(C)** rfhSP-D immobilised on a CM5 chip via amine coupling. Data is corrected for non-specific binding of the HRV to an empty flow cell and for buffer alone binding to the immobilised proteins.

To further characterise the interaction between SP-D and HRVs sugar competition studies were undertaken as binding abolition of SP-D to HRV in EDTA suggested involvement of the CRD of SP-D. HRV1B and HRV16 were flowed over immobilised multimeric nhSP-D, dodecameric nhSP-D and rfhSP-D in the presence of sugars (0-40 mM). All of the sugars used (ManNAc, maltose, glucose and galactose) inhibited HRV1B and HRV16

binding to multimeric nhSP-D, dodecameric nhSP-D and rfhSP-D in a concentration dependent manner (chromatograms not shown). An example of chromatograms from a competition experiment on each of the immobilised forms of SP-D with HRV1B in the presence of maltose is shown in Figure 5-21.

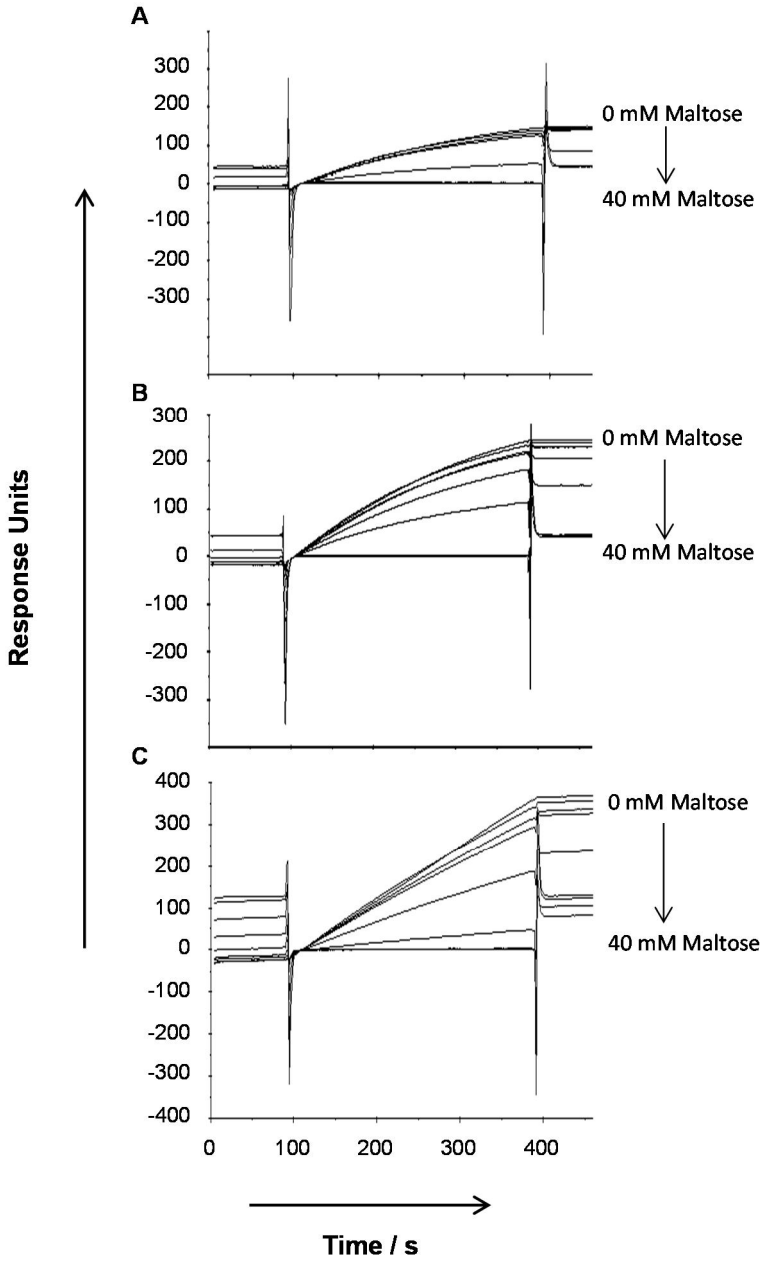

Figure 5-21 SPR response analyses of HRV1B in the presence of maltose. HRV1B was diluted 1 in 9 in buffer containing 5 mM $CaCl_2$ and varying concentrations of maltose (0 - 40 mM). HRV1B was allowed to bind to **(A)** multimeric nhSP-D, **(B)** dodecameric nhSP-D or **(C)** rfhSP-D immobilised on a CM5 chip via amine coupling. Data is corrected for non-specific binding of HRV to an empty flow cell and for buffer alone binding to the immobilised proteins.

The SPR response in the presence of sugar was normalised to the response in the absence of sugar, considering this to be maximal binding. An example of

the effect of sugar on SPR response can be seen in Figure 5-21. On surfaces with each of the forms of SP-D immobilised calculations of the IC_{50} values (i.e. the concentration of sugar at which there was half maximal binding) are shown in Figure 5-22. When HRV1B was flowed over SP-D the relative affinity order based on the IC_{50} values were in the order of ManNAc < maltose < glucose < galactose, Table 5-3. This was also observed with HRV16 and rfhSP-D. The order was different for HRV16 with dodecameric nhSP-D and multimeric nhSP-D, the IC_{50} values were in the order of maltose < glucose < ManNAc < galactose, Table 5-3.

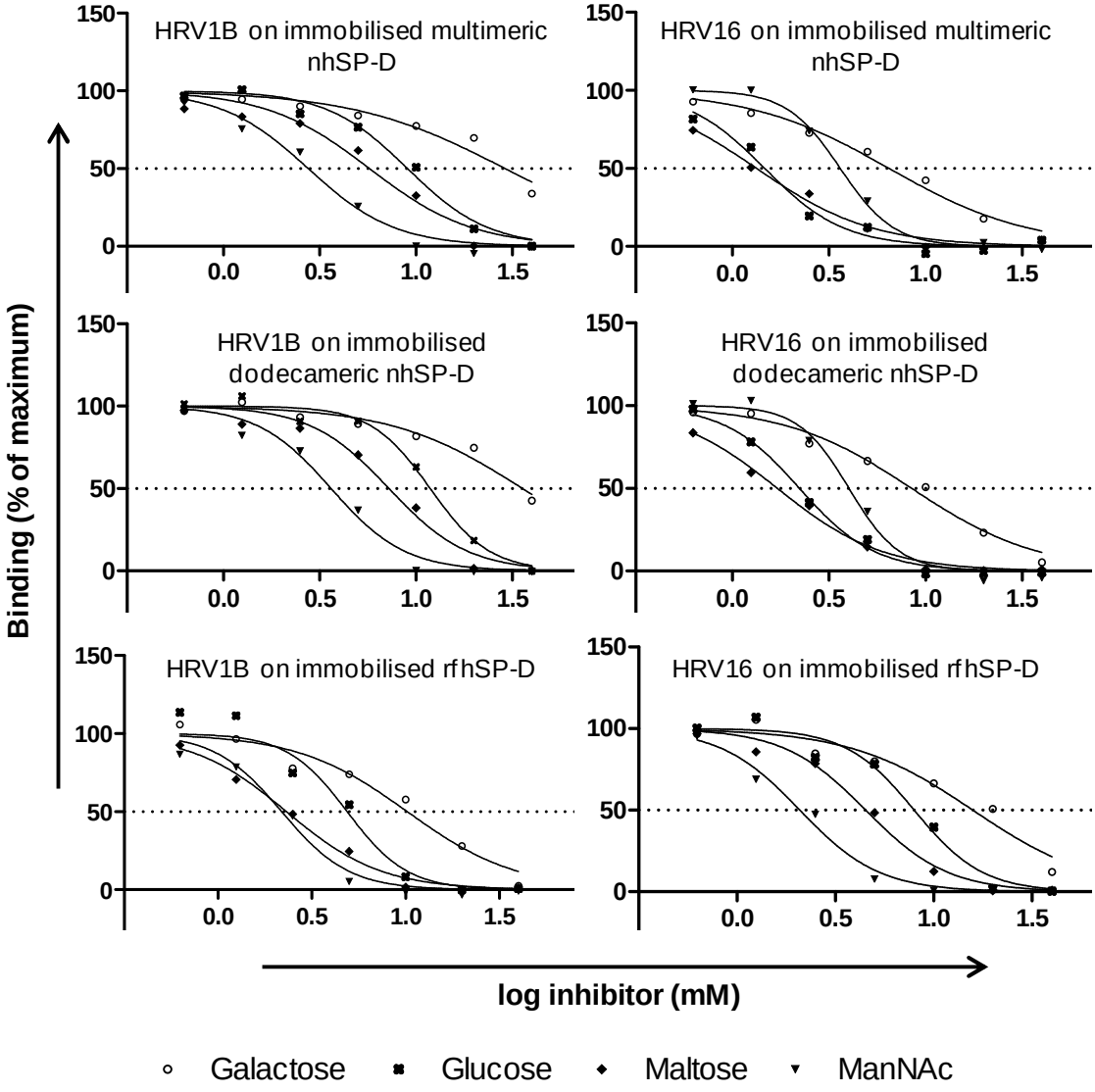

Figure 5-22 SPR analysis of the effect of sugars on the interaction between HRV and SP-D. HRV1B or HRV16 were diluted in running buffer containing 5 mM $CaCl_2$ and varying concentrations of sugar (0-40 mM). HRV1B or HRV16 were allowed to bind to different forms of SP-D (as indicated) immobilised on a CM5 chip via amine coupling. Data are represented as a percentage of maximal binding which was taken to be the maximum response in the absence of sugar.

		dodecameric nhSP-D	rfhSP-D	multimeric nhSP-D
HRV1B	ManNAc (mM)	3.624	2.087	2.756
	Maltose (mM)	7.239	4.513	5.732
	Glucose (mM)	11.85	7.964	9.033
	Galactose (mM)	35.71	15.81	29.01
HRV16	ManNAc (mM)	4.017	2.186	3.619
	Maltose (mM)	1.711	2.318	1.335
	Glucose (mM)	2.227	4.883	1.471
	Galactose (mM)	8.469	10.22	6.471

Table 5-3 IC_{50} values for sugar inhibition of HRV1B and HRV16 binding to SP-D. HRV1B or HRV16 diluted in 0-40 mM ManNAc, maltose, glucose or galactose were flowed over the surface of immobilised SP-D. Values were plotted as a percentage of maximal binding and the IC_{50} value calculated.

5.4 Discussion

The collectins SP-A and SP-D are known to interact directly with microorganisms. This can lead to agglutination, opsonisation and direct microbial killing [67, 127, 129, 247, 252]. It was previously unknown if nhSP-A, nhSP-D or rfhSP-D could bind to HRV; an aim of this study was therefore to elucidate if this occurs. This aim was addressed using several techniques, ligand blot, a solid phase binding assay, co-immunoprecipitation and SPR.

5.4.1 Ligand Blot

As an initial investigation into the interaction between HRV16 and rfhSP-D, using established experimental techniques, a ligand blot was conducted. It was found that rfhSP-D did not bind to reduced HRV16 samples immobilised on PVDF membrane. This was also the case for reduced RSV A2. Conformations of proteins run on SDS-PAGE are disrupted and this is a possible cause of rfhSP-D not binding to the proteins, but it was hoped that there may be a non-conformational dependent epitope to which rfhSP-D could bind HRV. Glycans are not disrupted by SDS-PAGE and so it was hoped that the rfhSP-D would be able to bind to these moieties in RSV, as it is known that rfhSP-D binds to the glycosylated G protein on RSV [111]. Conformational disruption may however have changed how the glycosylated moieties were presented, perhaps separating glycosylation sites and as rfhSP-D binds synergistically the binding may have been weakened such that the rfhSP-D wasn't detected. rfhSP-D did, however, bind to proteins in the HeLa cell lysate, highlighting the need for pure HRV16 for binding studies. This is not an ideal technique to investigate if binding occurs between rfhSP-D and HRV16 but as SDS-PAGE and antibodies to rfhSP-D were readily available it provided a rapid means to see if binding could be detected.

5.4.2 Solid Phase Binding Assay

An alternative technique used to investigate binding of HRV16 and rfhSP-D or nhSP-D was a solid phase binding assay, as was performed to examine SP-D binding to IAV and RSV G protein [111, 228, 229]. This method had not previously been conducted in the laboratory and therefore required optimisation. Initially different dilutions of HRV16 infected and uninfected HeLa cell lysate were immobilised on the plate, alongside RSV A2 infected and uninfected Hep-2C cell lysate as a positive control. It would be expected that the rfhSP-D would bind to RSV A2 as previously G protein from this serotype was isolated and used in a solid phase binding assay [111]. The RSV A2 infected Hep-2C cell lysate will contain this G protein and therefore rfhSP-D should bind. Binding of rfhSP-D to RSV A2 was not observed in this experiment; it appears that rfhSP-D may bind to proteins within the Hep-2C cell lysate, as binding in the infected cell lysate was not above that observed when the cell lysate was uninfected. It may also be that the Hep-2C cellular proteins are bulky and therefore prevent access of rfhSP-D to the G-protein. Subsequent to completion of research for this project other members of the laboratory in Southampton have also attempted to show binding of SP-D to RSV A2 and were unsuccessful (personal communication with Dr. Madsen). This may be a result of a mutation in the RSV that has occurred during amplification; the RSV A2 strain therefore needs to be characterised using sequence analysis to determine if this has occurred.

There appears to be rfhSP-D binding to HeLa cell proteins, highlighting again the need for pure HRV16 virions. To rectify this HRV16 purified by sucrose density gradient ultracentrifugation was used instead of HRV16 infected HeLa cell lysate. Ideally a positive control of pure RSV would also

have been conducted, however, none was available. No clear rfhSP-D binding to the sucrose density gradient purified HRV16 was detected. This could be due to the presence of sucrose interfering with interactions between rfhSP-D and HRV16. The binding pattern seen with the pure HRV16 may suggest that there is non-specific binding of rfhSP-D to the maxisorp plate. As the HRV16 is diluted more binding is seen, possibly due to the HRV16 proteins becoming more spaced out on the plate and thus allowing a greater proportion of the rfhSP-D to bind to the plate. This should be prevented by the blocking step so the choice of blocking solution was addressed.

The original blocking solution used in the solid phase binding assays was 2 % (w/v) BSA as previously used in the literature [229]. To test the blocking solution BSA was serially diluted in empty wells and rfhSP-D and dodecameric nhSP-D at 10 μg/ml was applied. Binding of dodecameric nhSP-D was high even with the highest concentration of BSA. A blocking solution of 5 % (w/v) skimmed milk was also tested in the same manner and non-specific binding of dodecameric nhSP-D was even higher than that observed with 2 % BSA. Non-specific rfhSP-D binding was less than that of dodecameric nhSP-D, most likely due to dodecameric nhSP-D containing higher order oligomeric structures with more CRDs than rfhSP-D. The synergistic action between the CRDs on dodecameric nhSP-D results in greater avidity and therefore binding of dodecameric nhSP-D compared to rfhSP-D. Only non-specific binding of dodecameric nhSP-D was assessed in further blocking solution optimisation due to the greatest level of non-specific binding being observed with dodecameric nhSP-D.

As BSA was the most effective blocking solution in the first experiment the concentration of BSA was increased to 5 % (w/v) to see if this could be further improved. Another blocking solution containing both 5 % (w/v) BSA

and 5 % (w/v) skimmed milk was also tested. Both blocking solutions decreased non-specific binding to a much greater extent than using wash buffer alone, but not to an acceptable level to be able to observe true binding between SP-D and HRV16.

The aforementioned experiments were on empty wells that had been incubated overnight with bicarbonate buffer, as this is the coating buffer used when proteins are immobilised onto the plate. It was hypothesised that the coating buffer was altering the charge on the plate's surface making it more "sticky" to the hydrophilic SP-D proteins. A coating of protein, HRV16 infected or uninfected HeLa cell lysate, or BSA was immobilised onto the plate in order to see if this resulted in decreased non-specific binding. Increasing concentrations of BSA blocking solution, up to 5 % (w/v), were then evaluated. In all wells the BSA concentration in the blocking solution made little difference to the level of binding observed; however the level of binding in wells containing HRV16 infected and uninfected HeLa cell lysate was approximately three times that seen when wells were coated with BSA. This provides further evidence that dodecameric nhSP-D binds to a protein within the HeLa cell lysate. The level of non-specific binding was reduced when BSA was present during coating, compared to no protein in the coating stage. This may confirm the hypothesis that the charge on the plate is altered by incubation with bicarbonate buffer.

To resolve problems regarding non-specific binding of SP-D the binding assay could have been switched around. This would involve immobilising the SP-D onto the plate and adding the HRV on top which would then be detected with an anti-HRV antibody such as R16-7. As the stocks of R16-7 were not readily available and this technique would have used large amounts of the antibody other techniques were explored.

5.4.3 Co-immunoprecipitation

Initial co-immunoprecipitation experiments to look at binding between HRV and rfhSP-D were going to be conducted using HRV infected HeLa cell lysate. It was hoped that the R16-7 monoclonal antibody would specifically recognise only the HRV VP2 protein that it was raised against and thus the presence of HeLa cell proteins would not be a problem. It became apparent that using HRV infected HeLa cell lysate was unsuitable as the R16-7 mAb was binding to a component in the HeLa cell lysate itself (found using mock infected HeLa cell lysate) and the rfhSP-D was binding to this. Binding between HRV could not be specifically isolated from rfhSP-D binding to components of the HeLa cell lysate. It is likely that the binding to a component in the HeLa cell lysate is related to the capacity for SP-D to bind to apoptotic and necrotic cells [71, 253]. The protocol was refined to use HRV that had been sucrose density gradient purified and buffer swapped into virus buffer. Negative controls using virus buffer without HRV showed that no precipitation of rfhSP-D occurred and therefore any rfhSP-D that was detectable by western blot when HRV was included in the preparation has precipitated due to binding to HRV. HRV1B was bound by the rfhSP-D as it was detected by western blot, HRV16 was not. This is the first discovery that HRV1B is bound by rfhSP-D. It was unclear from these experiments whether HRV16 is not bound by rfhSP-D, or whether the amount of HRV16 in the experiment was too low to result in a level of rfhSP-D binding detectable by western blot. This is possible as the viral titre of the HRV16 preparation was an order of magnitude lower than that of the HRV1B preparation (1.73×10^6 ffu/ml and 1.10×10^7 ffu/ml respectively).

The co-immunoprecipitation experiment design was swapped to capture rfhSP-D onto a bead and then any HRV that was detected by western blot was there as a result of binding to rfhSP-D. This experimental design posed problems as the anti-rfhSP-D antibody used to immobilise the rfhSP-D onto the protein A bead was detected by either the R16-7 anti-HRV mAb, or by the goat-anti-mouse-HRP secondary antibody; this was distinguishable as a band at 25 kDa, corresponding to the molecular weight of an antibody light chain, and a band at 60 kDa, corresponding to the molecular weight of an antibody heavy chain. This could have been rectified by cross-linking the antibody to the beads and then adding this to a solution of pre-incubated rfhSP-D and HRV. A 60 kDa band was detected when protein A beads alone were run on western blot and probed for HRV; it is unclear what this band is. The protein A immobilised onto the polystyrene bands is, according to the manufacturer, a recombinant form of protein A that is 32 kDa (user manual, "Dynabeads® Protein A" by Dynal Biotech" rev no 003). It is possible that the 60 kDa band observed is a dimer of the recombinant protein A.

An initial investigation as to whether it is possible to utilise this co-immunoprecipitation method to detect nhSP-A binding to HRV showed that it was not suitable due to nhSP-A becoming insoluble during the procedure. This is likely due to nhSP-A being a large protein in comparison with rfhSP-D. The centrifugation is essential to be able to wash the beads before analysis and therefore this technique cannot be used to look at binding between nhSP-A and HRV. A way to negate this problem would be to use magnetic beads and a magnetic stand; this equipment was not available so alternative methods were explored.

5.4.4 SPR

SPR experiments measure binding in real time and with high precision. This technique was used to assess binding between nhSP-A, multimeric nhSP-D, dodecameric nhSP-D and rfhSP-D with HRV1B and HRV16. The collectins were immobilised onto the surface of a Biacore chip and HRV1B or HRV16 were flowed over the surface. Both HRV1B and HRV16 were found to bind to multimeric nhSP-D, dodecameric nhSP-D and rfhSP-D, the binding was titratable and calcium dependent as the binding was inhibited in the presence of EDTA. This indicates that the CRD is involved in binding of SP-D to these HRVs as the rfhSP-D (lacking the collagen and N-terminus) retained the ability to bind to the HRVs. The CRD is further implicated as the CRD is influenced by the presence of calcium; calcium is required for collectin binding to oligosaccharides via the CRD and the crystal structure shows the presence of calcium causes conformational changes in the CRD [47, 254, 255]. Unexpectedly, competitive binding inhibition of SP-D to HRV was observed with experiments incorporating varying concentrations of sugars. This would usually suggest that the SP-D is binding to a carbohydrate residue on the HRV; however HRV is a non-enveloped virus and therefore glycosylation is unlikely. There are no publications suggesting that any of the capsid proteins of HRV are glycosylated and hence it is most likely that the interaction between SP-D and HRV is a protein-protein interaction. As a further investigative step it may be worth deglycosylating HRV, for instance by treating with Endoglycosidase H which selectively removes high mannose glycans, to elucidate whether SP-D is binding to such moieties. It is possible that the binding site for HRV on SP-D is near to the CRD and that a change in conformation induced upon binding to sugars could sterically inhibit binding to HRV. SP-D has previously been reported

to bind in a calcium dependent manner to lipids lacking carbohydrate moieties, and this was attenuated in the presence of sugars [256].

For both HRV1B and HRV16 the binding affinity was high with all forms of SP-D as the K_D values were all in the pico- or femto- mole ranges. By comparison with other protein-protein interactions, antibody and protein interactions tend to have K_D values in the range of 0.1 and 1 nM, with only some high affinity interactions being below this [257]. The K_D values for HRV with HeLa cells are in the picomole range as opposed to the femtomole range, suggesting the high affinity with SP-D could be important [258]. The low K_D values show that there is rapid recognition and binding of the HRV and SP-D (indicated by a high k_a or rapid "on rate") and a stable complex formation (indicated by a low k_d or slow "off rate"). Multimeric nhSP-D had the greatest affinity for HRV1B as the K_D was 0.953 femtomole, dodecameric nhSP-D and rfhSP-D had similar K_D's for HRV1B (1.46 and 0.47 pM respectively). The higher affinity of multimeric nhSP-D may be expected due to a greater number of CRDs and hence greater avidity compared to dodecameric nhSP-D and rfhSP-D. With HRV16 multimeric nhSP-D and dodecameric nhSP-D had similar affinities (K_D values of 70.6 and 60.4 pM respectively) whereas the affinity with rfhSP-D was lower (K_D value of 229 pM). This is again likely due to avidity that occurs with the oligomeric forms of SP-D that is not possible with the rfhSP-D which has single trimeric CRDs. The differences in the K_D values between HRV1B and HRV16 may suggest that the binding site on the each virus is different; this could be the case as the viruses have different surface properties, as demonstrated by Vlasak and colleagues [259].

The molar ratios of each form of SP-D and HRV were calculated to account for the differing amounts of proteins immobilised on the chip surface. As

may be expected due to having only one trimeric CRD rfhSP-D had the lowest molar ratio with both HRV1B and HRV16, dodecameric nhSP-D had the next lowest and multimeric nhSP-D bound the most. This reflects the number of CRDs that are in each molecule. It would however be expected that the multimeric form of nhSP-D would bind more HRV than was observed, as in comparison to dodecameric nhSP-D it only bound approximately twice the number of HRV particles. This expectation is on the assumption that the multimeric nhSP-D in this preparation is similar to that observed by Crouch and associates in which the multimeric nhSP-D had approximately 25 trimeric CRDs [260], compared to dodecameric nhSP-D which only has four trimeric CRDs. To determine the number of CRDs with the multimeric nhSP-D preparation used in this project TEM or atomic force microscopy could be conducted.

Four different sugars competed with HRV1B and HRV16 for binding to immobilised SP-D. The sugar inhibition of HRV1B and HRV16 binding to SP-D differed. Binding of all forms of SP-D to HRV1B were inhibited in the order of ManNAc > maltose > glucose > galactose. This was also seen with HRV16 and rfhSP-D. This reflects the relative affinities that SP-D has for these sugars [261]. For dodecameric nhSP-D and multimeric nhSP-D and HRV16 the order was maltose > glucose > ManNAc > galactose. It is less clear why this is so, it is possible that this is an artefact of the experiment and hence the experiment requires repeating. It may also be that this is again reflecting the differing surface properties of the HRV1B and HRV16 which may cause the SP-D to bind to each virus in a different way.

No binding of nhSP-A to either HRV1B or HRV16 was observed, this suggests that the binding of SP-D to these viruses is specific. The differences in binding may be a result of the differing structures of nhSP-A and nhSP-D.

The arrangement of the CRDs of nhSP-A is different to nhSP-D; for nhSP-A the CRDs are clustered in a "bouquet of flowers" formation whereas dodecameric nhSP-D they are in a "cruciform" formation. The trimeric structure of the CRDs of nhSP-A and nhSP-D also differ. The CRD of nhSP-A has a flat conformation, resembling a "T" shape, whereas nhSP-D has a conformation resembling a "Y" [47]. This could hinder the ability of nhSP-A to interact with the HRV. For instance, if the SP-D is binding to the dome of the HRV the "Y" shape could be advantageous in allowing the SP-D molecule to have maximal contact with the surface of the virus. Another possible suggestion for why nhSP-A did not bind to HRV are indicated from previous studies with ligands such as the RSV attachment protein, G, which is ≥ 60 % glycosylated by mass, may suggest that nhSP-A has specificity for highly glycosylated ligands [114, 115].

To ensure that the interaction between SP-D and HRV is specific a protein to which SP-D has not previously been found to bind, BSA, was flowed over the surface of the immobilised SP-D [262]. No binding to BSA was seen whilst in the same experiment binding to HRV1B was detected suggesting that the interaction with HRV is specific.

The site of binding of SP-D on HRV1B was explored through use of a mAb, R16-7, directed against the capsid protein VP2. A large excess of antibody to virus was used and no inhibition of binding to any form of SP-D was seen. It may be expected that binding of a non-neutralising antibody to the surface HRV would increase the mass of the HRV particle detected by SPR upon binding to the immobilised SP-D, and hence an increase in the RU value detected. There would however only be a small increase in the mass of the HRV upon binding of antibody. There are over 60 copies of VP2 on the surface of HRV, however, steric hindrance would only permit a few anti-

HRV antibodies to bind to the HRV virion. This is due to the HRV particle being 25-30 nm in diameter and the footprint of an antibody being approximately 15 nm [263, 264]. Due to HRV having a very large mass of 8000 kDa an increase in mass of approximately 450-700 kDa due to antibody binding is unlikely to be detected on the SPR sensorgram. An alternative explanation for the lack of increase in mass detected could be that the molecule that is binding to the immobilised SP-D is not HRV, and hence the antibody has no effect on the binding detected. Although this cannot be entirely excluded, it is unlikely. This is based on the TEM of the purified HRV preparation showing only the spherical HRV particles and no contaminating proteins. Based on this experiment and the lack of inhibition of HRV binding in the presence of the anti-HRV mAb, it appears that VP2 is not the site of binding. This approach could also be extended to include HRV16, as mentioned previously it is possible that SP-D is binding to a different site on each of the HRV serotypes.

5.4.5 Conclusions and Future Directions

SP-D binding to HRV could imply that they would be expected to inhibit HRV infection. Direct binding of nhSP-D and rfhSP-D neutralises infectivity of IAV and RSV [27, 111]. Binding of nhSP-D to RSV and IAV occurs via the CRD in a calcium dependent manner [62, 64, 111]. Whether SP-D can potentially inhibit infection could be explored further using SPR by exploring whether binding of SP-D to HRV interferes with HRVs interaction with its receptor. The receptor for the HRV, LDLR for HRV1B and ICAM-1 for HRV16, could be immobilised onto the surface of a Biacore chip [142-146]. HRV1B or HRV16 pre-incubated with SP-D could then be flowed over the immobilised receptor; free HRV would be expected to bind to the

receptor, if the SP-D is able to inhibit HRV binding to the receptor this would suggest that SP-D would inhibit infection *in vitro*.

Binding of SP-D to HRV could also potentially increase uptake into some host cells, as in the case of nhSP-A and RSV [114]. nhSP-A mediated RSV uptake into monocytes increases production of TNF-α and reduces IL-10 production, this is a reversal of what is observed in the absence of nhSP-A [115]. The enhanced production of pro-inflammatory TNF-α may be beneficial as it may limit further viral replication [265].

Further characterisation of the interaction between SP-D and HRV needs to be conducted. This could involve site directed mutagenesis of each component to elucidate the site of binding on the HRV and determine which amino acids are involved. It may also be of value to determine if binding still occurs in a biological environment, this could be achieved by conducting binding assays in BAL fluid which contains lipids and other competing proteins.

In summary, although the precise site(s) of binding of SP-D to HRV have not been defined it is probable that binding occurs in close proximity to the calcium or sugar binding sites within the CRD. This is drawn from evidence of an inhibitory effect of EDTA and the ability for competing sugars to completely inhibit HRV binding. These inhibitory effects could be a result of overlapping binding sites, steric effects at the ligand binding surface or conformational changes as a result of the removal of calcium or addition of sugars. This is the first report of the HRV capsid being bound by a component of the innate immune system.

6. Chapter 6: Effect of Collectins on *In Vitro* Rhinovirus Infection

6.1 Introduction

It was investigated whether the presence of collectins could attenuate the level of HRV infection. This was based on observations that SP-D binds to HRV, which could potentially sterically inhibit HRV from binding to its receptor. SP-D sterically inhibiting the binding of the viral hemagglutinin of IAV to sialic acid components on host cells is thought to play a role in the anti-IAV activity of SP-D [101, 248]. HRV16 binds to ICAM-1 and HRV1B binds to members of the LDLR family, this is a pre-requisite for entry into the cell which is the site for HRV replication. Hypothetically, less HRV being able to bind its receptor would therefore lead to reduced replication of HRV.

6.2 Materials and Methods

6.2.1 Fluorescent Focus Reduction Assay

To conduct the fluorescent focus reduction assay (FFRA) HeLa cells were seeded at a density of 1.56 x 10^5 cells/well or 16HBE cells were seeded at 4 x 10^5 cells/well in a 24 well plate; these were left to adhere for three hours at 37 °C, 5 % CO_2. A co-incubation assay was performed in which various concentrations of collectins (as indicated), were incubated with HRV1B or HRV16 (at a pre-established dose sufficient to result in 25 % infection of cells) in a final volume of 500 µl of serum starved media. The inoculum was incubated for one hour with rocking at room temperature. Media was removed from cells and washed with PBS. The above inoculum was applied

to the cells and left rocking at 30 o.p.m for one hour at room temperature before transferring into 33 °C, 5 % CO_2 for 17 hours.

After 17 hours incubation the media was removed and cells were washed twice in PBS prior to fixing in 1 % paraformaldehyde in PBS, 500 µl per well, for one hour at room temperature. Cells were stained and the number of infected cells determined as described in section 3.2.4. The number of infected cells in wells with collectin were related to the number of infected cells in control wells were no collectin was present, and expressed as a percentage of control infection.

6.2.2 Flow Cytometry

Assays were set up as detailed in 6.2.1 but instead of fixing the cells on the plate they were removed by trypsin treatment and fixed and stained as detailed in section 2.1.8.

Some assays were performed in 48 well plates (Greiner Bio-One) as opposed to 24 well plates as described in section 6.2.1. In these plates HeLa cells were seeded at 7.8 x 10^4 cells/well and 16HBE cells were seeded at 2 x 10^5 cells/well; all volumes were reduced by 50 %.

An alternative assay involving rfhSP-D was also conducted, this was a pre-inoculation assay. In the pre-inoculation assay serum starved media containing the appropriate concentration of rfhSP-D was incubated on PBS washed HeLa cells for two hours prior to addition of HRV16. The plate containing HRV16 was rocked and then incubated as for the co-incubation assay described in section 6.2.1. After the incubation period cells were fixed and stained as detailed in section 2.1.8.

6.2.3 Cytokine Analysis

Eight cytokines were analysed, IL-13, IL-4, IL-1β, IP-10, TNF-α, IL-6, IL-8 and RANTES. These cytokines were measured in conditioned cell media taken from HeLa cells 17 hours post infection; the cells had been infected with HRV16 that had been co-incubated for one hour with multimeric nhSP-D prior to infection as described in section 6.2.1. The conditioned cell media was stored at -80°C until cytokine analysis. The cytokines were measured using the MILLIPLEX® multi analyte panel kit from the human cytokine/chemokine magnetic bead panel (Merck Millipore), as per manufactures' instructions. In brief, a standard curve from 10000 pg/ml to 3.2 pg/ml was prepared using the provided standard as well as two quality controls. On a 96 well plate 200 µl of wash buffer was added to each well and incubated for ten minutes at room temperature. The standard and controls were applied to the plate, 25 µl per well. Assay buffer, 25 µl, was added to the sample wells and 25 µl of DMEM was added to the standard curve and control wells. A 25 µl volume of the sample cell supernatant that had been stored at -80 °C was then added to the plate in duplicate prior to addition of 25 µl of beads. The plate was incubated overnight at 4 °C with shaking. After washing twice with the provided wash buffer 25 µl of detection antibody was added to the plate for 1 hour at room temperature. Streptavadin-Phycoerythrin was added to each well for 30 minutes at room temperature and then washed; finally, 150 µl of sheath fluid was added to each well. The MILLIPLEX® beads were analysed using a MAGPIX® instrument with xPONENT software version 4.1.

6.2.4 Primary Nasal Epithelial Cell Culture

Primary nasal epithelial cells (PNECs) were obtained from the inferior turbinates of subjects by nasal brushing biopsy, using 2 mm diameter bronchoscopy brushes (Olympus Endotherapy). The cells were a kind gift from Dr. C. L. Myers (Child Health, University of Southampton). Cells were cultured in collagen coated wells with Bronchial Epithelial Cell Growth Media (BEGM™) (Lonza, Basel, Switzerland) supplemented with 50 U/ml penicillin and 50 U/ml streptomycin (both Invitrogen) and 1 % gentamicin and nystatin and routinely kept at 37 °C, 5 % CO_2. The cells were infected as described in section 6.2.1 at passage two and a density of 8.3 x 10^4 cells/well in a 48 well plate. The cells were infected with a MOI of 20, 13 or 10.

6.3 Results

6.3.1 Validation of Flow Cytometry

An assay utilising the technique of flow cytometry was developed and validated to increase the accuracy and speed at which the effect of collectins on HRV infection could be assessed. The method of FFA took a large amount of time and there was potential for incorporating bias. Flow cytometry allows a larger number of cells to be counted independent of user judgement. Initially the method had to be optimised to ensure detection of HRV infection. Cells were permeabilised using Cytofix/Cytoperm™ (BD biosciences) and stained using the anti-HRV antibody R16-7 which was detected using a goat-anti-mouse-APC secondary antibody (Invitrogen). The two antibodies were titrated to determine the optimal concentration (data not shown). As can be seen in Figure 6-1 there is a clear population of cells labelled with APC in the HRV infected cells that is not visible in the uninfected cells. In all experiments, to account for any non-specific binding

of the secondary antibody, the fluorescence observed in the control (stained uninfected samples) was subtracted from experimental samples.

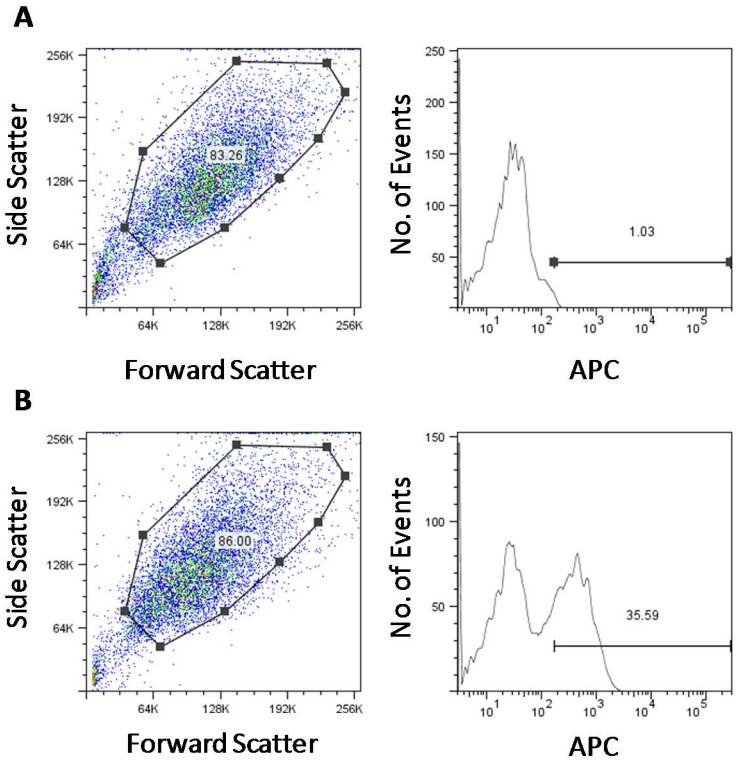

Figure 6-1 Comparison of (A) uninfected vs. (B) HRV16 infected HeLa cells using flow cytometry. HeLa cells were, or were not infected with HRV16 and incubated for 17 hours. The cells were then fixed and stained using R16-7 at 70 ng/ml and goat-anti-mouse-APC secondary antibody at 1 $\mu g/ml$. HRV16 infection was assessed using flow cytometry using a FACS Aria and analysed using FlowJo software version 7.6.5.

The methods of flow cytometry and FFA were compared by analysing two plates that were infected with HRV16 at the same time; this was performed with both HeLa cells and 16HBE cells,

Figure 6-2 A and B respectively.

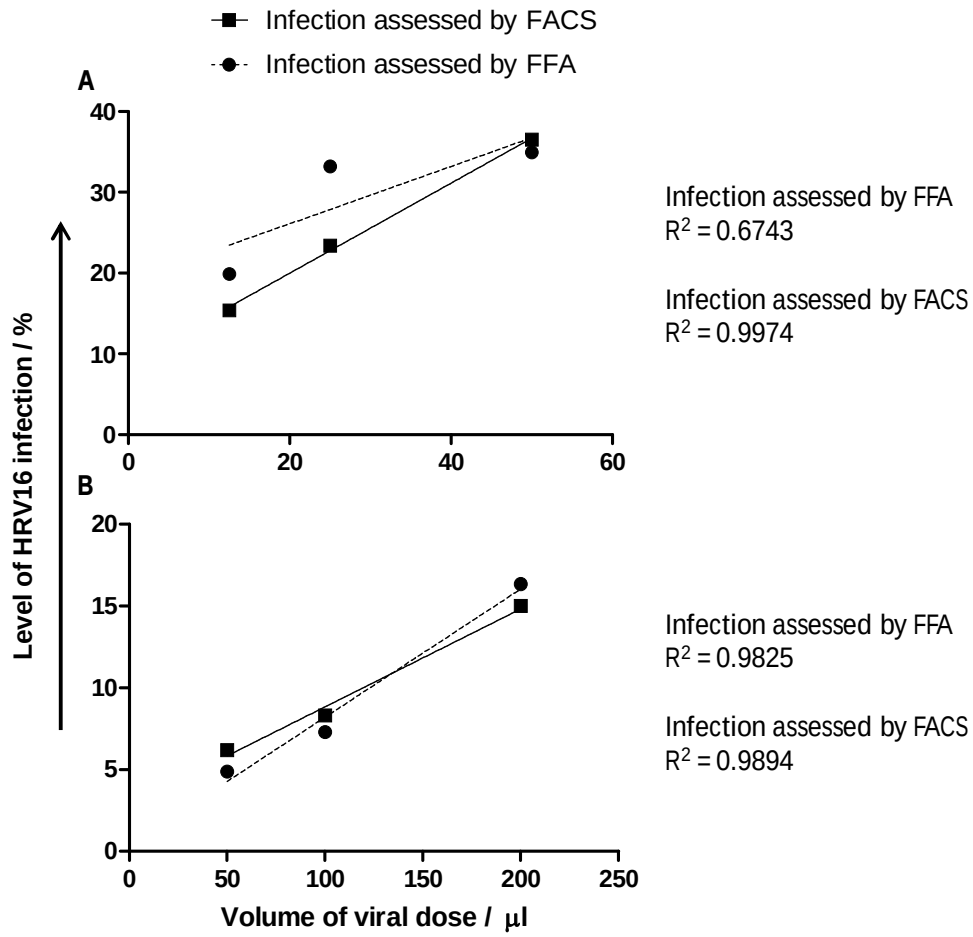

Figure 6-2 Comparison of HRV16 infection of (A) HeLa cells and (B) 16HBE cells assessed by FFA and flow cytometry (FACS). Monolayers of HeLa or 16HBE cells were infected with the indicated dose of HRV16 in a 24 well plate. Plates were rocked for one hour at room temperature before incubating for 17 hours at 33 °C. Cells were either trypsinised and stained for flow cytometry analysis or fixed using 1 % paraformaldehyde and stained for FFA analysis. Data are mean of duplicate wells.

The techniques of FFA and flow cytometry both showed a dose dependent increase in the level of HRV16 infection detected. The methods were comparable, except for one discrepancy with the level of infection detected with a viral dose of 25 µl on HeLa cells resulting in 33 % infection being detected by FFA compared to 23 % detected by flow cytometry, Figure 6-2.

6.3.2 *In Vitro* HRV Infection of HeLa Cells

The initial step to be able to conduct assays to investigate the effect of collectin on HRV infection was to determine the appropriate viral dose using the stocks that would be used throughout the assays conducted on HeLa cells. A viral dose that resulted in approximately 25 % infection was desirable as this is a large enough infection level to detect accurately but is not maximal. Submaximal infection levels should allow identification of any reduction or increase in infection as a result of the presence of collectins. Both HRV1B and HRV16 were titrated on monolayers of HeLa cells and the level of infection was analysed using flow cytometry, Figure 6-3.

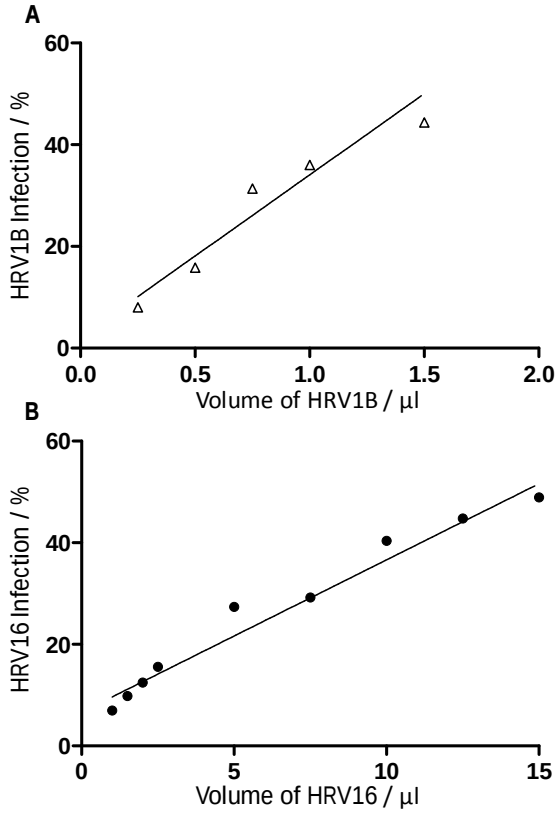

Figure 6-3 Determining viral dose for *in vitro* HeLa cell studies.
Monolayers of HeLa cells in 48 well plates were infected with varying doses of (**A**) HRV1B or (**B**) HRV16. The level of infection was determined by flow cytometry. Data are mean of duplicate wells.

Based on the data in Figure 6-3 to achieve a 25 % infection level in a 48 well plate HeLa cells required a HRV1B dose of 0.7 μl/well (MOI of 0.1) and a HRV16 dose of 4.6 μl/well (MOI of 0.5).

6.3.3 Effect of Pre-incubation of Collectins on HeLa Cells prior to *In Vitro* HRV Infection

To investigate whether the presence of collectins had any effect on the level of HRV infection HeLa cells were pre-treated with varying concentrations of rfhSP-D for two hours prior to addition of HRV16 at an MOI of 0.5, rfhSP-D was not removed when HRV16 was added. Cells were incubated for 17 hours and then stained for analysis by flow cytometry. Figure 6-4 demonstrates that there was no statistical difference between the untreated control cells and the cells that were pre-incubated with rfhSP-D prior to addition of HRV16.

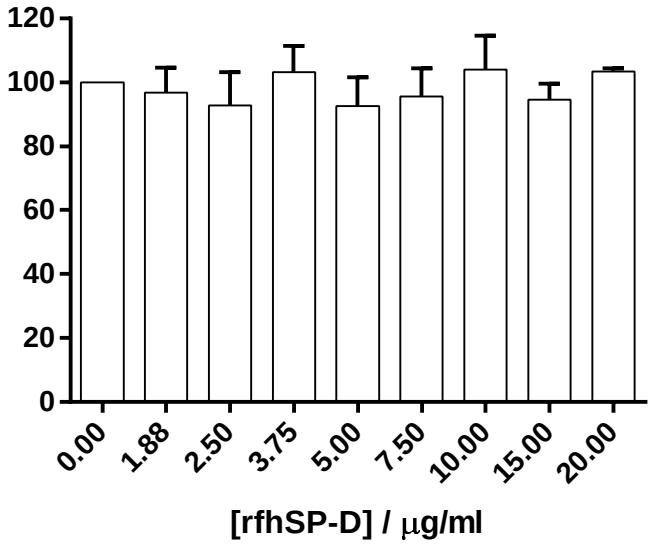

Figure 6-4 Effect of pre-treatment of HeLa cells with rfhSP-D prior to infection with HRV16. Monolayers of HeLa cells were pre-treated with varying concentrations of rfhSP-D; this was left for two hours at 37 °C prior to addition of HRV16. HRV16 infected cells were left 17 hours at 33 °C before fixing and staining for FACS analysis to determine the level of infection. All data are normalised to the control, where no rfhSP-D was present but they were infected with HRV16. Data are mean +S.E.M of three experiments and were analysed using one way ANOVA, no statistical significance was found.

As there were no differences observed with rfhSP-D pre-treatment of cells the experimental set up was altered. The HRV was instead co-incubated with the collectins prior to inoculation of the cells.

6.3.4 Effect of Co-incubation of Collectins and HRV prior to *In Vitro* Infection of HeLa Cells

The effect of co-incubation of collectins with HRV prior to inoculation of HeLa cells was assessed. Cells were inoculated with HRV16 at a MOI of 0.5 or HRV1B at a MOI of 0.1 (as determined in 6.3.2) that had been pre-incubated with serial dilutions of collectins (as indicated), Figure 6-5 and

Figure 6-6. Infection was determined using the FFRA or flow cytometry; the results are expressed as the percentage of control infectivity in each experiment (where cells were infected with HRV but no collectin was applied).

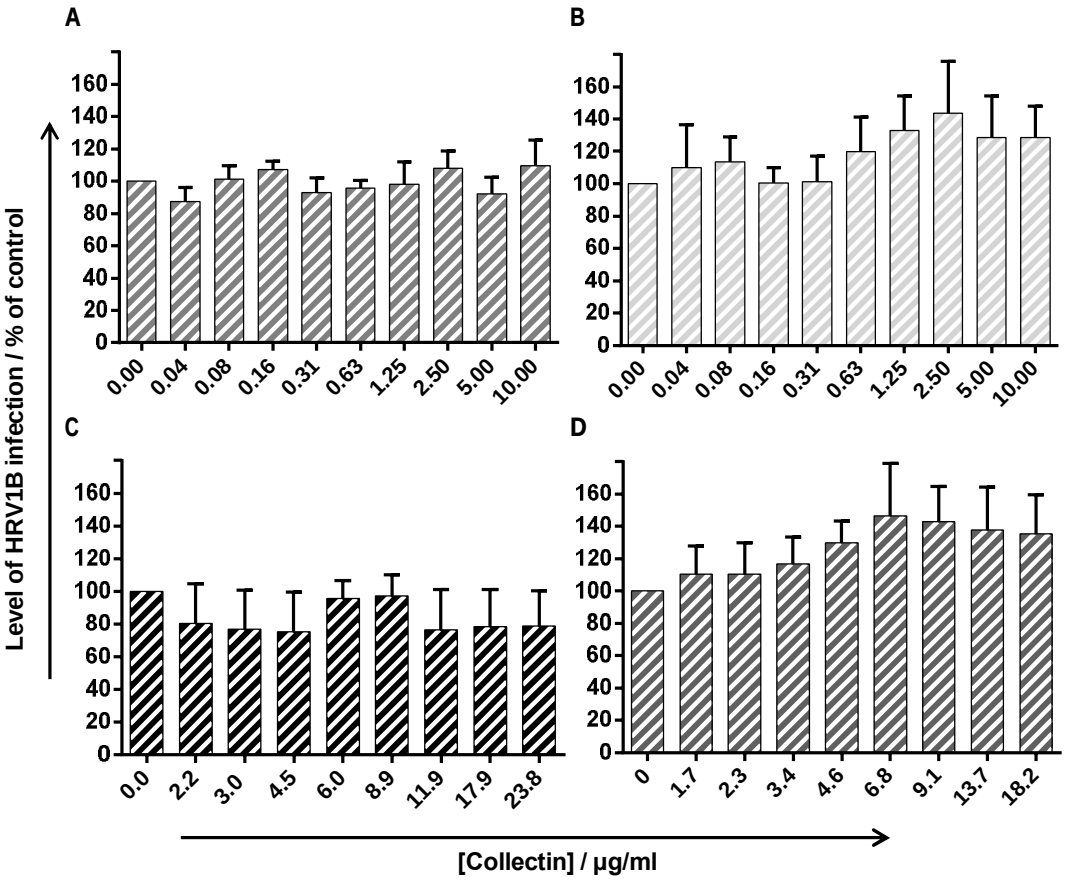

Figure 6-5 HRV1B infection of HeLa cells in the presence of rfhSP-D *in vitro*. HRV1B and multimeric nhSP-D **(A)**, dodecameric nhSP-D **(B)**, rfhSP-D **(C)** or nhSP-A **(D)** (final concentration indicated) were co-incubated for one hour at room temperature with agitation prior to inoculation of monolayers of HeLa cells. Inoculated cells were left 17 hours at 33 °C. The numbers of infected cells were counted using the FFRA or flow cytometry. Results are expressed as a percentage of infected control, where no collectin was applied. Data is the mean of at least three experiments, + S.E.M.

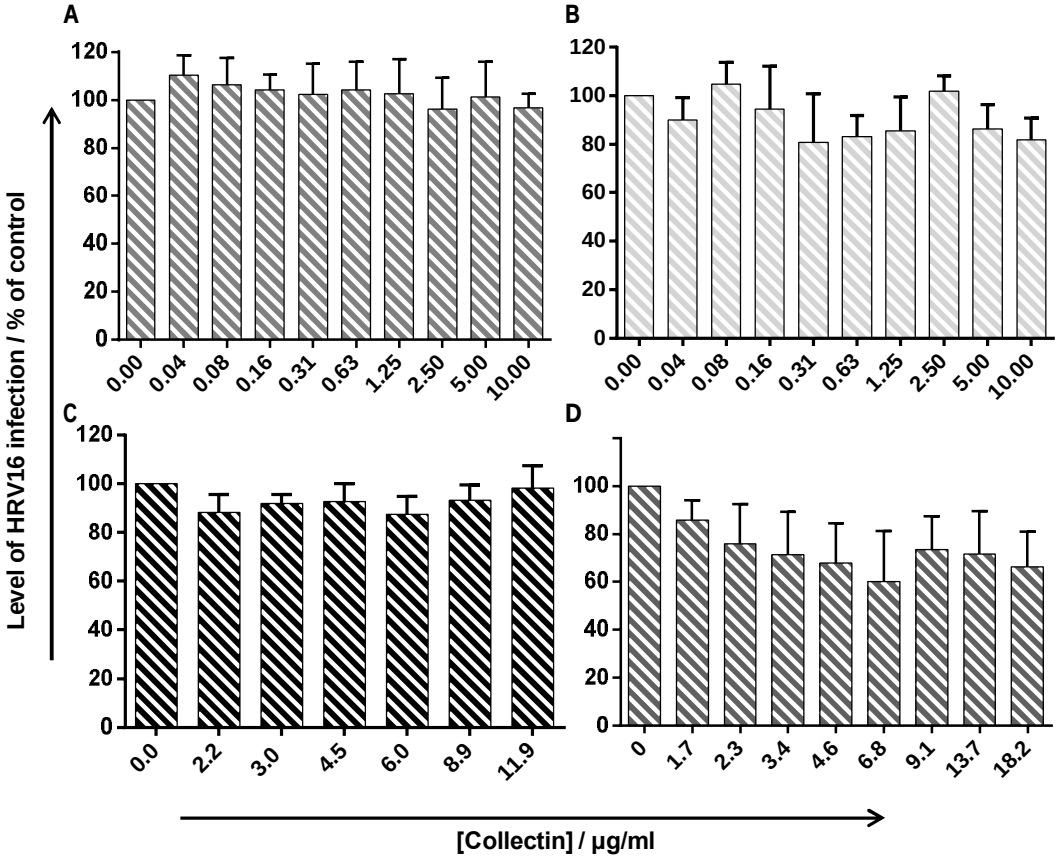

Figure 6-6 HRV16 infection of HeLa cells in the presence of rfhSP-D *in vitro*. HRV16 and multimeric nhSP-D **(A),** dodecameric nhSP-D **(B)**, rfhSP-D **(C)** or nhSP-A **(D)** (final concentration indicated) were co-incubated for one hour at room temperature with agitation prior to inoculation of monolayers of HeLa cells. Inoculated cells were left 17 hours at 33 °C. The numbers of infected cells were counted using the FFRA or flow cytometry. Results are expressed as a percentage of infected control, where no collectin was applied. Data is the mean of at least three experiments, + S.E.M.

Figure 6-5 and Figure 6-6 show there are no significant differences between the control infected with HRV1B or HRV16 without collectin and those with collectin at all concentrations. The results were variable as demonstrated by large S.E.M.

6.3.5 Cytokine Analysis

Several different cytokines in cell media from infections measured in Figure 6-6 were analysed using the MILLIPLEX® multi analyte panel (Merck Millipore). As an initial investigative look at the cytokine profile only samples and controls from HeLa cells infected with HRV16 that had been co-incubated with multimeric nhSP-D were analysed. Eight different cytokines were analysed, IL-13, IL-4, IL-1β, IP-10, TNF-α, IL-6, IL-8 and RANTES. These cytokines were chosen due to their known relevance to HRV infection and potential causative role in asthma exacerbations [209, 210].

In all the samples tested IL-13, IL-4, IL-1β, IP-10 and TNF-α cytokine levels were all at background. The results for IL-6, IL-8 and RANTES can be seen in Figure 6-7, there were no statistically significant differences in the levels of IL-6, IL-8 or RANTES when infected with HRV16 compared to uninfected and in the presence or absence of multimeric nhSP-D. Only two out of the three experiments analysed for IL-6 had levels of IL-6 that were above the detection limit of the assay, and thus only those results are shown. The number of beads measured in each sample was approximately ten; this is less than the 50 beads that are desirable for maximal reliability of the assay.

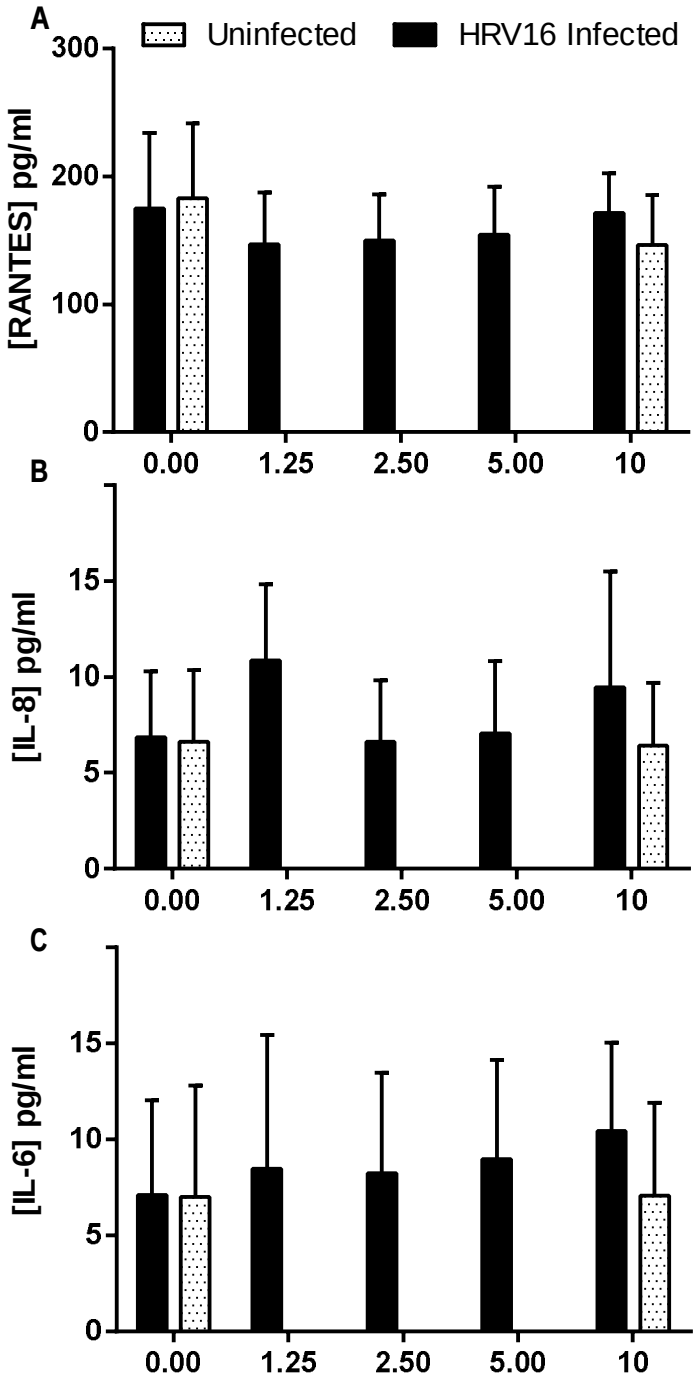

Figure 6-7 Analysis of cytokines in cell supernatant from HeLa cells infected with HRV16 co-incubated with multimeric nhSP-D prior to infection. The cell media from the experiment described in Figure 6-6 A was measured at 17 hours post infection using MILLIPLEX® multi analyte panel (Merck Millipore) measured on a MAGPIX® Instrument with xPONENT software version 4.1. Results are shown for (**A**) RANTES, (**B**) IL-8 and (**C**) IL-6, data are mean + S.E.M. of cytokines measured in three separate assays, all in duplicate.

6.3.6 *In Vitro* HRV Infection of 16HBE Cells

It was desirable to explore the effect of collectins on HRV infection in a more relevant model of the natural target of HRV. HeLa cells provided a good starting point for infection studies as they are easily infected and readily available in the laboratory, however, they are a cervical epithelial cell line. 16HBEs are a SV-40 transformed human bronchial epithelial cell line and so more closely resemble the natural target of HRV [266].

As with *in vitro* experiments in HeLa cells the initial step to enable *in vitro* experiments in 16HBE cells was to determine the appropriate viral dose using the HRV stock that would be used. An infection level that was submaximal but still reliably detectable was desirable to ensure changes in the level of infection in the presence of collectins would be identified. HRV16 was titrated on monolayers of 16HBE cells and the level of infection was analysed using the FFA, Figure 6-8. The maximal infection rate with a high dose of HRV16 was 17 % (MOI = 3).

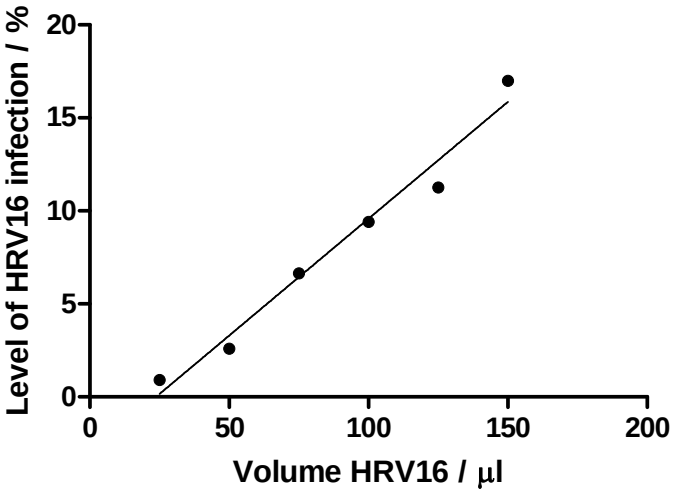

Figure 6-8 Determining viral dose for *in vitro* 16HBE cell studies.
Monolayers of 16HBE cells were infected with varying doses of HRV16 on a 24 well plate. The level of infection was determined by FFA. Data are mean of duplicate wells.

As the maximal infection rate was only 17 % the target infection rate in the assays was reduced to 10 %. This equated to 100 µl of HRV16 per well of a 24 well plate, an MOI of 2. The effect of co-incubation of rfhSP-D with HRV16 on the level of HRV16 infection was assessed, Figure 6-9. There was no statistically significant difference in the level of infection in the presence of rfhSP-D when compared to HRV16 infection without rfhSP-D pre-incubation.

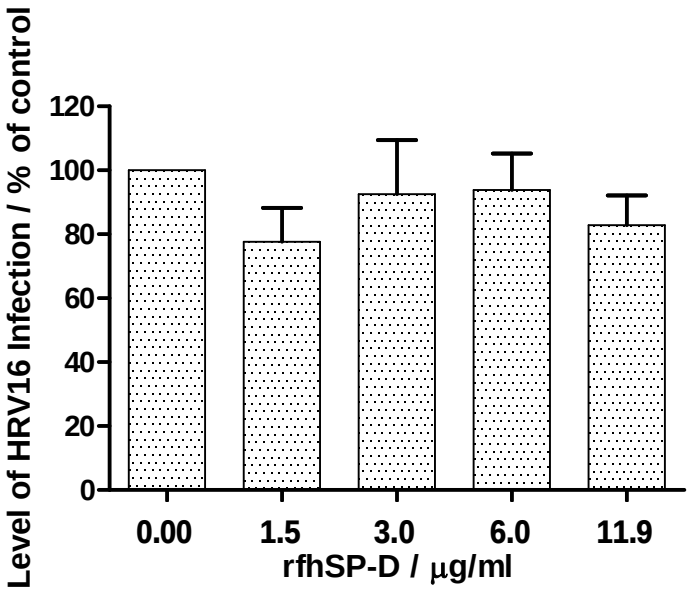

Figure 6-9 HRV16 infection in the presence of rfhSP-D *in vitro* in 16HBE cells. HRV16 and rfhSP-D were pre-incubated for one hour at room temperature prior to inoculation of monolayers of 16HBE cells. Inoculated cells were left 17 hours at 33 °C. The numbers of infected cells were counted using the FFA or assessed using flow cytometry. Results are expressed as a percentage of infected control, where no collectin was applied. Data is the mean of at least four experiments, + S.E.M.

6.3.7 Effect of Co-incubation of Collectins and HRV prior to *In Vitro* Infection of PNEC Cultures

As a model of the natural target of HRV, PNECs were infected with HRV1B in submerged culture *in vitro* to investigate whether the presence of multimeric nhSP-D altered the infection level observed. This was a first look experiment. As with previous assays using other cell types the HRV1B was co-incubated for one hour with multimeric nhSP-D and this was applied to the cells. After incubation for 17 hours the level of infection was assessed using flow cytometry.

Figure 6-10 shows the monolayers of PNECs were successfully infected with HRV1B; this is visible as cell rounding in images Figure 6-10 C and D that is

not visible in Figure 6-10 A and B. The presence of 20 μg/ml multimeric nhSP-D appears to have had no effect on the morphology of the PNECs.

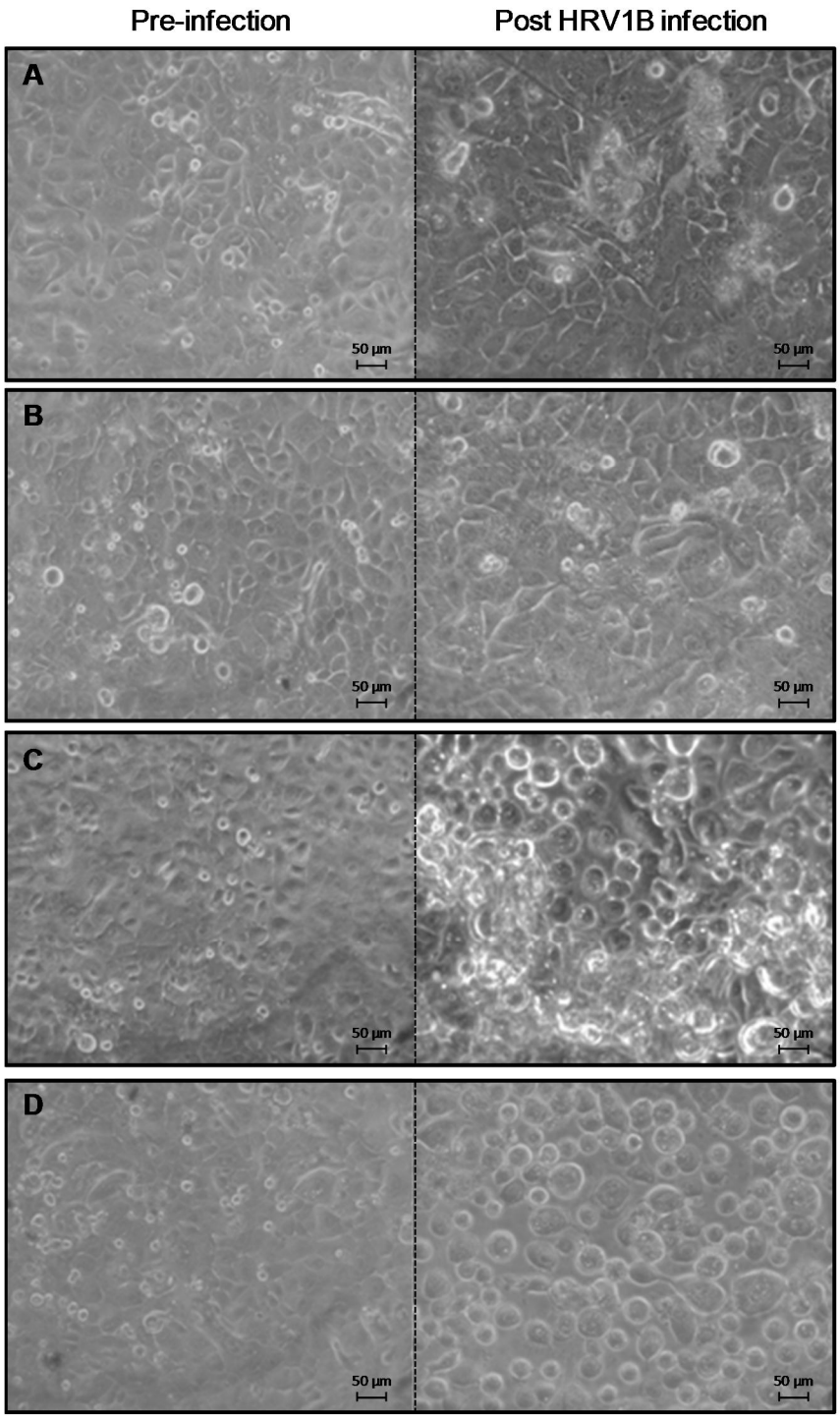

Figure 6-10 HRV1B infection of PNECs in the presence and absence of multimeric nhSP-D. PNECs were infected, or not, with HRV1B (MOI = 13) that had or had not been pre-incubated for one hour with multimeric nhSP-D at a concentration of 20 µg/ml. **(A)** No HRV1B, no multimeric nhSP-D, **(B)** No HRV1B, 20 µg/ml multimeric nhSP-D, **(C)** HRV1B infected, no multimeric nhSP-D, **(D)** HRV1B infected, 20 µg/ml multimeric nhSP-D. Images were taken prior to infection with HRV1B and 17 hours post infection.

As measured by flow cytometry the level of infection in wells infected with HRV1B with no treatment were 12 %, 15 % and 13 % when infected with a MOI of 20, 13 and 10 respectively, suggesting this is the maximal level of infection that can be observed in PNECs. When comparing wells that did receive multimeric nhSP-D to those that did not, Figure 6-11, there was no consistency with the response observed with each viral dose. With a very high viral dose (MOI of 20) the presence of multimeric nhSP-D increased the level of infection by 19 %. With a slightly lower viral dose (MOI of 13) the presence of the multimeric nhSP-D decreased the infection by 28 %. With the lowest MOI of HRV1B used (MOI of 10) there was a 5 % increase in the level of infection when the HRV1B was pre-incubated with multimeric nhSP-D compared to when multimeric nhSP-D was absent.

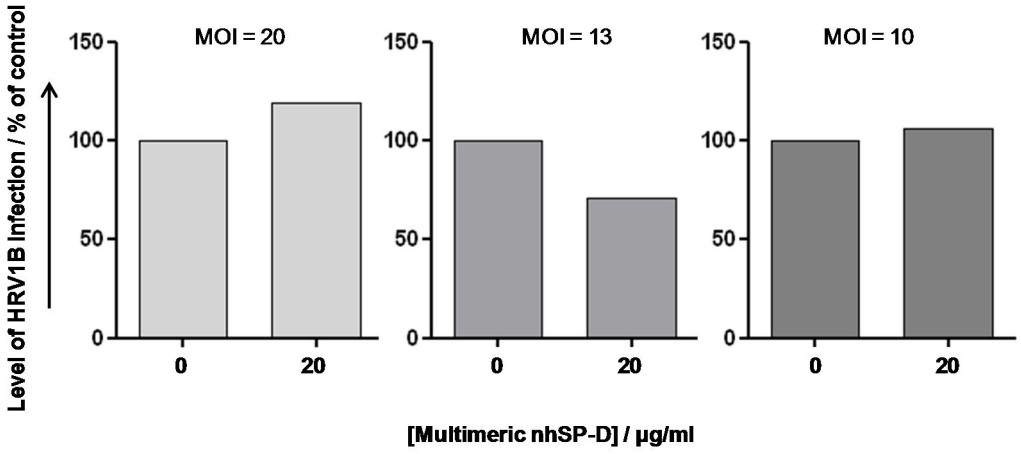

Figure 6-11 Effect of co-incubation of HRV1B with multimeric nhSP-D on the level of HRV1B infection of PNECs. PNECs were infected with HRV1B (MOI as indicated) after a one hour co-incubation with multimeric nhSP-D. The level of infection was normalised to where cells had been infected with the same amount of HRV but no multimeric nhSP-D. Infection with a MOI of 20 and 13 were conducted on duplicate wells, infection with a MOI of 10 was conducted on single wells.

6.4 Discussion

Investigations into whether collectins are able to alter the level of HRV infection *in vitro* were conducted. These experiments are important as they give an indication as to whether the novel interaction that has been identified in this project between SP-D and HRV may be functionally important. It has previously been found that collectin binding to viruses can lead to inhibition of cellular infection, increased phagocytosis and viral agglutination [63, 64, 101, 248].

6.4.1 Flow Cytometry to Detect HRV Infection

The technique of flow cytometry was optimised to detect HRV infection and compared to the FFA for use to determine the level of HRV infection *in vitro*. Flow cytometry was preferable to the FFA technique as the accuracy is higher due to 10,000 cells per well being counted as opposed to approximately 1000 in the FFA, flow cytometry is also much quicker to conduct. The technique of FFA relies on the observer selecting different fields of view of the well in a non-bias manner and correctly counting the cells. Flow cytometry removes this potential for bias and error.

The levels of HRV infection of HeLa cells and 16HBE cells determined by flow cytometry and FFA were comparable. The technique of flow cytometry was therefore validated for use in these *in vitro* studies.

6.4.2 Collectins and *In Vitro* Infection of HeLa cells

The dose of HRV1B and HRV16 required to achieve 25 % infection of HeLa cell cultures was established. A 25 % infection rate was chosen as this was submaximal (infection levels of in excess of 50 % were observed with

relatively low doses of HRV) yet still a reliably detected level of infection. An infection level that is submaximal is preferable as this allows detection of any infection level changes. An assay in which all cells were infected and there is surplus HRV would not permit detection of increases in HRV infection, as there are no more cells to infect.

Pre-incubation of rfhSP-D on HeLa cells prior to infection with HRV16 had no effect on the level of HRV infection observed. It was hypothesised that the presence of rfhSP-D prior to HRV16 infection would mimic what would happen if rfhSP-D was to be given prophylactically, and may result in priming of the cells to stop infection. It is possible, though not previously reported, that nhSP-A and nhSP-D may be able to bind to ICAM-1 directly. ICAM-1 has multiple *N*-glycosylation sites, thus it is possible that nhSP-A or nhSP-D could bind to these residues thereby sterically hindering attachment of HRV [267]. SP-D is known to bind in a calcium dependent manner to *N*-glycosylated sites on the signal regulatory protein α (SIRPα), this interaction can be inhibited by the presence of sugars such as glucose and maltose and by treatment with *N*-glycosidase F [268]. The structure of SIRPα is not too dissimilar to that of ICAM-1; both are type-I transmembrane proteins belonging to the immunoglobulin superfamily and have extracellular immunoglobulin-like domains that are *N*-glycosylated. Pre-treatment of cells with rfhSP-D could also attenuate the response of the cells to HRV infection. This could have been measured in the model used here by detection using quantitative real-time PCR to detect changes in the RNA expression and Luminex or ELISA to measure the release of cytokines upon priming with rfhSP-D. Even if rfhSP-D did not have a "priming" effect the pre-treatment of cells would result in the rfhSP-D being in place as the HRV was added to the cell culture, allowing opportunity for the rfhSP-D to bind the virus.

No reduction in virus infection was observed when collectins (multimeric nhSP-D, dodecameric nhSP-D, rfhSP-D and nhSP-A) were co-incubated with HRV1B and HRV16 before infection of HeLa cells. Co-incubation of SP-D with RSV and IAV inhibits infection as measured by FFA [111, 269]. In the case of SP-D binding to HRV1B and HRV16 it is possible that the SP-D binds to a location on the viral capsid that does not prevent attachment to ICAM-1 or LDLR. If SP-D binds to VP3 on the viral capsid this would not prevent binding to ICAM-1 or LDLR, as exemplified in Figure 6-12. It is also possible that the assay used was not sensitive enough to detect small decreases or increases in the level of infection. The experimental results were variable, in some repeats the level of infection was decreased with the addition of collectins compared to untreated infected controls, whereas in other repeats the level of infection was increased and in some cases the infection level was unchanged. This makes it difficult to draw firm conclusions as to the effect of collectins on HRV infection.

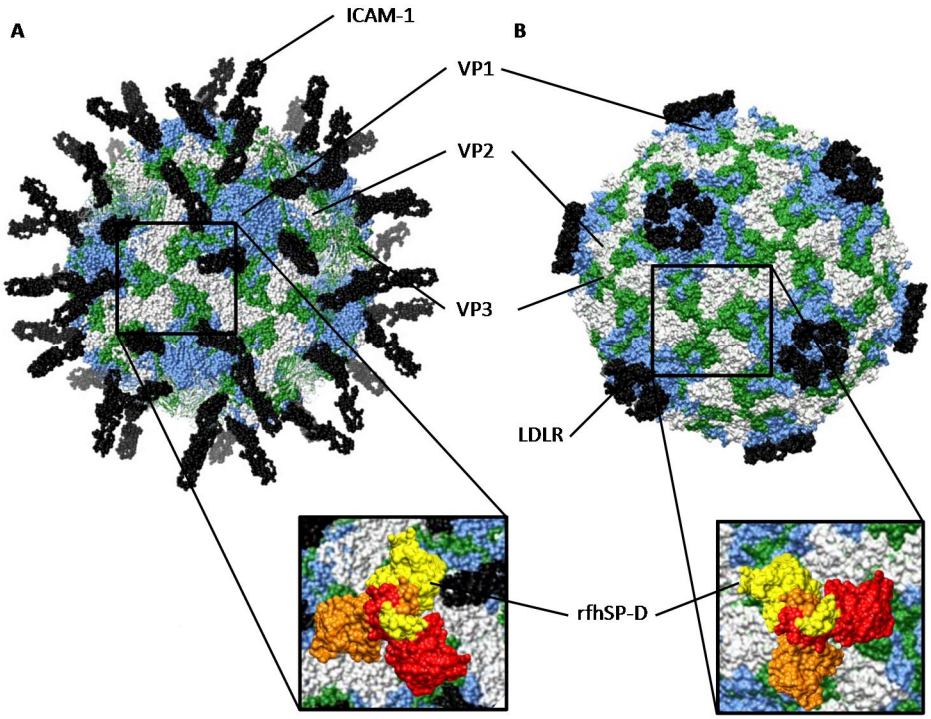

Figure 6-12 A model showing the potential binding site of SP-D on HRV. Representation of a potential binding site on HRV that would not prevent binding to the cellular receptor (ICAM-1 or LDLR) on host cells. **A**. HRV16 is shown in complex with the first two domains of ICAM-1; **B.** HRV2 is shown in complex with a fragment of its receptor LDLR. The VP3 protein (green) is in a trimeric formation, as indicated, which may be the target of SP-D binding, as shown by an overlay of rfhSP-D. VP1 (blue) and VP2 (white) are also visible on the surface of the viral capsid. Diagram is approximately to scale. Crystal structures produced using the UCSF Chimera package version 1.6, PDB codes 1PW9, 1D3E and 1V9U for rfhSP-D, HRV16 complexed with fragments of ICAM-1 and HRV2 complexed with fragments of LDLR, respectively.

The *in vitro* assay used in this study indirectly assessed the ability of nhSP-D, rfhSP-D and nhSP-A to reduce HRV attachment and infection of cells. The assay assessed HRV infection at 17 hours post infection; when the cells were fixed and stained at earlier time points (four and six hours post infection) no infected cells were detected using the mAb. At four and six hours post infection, as shown by Grunert *et al.* using T.E.M and radioactive labelling of viral RNA, the HRV will have attached to the cells and have been

internalised [270]; this was not detected. This indicates that the HRV had to replicate to a level that was detectable by FFA and flow cytometry. Due to the replication time of the virus (8-10 hours) [270] it is unlikely that at 17 hours post infection any secondary infection was detected. The immunofluorescent staining also appeared as single infected cells rather than "islands of cells" that would be expected if secondary infection was being observed. This assay is therefore indirectly assessing prevention of infection by the collectins as if less HRV was initially able to enter the cells then less HRV will be detected. It is unlikely that the collectins would be able to directly inhibit replication of the HRV as they are not found intracellulary. The assay may be improved by using a more sensitive method of assessing HRV infection such as real-time PCR. Using quantitative real-time PCR (qPCR) it would be possible to detect both the positive strand RNA and negative strand (replicative) RNA [216]. This more sensitive method may be advantageous as the amount of virus that has been able to attach to cells and infect cells could be measured directly at an earlier time point, before HRV has replicated. A downfall of this may be that extracellular HRV attached to the surface of cells would be detected, rather than only the intracellular HRV that has been able to infect cells.

An alternative method that could be used would be to label HRV, for instance with fluorescein isothiocyanate (FITC) and detect infection of cells. The level of infection could be assessed by flow cytometry. A potential downfall of this method is that the number of viral particles that have infected the cells may be too low to detect, as was found with FFA and flow cytometry detection of HRV infection at early time points using an antibody directed against HRV.

It may be expected that nhSP-A would not have any effect on HRV infection as there was no binding observed when measured by SPR, indeed no significant change in infection levels were observed when HRV was co-incubated with nhSP-A prior to infection of HeLa cells. However, the absence of nhSP-A binding to HRV does not mean that nhSP-A will not have importance biologically during HRV infections. nhSP-A has been shown to indirectly enhance phagocytosis of pathogens both *in vitro* and *in vivo* by regulating surface expression of receptors that are important in the immune-cell response to pathogens. For example, nhSP-A enhances phagocytosis of *Streptococcus pneumoniae* by increasing expression of scavenger receptor A [130]. Expression of the mannose receptor on human monocyte-derived macrophages is also increased by nhSP-A, leading to enhanced uptake of *Mycobacterium tuberculosis* lipoarabinomannan-coated microspheres [271]. In addition to these functions Wright and colleagues demonstrated that nhSP-A can act as an activation ligand; coating of particles in an opsonin such as IgG can lead to nhSP-A enhanced uptake by direct activation of the cell [272].

Further *in vitro* studies may show that there is increased uptake of HRV into HeLa cells in the presence of collectins. An increased uptake into epithelial cells may be beneficial to the host as the free HRV would be actively taken into the cells for targeted cell clearance by apoptosis, rather than being able to replicate within the cell and cause cell lysis and viral spread [208, 273].

If further *in vitro* infection studies in airway epithelial cells conclusively find there is no difference in the infection level in the presence and absence of collectins it is still possible that binding of SP-D to HRV could have biological significance. SP-D has been shown to act as an opsonin, increasing phagocytosis and therefore clearance of the virus and resolution of infection. Studies with SP-D and IAV have also shown that the presence of SP-D

protects neutrophils from the depressing effect of IAV on the respiratory burst by neutrophils in response to other stimuli, as well as increasing neutrophil uptake of the virus [102, 103]. These functions of SP-D with IAV were dependent on an ability to agglutinate the IAV and a higher multimeric state of the SP-D. SP-D also increases phagocytosis of RSV by alveolar macrophages and neutrophils, observed both *in vitro* and *in vivo* [64]. Due to the clear role SP-D can play in viral phagocytosis investigation into the effect of SP-D on HRV uptake by neutrophils or macrophages is required, regardless of further *in vitro* infection study results.

6.4.3 Effect of Collectins on Cytokine Release by HeLa Cells in Response to HRV Infection

The host response to HRV infection is important in limiting infection. Much of the symptoms of HRV infections and pathogenesis of HRV induced exacerbations of chronic airway diseases such as asthma are however attributed to the host response. The host response incorporates the release of inflammatory mediators, including cytokines, and the recruitment of immune cells. This crucial role of cytokines in causing the pathology associated with HRV infection is hypothesised because unlike in other viral infections, such as IAV and adenovirus, there is little cell cytotoxicity [274, 275]. There are numerous different proinflammatory cytokines and chemokines that have been reported to be induced as a result of HRV infection *in vitro* and *in vivo*. The cytokines include IL-1β, IL-2, IL-4, IL-6, IL-8, IL-11, IL-12, IL-13, IL-16, G-CSF, GM-CSF, TNF-α, and IFNs whilst the chemokines include RANTES, eotaxin and eotaxin-2 [209, 220, 221, 276-279]. Eight different cytokines (IL-13, IL-4, IL-1β, IP-10, TNF-α, IL-6, IL-8 and RANTES) were analysed using a MILLIPLEX® magnetic bead based multi analyte panel in the cell culture supernatants taken from HeLa cells that had

been infected with HRV co-incubated with multimeric nhSP-D. These cytokines were chosen due to their potential involvement in pathogenesis associated with HRV infection and chronic lung diseases [209, 210]. The assay was not optimal due to a low number of beads in each of the samples (ten beads opposed to the desired 50). This will not have affected the overall assay result but a larger number of beads would have increased the reliability of the concentration values.

RANTES is chemotactic for eosinophils, monocytes and T cells. Increased levels of RANTES are found in children who are infected with HRV and have wheeze compared to children who are infected with HRV but do not have wheeze [199]. This suggests RANTES may have an important role in HRV associated pathogenesis in lung diseases. RANTES was detected in the cell supernatant from uninfected cells not treated with multimeric nhSP-D, when the cells were infected with HRV16 the level of RANTES detected did not change. Pre-incubation of HRV16 with multimeric nhSP-D did not alter the RANTES level detected. *In vitro* in primary bronchial epithelial cells (PBECs) and *in vivo* in mice large increases in protein levels of RANTES are detected upon infection with HRV [200, 280]. The lack of RANTES increase when cells were infected with HRV in the experiments described here may be attributed to the short time course (17 hours) of the experiment. In the published PBEC experiments the cells were infected for 48 hours before analysis for RANTES, and in the murine studies there was only a slight but significant increase in RANTES at eight hours post infection with peak RANTES levels observed 24 hours post infection.

As with RANTES there were measurable levels of IL-8 in the HeLa cell supernatants but there was no difference in the level of IL-8 detected either in the presence or absence if multimeric nhSP-D or with HRV16 infection.

When Johnston and colleagues infected a respiratory cell line, A549 cells, with HRV, IL-8 was released in a time-dependent manner; at six hours post infection there was a small but statistically significant increase in IL-8 released by HRV infected cells compared to uninfected controls. IL-8 release continued to increase in HRV infected cultures until the experiment was stopped at 120 hours post infection [278]. This increase in IL-8 had previously been found by Zhu and colleagues, however in their experiments the increase in IL-8 levels was more rapid, with a large increase detected at four hours post infection [221]. It is unclear why there was no increased in IL-8 levels observed in the experiments conducted here. It is possible that the lower MOI of 0.5 used in the experiments reported here was not a large enough viral dose to elicit a response, the experiments by Johnston *et al.* and Zhu *et al.* both used a MOI of 1 in their experiments examining IL-8 release at early time points [221, 278]. Johnston *et al.* did however detect IL-8 significantly raised compared to control at 24 hours post infection when A549 cells were infected with HRV at an MOI of 0.1. Based on the previous studies mentioned above, it may be expected that there would be detectable release of IL-8 by 17 hours post infection and these HeLa cells are capable of producing IL-8 as there is basal expression of IL-8 present.

An increase in IL-8 in the nasal secretions of HRV infected healthy volunteers has been observed, but interestingly there was no correlation between the HRV infected volunteers symptom scores and level of IL-8 [221]. IL-8 is thought to have a potential role in the pathogenesis of HRV exacerbations of asthma. This is due to IL-8 being a potent chemoattractant for neutrophils which are known to be rapidly recruited to the lung. Upon activation neutrophils produce neutrophil elastase which could contribute to airway obstruction and up-regulation of goblet cell mucus production [211]. In asthmatic patients who were monitored upon development of cold

symptoms, those who had exacerbations were found to have higher neutrophil counts in their sputum than patients who did not have an exacerbation, suggesting neutrophils may have an important role in exacerbations [281].

IL-6 was the only other cytokine that was detected in the cell supernatants from HRV infected HeLa cells. Levels of IL-6 above the detection limit of the assay were found in two out of three experiments analysed. In the two experiments that had clear IL-6 detected there was no difference between uninfected HeLa cells and those that had been infected with HRV16. There was a general trend in the HRV16 infected cells that had been co-incubated with multimeric nhSP-D that the higher the concentration of multimeric nhSP-D, the greater the release of IL-6, although this was not statistically significant. Previously IAV infection of SP-D deficient mice has been found to cause increased expression of IL-6 in response to infection, and instillation of SP-D reduced the IL-6 levels [100]. It is therefore unclear why the IL-6 level in the model used here would increase. It is possible that the increase in IL-6 release in the presence of increasing concentrations of multimeric nhSP-D may be due to endotoxin contamination of the preparation. Endotoxin has been shown to induce IL-6 release by epithelial cells [282, 283].

The level of IL-6 detected was very low (5-15 pg/ml); in an experiment in which BEAS-2B cells (a bronchial epithelial cell line) were infected with HRV IL-6 levels were found to be ~100 pg/ml at 14 hours post infection. This experiment however used a much higher viral dose with an MOI of 30 [284]. In a separate study conducted by Zhu *et al.* IL-6 induction in A549 cells and MRC-5 lung fibroblasts was detected upon infection with HRV (MOI of 3), this was significantly increased from baseline within four to eight hours to a

concentration of ~7500 pg/ml and ~2500 pg/ml for A549 cells and MRC-5 lung fibroblasts respectively. The IL-6 production appeared to be HRV specific as sucrose density gradient purified HRV stimulated the production of IL-6, and the production was also dependent upon replication as UV irradiated HRV did not elicit IL-6 production [276].

The exact role of IL-6 in HRV exacerbations of asthma and COPD is unclear, however due to its up-regulation during HRV infection of human volunteers it is thought to be involved in causing airway and systemic inflammation [276]. Experimental evidence suggests that IL-6 may be at least partially responsible for causing fever and infiltration of lymphocytes by increasing vascular permeability and expression of ICAM-1 [285, 286]. IL-6 is a stimulus for myelopoiesis and thus causes increases in peripheral neutrophil numbers. This was demonstrated by injecting rats with a recombinant form of IL-6 which caused an initial peak of neutrophils in the peripheral circulation at 90 minutes followed by a second peak between four and 12 hours [287]. In addition, it is thought IL-6 could contribute to antibody production after HRV infection due to its role in induction of terminal differentiation and antibody production by B lymphocytes [288]. IL-6 is clearly an important cytokine in the limitation of HRV infection as a single nucleotide polymorphism causing in lower production of IL-6 results in worse HRV symptoms [289].

IP-10 is chemotactic for Th1 lymphocytes and NK cells and has been associated with HRV pathology. HRV infection of human volunteers increases IP-10 in nasal lavage and the level of IP-10 correlates with symptom severity and viral titre [219, 290]. Several studies have found HRV infection induces production of IP-10 by epithelial cells [219, 290, 291]. In the cytokine analysis conducted in this study no IP-10 was detected in the cell

supernatant of HRV infected HeLa cells. This discrepancy is likely due to the infection period prior to measuring cytokines being 17 hours in this assay, whereas in previous reports of IP-10 induction the cytokine was detected at 24 hours and found to peak at 48 hours post infection [290].

The pre-treatment of a lung epithelial cell line (H292) with IL-13 and IL-4 can increase ICAM-1 expression with an associated increase in viral titre when subsequently infected with HRV. This may be important in the induction of HRV induced exacerbations of asthma due to IL-13 and IL-4 levels being elevated in asthmatics [292-294]. Due to the potential role of these cytokines in the pathogenesis of HRV induced asthma exacerbations it was of interest to analyse if the presence of collectins during HRV infection attenuated the release of IL-13 and IL-4. No IL-13 or IL-4 was detected in any of the samples tested, either in uninfected or HRV infected samples.

Human tracheal epithelial cells infected with HRV produce both IL-1β and TNF-α, as with IL-13, IL-1β is able to up-regulate the expression of ICAM-1 [295]. IL-1β is found in the nasal secretions of HRV infected volunteers who are symptomatic of colds, whereas in HRV infected volunteers who are asymptomatic no IL-1β is detected; this may suggest a role for IL-1β in causing the familiar symptoms associated with a having a cold [189, 296]. One study has however found that, unlike in the asthmatic volunteers they studied, healthy volunteers infected with HRV had no increase in IL-1β in nasal secretions [297]. TNF-α is released in response to HRV infection, the cytokine has been shown to be up-regulated in the nasal secretions of HRV infected children and *in vitro* human tracheal epithelial cells infected with HRV release TNF-α [298-300]. TNF-α is chemotactic for neutrophils and monocytes, which may be dependent on TNF-α induced release of other cytokines such as IL-8 [301]. As mentioned previously, an influx of

inflammatory cells is associated with the pathogenesis of HRV induced asthma exacerbations. Pre-treatment of H292 cells with TNF-α has been demonstrated to increase ICAM-1 expression associated with HRV infection [196]. This up regulation in ICAM-1 expression could lead to enhanced viral replication in addition to increased inflammatory cell recruitment. Due to the potential roles of IL-1β and TNF-α in pathogenesis caused by HRV infection it was of interest to investigate if these cytokines were induced in the infection assay used here. Neither of the cytokines were detected in any of the cell culture supernatants tested.

The reason for the absence of any significant differences in the levels of cytokines measured after infection of HeLa cells with HRV16 is unclear. It is possible that the time point at which the cytokines were measured, 17 hours, was too early to detect changes. This however should not be the case for IL-8 and IL-6 which have been seen in previous assays to be up-regulated quickly in response to HRV infection. The main discrepancy is that the cells used in most other studies investigating cytokines are cell lines or primary cells that are epithelial cells from the airway, rather than HeLa cells which are a cervical epithelial cell line. The lack of response observed could be attributed to this, however, it is known that HeLa cells are capable of producing a large array of cytokines [302]. The most appropriate *in vitro* model to assess the effect of collectins on the cytokine profile of HRV infected cells would be to use differentiated PNECs or PBECs on an air liquid interface (ALI) culture as these most closely resemble to natural target of HRV. Recent advances in tissue engineering are allowing the development of *in vitro* models in which microfluidics are incorporated into the ALI culture to allow a more accurate representation of the *in vivo* environment [303]. In these microfluidic systems it is also possible to assess

recruitment of cells by including, for instance neutrophils, in the cell media that is flowed under basal surface of the cells.

Some studies also used a very high MOI of HRV, to which they saw a large response in the level of cytokines released into the cell supernatant. A low dose of HRV used in the experiments described here could therefore be a factor in accounting for the lack of cytokine response upon HRV infection. Other studies did however use lower doses of HRV similar to those used here, and therefore the viral dose may not be the limiting factor.

6.4.4 Collectins and *In Vitro* Infection of 16HBE cells

An *in vitro* assay, similar to that discussed above infecting HeLa cells with HRV co-incubated prior to infection with collectins, was repeated using HRV16 and rfhSP-D applied to 16HBE cells. 16HBE cells are a cell line of transformed bronchial epithelial cells; these were chosen as a more relevant model of the natural target of HRV (nasal epithelial cells and bronchial epithelial cells) [227, 304, 305]. A single serotype of HRV and only rfhSP-D was investigated as this was a first look into whether the cell type influenced the result observed in HeLa cell experiments.

An initial experiment was conducted to establish the appropriate dose of HRV16 to infect 16HBE cells with. Interestingly a maximal infection level of 17 % was attained with an MOI of 3. To be able to detect changes in the level of infection a submaximal infection rate of 10 % was used, this was an MOI of 2. With a dose of rfhSP-D at 10 μg/ml, this equates to approximately 70 million molecules of rfhSP-D for every viral particle, or approximately 1.1 million molecules of rfhSP-D per copy of each viral capsid protein, despite the large virus dose.

As with the HeLa cell experiments there was no statistical difference observed in the level of HRV infection in the presence of rfhSP-D when compared to the level of infection in the absence of rfhSP-D. There was a general trend that in the presence of rfhSP-D there was a slight decrease in the level of infection; however, as mentioned previously this was not statistically significant. The lack of statistical significance is likely attributed to the fact that the results were again variable, with some repeats showing a decrease, whilst others showing no difference or even a slight increase. It may be valuable as discussed above in section 6.4.2 to repeat these experiments using more sensitive techniques to detect HRV, such as qPCR.

6.4.5 Collectins and *In Vitro* Infection of PNECs

PNECs are the natural target of HRV *in vivo*, and therefore *in vitro* infection of PNECs is a better model than the cell lines that were used previously [305]. The PNECs used were in submerged culture, thus the cells were undifferentiated. Differentiation of cells can be achieved by using PNECs that have been cultured at an ALI; in these cultures it is possible to distinguish mucus secreting goblet cells, ciliated cells and columnar cells [306, 307]. ALI cultures are more difficult to maintain and therefore as a first look at PNECs the submerged cultures were used.

An initial experiment of HRV infection of PNECs was conducted. This experiment had two principle aims. Firstly, to infect with HRV and to detect this infection as this had not been previously done in the laboratory. Secondly, to add in multimeric nhSP-D to see if this affected the level of HRV infection in comparison to PNECs infected without the presence of the collectin.

HRV1B infection of the PNECs was detected, this was visible under light microscopy as cell rounding. The infection was quantified using flow cytometry and found to be 12 %, 15 % and 13 % when infected with a MOI of 20, 13 and 10 respectively. This suggests that around 13 % is the maximal level of infection that can be observed in PNECs in these conditions. The MOIs used were very high; these were chosen based on previous literature suggesting that PNECs are difficult to infect with HRV [306, 307]. With the high dose of multimeric nhSP-D there should have been sufficient SP-D molecules present to have an effect. With the highest MOI of 20 there will have been approximately 650,000 multimeric nhSP-D molecules per every HRV particle; this is an approximation but gives an indication that there was an excess of SP-D to HRV.

As seen previously with HeLa cell and 16HBE cell experiments the effect of multimeric nhSP-D on HRV infection was variable. At the highest MOI of HRV1B used (MOI = 20) the presence of multimeric nhSP-D increased infection, with an MOI of 13 the presence of multimeric nhSP-D decreased infection but with the lowest MOI of HRV1B (MOI = 10) there was no difference when multimeric nhSP-D was present. This obviously warrants further investigation to be able to draw firm conclusions as to the effect of multimeric nhSP-D on HRV1B infection of PNECs. The more sensitive method of qPCR may be used here, as discussed for other *in vitro* experiments. Cytokine analysis on the cell culture supernatants from these experiments could provide valuable information regarding the effect of SP-D on the cellular response to HRV. The greater relevance of these cells to the *in vivo* target of HRV infection makes them a valuable model to assess the effect of SP-D.

6.4.6 Future Directions

There are many potentially exciting avenues that future research investigating the functional consequences of the interaction between HRV and SP-D could take. Firstly, as discussed above, further *in vitro* experiments are required to conclusively investigate the effect of collectins on the level of HRV infection and the cellular responses to HRV. These *in vitro* assays should ideally be conducted with biologically relevant cells such as PNECs or PBECs but if this is not possible airway derived cell lines could also be used. A time course approach into how collectins effect HRV infection and cellular responses would be particularly interesting. As highlighted previously many assays investigating cytokines released in response to HRV infection are conducted over a much longer period, often 24 to 48 hours, compared with the short time course of 17 hours used in the experiments reported here.

Experiments to explore whether the binding of SP-D to HRV results in enhanced clearance of the virus by aggregation and enhanced phagocytosis would be valuable. Aggregation is observed with IAV and is dependent on the level of multimerisation of the SP-D molecule, this may suggest that the rfhSP-D may not be as effective as the native molecules at aiding HRV clearance by this mechanism [104]. To measure the effect of SP-D on aggregation of IAV a similar method as used by Hartshorn *et al.* could be used; this involves the measurement of light transmission through preparations of virus to which SP-D is added [308]. The level of phagocytosis by SP-D could be assessed by incubating SP-D with HRV that is labelled with a tag such as pHrodo™ (Invitrogen) and incubating the SP-D/HRV-pHrodo with phagocytes. The pHrodo™ only fluoresces when in an acidic environment, thus increased fluorescence as measured by flow

cytometry indicates uptake into the acidic endosome of the phagocyte. This method has previously been used to examine phagocytosis of pHrodo™ labelled bacteria by neutrophils [309]. Modification of phagocyte function could also be explored. The presence of SP-D incubated with IAV and neutrophils ameliorates the depression of neutrophil superoxide responses observed with IAV alone [102, 310]. It would be interesting to explore if SP-D modifies the response of phagocytes to the presence of HRV.

Co-crystallisation studies of HRV and SP-D would help elucidate the site of binding between SP-D and the virus. This could explain whether SP-D would be expected to inhibit binding to the cellular receptor, or not. Mutagenesis studies of the SP-D molecule or the surface of HRV could also be performed to help elucidate where binding occurs.

A potentially very effective experiment to determine whether SP-D and SP-A have functional importance during HRV infection would be to compare the *in vivo* response of SP-D knockout and SP-A knockout mice infected with HRV compared to wild type mice. This would only be possible with minor group HRVs, such as HRV1B, as mice do not have a homologous receptor for ICAM-1 and consequently do not become infected with major group HRVs. Knockout mice clearly show the significance of SP-D in controlling IAV and RSV infection. In a study by Hawgood *et al.* SP-D knockout mice were unable to gain weight for the first week after IAV infection, whilst wild type mice steadily gained weight [101]. In the same study the SP-D knockout mice also had an increased viral load in the lungs; two days post infection the viral load was 40 times that of wild type mice and was 150-fold greater on day four; the viral load then fell dramatically between days four and six. Viral load in SP-A knockout mice was also significantly increased two days post IAV infection but to a much lesser extent than in SP-D knockout mice

[101]. The importance of SP-A and SP-D in controlling RSV infection has also been clearly demonstrated by infecting SP-A and SP-D knockout mice; lung viral titres were significantly increased in both types of knockout mice compared to wild type mice at three and five days post RSV infection. These increased viral loads correlated with significantly increased proinflammatory cytokines in lung homogenates from the SP-A and SP-D knockout mice compared to wild type mice [63, 64].

The HRV infected mice could also be treated with rfhSP-D or nhSP-D and the outcome of infection compared to those without treatment, as performed by LeVine *et al.* in infection experiments using IAV and by Hickling *et al.* in experiments using RSV [100, 111]. A humanised ICAM-1 mouse developed by Bartlett *et al.* could also be used to determine if exogenous treatment with SP-D is beneficial during major group HRV infection [200]. These models would permit assessment of any changes in the cytokine response upon HRV infection when treated with collectins.

7. Chapter 7: Summary and Future Directions

HRV infections are a major cause of the common cold and exacerbations of chronic airways diseases such as asthma and COPD [153, 311]. The high incidence of HRV infections has great socio-economic impact due to reduced quality of life, lost days from work and school, and cost to healthcare services due to hospitalisation. The innate immune system is very important in the pulmonary defence against HRV. The large number of HRV serotypes (>100) result in frequent infections with serotypes of HRV to which people are immunologically naïve, and thus do not have protective antibodies. The innate immune system is instrumental in resolving HRV infection when no antibodies are present as the production of HRV-neutralising antibodies are only seen after the infection has been resolved [206]. Furthermore, defects in the innate immune system of asthmatics have been implicated as an underlying cause of the exaggerated effect of HRV infection in this population [208, 214, 215].

SP-A and SP-D have a well-established role in innate immunity in the lung. The proteins have many functions including the agglutination of pathogens, alteration of cellular responses to pathogens and opsonisation of pathogens for increased uptake by phagocytes [64, 116, 126, 129, 131]. SP-A, SP-D and rfhSP-D have all previously been shown to have antiviral properties [62, 63, 65, 100, 101, 111]. The previously reported antiviral activities of SP-A and SP-D and their localisation in the upper and lower airway epithelium were the foundation for developing the research question addressed in this thesis; **can SP-A, SP-D and rfhSP-D bind to and inhibit infectivity of HRV?**

A novel interaction between nhSP-D and rfhSP-D with HRV1B and HRV16 has been identified in this thesis. This is an exciting discovery as no other

component of the innate immune system was previously known to interact with the surface of HRV. The CRD was found to be the likely site of interaction between SP-D and HRV; this is based on the finding that the interaction was calcium dependent and inhibited by sugars. There are three calcium binding sites in the CRD of SP-D; calcium occupation of these binding sites results in a conformational change in the CRD [46]. In addition, the rfhSP-D which consists of the CRD and neck region, but lacks the collagen region and N-terminus of nhSP-D, retained the ability to bind to HRV. The absence of glycosylation on HRV, which is a nonenveloped virus, suggests that there is a protein-protein interaction between SP-D and HRV. Although the most common interaction of SP-A and SP-D with pathogens is through binding to carbohydrate moieties on the pathogen's surface, SP-D does participate in protein-protein interactions. For example, SP-D has been shown to bind in a calcium dependent manner to IgE, and this interaction can be inhibited by the presence of sugars. IgE is a highly glycosylated protein, however, SP-D does not appear to bind to carbohydrate moieties on the molecule as treatment with Endoglycosidase H and N-glycosidase F did not inhibit SP-D binding [312]. Protein-protein interactions also occur between SP-D and IgG [313]. Co-crystallisation studies would allow better characterisation of the interaction between SP-D and HRV.

The functional consequence of SP-D binding to HRV requires further investigation. The *in vitro* studies conducted as part of this thesis examined the effect of co-incubation of HRV with the collectins prior to infection of HeLa cells, and preliminary work was conducted on 16HBE cells and PNECs; no significant change in the subsequent level of infection was observed. In light of this, it is tempting to speculate that the site of binding on HRV may be VP3 of the viral capsid. SP-D binding to VP3 would leave the canyon and dome on the five-fold axis accessible, thereby allowing

binding to ICAM-1 and LDLR, the major and minor group receptors, respectively. A SPR assay involving immobilisation of the receptor and flowing HRV co-incubated with SP-D over the surface may help elucidate if receptor binding can occur in the presence of SP-D. If the HRV is still able to bind to its receptor even after co-incubation with SP-D this would imply HRV would still be able to infect host cells. Other functional aspects also require investigation. SP-D binding to IAV and RSV has previously been shown to act as an opsonin resulting in enhanced uptake by phagocytes [64, 102]. Dodecameric and multimeric nhSP-D can also induce the agglutination of IAV, which enhances clearance of the pathogens by mucociliary clearance, reduces the number of infectious particles as well as increasing uptake by phagocytes [27]. It would be interesting to explore if either of these also occur with HRV that has been bound by SP-D. The effect of SP-D on the uptake and presentation of HRV by DCs could also warrant investigation; SP-D has previously been shown to augment pathogen uptake and antigen presentation by DCs [87, 88].

Murine studies in SP-A or SP-D deficient mice would allow further characterisation of the functional importance of the proteins during HRV infection. Preliminary work was undertaken in this thesis to develop the appropriate viral dose (Appendix 2); this work could form the basis of further experiments. As the functions of SP-A and SP-D are multifaceted *in vivo* studies would allow a greater understanding in comparison to *in vitro* studies. The *in vivo* mouse experiments could also be extended to test rfhSP-D as an exogenous treatment, and potentially assess the anti-HRV effectiveness of nhSP-D and rfhSP-D in sensitised transgenic mice that are an asthmatic or COPD exacerbation model [200]. This would help determine if nhSP-D and rfhSP-D are potential therapeutics for patient groups that are vulnerable to HRV induced exacerbations. As a therapy rfhSP-D could be

given prophylactically to patients with chronic airways disease during periods of increased risk of HRV induced exacerbation; for example, in the autumn when children return to school [153, 314]. Use of rfhSP-D is an attractive prospective therapeutic as it can potentially be produced on a large scale with relative ease.

Development of nhSP-D and rfhSP-D as therapeutics could have immense impact on patient groups in which HRV infection can lead to exacerbations of disease that can cause irreversible lung damage and hospitalisation [151, 152]. Currently there are no specific therapeutics to treat HRV exacerbations. There has been a great deal of research into developing anti-HRV therapies, but none have been approved for use in the prevention or treatment of the common cold [315-317]. A currently promising therapy is one that addresses the aberrant IFN response observed in asthmatic patients during HRV infection; the therapy involves inhalation of IFN-β and has just completed phase II trials (Synairgen plc. press release, 10th August 2012). A second therapy in clinical development by Biota Holding Ltd. is BTA-798 (Vapendavir), a capsid binder that is thought to inhibit HRV attachment to cellular receptors, has also completed phase II trials [317]. A major hurdle in the treatment of HRV infections is that treatments must have minimal side effects and be fast acting, as the time from first detection of HRV symptoms to peak symptoms is generally 24-36 hours. The other hurdle in the development of HRV treatments is the inability to accurately diagnose a HRV infection clinically. Although HRV is the main cause of the common cold (30-50 %), many other viruses also cause common cold symptoms, including coronavirus, adenovirus, parainfluenza virus, and RSV [135, 318-320]; consequently if HRV-specific treatments are to be successful, a rapid reliable diagnostic test is required, which is currently unavailable. A potential benefit of exogenous SP-D treatment is that it may also be effective

against other respiratory viruses that cause the common cold. There is a wealth of research demonstrating the antiviral effects of SP-A and SP-D against RSV, and SP-A and SP-D have been implicated as potentially important in antiviral activities against coronavirus, adenovirus and parainfluenza virus, although relatively little is known about their interactions with these viruses [63, 64, 111, 120, 321, 322]. Due to these viruses being causes of exacerbations of chronic airways diseases the effect of SP-A and SP-D against these viruses also warrants further investigation [153, 311, 323].

How SP-A and SP-D levels change during HRV infection is currently unknown, this would be interesting to investigate. During other viral infections there are different consequences of infection on SP-A and SP-D levels. Reduced SP-A and SP-D levels in children with severe RSV infection have been reported [324]. It is not clear if low SP-A and SP-D levels lead to increased susceptibility to RSV infection, or whether the infection causes a decrease in SP-A and SP-D levels in BAL. It is however possible that reduced levels of surfactant proteins may contribute to the pathogenesis of respiratory failure seen in severe RSV infection. Low SP-A and SP-D levels during infection could be due to several factors, for example, RSV infection of type II cells could prevent SP synthesis. In addition, the opsonising activity of SP-A and SP-D would increase uptake of SP-A and SP-D bound RSV into phagocytes and consequently reduce the concentration in BAL. The reduction in SP-A and SP-D levels during RSV infection are in contrast to what has been observed *in vivo* in murine IAV infection, where increased SP-D levels are seen [98, 101]. Characterising the levels of SP-D in BAL from asthmatics has not been extensively examined and has been somewhat contradictory [325, 326]. Characterisation would be interesting as if SP-D is shown to have important anti-HRV activity a low SP-D level may predispose

individuals to HRV exacerbations and be indicative of patients who would benefit from exogenous SP-D treatment.

Polymorphisms in the SP-D gene can be instrumental in causing increased risk of infection. This is exemplified by the single nucleotide polymorphism (SNP) that results in an exchange of Threonine for Methionine at amino acid 11 in the N-terminus of SP-D; the SNP can alter immunity to RSV and *M. tuberculosis* due to changing the oligomeric state of the protein [109, 327, 328]. A SNP that causes an Alanine to Threonine switch at position 160 in the CRD of SP-D can increase the risk of RSV infection in children [110]. Whether polymorphisms are associated with increased occurrence or more severe HRV infection would be interesting to explore, especially if SP-D deficient mice demonstrate a fundamental role of SP-D in HRV infections.

The use of rfhSP-D as a therapeutic would obviously require careful assessment. It has been reported that wild-type trimeric neck-CRD fragments of SP-D are not capable of carrying out some of the functions of the oligomerised molecule; for instance agglutination of IAV [241, 329, 330]. If agglutination is a critical mechanism by which HRV is cleared *in vivo* this may lead to impaired clearance of HRV if the rfhSP-D is binding, thereby preventing endogenous nhSP-D binding, but not enhancing clearance.

In conclusion, a novel interaction between SP-D and HRV has been discovered; this broadens our current knowledge of the targets of SP-D. Further investigation into the functional consequences of SP-D binding to HRV is warranted. If SP-D is found to enhance clearance and minimise the inflammatory reaction to HRV infection it could be developed as a future therapeutic to HRV infections. This would be of great importance in patients

who experience exacerbations of airways disease as a result of HRV infection, for which there is no approved antiviral treatment.

8. Appendices

8.1 Appendix 1: Amplification of HRV16

8.1.1 Infection Media

DMEM (with high glucose and GlutaMAX) (Invitrogen) supplemented with:

14 mM HEPES (Sigma-Aldrich)

0.8 mM 7.5 % $NaHCO_3$ (Sigma-Aldrich)

4 % v/v 29.5 g/L Tryptose phosphate broth solution (Sigma-Aldrich)

0.1 mM Non-essential amino acids (Invitrogen)

4 % v/v FBS

50 U/ml penicillin (Invitrogen)

50 mg/ml streptomycin (Invitrogen)

20 mM $MgCl_2$

8.2 Appendix 2: Preliminary Murine Studies

8.3 Introduction

The investigation of the role of SP-A and SP-D during HRV infection *in vivo* would be of great value. Both SP-A and SP-D deficient mouse models, and an inducible SP-D knockout mouse (iDKO) have been developed and would allow determination of the effect of these collectins *in vivo* during HRV infection. The rfhSP-D could also be tested as a potential therapy against HRV infections *in vivo.* Preliminary experiments were undertaken to develop a murine HRV infection model. This initially sought to establish the

viral dose, appropriate time of detection and method of detecting HRV infection. The HRV used was HRV1B, a minor group HRV, as this has previously been shown to attach to mouse airway epithelial cells and successfully replicate in the mouse *in vivo* as it can attach to the mouse homologue of the human LDLR [216, 331]. Major group HRVs that use ICAM-1 as their cellular receptor do not bind to the murine ICAM-1 homologue.

8.4 Materials and Methods

8.4.1 Source of Wild-Type and Knockout Mice

Pathogen free wild-type C57BL/6 mice were obtained from the breeding colony at the Biomedical Research Facility (BRF) at the University of Southampton. The iDKO mouse is a triple transgenic mouse, genetically engineered to express rat SP-D in the distal airway epithelia in response to tetracycline; these mice were originally sourced from Professor J. Whitsett and a breeding colony has been established at the BRF at the University of Southampton [332].

All mice were housed in the Biomedical Research Facility at the Southampton General Hospital in accordance with general animal welfare practices under the home office project licence 30/2691 and personal licence 30/9155.

8.4.2 BAL of Animals

Mice and rats were sacrificed by asphyxiation with carbon dioxide and the BAL was conducted with sterile PBS containing 0.2 mM EDTA. The lungs were lavaged four times with 1 ml.

8.4.3 Cytospin Preparations of Alveolar Macrophages

Alveolar macrophages were isolated from the BAL described in section **Error! Reference source not found.**. Red blood cells were removed by adding 1 ml red blood cell lysis buffer (0.15 M NH_4Cl, 10 mM $KHCO_3$, 0.12 mM EDTA) to cell pellets, cells were then vortexed for three minutes before centrifuging at 200 x g for five minutes. Cell pellets were resuspended in PBS containing 0.2 mM EDTA. Aliquots taken from the resuspended cells were stained with trypan blue and counted by hemocytometer. Cytospins were prepared using a Cytospin 3 (Thermo Shandon Ltd) and a standard protocol. The cytospin preparations were stained with Speedy Diff (Clin-tech Ltd, Guildford, UK), as per manufacturer's instructions.

8.4.4 Infection of Mice with HRV

A total of 15 iDKO mice, removed from tetracycline (previously receiving 1 μg/ml in the drinking water) for 72 hours, were infected with sucrose density gradient purified HRV1B suspended in virus buffer (10 mM Tris, 50 mM $MgCl_2$) at a titre of 1.1×10^7 ffu/ml. As a control, five mice were also mock infected with virus buffer alone. Mice were anesthetised by inhalation of isoflurane. The mice were then weighed and infected intranasally with HRV1B at 2.5 μl/g body weight. Four mice per day were sacrificed by intraperitoneal injection with 250 μl phenolbarbitol, this was performed one, two, three, four or seven days post infection.

8.4.5 Analysis of Infection of Mice

RNA was extracted from the left lung tissue that had been frozen in liquid nitrogen upon removal and stored at -80°C until analysis. RNA was extracted using the RNeasy® Mini kit (Qiagen, Crawley, UK) as recommended by the manufacturer. In brief, the frozen lung was homogenised in 20 μl RLT buffer/mg tissue. The homogenised tissue was clarified by centrifugation at 20,000 x g for three minutes. To the supernatant 600 μl of 70 % ethanol was added before being transferred to an RNeasy Mini spin column and centrifuging for 15 seconds at 8000 x g. The spin column was washed with 700 μl RW1 buffer and twice with 500 μl RPE buffer, centrifuging the column for 15 seconds at 8000 x g after the addition of each buffer. RNA was eluted from the spin column with 30 μl RNase-free water.

RNA concentration was determined using a Nanodrop ND-1000 Spectrophotometer (Thermo Scientific). Complementary DNA (cDNA) was produced from 2 μg of RNA using SuperScript® III reverse transcriptase kit (Invitrogen) as per manufacturer's instructions.

Quantitative real-time PCR (qPCR) was undertaken using the "Quantification of human rhinovirus 1B polyprotein gene, standard kit" from PrimerDesign (Southampton, UK). Reactions were conducted in duplicate according to manufacturers' instructions, in a 10 μl volume, with 1 μl cDNA and run on the Applied Biosystems 7900HR Fast Real-Time PCR System. Normalising gene 18S rRNA (purchased from PrimerDesign) was also analysed. qPCR consisted of initial enzyme activation of ten minutes at 95 °C, followed by 50 cycles of denaturation at 95 °C for ten seconds and data collection at 60 °C for 60 seconds. HRV RNA data was analysed relative to

18S gene expression using a standard ΔC_T calculation as undertaken by Wicks *et al.*, and normalised to the sample with the lowest detected RNA, Mouse 3 from day four [333].

8.5 Results

8.5.1 Characterisation of iDKO Mice

The iDKO mice were characterised in terms of the switching off of SP-D production upon the withdrawal of tetracycline, as they have been engineered to do [332]. The BAL from three groups of mice were analysed, wild type mice (C57BL/6 mice), iDKO mice receiving tetracycline and iDKO mice withdrawn from tetracycline for 48 hours prior to culling. In addition, the BAL from a wild type rat was also analysed as the SP-D induced by tetracycline in the iDKO mice is rat SP-D.

The macrophages from the mice and rat were analysed by Speedy Diff staining of cytospun preparations, representative images are shown in Figure 8-1. The iDKO mice withdrawn from tetracycline and therefore SP-D deficient were foamy in appearance and occasionally multinucleated, Figure 8-1 A. The iDKO mice receiving tetracycline had macrophages that appeared similar to those from iDKO mice withdrawn from tetracycline and were noticeably different to those from wild type mice and rat, which were normal in appearance Figure 8-1 C and D.

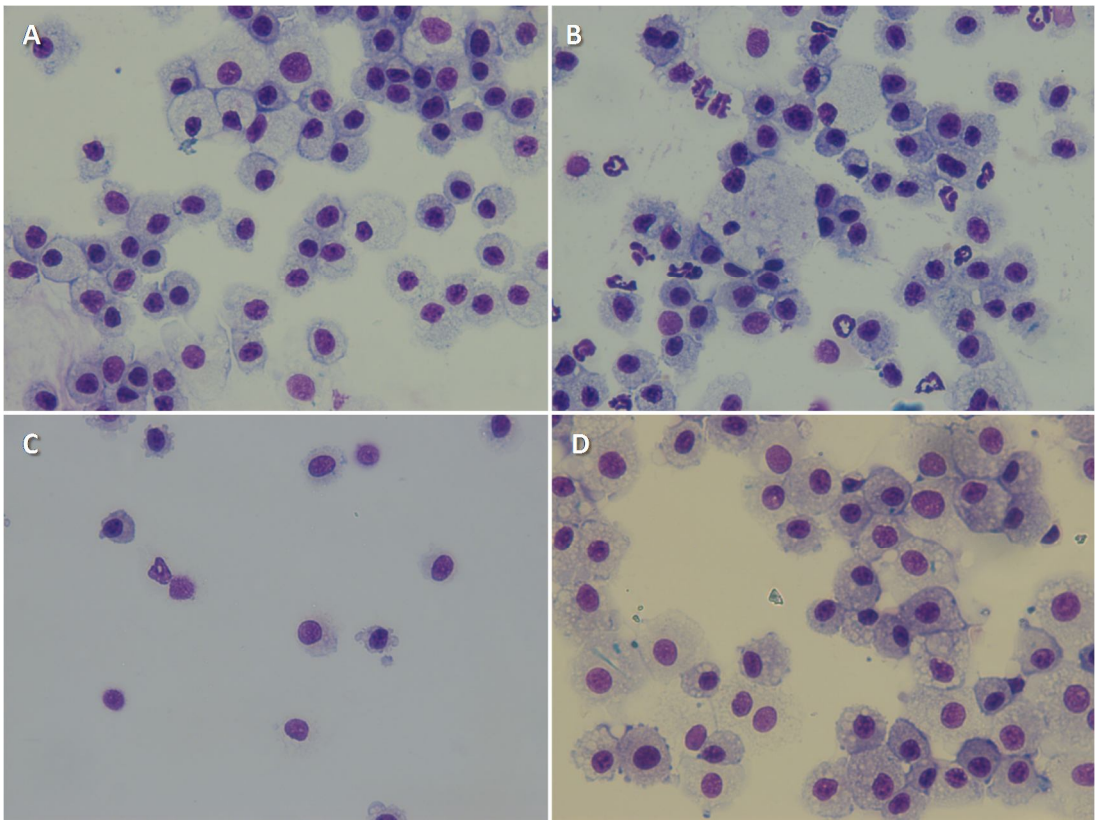

Figure 8-1 Cytospin of alveolar macrophages from (A) iDKO mice withdrawn from tetracycline for 48 hours (B) iDKO receiving tetracycline (C) wild type mice and (D) wild type rat. Animals were lavaged using PBS containing 0.2 mM EDTA. Alveolar macrophages were isolated by treating cell pellets from BAL with red blood cell lysis buffer. A cytospin was then performed and the cells were stained using Speedy Diff.

Clarified lavage from the experiment shown in Figure 8-1 was analysed for the presence of SP-D by western blot, Figure 8-2. This was to assess if the administration of tetracycline was successfully inducing the expression of SP-D in the airways of iDKO mice and that the withdrawal of tetracycline resulted in the switching off of SP-D expression. Recombinant mouse neck and CRD was run alongside the samples as a positive control for the SP-D from wild type mice. All of the samples tested contained a band at approximately 49 kDa. The 49 kDa band is faint in all of the samples tested, including the two out of three of the BAL samples from wild type mice. There does not seem to be any difference in the 49 kDa band seen in samples from iDKO mice withdrawn from tetracycline, and therefore should have

had expression of SP-D turned off, and the iDKO mice receiving tetracycline. As previously reported the rabbit-anti-mouse SP-D antibody used in the western blot does recognise rat SP-D (personal communication with Dr. R. M. Mackay), as a clear band is visible in the BAL sample from the rat.

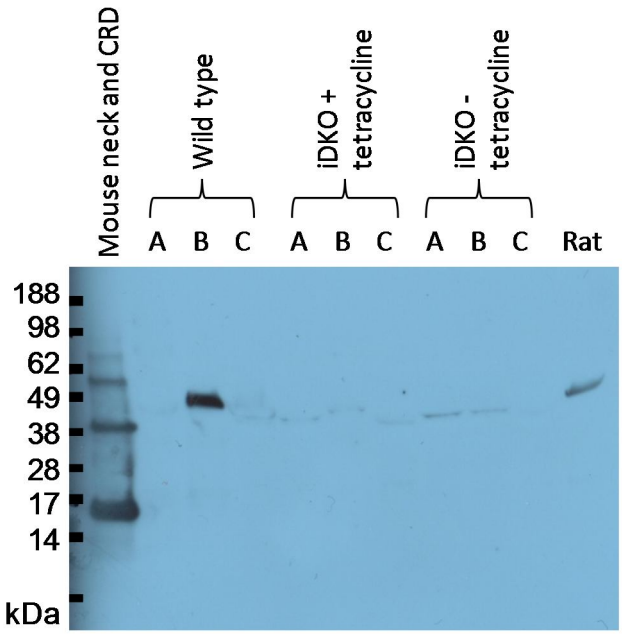

Figure 8-2 Western blot analysis of SP-D content of BAL from wild type and iDKO mice with and without treatment with tetracycline. BAL from mice was concentrated using StrataClean resin (Stratagene), the samples were then reduced and run on a 12 % NuPAGE gel. Once transferred to PVDF the proteins were probed using a rabbit-anti-mouse SP-D primary antibody at 1.5 ng/ml (previously shown to recognise rat SP-D, personal communication with Dr. R. M. MacKay) and anti-rabbit alkaline phosphatase conjugated secondary antibody solution and detection solution (Invitrogen).

8.5.2 HRV Infection of iDKO Mice

A preliminary experiment was set up to determine if HRV1B infection could be caused in iDKO mice and to establish the most appropriate time point to detect infection.

HRV1B RNA in the lung was detected using qPCR. No HRV1B RNA was detected in any of the control mice mock infected with virus buffer only. All qPCR negative controls were also successful. HRV1B RNA was detected in all three HRV1B infected mice killed one day post-inoculation, and in two out of the three HRV1B infected mice killed two days post-inoculation, but at much lower levels than detected at one day post-innoculation, as demonstrated by Figure 8-3. The amount of RNA detected was below that of the HRV1B standard curve (<20 copies viral RNA) and therefore the copy number could not be quantified. No HRV1B RNA was detected at any of the later time points (three, four and seven days post-inoculation), except very low levels in one mouse four days post-inoculation.

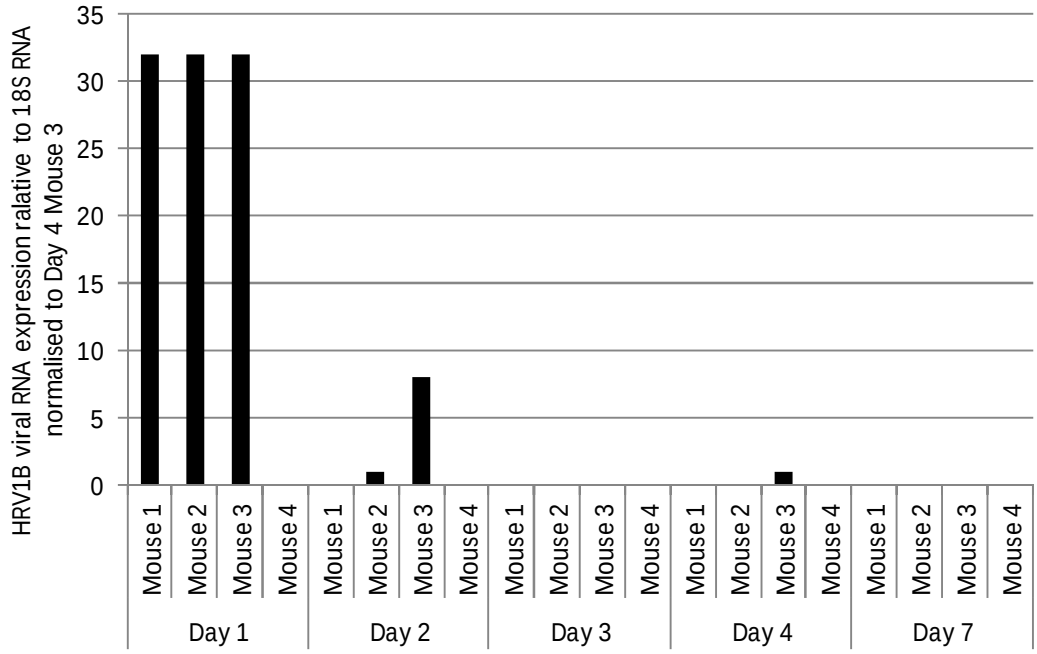

Figure 8-3 HRV1B RNA detected in the lungs of HRV1B infected mice. iDKO mice, withdrawn from tetracyclin for 72 hours and therefore not expressing SP-D, were inoculated with HRV1B by intranasal instillation or mock infected with virus buffer (mouse 4 on each day). Mice were sacrificed on the indicated day and RNA was extracted from the left lung and analysed for viral RNA. Data is expressed relative to 18S RNA and normalised to Mouse 3 from Day 4.

8.6 Discussion

The alveolar macrophages from iDKO mice that were and were not receiving tetracycline had a foamy macrophage appearance, as observed in SP-D deficient mice [91]. This suggests that even whilst on tetracycline treatment the mice are not expressing the correct level of SP-D to maintain a normal macrophage phenotype. The immunoblot analysis of BAL from iDKO mice that were and were not receiving tetracycline showed a band at approximately 49 kDa in all of the samples tested. This faint 49 kDa band may be detection of low levels of SP-D, or it could potentially be cross reactivity with the immunoglobulin heavy chain (~50 kDa) of IgA that would be present in BAL. The presence of foamy macrophages in BAL from iDKO mice receiving tetracycline indicates a SP-D deficiency, thereby suggesting that the 49 kDa band is most likely to be cross reactivity with the immunoglobulin heavy chain as opposed to SP-D. There should be no SP-D detected in iDKO mice withdrawn from tetracycline as these mice should not be expressing SP-D. It is difficult to directly compare SP-D levels in BAL as recovery of lavage may not be the same between mice, despite every effort to do so. These results indicate that careful characterisation of the iDKO mice is required before future experiments to ensure the mice are expressing, or not expressing SP-D as expected. The dosing of tetracycline should be addressed as this may be insufficient and therefore be leading to inadequate expression of SP-D that leads to the foamy macrophage phenotype.

The use of iDKO mice is favourable to SP-D knockout mice as the latter develop an abnormal phenotype characterised by aberrant surfactant homeostasis, emphysematous and fibrotic changes, accumulation of alveolar macrophages and abnormal alveolar cell morphology [334, 335]. In HRV infection studies in which the aim is to assess the effect of SP-D on the

immune defence to the virus, it is preferable to use iDKO mice which do not have an abnormal phenotype if SP-D expression has only been switched off for a short period; this allows better determination of the specific effects of SP-D.

The preliminary HRV1B inoculation of iDKO mice showed that the HRV1B was successfully delivered into the lungs of the mice, as HRV RNA was detected by qPCR at one day post-inoculation. There was not enough RNA detected to be able to quantify relative to the HRV1B standard curve and thus determine HRV1B copy number could not be established. This suggests that the dose given to the mice was too low. It is difficult to compare the viral dose used here to those used in the literature because viral titre is given as a $TCID_{50}$ value; the $TCID_{50}$ is highly dependent on how susceptible the cells used in the assay are to the HRV, as shown in section 3.3.2 with HeLa cells of differing passage number. The viral dose given to mice in experiments detailed in the literature often appear greater than the dose used here; the titre of the stock used here was 1.1×10^7 ffu/ml, whereas typical titres of virus used in the literature are an order of magnitude higher, but this is not true for all studies as a study by Bartlett *et al.* used a dose of 5×10^6 $TCID_{50}$ [200, 216, 336]. The reports in the literature show detection of HRV1B RNA up until day seven, with a peak 18 hours post-inoculation; this was not seen in the experiment reported here [216]. This discrepancy is likely due to a lower viral dose given to the mice, and thus the mice were able to clear the infection more rapidly. Some of the differences may also be attributed to the strain of mice used, in a previous study by Nagarkar *et al*. BALB/c mice demonstrated greater levels of airway inflammation in response to HRV1B compared with C57BL/6 mice; this shows differing immune responses to the infection [217].

To refine the HRV infection studies the titre of the HRV needs to be increased to enable a larger dose of virus to be given to the animals; this will allow quantification of infection and thus it will be possible to follow the immune response to the virus in the presence and absence of SP-D. It will be important to establish reliable protocols for the infection and detection of infection *in vivo* before assessment of the importance of SP-D against HRV can be conducted.

Expansion of the methods of determining infection in the HRV1B inoculated mice would need to be encompassed in future studies. The qPCR used here detected positive-strand RNA, which is the genomic form of viral RNA. Negative-strand RNA could also be detected which is the replicative form of RNA and thus would give an indication of HRV replication [216]. Lung sections could also be stained with an anti-HRV antibody to determine cellular infection. The infectivity of the HRV in the lungs could be tested by overlaying homogenised lungs onto monolayers of HeLa cells and measuring the titre as conducted by Newcomb *et al.* [216]. Determination of the level of inflammation induced by HRV in wild-type and SP-D deficient mice would also be interesting, to observe if SP-D has an important role in HRV infections. These are all methods that would be useful in allowing comparisons between SP-D deficient mice and wild type mice.

Future *in vivo* studies could incorporate the use of transgenic mice expressing a mouse-human ICAM-1 chimera and a model of allergic airway inflammation, the mouse can be infected with major group HRVs, such as HRV16 [200]. This would permit assessment of rfhSP-D as a therapeutic to HRV as a cause of exacerbations. *In vivo* experiments would provide a fantastic opportunity to assess the importance of SP-D in HRV infection and

observe if the novel interaction found in this thesis has an immunological role.

9. References

1. Pattle R. Properties, function and origin of the alveolar lining layer. Nature 1955;175:1125-6.

2. Hoekstra RE, Jackson JC, Myers TF, et al. Improved neonatal survival following multiple doses of bovine surfactant in very premature neonates at risk for respiratory distress syndrome. Pediatrics 1991;88:10-8.

3. Liechty EA, Donovan E, Purohit D, et al. Reduction of neonatal mortality after multiple doses of bovine surfactant in low birth weight neonates with respiratory distress syndrome. Pediatrics 1991;88:19-28.

4. Corbet A, Bucciarelli R, Goldman S, Mammel M, Wold D, Long W. Decreased mortality rate among small premature infants treated at birth with a single dose of synthetic surfactant: a multicenter controlled trial. American Exosurf Pediatric Study Group 1. J Pediatr 1991;118:277-84.

5. Veldhuizen R, Nag K, Orgeig S, Possmayer F. The role of lipids in pulmonary surfactant. Biochim Biophys Acta 1998;1408:90-108.

6. Oosterlaken-Dijksterhuis MA, Haagsman HP, van Golde LM, Demel RA. Characterization of lipid insertion into monomolecular layers mediated by lung surfactant proteins SP-B and SP-C. Biochemistry 1991;30:10965-71.

7. Nogee LM, Garnier G, Dietz HC, et al. A mutation in the surfactant protein B gene responsible for fatal neonatal respiratory disease in multiple kindreds. J Clin Invest 1994;93:1860-3.

8. Vorbroker DK, Profitt SA, Nogee LM, Whitsett JA. Aberrant processing of surfactant protein C in hereditary SP-B deficiency. Am J Physiol 1995;268:L647-L656.

9. Nogee LM, Dunbar AE, III, Wert SE, Askin F, Hamvas A, Whitsett JA. A mutation in the surfactant protein C gene associated with familial interstitial lung disease. N Engl J Med 2001;344:573-9.

10. Nogee LM, Dunbar AE, III, Wert S, Askin F, Hamvas A, Whitsett JA. Mutations in the surfactant protein C gene associated with interstitial lung disease. Chest 2002;121:20S-1S.

11. Epaud R, Ikegami M, Whitsett JA, Jobe AH, Weaver TE, Akinbi HT. Surfactant protein B inhibits endotoxin-induced lung inflammation. Am J Respir Cell Mol Biol 2003;28:373-8.

12. Holmskov U, Teisner B, Willis AC, Reid KB, Jensenius JC. Purification and characterization of a bovine serum lectin (CL-43) with structural homology to conglutinin and SP-D and carbohydrate specificity similar to mannan-binding protein. J Biol Chem 1993;268:10120-5.

13. Lu J, Wiedemann H, Holmskov U, Thiel S, Timpl R, Reid KB. Structural similarity between lung surfactant protein D and conglutinin. Two distinct, C-type lectins containing collagen-like sequences. Eur J Biochem 1993;215:793-9.

14. Hansen S, Holmskov U. Lung surfactant protein D (SP-D) and the molecular diverted descendants: conglutinin, CL-43 and CL-46. Immunobiology 2002;205:498-517.

15. Hansen S, Selman L, Palaniyar N, et al. Collectin 11 (CL-11, CL-K1) is a MASP-1/3-associated plasma collectin with microbial-binding activity. J Immunol 2010;185:6096-104.

16. Pastva AM, Wright JR, Williams KL. Immunomodulatory roles of surfactant proteins A and D: implications in lung disease. Proc Am Thorac Soc 2007;4:252-7.

17. Madsen J, Kliem A, Tornoe I, Skjodt K, Koch C, Holmskov U. Localization of lung surfactant protein D on mucosal surfaces in human tissues. J Immunol 2000;164:5866-70.

18. Miyamura K, Malhotra R, Hoppe HJ, et al. Surfactant proteins A (SP-A) and D (SP-D): levels in human amniotic fluid and localization in the fetal membranes. Biochim Biophys Acta 1994;1210:303-7.

19. Leth-Larsen R, Floridon C, Nielsen O, Holmskov U. Surfactant protein D in the female genital tract. Mol Hum Reprod 2004;10:149-54.

20. Brauer L, Kindler C, Jager K, et al. Detection of surfactant proteins A and D in human tear fluid and the human lacrimal system. Invest Ophthalmol Vis Sci 2007;48:3945-53.

21. Brauer L, Schicht M, Stengl C, et al. Detection of surfactant proteins A, B, C, and D in human gingiva and saliva. Biomed Tech (Berl) 2012;57:59-64.

22. Kim JK, Kim SS, Rha KW, et al. Expression and localization of surfactant proteins in human nasal epithelium. Am J Physiol Lung Cell Mol Physiol 2007;292:L879-L884.

23. Chailley-Heu B, Rubio S, Rougier JP, et al. Expression of hydrophilic surfactant proteins by mesentery cells in rat and man. Biochem J 1997;328 (Pt 1):251-6.

24. MacNeill C, Umstead TM, Phelps DS, et al. Surfactant protein A, an innate immune factor, is expressed in the vaginal mucosa and is present in vaginal lavage fluid. Immunology 2004;111:91-9.

25. Madsen J, Tornoe I, Nielsen O, Koch C, Steinhilber W, Holmskov U. Expression and localization of lung surfactant protein A in human tissues. Am J Respir Cell Mol Biol 2003;29:591-7.

26. Strong P, Kishore U, Morgan C, Lopez BA, Singh M, Reid KB. A novel method of purifying lung surfactant proteins A and D from the lung lavage of alveolar proteinosis patients and from pooled amniotic fluid. J Immunol Methods 1998;220:139-49.

27. Hartshorn K, Chang D, Rust K, White M, Heuser J, Crouch E. Interactions of recombinant human pulmonary surfactant protein D and SP-D multimers with influenza A. Am J Physiol 1996;271:L753-L762.

28. Ogasawara Y, McCormack FX, Mason RJ, Voelker DR. Chimeras of surfactant proteins A and D identify the carbohydrate recognition domains as essential for phospholipid interaction. J Biol Chem 1994;269:29785-92.

29. Strong P, Reid KB, Clark H. Intranasal delivery of a truncated recombinant human SP-D is effective at down-regulating allergic hypersensitivity in mice sensitized to allergens of Aspergillus fumigatus. Clin Exp Immunol 2002;130:19-24.

30. Clark H, Palaniyar N, Hawgood S, Reid KB. A recombinant fragment of human surfactant protein D reduces alveolar macrophage apoptosis and pro-inflammatory cytokines in mice developing pulmonary emphysema. Ann N Y Acad Sci 2003;1010:113-6.

31. Knudsen L, Ochs M, Mackay R, et al. Truncated recombinant human SP-D attenuates emphysema and type II cell changes in SP-D deficient mice. Respir Res 2007;8:70.

32. Clark H, Reid KB. Structural requirements for SP-D function in vitro and in vivo: therapeutic potential of recombinant SP-D. Immunobiology 2002;205:619-31.

33. Haczku A. Protective role of the lung collectins surfactant protein A and surfactant protein D in airway inflammation. J Allergy Clin Immunol 2008;122:861-79.

34. Hakansson K, Lim NK, Hoppe HJ, Reid KB. Crystal structure of the trimeric alpha-helical coiled-coil and the three lectin domains of human lung surfactant protein D. Structure 1999;7:255-64.

35. Hakansson K, Reid KB. Collectin structure: a review. Protein Sci 2000;9:1607-17.

36. Hoppe HJ, Barlow PN, Reid KB. A parallel three stranded alpha-helical bundle at the nucleation site of collagen triple-helix formation. FEBS Lett 1994;344:191-5.

37. White RT, Damm D, Miller J, et al. Isolation and characterization of the human pulmonary surfactant apoprotein gene. Nature 1985;317:361-3.

38. Katyal SL, Singh G, Locker J. Characterization of a second human pulmonary surfactant-associated protein SP-A gene. Am J Respir Cell Mol Biol 1992;6:446-52.

39. Crouch E, Persson A, Chang D, Heuser J. Molecular structure of pulmonary surfactant protein D (SP-D). J Biol Chem 1994;269:17311-9.

40. Haagsman HP, White RT, Schilling J, et al. Studies of the structure of lung surfactant protein SP-A. Am J Physiol 1989;257:L421-L429.

41. Hattori A, Kuroki Y, Katoh T, et al. Surfactant protein A accumulating in the alveoli of patients with pulmonary alveolar proteinosis: oligomeric structure and interaction with lipids. Am J Respir Cell Mol Biol 1996;14:608-19.

42. Voss T, Schafer KP, Nielsen PF, et al. Primary structure differences of human surfactant-associated proteins isolated from normal and proteinosis lung. Biochim Biophys Acta 1992;1138:261-7.

43. Crouch EC. Structure, biologic properties, and expression of surfactant protein D (SP-D). Biochim Biophys Acta 1998;1408:278-89.

44. Drickamer K. Two distinct classes of carbohydrate-recognition domains in animal lectins. J Biol Chem 1988;263:9557-60.

45. Weis WI, Kahn R, Fourme R, Drickamer K, Hendrickson WA. Structure of the calcium-dependent lectin domain from a rat mannose-binding protein determined by MAD phasing. Science 1991;254:1608-15.

46. Shrive AK, Tharia HA, Strong P, et al. High-resolution structural insights into ligand binding and immune cell recognition by human lung surfactant protein D. J Mol Biol 2003;331:509-23.

47. Head JF, Mealy TR, McCormack FX, Seaton BA. Crystal structure of trimeric carbohydrate recognition and neck domains of surfactant protein A. J Biol Chem 2003;278:43254-60.

48. Shang F, Rynkiewicz MJ, McCormack FX, et al. Crystallographic complexes of surfactant protein A and carbohydrates reveal ligand-induced conformational change. J Biol Chem 2011;286:757-65.

49. van Eijk M, White MR, Crouch EC, et al. Porcine pulmonary collectins show distinct interactions with influenza A viruses: role of the N-linked oligosaccharides in the carbohydrate recognition domain. J Immunol 2003;171:1431-40.

50. van Eijk M, van de Lest CH, Batenburg JJ, et al. Porcine surfactant protein D is N-glycosylated in its carbohydrate recognition domain and is assembled into differently charged oligomers. Am J Respir Cell Mol Biol 2002;26:739-47.

51. Winn MD, Ballard CC, Cowtan KD, et al. Overview of the CCP4 suite and current developments. Acta Crystallogr D Biol Crystallogr 2011;67:235-42.

52. Potterton E, Briggs P, Turkenburg M, Dodson E. A graphical user interface to the CCP4 program suite. Acta Crystallogr D Biol Crystallogr 2003;59:1131-7.

53. Zhang P, McAlinden A, Li S, et al. The amino-terminal heptad repeats of the coiled-coil neck domain of pulmonary surfactant protein d are necessary for the assembly of trimeric subunits and dodecamers. J Biol Chem 2001;276:19862-70.

54. Kramer RZ, Vitagliano L, Bella J, et al. X-ray crystallographic determination of a collagen-like peptide with the repeating sequence (Pro-Pro-Gly). J Mol Biol 1998;280:623-38.

55. Lu J, Willis AC, Reid KB. Purification, characterization and cDNA cloning of human lung surfactant protein D. Biochem J 1992;284 (Pt 3):795-802.

56. Voss T, Eistetter H, Schafer KP, Engel J. Macromolecular organization of natural and recombinant lung surfactant protein SP 28-36. Structural homology with the complement factor C1q. J Mol Biol 1988;201:219-27.

57. Brown-Augsburger P, Chang D, Rust K, Crouch EC. Biosynthesis of surfactant protein D. Contributions of conserved NH2-terminal cysteine residues and collagen helix formation to assembly and secretion. J Biol Chem 1996;271:18912-9.

58. Floros J, Steinbrink R, Jacobs K, et al. Isolation and characterization of cDNA clones for the 35-kDa pulmonary surfactant-associated protein. J Biol Chem 1986;261:9029-33.

59. Brown-Augsburger P, Hartshorn K, Chang D, et al. Site-directed mutagenesis of Cys-15 and Cys-20 of pulmonary surfactant protein D. Expression of a trimeric protein with altered anti-viral properties. J Biol Chem 1996;271:13724-30.

60. McCormack FX, Damodarasamy M, Elhalwagi BM. Deletion mapping of N-terminal domains of surfactant protein A. The N-terminal segment is required for phospholipid aggregation and specific inhibition of surfactant secretion. J Biol Chem 1999;274:3173-81.

61. Zhang M, Damodarasamy M, Elhalwagi BM, McCormack FX. The longer isoform and Cys-1 disulfide bridge of rat surfactant protein A are not essential for phospholipid and type II cell interactions. Biochemistry 1998;37:16481-8.

62. Hartshorn KL, Crouch EC, White MR, et al. Evidence for a protective role of pulmonary surfactant protein D (SP-D) against influenza A viruses. J Clin Invest 1994;94:311-9.

63. LeVine AM, Gwozdz J, Stark J, Bruno M, Whitsett J, Korfhagen T. Surfactant protein-A enhances respiratory syncytial virus clearance in vivo. J Clin Invest 1999;103:1015-21.

64. LeVine AM, Elliott J, Whitsett JA, et al. Surfactant protein-d enhances phagocytosis and pulmonary clearance of respiratory syncytial virus. Am J Respir Cell Mol Biol 2004;31:193-9.

65. Benne CA, Kraaijeveld CA, van Strijp JA, et al. Interactions of surfactant protein A with influenza A viruses: binding and neutralization. J Infect Dis 1995;171:335-41.

66. Ofek I, Mesika A, Kalina M, et al. Surfactant protein D enhances phagocytosis and killing of unencapsulated phase variants of Klebsiella pneumoniae. Infect Immun 2001;69:24-33.

67. Kuan SF, Rust K, Crouch E. Interactions of surfactant protein D with bacterial lipopolysaccharides. Surfactant protein D is an Escherichia coli-binding protein in bronchoalveolar lavage. J Clin Invest 1992;90:97-106.

68. Madan T, Kishore U, Singh M, et al. Surfactant proteins A and D protect mice against pulmonary hypersensitivity induced by Aspergillus fumigatus antigens and allergens. J Clin Invest 2001;107:467-75.

69. Malhotra R, Haurum J, Thiel S, Jensenius JC, Sim RB. Pollen grains bind to lung alveolar type II cells (A549) via lung surfactant protein A (SP-A). Biosci Rep 1993;13:79-90.

70. Wang JY, Kishore U, Lim BL, Strong P, Reid KB. Interaction of human lung surfactant proteins A and D with mite (Dermatophagoides pteronyssinus) allergens. Clin Exp Immunol 1996;106:367-73.

71. Palaniyar N, Clark H, Nadesalingam J, Hawgood S, Reid KB. Surfactant protein D binds genomic DNA and apoptotic cells, and enhances their clearance, in vivo. Ann N Y Acad Sci 2003;1010:471-5.

72. Crouch EC, Persson A, Griffin GL, Chang D, Senior RM. Interactions of pulmonary surfactant protein D (SP-D) with human blood leukocytes. Am J Respir Cell Mol Biol 1995;12:410-5.

73. Tino MJ, Wright JR. Surfactant proteins A and D specifically stimulate directed actin-based responses in alveolar macrophages. Am J Physiol 1999;276:L164-L174.

74. Cai GZ, Griffin GL, Senior RM, Longmore WJ, Moxley MA. Recombinant SP-D carbohydrate recognition domain is a chemoattractant for human neutrophils. Am J Physiol 1999;276:L131-L136.

75. Wright JR, Youmans DC. Pulmonary surfactant protein A stimulates chemotaxis of alveolar macrophage. Am J Physiol 1993;264:L338-L344.

76. Gardai SJ, Xiao YQ, Dickinson M, et al. By binding SIRPalpha or calreticulin/CD91, lung collectins act as dual function surveillance molecules to suppress or enhance inflammation. Cell 2003;115:13-23.

77. Sato M, Sano H, Iwaki D, et al. Direct binding of Toll-like receptor 2 to zymosan, and zymosan-induced NF-kappa B activation and TNF-alpha secretion are down-regulated by lung collectin surfactant protein A. J Immunol 2003;171:417-25.

78. Sano H, Sohma H, Muta T, Nomura S, Voelker DR, Kuroki Y. Pulmonary surfactant protein A modulates the cellular response to smooth and rough lipopolysaccharides by interaction with CD14. J Immunol 1999;163:387-95.

79. Borron PJ, Crouch EC, Lewis JF, Wright JR, Possmayer F, Fraher LJ. Recombinant rat surfactant-associated protein D inhibits human T lymphocyte proliferation and IL-2 production. J Immunol 1998;161:4599-603.

80. Borron P, Veldhuizen RA, Lewis JF, et al. Surfactant associated protein-A inhibits human lymphocyte proliferation and IL-2 production. Am J Respir Cell Mol Biol 1996;15:115-21.

81. Borron PJ, Mostaghel EA, Doyle C, Walsh ES, McHeyzer-Williams MG, Wright JR. Pulmonary surfactant proteins A and D directly suppress CD3+/CD4+ cell function: evidence for two shared mechanisms. J Immunol 2002;169:5844-50.

82. Mukherjee S, Giamberardino C, Thomas J, et al. Surfactant protein A integrates activation signal strength to differentially modulate T cell proliferation. J Immunol 2012;188:957-67.

83. Sertl K, Takemura T, Tschachler E, Ferrans VJ, Kaliner MA, Shevach EM. Dendritic cells with antigen-presenting capability reside in airway epithelium, lung parenchyma, and visceral pleura. J Exp Med 1986;163:436-51.

84. Jakel A, Sim RB. The human lung surfactant proteins A (SP-A) and D (SP-D) share similar binding mechanisms and common ligands on macrophages and dendritic cells. JUNQ 2012;2:12-8.

85. Ledford JG, Lo B, Kislan MM, et al. Surfactant protein-A inhibits mycoplasma-induced dendritic cell maturation through regulation of HMGB-1 cytokine activity. J Immunol 2010;185:3884-94.

86. Brinker KG, Garner H, Wright JR. Surfactant protein A modulates the differentiation of murine bone marrow-derived dendritic cells. Am J Physiol Lung Cell Mol Physiol 2003;284:L232-L241.

87. Brinker KG, Martin E, Borron P, et al. Surfactant protein D enhances bacterial antigen presentation by bone marrow-derived dendritic cells. Am J Physiol Lung Cell Mol Physiol 2001;281:L1453-L1463.

88. Hansen S, Lo B, Evans K, Neophytou P, Holmskov U, Wright JR. Surfactant protein D augments bacterial association but attenuates major histocompatibility complex class II presentation of bacterial antigens. Am J Respir Cell Mol Biol 2007;36:94-102.

89. Savill J. Apoptosis in resolution of inflammation. J Leukoc Biol 1997;61:375-80.

90. Vandivier RW, Ogden CA, Fadok VA, et al. Role of surfactant proteins A, D, and C1q in the clearance of apoptotic cells in vivo and in vitro: calreticulin and CD91 as a common collectin receptor complex. J Immunol 2002;169:3978-86.

91. Clark H, Palaniyar N, Strong P, Edmondson J, Hawgood S, Reid KB. Surfactant protein D reduces alveolar macrophage apoptosis in vivo. J Immunol 2002;169:2892-9.

92. Johnson NP, Mueller J. Updating the accounts: global mortality of the 1918-1920 "Spanish" influenza pandemic. Bull Hist Med 2002;76:105-15.

93. Kates M, Allison AC, Tyrell DA, James AT. Origin of lipids in influenza virus. Cold Spring Harb Symp Quant Biol 1962;27:293-301.

94. Couceiro JN, Paulson JC, Baum LG. Influenza virus strains selectively recognize sialyloligosaccharides on human respiratory epithelium; the role of the host cell in selection of hemagglutinin receptor specificity. Virus Res 1993;29:155-65.

95. Nayak DP, Hui EK, Barman S. Assembly and budding of influenza virus. Virus Res 2004;106:147-65.

96. Hartshorn KL, Webby R, White MR, et al. Role of viral hemagglutinin glycosylation in anti-influenza activities of recombinant surfactant protein D. Respir Res 2008;9:65.

97. Anders EM, Hartley CA, Jackson DC. Bovine and mouse serum beta inhibitors of influenza A viruses are mannose-binding lectins. Proc Natl Acad Sci U S A 1990;87:4485-9.

98. Reading PC, Morey LS, Crouch EC, Anders EM. Collectin-mediated antiviral host defense of the lung: evidence from influenza virus infection of mice. J Virol 1997;71:8204-12.

99. Kilbourne ED, Laver WG, Schulman JL, Webster RG. Antiviral activity of antiserum specific for an influenza virus neuraminidase. J Virol 1968;2:281-8.

100. LeVine AM, Whitsett JA, Hartshorn KL, Crouch EC, Korfhagen TR. Surfactant protein D enhances clearance of influenza A virus from the lung in vivo. J Immunol 2001;167:5868-73.

101. Hawgood S, Brown C, Edmondson J, et al. Pulmonary collectins modulate strain-specific influenza a virus infection and host responses. J Virol 2004;78:8565-72.

102. Hartshorn KL, White MR, Shepherd V, Reid K, Jensenius JC, Crouch EC. Mechanisms of anti-influenza activity of surfactant proteins A and D: comparison with serum collectins. Am J Physiol 1997;273:L1156-L1166.

103. Hartshorn KL, Reid KB, White MR, et al. Neutrophil deactivation by influenza A viruses: mechanisms of protection after viral opsonization with collectins and hemagglutination-inhibiting antibodies. Blood 1996;87:3450-61.

104. White M, Kingma P, Tecle T, et al. Multimerization of surfactant protein D, but not its collagen domain, is required for antiviral and opsonic activities related to influenza virus. J Immunol 2008;181:7936-43.

105. Kim HW, Arrobio JO, Brandt CD, et al. Epidemiology of respiratory syncytial virus infection in Washington, D.C. I. Importance of the virus in different respiratory tract disease syndromes and temporal distribution of infection. Am J Epidemiol 1973;98:216-25.

106. Falsey AR, Hennessey PA, Formica MA, Cox C, Walsh EE. Respiratory syncytial virus infection in elderly and high-risk adults. N Engl J Med 2005;352:1749-59.

107. Levine S, Klaiber-Franco R, Paradiso PR. Demonstration that glycoprotein G is the attachment protein of respiratory syncytial virus. J Gen Virol 1987;68 (Pt 9):2521-4.

108. Walsh EE, Brandriss MW, Schlesinger JJ. Purification and characterization of the respiratory syncytial virus fusion protein. J Gen Virol 1985;66 (Pt 3):409-15.

109. Lahti M, Lofgren J, Marttila R, et al. Surfactant protein D gene polymorphism associated with severe respiratory syncytial virus infection. Pediatr Res 2002;51:696-9.

110. Thomas NJ, DiAngelo S, Hess JC, et al. Transmission of surfactant protein variants and haplotypes in children hospitalized with respiratory syncytial virus. Pediatr Res 2009;66:70-3.

111. Hickling TP, Bright H, Wing K, et al. A recombinant trimeric surfactant protein D carbohydrate recognition domain inhibits respiratory syncytial virus infection in vitro and in vivo. Eur J Immunol 1999;29:3478-84.

112. Ghildyal R, Hartley C, Varrasso A, et al. Surfactant protein A binds to the fusion glycoprotein of respiratory syncytial virus and neutralizes virion infectivity. J Infect Dis 1999;180:2009-13.

113. Sano H, Nagai K, Tsutsumi H, Kuroki Y. Lactoferrin and surfactant protein A exhibit distinct binding specificity to F protein and differently modulate respiratory syncytial virus infection. Eur J Immunol 2003;33:2894-902.

114. Hickling TP, Malhotra R, Bright H, McDowell W, Blair ED, Sim RB. Lung surfactant protein A provides a route of entry for respiratory syncytial virus into host cells. Viral Immunol 2000;13:125-35.

115. Barr FE, Pedigo H, Johnson TR, Shepherd VL. Surfactant protein-A enhances uptake of respiratory syncytial virus by monocytes and U937 macrophages. Am J Respir Cell Mol Biol 2000;23:586-92.

116. van Iwaarden JF, van Strijp JA, Ebskamp MJ, Welmers AC, Verhoef J, van Golde LM. Surfactant protein A is opsonin in phagocytosis of herpes simplex virus type 1 by rat alveolar macrophages. Am J Physiol 1991;261:L204-L209.

117. van Iwaarden JF, van Strijp JA, Visser H, Haagsman HP, Verhoef J, van Golde LM. Binding of surfactant protein A (SP-A) to herpes simplex virus type 1-infected cells is mediated by the carbohydrate moiety of SP-A. J Biol Chem 1992;267:25039-43.

118. Gaiha GD, Dong T, Palaniyar N, Mitchell DA, Reid KB, Clark HW. Surfactant protein A binds to HIV and inhibits direct infection of CD4+ cells, but enhances dendritic cell-mediated viral transfer. J Immunol 2008;181:601-9.

119. Meschi J, Crouch EC, Skolnik P, et al. Surfactant protein D binds to human immunodeficiency virus (HIV) envelope protein gp120 and inhibits HIV replication. J Gen Virol 2005;86:3097-107.

120. Leth-Larsen R, Zhong F, Chow VT, Holmskov U, Lu J. The SARS coronavirus spike glycoprotein is selectively recognized by lung

surfactant protein D and activates macrophages. Immunobiology 2007;212:201-11.

121. Geertsma MF, Nibbering PH, Haagsman HP, Daha MR, van FR. Binding of surfactant protein A to C1q receptors mediates phagocytosis of Staphylococcus aureus by monocytes. Am J Physiol 1994;267:L578-L584.

122. Kabha K, Schmegner J, Keisari Y, Parolis H, Schlepper-Schaeffer J, Ofek I. SP-A enhances phagocytosis of Klebsiella by interaction with capsular polysaccharides and alveolar macrophages. Am J Physiol 1997;272:L344-L352.

123. Gaynor CD, McCormack FX, Voelker DR, McGowan SE, Schlesinger LS. Pulmonary surfactant protein A mediates enhanced phagocytosis of Mycobacterium tuberculosis by a direct interaction with human macrophages. J Immunol 1995;155:5343-51.

124. Ferguson JS, Voelker DR, McCormack FX, Schlesinger LS. Surfactant protein D binds to Mycobacterium tuberculosis bacilli and lipoarabinomannan via carbohydrate-lectin interactions resulting in reduced phagocytosis of the bacteria by macrophages. J Immunol 1999;163:312-21.

125. van Iwaarden JF, Pikaar JC, Storm J, et al. Binding of surfactant protein A to the lipid A moiety of bacterial lipopolysaccharides. Biochem J 1994;303 (Pt 2):407-11.

126. McNeely TB, Coonrod JD. Aggregation and opsonization of type A but not type B Hemophilus influenzae by surfactant protein A. Am J Respir Cell Mol Biol 1994;11:114-22.

127. Wu H, Kuzmenko A, Wan S, et al. Surfactant proteins A and D inhibit the growth of Gram-negative bacteria by increasing membrane permeability. J Clin Invest 2003;111:1589-602.

128. Pikaar JC, Voorhout WF, van Golde LM, Verhoef J, van Strijp JA, van Iwaarden JF. Opsonic activities of surfactant proteins A and D in phagocytosis of gram-negative bacteria by alveolar macrophages. J Infect Dis 1995;172:481-9.

129. Hartshorn KL, Crouch E, White MR, et al. Pulmonary surfactant proteins A and D enhance neutrophil uptake of bacteria. Am J Physiol 1998;274:L958-L969.

130. Kuronuma K, Sano H, Kato K, et al. Pulmonary surfactant protein A augments the phagocytosis of Streptococcus pneumoniae by alveolar macrophages through a casein kinase 2-dependent increase of cell surface localization of scavenger receptor A. J Biol Chem 2004;279:21421-30.

131. O'Riordan DM, Standing JE, Kwon KY, Chang D, Crouch EC, Limper AH. Surfactant protein D interacts with Pneumocystis carinii and mediates organism adherence to alveolar macrophages. J Clin Invest 1995;95:2699-710.

132. Zimmerman PE, Voelker DR, McCormack FX, Paulsrud JR, Martin WJ. 120-kD surface glycoprotein of Pneumocystis carinii is a ligand for surfactant protein A. J Clin Invest 1992;89:143-9.

133. Madan T, Eggleton P, Kishore U, et al. Binding of pulmonary surfactant proteins A and D to Aspergillus fumigatus conidia enhances phagocytosis and killing by human neutrophils and alveolar macrophages. Infect Immun 1997;65:3171-9.

134. Schelenz S, Malhotra R, Sim RB, Holmskov U, Bancroft GJ. Binding of host collectins to the pathogenic yeast Cryptococcus neoformans: human surfactant protein D acts as an agglutinin for acapsular yeast cells. Infect Immun 1995;63:3360-6.

135. Makela MJ, Puhakka T, Ruuskanen O, et al. Viruses and bacteria in the etiology of the common cold. J Clin Microbiol 1998;36:539-42.

136. Price WH. The isolation af a new virus associated with respiratory clinical disease in humans. Proc Natl Acad Sci U S A 1956;42:892-6.

137. Pelon W, Mogabgab WJ, PHILLIPS IA, PIERCE WE. A cytopathogenic agent isolated from naval recruits with mild respiratory illnesses. Proc Soc Exp Biol Med 1957;94:262-7.

138. Lauber C, Gorbalenya AE. Toward genetics-based virus taxonomy: comparative analysis of a genetics-based classification and the taxonomy of picornaviruses. J Virol 2012;86:3905-15.

139. Ledford RM, Patel NR, Demenczuk TM, et al. VP1 sequencing of all human rhinovirus serotypes: insights into genus phylogeny and

susceptibility to antiviral capsid-binding compounds. J Virol 2004;78:3663-74.

140. Andries K, Dewindt B, Snoeks J, et al. Two groups of rhinoviruses revealed by a panel of antiviral compounds present sequence divergence and differential pathogenicity. J Virol 1990;64:1117-23.

141. Palmenberg AC, Spiro D, Kuzmickas R, et al. Sequencing and analyses of all known human rhinovirus genomes reveal structure and evolution. Science 2009;324:55-9.

142. Hofer F, Gruenberger M, Kowalski H, et al. Members of the low density lipoprotein receptor family mediate cell entry of a minor-group common cold virus. Proc Natl Acad Sci U S A 1994;91:1839-42.

143. Marlovits TC, Abrahamsberg C, Blaas D. Very-low-density lipoprotein receptor fragment shed from HeLa cells inhibits human rhinovirus infection. J Virol 1998;72:10246-50.

144. Greve JM, Davis G, Meyer AM, et al. The major human rhinovirus receptor is ICAM-1. Cell 1989;56:839-47.

145. Staunton DE, Merluzzi VJ, Rothlein R, Barton R, Marlin SD, Springer TA. A cell adhesion molecule, ICAM-1, is the major surface receptor for rhinoviruses. Cell 1989;56:849-53.

146. Tomassini JE, Graham D, DeWitt CM, Lineberger DW, Rodkey JA, Colonno RJ. cDNA cloning reveals that the major group rhinovirus receptor on HeLa cells is intercellular adhesion molecule 1. Proc Natl Acad Sci U S A 1989;86:4907-11.

147. Reischl A, Reithmayer M, Winsauer G, Moser R, Gosler I, Blaas D. Viral evolution toward change in receptor usage: adaptation of a major group human rhinovirus to grow in ICAM-1-negative cells. J Virol 2001;75:9312-9.

148. Vlasak M, Goesler I, Blaas D. Human rhinovirus type 89 variants use heparan sulfate proteoglycan for cell attachment. J Virol 2005;79:5963-70.

149. Bochkov YA, Palmenberg AC, Lee WM, et al. Molecular modeling, organ culture and reverse genetics for a newly identified human rhinovirus C. Nat Med 2011;17:627-32.

150. Fendrick AM, Monto AS, Nightengale B, Sarnes M. The economic burden of non-influenza-related viral respiratory tract infection in the United States. Arch Intern Med 2003;163:487-94.

151. Papi A, Bellettato CM, Braccioni F, et al. Infections and airway inflammation in chronic obstructive pulmonary disease severe exacerbations. Am J Respir Crit Care Med 2006;173:1114-21.

152. Corne JM, Marshall C, Smith S, et al. Frequency, severity, and duration of rhinovirus infections in asthmatic and non-asthmatic individuals: a longitudinal cohort study. Lancet 2002;359:831-4.

153. Johnston SL, Pattemore PK, Sanderson G, et al. Community study of role of viral infections in exacerbations of asthma in 9-11 year old children. BMJ 1995;310:1225-9.

154. Nicholson KG, Kent J, Ireland DC. Respiratory viruses and exacerbations of asthma in adults. BMJ 1993;307:982-6.

155. Rossmann MG, Arnold E, Erickson JW, et al. Structure of a human common cold virus and functional relationship to other picornaviruses. Nature 1985;317:145-53.

156. Bella J, Rossmann MG. Review: rhinoviruses and their ICAM receptors. J Struct Biol 1999;128:69-74.

157. Tomassini JE, Maxson TR, Colonno RJ. Biochemical characterization of a glycoprotein required for rhinovirus attachment. J Biol Chem 1989;264:1656-62.

158. Papi A, Johnston SL. Rhinovirus infection induces expression of its own receptor intercellular adhesion molecule 1 (ICAM-1) via increased NF-kappaB-mediated transcription. J Biol Chem 1999;274:9707-20.

159. Marlin SD, Springer TA. Purified intercellular adhesion molecule-1 (ICAM-1) is a ligand for lymphocyte function-associated antigen 1 (LFA-1). Cell 1987;51:813-9.

160. Diamond MS, Staunton DE, de Fougerolles AR, et al. ICAM-1 (CD54): a counter-receptor for Mac-1 (CD11b/CD18). J Cell Biol 1990;111:3129-39.

161. McClelland A, deBear J, Yost SC, Meyer AM, Marlor CW, Greve JM. Identification of monoclonal antibody epitopes and critical residues

for rhinovirus binding in domain 1 of intercellular adhesion molecule 1. Proc Natl Acad Sci U S A 1991;88:7993-7.

162. Register RB, Uncapher CR, Naylor AM, Lineberger DW, Colonno RJ. Human-murine chimeras of ICAM-1 identify amino acid residues critical for rhinovirus and antibody binding. J Virol 1991;65:6589-96.

163. Kolatkar PR, Bella J, Olson NH, Bator CM, Baker TS, Rossmann MG. Structural studies of two rhinovirus serotypes complexed with fragments of their cellular receptor. EMBO Journal 18(22):6249-59, 1999.

164. Rossmann MG, Palmenberg AC. Conservation of the putative receptor attachment site in picornaviruses. Virology 1988;164:373-82.

165. Smith TJ, Chase ES, Schmidt TJ, Olson NH, Baker TS. Neutralizing antibody to human rhinovirus 14 penetrates the receptor-binding canyon. Nature 1996;383:350-4.

166. Hewat EA, Neumann E, Conway JF, et al. The cellular receptor to human rhinovirus 2 binds around the 5-fold axis and not in the canyon: a structural view. EMBO J 2000;19:6317-25.

167. Verdaguer N, Fita I, Reithmayer M, Moser R, Blaas D. X-ray structure of a minor group human rhinovirus bound to a fragment of its cellular receptor protein. Nat Struct Mol Biol 2004;11:429-34.

168. Go GW, Mani A. Low-density lipoprotein receptor (LDLR) family orchestrates cholesterol homeostasis. Yale J Biol Med 2012;85:19-28.

169. Suzuki T, Yamaya M, Kamanaka M, et al. Type 2 rhinovirus infection of cultured human tracheal epithelial cells: role of LDL receptor. Am J Physiol Lung Cell Mol Physiol 2001;280:L409-L420.

170. Greve JM, Forte CP, Marlor CW, et al. Mechanisms of receptor-mediated rhinovirus neutralization defined by two soluble forms of ICAM-1. J Virol 1991;65:6015-23.

171. DeTulleo L, Kirchhausen T. The clathrin endocytic pathway in viral infection. EMBO J 1998;17:4585-93.

172. Nurani G, Lindqvist B, Casasnovas JM. Receptor priming of major group human rhinoviruses for uncoating and entry at mild low-pH environments. J Virol 2003;77:11985-91.

173. Zhao R, Hadfield AT, Kremer MJ, Rossmann MG. Cations in human rhinoviruses. Virology 1997;227:13-23.

174. Gruenberger M, Wandl R, Nimpf J, et al. Avian homologs of the mammalian low-density lipoprotein receptor family bind minor receptor group human rhinovirus. J Virol 1995;69:7244-7.

175. Schober D, Kronenberger P, Prchla E, Blaas D, Fuchs R. Major and minor receptor group human rhinoviruses penetrate from endosomes by different mechanisms. J Virol 1998;72:1354-64.

176. Prchla E, Kuechler E, Blaas D, Fuchs R. Uncoating of human rhinovirus serotype 2 from late endosomes. J Virol 1994;68:3713-23.

177. Prchla E, Plank C, Wagner E, Blaas D, Fuchs R. Virus-mediated release of endosomal content in vitro: different behavior of adenovirus and rhinovirus serotype 2. J Cell Biol 1995;131:111-23.

178. Duechler M, Skern T, Sommergruber W, et al. Evolutionary relationships within the human rhinovirus genus: comparison of serotypes 89, 2, and 14. Proc Natl Acad Sci U S A 1987;84:2605-9.

179. Pelletier J, Sonenberg N. Internal initiation of translation of eukaryotic mRNA directed by a sequence derived from poliovirus RNA. Nature 1988;334:320-5.

180. Macejak DG, Sarnow P. Internal initiation of translation mediated by the 5' leader of a cellular mRNA. Nature 1991;353:90-4.

181. Kitamura N, Semler BL, Rothberg PG, et al. Primary structure, gene organization and polypeptide expression of poliovirus RNA. Nature 1981;291:547-53.

182. Skern T, Sommergruber W, Blaas D, et al. Human rhinovirus 2: complete nucleotide sequence and proteolytic processing signals in the capsid protein region. Nucleic Acids Res 1985;13:2111-26.

183. Li X, Lu HH, Mueller S, Wimmer E. The C-terminal residues of poliovirus proteinase 2A(pro) are critical for viral RNA replication but not for cis- or trans-proteolytic cleavage. J Gen Virol 2001;82:397-408.

184. Van Dyke TA, Flanegan JB. Identification of poliovirus polypeptide P63 as a soluble RNA-dependent RNA polymerase. J Virol 1980;35:732-40.

185. Love RA, Maegley KA, Yu X, et al. The crystal structure of the RNA-dependent RNA polymerase from human rhinovirus: a dual function target for common cold antiviral therapy. Structure 2004;12:1533-44.

186. Rombaut B, Vrijsen R, Boeye A. New evidence for the precursor role of 14 S subunits in poliovirus morphogenesis. Virology 1990;177:411-4.

187. Palmenberg AC. In vitro synthesis and assembly of picornaviral capsid intermediate structures. J Virol 1982;44:900-6.

188. Jacobson MF, Baltimore D. Morphogenesis of poliovirus. I. Association of the viral RNA with coat protein. J Mol Biol 1968;33:369-78.

189. Proud D, Gwaltney JM, Jr., Hendley JO, Dinarello CA, Gillis S, Schleimer RP. Increased levels of interleukin-1 are detected in nasal secretions of volunteers during experimental rhinovirus colds. J Infect Dis 1994;169:1007-13.

190. Laza-Stanca V, Stanciu LA, Message SD, Edwards MR, Gern JE, Johnston SL. Rhinovirus replication in human macrophages induces NF-kappaB-dependent tumor necrosis factor alpha production. J Virol 2006;80:8248-58.

191. Gern JE, Dick EC, Lee WM, et al. Rhinovirus enters but does not replicate inside monocytes and airway macrophages. J Immunol 1996;156:621-7.

192. Johnston SL, Papi A, Monick MM, Hunninghake GW. Rhinoviruses induce interleukin-8 mRNA and protein production in human monocytes. J Infect Dis 1997;175:323-9.

193. Parry DE, Busse WW, Sukow KA, Dick CR, Swenson C, Gern JE. Rhinovirus-induced PBMC responses and outcome of experimental infection in allergic subjects. J Allergy Clin Immunol 2000;105:692-8.

194. Stockl J, Vetr H, Majdic O, Zlabinger G, Kuechler E, Knapp W. Human major group rhinoviruses downmodulate the accessory function of monocytes by inducing IL-10. J Clin Invest 1999;104:957-65.

195. Douglass JA, Dhami D, Gurr CE, et al. Influence of interleukin-8 challenge in the nasal mucosa in atopic and nonatopic subjects. Am J Respir Crit Care Med 1994;150:1108-13.

196. Sethi SK, Bianco A, Allen JT, Knight RA, Spiteri MA. Interferon-gamma (IFN-gamma) down-regulates the rhinovirus-induced expression of intercellular adhesion molecule-1 (ICAM-1) on human airway epithelial cells. Clin Exp Immunol 1997;110:362-9.

197. Fleming HE, Little FF, Schnurr D, et al. Rhinovirus-16 colds in healthy and in asthmatic subjects: similar changes in upper and lower airways. Am J Respir Crit Care Med 1999;160:100-8.

198. Diwen Q. In Vitro Studies of Neutrophil Interaction with Rhinovirus. National University of Singapore: 2004.

199. Pacifico L, Iacobini M, Viola F, Werner B, Mancuso G, Chiesa C. Chemokine concentrations in nasal washings of infants with rhinovirus illnesses. Clin Infect Dis 2000;31:834-8.

200. Bartlett NW, Walton RP, Edwards MR, et al. Mouse models of rhinovirus-induced disease and exacerbation of allergic airway inflammation. Nat Med 2008;14:199-204.

201. Avila PC, Abisheganaden JA, Wong H, et al. Effects of allergic inflammation of the nasal mucosa on the severity of rhinovirus 16 cold. J Allergy Clin Immunol 2000;105:923-32.

202. Domachowske JB, Dyer KD, Adams AG, Leto TL, Rosenberg HF. Eosinophil cationic protein/RNase 3 is another RNase A-family ribonuclease with direct antiviral activity. Nucleic Acids Res 1998;26:3358-63.

203. Fraenkel DJ, Bardin PG, Sanderson G, Lampe F, Johnston SL, Holgate ST. Lower airways inflammation during rhinovirus colds in normal and in asthmatic subjects. Am J Respir Crit Care Med 1995;151:879-86.

204. Gern JE, Vrtis R, Kelly EA, Dick EC, Busse WW. Rhinovirus produces nonspecific activation of lymphocytes through a monocyte-dependent mechanism. J Immunol 1996;157:1605-12.

205. Igarashi Y, Skoner DP, Doyle WJ, White MV, Fireman P, Kaliner MA. Analysis of nasal secretions during experimental rhinovirus upper respiratory infections. J Allergy Clin Immunol 1993;92:722-31.

206. Barclay WS, al-Nakib W, Higgins PG, Tyrrell DA. The time course of the humoral immune response to rhinovirus infection. Epidemiol Infect 1989;103:659-69.

207. Alper CM, Doyle WJ, Skoner DP, et al. Prechallenge antibodies: moderators of infection rate, signs, and symptoms in adults experimentally challenged with rhinovirus type 39. Laryngoscope 1996;106:1298-305.

208. Wark PA, Johnston SL, Bucchieri F, et al. Asthmatic bronchial epithelial cells have a deficient innate immune response to infection with rhinovirus. J Exp Med 2005;201:937-47.

209. Papadopoulos NG, Bates PJ, Bardin PG, et al. Rhinoviruses infect the lower airways. J Infect Dis 2000;181:1875-84.

210. Papadopoulos NG, Sanderson G, Hunter J, Johnston SL. Rhinoviruses replicate effectively at lower airway temperatures. J Med Virol 1999;58:100-4.

211. Cardell LO, Agusti C, Takeyama K, Stjarne P, Nadel JA. LTB(4)-induced nasal gland serous cell secretion mediated by neutrophil elastase. Am J Respir Crit Care Med 1999;160:411-4.

212. Hessel EM, Cruikshank WW, Van A, I, et al. Involvement of IL-16 in the induction of airway hyper-responsiveness and up-regulation of IgE in a murine model of allergic asthma. J Immunol 1998;160:2998-3005.

213. Mashikian MV, Tarpy RE, Saukkonen JJ, et al. Identification of IL-16 as the lymphocyte chemotactic activity in the bronchoalveolar lavage fluid of histamine-challenged asthmatic patients. J Allergy Clin Immunol 1998;101:786-92.

214. Papadopoulos NG, Stanciu LA, Papi A, Holgate ST, Johnston SL. A defective type 1 response to rhinovirus in atopic asthma. Thorax 2002;57:328-32.

215. Brooks GD, Buchta KA, Swenson CA, Gern JE, Busse WW. Rhinovirus-induced interferon-gamma and airway responsiveness in asthma. Am J Respir Crit Care Med 2003;168:1091-4.

216. Newcomb DC, Sajjan US, Nagarkar DR, et al. Human rhinovirus 1B exposure induces phosphatidylinositol 3-kinase-dependent airway inflammation in mice. Am J Respir Crit Care Med 2008;177:1111-21.

217. Nagarkar DR, Wang Q, Shim J, et al. CXCR2 is required for neutrophilic airway inflammation and hyperresponsiveness in a mouse model of human rhinovirus infection. J Immunol 2009;183:6698-707.

218. Kuo C, Lim S, King NJ, et al. Rhinovirus infection induces expression of airway remodelling factors in vitro and in vivo. Respirology 2011;16:367-77.

219. Wark PA, Bucchieri F, Johnston SL, et al. IFN-gamma-induced protein 10 is a novel biomarker of rhinovirus-induced asthma exacerbations. J Allergy Clin Immunol 2007;120:586-93.

220. Einarsson O, Geba GP, Zhu Z, Landry M, Elias JA. Interleukin-11: stimulation in vivo and in vitro by respiratory viruses and induction of airways hyperresponsiveness. J Clin Invest 1996;97:915-24.

221. Zhu Z, Tang W, Gwaltney JM, Jr., Wu Y, Elias JA. Rhinovirus stimulation of interleukin-8 in vivo and in vitro: role of NF-kappaB. Am J Physiol 1997;273:L814-L824.

222. Okun VM, Blaas D, Kenndler E. Separation and biospecific identification of subviral particles of human rhinovirus serotype 2 by capillary zone electrophoresis. Anal Chem 1999;71:4480-5.

223. Abraham G, Colonno RJ. Many rhinovirus serotypes share the same cellular receptor. J Virol 1984;51:340-5.

224. Reisdorph N, Thomas JJ, Katpally U, et al. Human rhinovirus capsid dynamics is controlled by canyon flexibility. Virology 2003;314:34-44.

225. Dans PE, Forsyth BR, Chanock RM. Density of infectious virus and complement-fixing antigens of two rhinovirus strains. J Bacteriol 1966;91:1605-11.

226. Martin SJ, Johnston MD, Clements JB. Purification and characterization of bovine enteroviruses. J Gen Virol 1970;7:103-13.

227. Mosser AG, Brockman-Schneider R, Amineva S, et al. Similar frequency of rhinovirus-infectible cells in upper and lower airway epithelium. J Infect Dis 2002;185:734-43.

228. White MR, Crouch E, Chang D, et al. Enhanced antiviral and opsonic activity of a human mannose-binding lectin and surfactant protein D chimera. J Immunol 2000;165:2108-15.

229. Hartshorn KL, White MR, Tecle T, et al. Reduced influenza viral neutralizing activity of natural human trimers of surfactant protein D. Respir Res 2007;8:9.

230. Lee WM, Monroe SS, Rueckert RR. Role of maturation cleavage in infectivity of picornaviruses: activation of an infectosome. J Virol 1993;67:2110-22.

231. Kaul P, Singh I, Turner RB. Effect of nitric oxide on rhinovirus replication and virus-induced interleukin-8 elaboration. Am J Respir Crit Care Med 1999;159:1193-8.

232. Korpi-Steiner NL, Bates ME, Lee WM, Hall DJ, Bertics PJ. Human rhinovirus induces robust IP-10 release by monocytic cells, which is independent of viral replication but linked to type I interferon receptor ligation and STAT1 activation. J Leukoc Biol 2006;80:1364-74.

233. McGregor S, Mayor HD. Biophysical Properties on Rhinovirus and Poliovirus. American Society for Microbiology 1968;2:149-54.

234. Gerin JL, Richter WR, Fenters JD, Holper JC. Use of zonal ultracentrifuge systems for biophysical studies of rhinoviruses. J Virol 1968;2:937-43.

235. Chapple PJ, Harris WJ. Biophysical studies of a rhinovirus. Ultracentrifugation and electron microscopy. Nature 1966;209:790-2.

236. Kapikian AZ, Almeida JD, Stott EJ. Immune electron microscopy of rhinoviruses. J Virol 1972;10:142-6.

237. Sorensen GL, Hoegh SV, Leth-Larsen R, et al. Multimeric and trimeric subunit SP-D are interconvertible structures with distinct ligand interaction. Mol Immunol 2009;46:3060-9.

238. Wright JR, Wager RE, Hawgood S, Dobbs L, Clements JA. Surfactant apoprotein Mr = 26,000-36,000 enhances uptake of liposomes by type II cells. J Biol Chem 1987;262:2888-94.

239. Xu X, Kilbourne ED, Hall HE, Cox NJ. Nonimmunoselected intrastrain genetic variation detected in pairs of high-yielding influenza A (H3N2) vaccine and parental viruses. J Infect Dis 1994;170:1432-8.

240. Crouch E, Tu Y, Briner D, et al. Ligand specificity of human surfactant protein D: expression of a mutant trimeric collectin that shows enhanced interactions with influenza A virus. J Biol Chem 2005;280:17046-56.

241. White MR, Boland P, Tecle T, et al. Enhancement of antiviral activity of collectin trimers through cross-linking and mutagenesis of the carbohydrate recognition domain. J Innate Immun 2010;2:267-79.

242. Duvoix A, Miranda E, Perez J, et al. Evaluation of full-length, cleaved and nitrosylated serum surfactant protein D as biomarkers for COPD. COPD 2011;8:79-95.

243. Punatar AD, Kusne S, Blair JE, Seville MT, Vikram HR. Opportunistic infections in patients with pulmonary alveolar proteinosis. J Infect 2012.

244. Ikegami M, Scoville EA, Grant S, et al. Surfactant protein-D and surfactant inhibit endotoxin-induced pulmonary inflammation. Chest 2007;132:1447-54.

245. Wright JR, Zlogar DF, Taylor JC, Zlogar TM, Restrepo CI. Effects of endotoxin on surfactant protein A and D stimulation of NO production by alveolar macrophages. Am J Physiol 1999;276:L650-L658.

246. Wang L, Brauner JW, Mao G, et al. Interaction of recombinant surfactant protein D with lipopolysaccharide: conformation and orientation of bound protein by IRRAS and simulations. Biochemistry 2008;47:8103-13.

247. Restrepo CI, Dong Q, Savov J, Mariencheck WI, Wright JR. Surfactant protein D stimulates phagocytosis of Pseudomonas aeruginosa by alveolar macrophages. Am J Respir Cell Mol Biol 1999;21:576-85.

248. Hartshorn KL, White MR, Voelker DR, Coburn J, Zaner K, Crouch EC. Mechanism of binding of surfactant protein D to influenza A viruses: importance of binding to haemagglutinin to antiviral activity. Biochem J 2000;351 Pt 2:449-58.

249. Xing L, Tjarnlund K, Lindqvist B, et al. Distinct cellular receptor interactions in poliovirus and rhinoviruses. EMBO J 2000;19:1207-16.

250. Doss M, White MR, Tecle T, et al. Interactions of alpha-, beta-, and theta-defensins with influenza A virus and surfactant protein D. J Immunol 2009;182:7878-87.

251. Malhotra R, Haurum JS, Thiel S, Sim RB. Binding of human collectins (SP-A and MBP) to influenza virus. Biochem J 1994;304 (Pt 2):455-61.

252. Griese M, Starosta V. Agglutination of Pseudomonas aeruginosa by surfactant protein D. Pediatr Pulmonol 2005;40:378-84.

253. Schagat TL, Wofford JA, Wright JR. Surfactant protein A enhances alveolar macrophage phagocytosis of apoptotic neutrophils. J Immunol 2001;166:2727-33.

254. Weis WI, Drickamer K, Hendrickson WA. Structure of a C-type mannose-binding protein complexed with an oligosaccharide. Nature 1992;360:127-34.

255. Taneva S, Voelker DR, Keough KM. Adsorption of pulmonary surfactant protein D to phospholipid monolayers at the air-water interface. Biochemistry 1997;36:8173-9.

256. DeSilva NS, Ofek I, Crouch EC. Interactions of surfactant protein D with fatty acids. Am J Respir Cell Mol Biol 2003;29:757-70.

257. Nahshol O, Bronner V, Notcovich A, Rubrecht L, Laune D, Bravman T. Parallel kinetic analysis and affinity determination of hundreds of monoclonal antibodies using the ProteOn XPR36. Anal Biochem 2008;383:52-60.

258. Colonno RJ, Condra JH, Mizutani S, Callahan PL, Davies ME, Murcko MA. Evidence for the direct involvement of the rhinovirus canyon in receptor binding. Proc Natl Acad Sci U S A 1988;85:5449-53.

259. Vlasak M, Blomqvist S, Hovi T, Hewat E, Blaas D. Sequence and structure of human rhinoviruses reveal the basis of receptor discrimination. J Virol 2003;77:6923-30.

260. Crouch EC. Surfactant protein-D and pulmonary host defense. Respir Res 2000;1:93-108.

261. Crouch EC, Smith K, McDonald B, et al. Species differences in the carbohydrate binding preferences of surfactant protein D. Am J Respir Cell Mol Biol 2006;35:84-94.

262. van de Wetering JK, van RA, Vaandrager AB, et al. Surfactant protein D binding to terminal alpha1-3-linked fucose residues and to Schistosoma mansoni. Am J Respir Cell Mol Biol 2004;31:565-72.

263. Sarma VR, Silverton EW, Davies DR, Terry WD. The three-dimensional structure at 6 A resolution of a human gamma Gl immunoglobulin molecule. J Biol Chem 1971;246:3753-9.

264. Kienberger F, Mueller H, Pastushenko V, Hinterdorfer P. Following single antibody binding to purple membranes in real time. EMBO Rep 2004;5:579-83.

265. Arnold R, Konig B, Galatti H, Werchau H, Konig W. Cytokine (IL-8, IL-6, TNF-alpha) and soluble TNF receptor-I release from human

peripheral blood mononuclear cells after respiratory syncytial virus infection. Immunology 1995;85:364-72.

266. Cozens AL, Yezzi MJ, Kunzelmann K, et al. CFTR expression and chloride secretion in polarized immortal human bronchial epithelial cells. Am J Respir Cell Mol Biol 1994;10:38-47.

267. Bloom JW, Madanat MS, Ray MK. Cell line and site specific comparative analysis of the N-linked oligosaccharides on human ICAM-1des454-532 by electrospray ionization mass spectrometry. Biochemistry 1996;35:1856-64.

268. Fournier B, Andargachew R, Robin AZ, et al. Surfactant protein D (Sp-D) binds to membrane-proximal domain (D3) of signal regulatory protein alpha (SIRPalpha), a site distant from binding domain of CD47, while also binding to analogous region on signal regulatory protein beta (SIRPbeta). J Biol Chem 2012;287:19386-98.

269. Hartshorn KL, Sastry KN, Chang D, White MR, Crouch EC. Enhanced anti-influenza activity of a surfactant protein D and serum conglutinin fusion protein. Am J Physiol Lung Cell Mol Physiol 2000;278:L90-L98.

270. Grunert HP, Wolf KU, Langner KD, Sawitzky D, Habermehl KO, Zeichhardt H. Internalization of human rhinovirus 14 into HeLa and ICAM-1-transfected BHK cells. Med Microbiol Immunol 1997;186:1-9.

271. Beharka AA, Gaynor CD, Kang BK, Voelker DR, McCormack FX, Schlesinger LS. Pulmonary surfactant protein A up-regulates activity of the mannose receptor, a pattern recognition receptor expressed on human macrophages. J Immunol 2002;169:3565-73.

272. Tenner AJ, Robinson SL, Borchelt J, Wright JR. Human pulmonary surfactant protein (SP-A), a protein structurally homologous to C1q, can enhance FcR- and CR1-mediated phagocytosis. J Biol Chem 1989;264:13923-8.

273. Tschopp J, Thome M, Hofmann K, Meinl E. The fight of viruses against apoptosis. Curr Opin Genet Dev 1998;8:82-7.

274. Winther B, Brofeldt S, Christensen B, Mygind N. Light and scanning electron microscopy of nasal biopsy material from patients with naturally acquired common colds. Acta Otolaryngol 1984;97:309-18.

275. Winther B, Gwaltney JM, Hendley JO. Respiratory virus infection of monolayer cultures of human nasal epithelial cells. Am Rev Respir Dis 1990;141:839-45.

276. Zhu Z, Tang W, Ray A, et al. Rhinovirus stimulation of interleukin-6 in vivo and in vitro. Evidence for nuclear factor kappa B-dependent transcriptional activation. J Clin Invest 1996;97:421-30.

277. Griego SD, Weston CB, Adams JL, Tal-Singer R, Dillon SB. Role of p38 mitogen-activated protein kinase in rhinovirus-induced cytokine production by bronchial epithelial cells. J Immunol 2000;165:5211-20.

278. Johnston SL, Papi A, Bates PJ, Mastronarde JG, Monick MM, Hunninghake GW. Low grade rhinovirus infection induces a prolonged release of IL-8 in pulmonary epithelium. J Immunol 1998;160:6172-81.

279. Papadopoulos NG, Papi A, Meyer J, et al. Rhinovirus infection up-regulates eotaxin and eotaxin-2 expression in bronchial epithelial cells. Clin Exp Allergy 2001;31:1060-6.

280. Schroth MK, Grimm E, Frindt P, et al. Rhinovirus replication causes RANTES production in primary bronchial epithelial cells. Am J Respir Cell Mol Biol 1999;20:1220-8.

281. Denlinger LC, Sorkness RL, Lee WM, et al. Lower airway rhinovirus burden and the seasonal risk of asthma exacerbation. Am J Respir Crit Care Med 2011;184:1007-14.

282. Khair OA, Devalia JL, Abdelaziz MM, Sapsford RJ, Tarraf H, Davies RJ. Effect of Haemophilus influenzae endotoxin on the synthesis of IL-6, IL-8, TNF-alpha and expression of ICAM-1 in cultured human bronchial epithelial cells. Eur Respir J 1994;7:2109-16.

283. Meyer TA, Noguchi Y, Ogle CK, et al. Endotoxin stimulates interleukin-6 production in intestinal epithelial cells. A synergistic effect with prostaglandin E2. Arch Surg 1994;129:1290-4.

284. Zalman LS, Brothers MA, Dragovich PS, et al. Inhibition of human rhinovirus-induced cytokine production by AG7088, a human rhinovirus 3C protease inhibitor. Antimicrob Agents Chemother 2000;44:1236-41.

285. LeMay LG, Vander AJ, Kluger MJ. Role of interleukin 6 in fever in rats. Am J Physiol 1990;258:R798-R803.

286. Chen Q, Fisher DT, Clancy KA, et al. Fever-range thermal stress promotes lymphocyte trafficking across high endothelial venules via an interleukin 6 trans-signaling mechanism. Nat Immunol 2006;7:1299-308.

287. Ulich TR, del CJ, Guo KZ. In vivo hematologic effects of recombinant interleukin-6 on hematopoiesis and circulating numbers of RBCs and WBCs. Blood 1989;73:108-10.

288. Hirano T, Yasukawa K, Harada H, et al. Complementary DNA for a novel human interleukin (BSF-2) that induces B lymphocytes to produce immunoglobulin. Nature 1986;324:73-6.

289. Doyle WJ, Casselbrant ML, Li-Korotky HS, et al. The interleukin 6 -174 C/C genotype predicts greater rhinovirus illness. J Infect Dis 2010;201:199-206.

290. Spurrell JC, Wiehler S, Zaheer RS, Sanders SP, Proud D. Human airway epithelial cells produce IP-10 (CXCL10) in vitro and in vivo upon rhinovirus infection. Am J Physiol Lung Cell Mol Physiol 2005;289:L85-L95.

291. Korpi-Steiner NL, Valkenaar SM, Bates ME, Evans MD, Gern JE, Bertics PJ. Human monocytic cells direct the robust release of CXCL10 by bronchial epithelial cells during rhinovirus infection. Clin Exp Allergy 2010;40:1203-13.

292. Bianco A, Sethi SK, Allen JT, Knight RA, Spiteri MA. Th2 cytokines exert a dominant influence on epithelial cell expression of the major

group human rhinovirus receptor, ICAM-1. Eur Respir J 1998;12:619-26.

293. Walker C, Bauer W, Braun RK, et al. Activated T cells and cytokines in bronchoalveolar lavages from patients with various lung diseases associated with eosinophilia. Am J Respir Crit Care Med 1994;150:1038-48.

294. Naseer T, Minshall EM, Leung DY, et al. Expression of IL-12 and IL-13 mRNA in asthma and their modulation in response to steroid therapy. Am J Respir Crit Care Med 1997;155:845-51.

295. Terajima M, Yamaya M, Sekizawa K, et al. Rhinovirus infection of primary cultures of human tracheal epithelium: role of ICAM-1 and IL-1beta. Am J Physiol 1997;273:L749-L759.

296. Yoon HJ, Zhu Z, Gwaltney JM, Jr., Elias JA. Rhinovirus regulation of IL-1 receptor antagonist in vivo and in vitro: a potential mechanism of symptom resolution. J Immunol 1999;162:7461-9.

297. de KJ, Grunberg K, Pons D, et al. Interleukin-1beta and interleukin-1ra levels in nasal lavages during experimental rhinovirus infection in asthmatic and non-asthmatic subjects. Clin Exp Allergy 2003;33:1415-8.

298. van Benten IJ, van Drunen CM, Koevoet JL, et al. Reduced nasal IL-10 and enhanced TNFalpha responses during rhinovirus and RSV-induced upper respiratory tract infection in atopic and non-atopic infants. J Med Virol 2005;75:348-57.

299. Noah TL, Henderson FW, Wortman IA, et al. Nasal cytokine production in viral acute upper respiratory infection of childhood. J Infect Dis 1995;171:584-92.

300. Suzuki T, Yamaya M, Sekizawa K, et al. Effects of dexamethasone on rhinovirus infection in cultured human tracheal epithelial cells. Am J Physiol Lung Cell Mol Physiol 2000;278:L560-L571.

301. Smart SJ, Casale TB. Pulmonary epithelial cells facilitate TNF-alpha-induced neutrophil chemotaxis. A role for cytokine networking. J Immunol 1994;152:4087-94.

302. Hazelbag S, Fleuren GJ, Baelde JJ, Schuuring E, Kenter GG, Gorter A. Cytokine profile of cervical cancer cells. Gynecol Oncol 2001;83:235-43.

303. Huh D, Matthews BD, Mammoto A, Montoya-Zavala M, Hsin HY, Ingber DE. Reconstituting organ-level lung functions on a chip. Science 2010;328:1662-8.

304. Gern JE, Galagan DM, Jarjour NN, Dick EC, Busse WW. Detection of rhinovirus RNA in lower airway cells during experimentally induced infection. Am J Respir Crit Care Med 1997;155:1159-61.

305. Winther B, Gwaltney JM, Jr., Mygind N, Turner RB, Hendley JO. Sites of rhinovirus recovery after point inoculation of the upper airway. JAMA 1986;256:1763-7.

306. Jang YJ, Lee SH, Kwon HJ, Chung YS, Lee BJ. Development of rhinovirus study model using organ culture of turbinate mucosa. J Virol Methods 2005;125:41-7.

307. Lopez-Souza N, Favoreto S, Wong H, et al. In vitro susceptibility to rhinovirus infection is greater for bronchial than for nasal airway epithelial cells in human subjects. J Allergy Clin Immunol 2009;123:1384-90.

308. Hartshorn KL, Sastry K, Brown D, et al. Conglutinin acts as an opsonin for influenza A viruses. J Immunol 1993;151:6265-73.

309. Bernardo J, Long HJ, Simons ER. Initial cytoplasmic and phagosomal consequences of human neutrophil exposure to Staphylococcus epidermidis. Cytometry A 2010;77:243-52.

310. Hartshorn KL, Collamer M, White MR, Schwartz JH, Tauber AI. Characterization of influenza A virus activation of the human neutrophil. Blood 1990;75:218-26.

311. Hutchinson AF, Ghimire AK, Thompson MA, et al. A community-based, time-matched, case-control study of respiratory viruses and exacerbations of COPD. Respir Med 2007;101:2472-81.

312. Deb R. An Investigation of the Roles of Lung Surfactant Proteins- A and -D in the Pulmonary Allergic Response. D. Phil Thesis, University of Oxford, 2006.

313. Nadesalingam J, Reid KB, Palaniyar N. Collectin surfactant protein D binds antibodies and interlinks innate and adaptive immune systems. FEBS Lett 2005;579:4449-53.

314. Gwaltney JM, Jr., Hendley JO, Simon G, Jordan WS, Jr. Rhinovirus infections in an industrial population. I. The occurrence of illness. N Engl J Med 1966;275:1261-8.

315. Senior K. FDA panel rejects common cold treatment. Lancet Infect Dis 2002;2:264.

316. Hayden FG, Hipskind GJ, Woerner DH, et al. Intranasal pirodavir (R77,975) treatment of rhinovirus colds. Antimicrob Agents Chemother 1995;39:290-4.

317. De Palma AM, Vliegen I, De CE, Neyts J. Selective inhibitors of picornavirus replication. Med Res Rev 2008;28:823-84.

318. Arruda E, Pitkaranta A, Witek TJ, Jr., Doyle CA, Hayden FG. Frequency and natural history of rhinovirus infections in adults during autumn. J Clin Microbiol 1997;35:2864-8.

319. Tyrrell DA, Cohen S, Schlarb JE. Signs and symptoms in common colds. Epidemiol Infect 1993;111:143-56.

320. Tyrrell DA, BYNOE ML, PETERSEN KB, SUTTON RN, PEREIRA MS. Inoculation of human volunteers with parainfluenza viruses types 1 and 3 (HA 2 and HA 1). Br Med J 1959;2:909-11.

321. Harrod KS, Trapnell BC, Otake K, Korfhagen TR, Whitsett JA. SP-A enhances viral clearance and inhibits inflammation after pulmonary adenoviral infection. Am J Physiol 1999;277:L580-L588.

322. Grubor B, Gallup JM, Meyerholz DK, et al. Enhanced surfactant protein and defensin mRNA levels and reduced viral replication during parainfluenza virus type 3 pneumonia in neonatal lambs. Clin Diagn Lab Immunol 2004;11:599-607.

323. Dimopoulos G, Lerikou M, Tsiodras S, et al. Viral epidemiology of acute exacerbations of chronic obstructive pulmonary disease. Pulm Pharmacol Ther 2012;25:12-8.

324. Kerr MH, Paton JY. Surfactant protein levels in severe respiratory syncytial virus infection. Am J Respir Crit Care Med 1999;159:1115-8.

325. Cheng G, Ueda T, Numao T, et al. Increased levels of surfactant protein A and D in bronchoalveolar lavage fluids in patients with bronchial asthma. Eur Respir J 2000;16:831-5.

326. Wang JY, Shieh CC, Yu CK, Lei HY. Allergen-induced bronchial inflammation is associated with decreased levels of surfactant proteins A and D in a murine model of asthma. Clin Exp Allergy 2001;31:652-62.

327. Leth-Larsen R, Garred P, Jensenius H, et al. A common polymorphism in the SFTPD gene influences assembly, function, and concentration of surfactant protein D. J Immunol 2005;174:1532-8.

328. Floros J, Lin HM, Garcia A, et al. Surfactant protein genetic marker alleles identify a subgroup of tuberculosis in a Mexican population. J Infect Dis 2000;182:1473-8.

329. Hartshorn KL, White MR, Tecle T, Sorensen G, Holmskov U, Crouch EC. Viral aggregating and opsonizing activity in collectin trimers. Am J Physiol Lung Cell Mol Physiol 2010;298:L79-L88.

330. Tecle T, White MR, Sorensen G, et al. Critical role for cross-linking of trimeric lectin domains of surfactant protein D in antiviral activity against influenza A virus. Biochem J 2008;412:323-9.

331. Tuthill TJ, Papadopoulos NG, Jourdan P, et al. Mouse respiratory epithelial cells support efficient replication of human rhinovirus. J Gen Virol 2003;84:2829-36.

332. Zhang L, Ikegami M, Dey CR, Korfhagen TR, Whitsett JA. Reversibility of pulmonary abnormalities by conditional replacement of surfactant protein D (SP-D) in vivo. J Biol Chem 2002;277:38709-13.

333. Wicks J, Haitchi HM, Holgate ST, Davies DE, Powell RM. Enhanced upregulation of smooth muscle related transcripts by TGF beta2 in asthmatic (myo) fibroblasts. Thorax 2006;61:313-9.

334. Botas C, Poulain F, Akiyama J, et al. Altered surfactant homeostasis and alveolar type II cell morphology in mice lacking surfactant protein D. Proc Natl Acad Sci U S A 1998;95:11869-74.

335. Korfhagen TR, Sheftelyevich V, Burhans MS, et al. Surfactant protein-D regulates surfactant phospholipid homeostasis in vivo. J Biol Chem 1998;273:28438-43.

336. Nagarkar DR, Bowman ER, Schneider D, et al. Rhinovirus infection of allergen-sensitized and -challenged mice induces eotaxin release from functionally polarized macrophages. J Immunol 2010;185:2525-35.